# Retinal plasticity in experimental glaucoma

## Paulina Anna Samsel

Thesis submitted to Cardiff University in accordance with the requirements for the degree of Doctor of Philosophy

Visual Neuroscience and Molecular Biology Group
School of Optometry and Vision Sciences
Cardiff University
June 2010

UMI Number: U517580

#### All rights reserved

#### INFORMATION TO ALL USERS

The quality of this reproduction is dependent upon the quality of the copy submitted.

In the unlikely event that the author did not send a complete manuscript and there are missing pages, these will be noted. Also, if material had to be removed, a note will indicate the deletion.



#### UMI U517580

Published by ProQuest LLC 2013. Copyright in the Dissertation held by the Author.

Microform Edition © ProQuest LLC.

All rights reserved. This work is protected against unauthorized copying under Title 17, United States Code.



ProQuest LLC 789 East Eisenhower Parkway P.O. Box 1346 Ann Arbor, MI 48106-1346

### CONTENTS

DECLARATION	I
Acknowledgements	VI
Contributions	VII
Abbreviations	IX
List of Figures	XII
List of Tables X	VIII
Chapter 1: Introduction	
1.1. Glaucoma	
1.1.1. Background	
1.1.2. Forms of glaucoma	2
1.1.3. Diagnostic aspects	
1.1.4. Research approaches to treatment	
1.1.5. Current treatments	
1.1.5.1. Effect of IOP reduction	
1.1.5.2. Pharmacotherapy	6
1.1.5.3. Surgery and laser techniques	
1.1.6. Mechanisms of RGC death in glaucoma	
1.1.6.1. Neurotrophic factor deprivation	
1.1.6.2. Hypoperfusion	8
1.1.6.3. Glial cell activation	9
1.1.6.4. Glutamate toxicity	10
1.1.6.5. Abnormal immune response	
1.1.7. Morphology and function of RGCs	
1.1.7.1. Morphology and function of RGC in glaucoma	14
1.1.8. Models of experimental glaucoma	
1.1.8.1. Mouse model of glaucoma	
1.1.8.2. Non-human primate model of IOP-induced optic nerve damage	
1.1.8.3. Rat model of IOP-induced optic nerve damage	
1.1.8.4. <i>In vitro</i> systems	21
1.1.8.4.1. Retinal explant culture	21
1.1.8.4.2. Retinal ganglion cell culture	21
1.2. Neuroplasticity	22
1.2.1. Neuroplasticity and diseases of the CNS	22
1.2.2. Regulators of neuroplasticity	
1.2.3. Neuroplasticity in the retina.	
1.2.4. Neurotrophins	
1.2.5. Perineuronal nets	
1.2.5.1. Structure and composition	
1.2.5.2. Functional roles of PNNs in plasticity.	
• •	
1.3. Hypothesis	
1.4. Project aims	31
Chapter 2: Materials and Methods	32
2.1. Ex vivo – retinal explant culture	33
2.1.1. Experimental animals	
2.1.2. Retinal dissection	
2.1.3. Culture conditions	
2.1.4. Cell viability assays	
2.1.4.1. Image capture of labelled RGCs	
2.1.4.2. Statistical analysis	
2.1.5. Gene gun processes	
2.1.5.1. Biolistic labelling	
2.1.5.2. Diolistic labelling	

2.1.5.3. Image capture of labelled RGCs	39
2.1.6. Effects of BDNF and caspase inhibitors on neuronal survival and the number of axonal	2.0
growth cones	39
2.2. In vivo - experimental glaucoma models	40
2.2.1. Introduction to animal techniques	40
2.2.2. Calibration of the Tonolab rebound tonometer in cannulated rat eye	40
2.2.3. Hypertonic saline model	41
2.2.3.1. Induction of glaucoma	41
2.2.3.1.1. Microneedle assembly	
2.2.3.1.2. Anaesthesia	
2.2.3.1.3. Surgical procedure	
2.2.3.2. IOP measurements	
2.2.3.3. Euthanasia	
2.2.4. Magnetic bead model	
2.2.4.1. Induction of glaucoma	44 17
2.2.4.2. Chondroithnase ABC and BDNF injections into a gradionnatous fat eye	48
• •	
2.3. Ex vivo evaluation of glaucomatous changes in experimental glaucoma models	53 53
2.3.1. Ex vivo FD-OCT imaging	53
2.3.2. Protectist laberting	
2.3.3.1. Retinal dissection	
2.3.3.2. Preparation of dye-coated particles and diolistic labelling	
2.3.3.3. Analysis of morphological parameters	5:
2.3.3.4. Neuron nuclei imaging and counting	
2.3.4. Croyosections of the anterior chamber	
2.4. Biochemical and immunohistochemical analyses of GAGs in a rat retina	5,
2.4. Biochemical analysis	50 54
2.4.1.1 Animals	
2.4.1.2. Guanidine extraction	
2.4.1.3. Protein assay	
2.4.1.4. SDS-PAGE	
2.4.1.5. Western blotting	
2.4.2. Immunohistochemistry	
2.4.2.1. Animals	
2.4.2.2. Preparation of wax sections	
2.4.2.3. Chondroitinase ABC digestion and immunostaining using DAB method	
Chapter 3: Retinal explant culture	61
•	
3.1. Introduction	62
3.2. Results	64
3.2.1. Assessment of retinal explant viability with calcein AM and propidium iodide	64
3.2.2. Evaluation of the biolistic transfection technique	
3.2.3. Assessment of the effect of ballistic transfection on tissue survival	71
3.2.4. Assessment of the morphology of labelled RGCs using the diolistic technique	
3.2.5. Effects of caspase inhibitors and BDNF on neuronal survival and the number of axonal	
growth cones	
3.2.5.1. Effects of caspase inhibitor on the survival of transfected RGCs	
3.2.5.2. Effects of caspase inhibitor on the number of axons in the proximity of the optic di	ISC
3.2.5.3. The number of axonal growth cones and the number of axons in the proximity of t	he
optic disc in BDNF-treated explants	
·	
3.3. Discussion	81 01
3.3.2.Effects of BDNF and caspase inhibitors on neuronal survival and the number of ax	
growth cones 85	viia
Brown source on	

3.4. Summary	86
Chapter 4: Experimental glaucoma: profiling intraocular pressure, cell loss and optic nervo	
4.1. Introduction	88
4.1.1. IOP profiles and cell loss	
4.1.2. OCT imaging studies: in vivo detection and monitoring of retinal damage in experim	ental
glaucomaglaucoma	89
4.1.3. Experimental design	
4.2. Results	93
4.2.1. Calibration of the Tonolab rebound tonometer in cannulated rat eyes	
4.2.2. Intraocular pressure elevation in the hyperonic saline model	96
4.2.3. Intraocular pressure elevation and cell loss in the magnetic bead model	100
4.2.3.1. Intraocular pressure elevation	
4.2.3.2. Neuron quantification in the RGCL	
4.2.4. OCT imaging	110
4.2.4.1. In vivo OCT imaging and quantification of RNFL thickness in a magnetic bead	
4.2.4.2. Evaluation of damage by ex vivo OCT imaging in hypertonic saline model	115
4.3. Discussion	
4.3.1. Evaluation of the Tonolab rebound tonometer	
4.3.2. Hypertonic saline model	
4.3.3. Magnetic bead model	
4.3.4. OCT imaging	
4.4. Summary	124
treated retinas	
5.2 Results	129
5.2.1. IOP profiles	
5.2.2. Quantification of dendrite morphology	
5.2.2.1. Dendrite morphology in glaucoma vs. control	
5.2.2.2. Dendrite morphology in the treated retinas vs. glaucomatous and control retinas	
5.2.2.2.1. Sholl plots	136
5.2.2.2. Dendrite morphology in chABC-injected glaucomatous eyes	139
5.2.2.2.3. Dendrite morphology in BDNF-injected glaucomatous eyes	
5.2.2.2.5. Dendrite morphology in cnABC+BDNF-injected glaucomatous eyes	
5.2.2.2.6. Summary of the results	
5.2.3. The presence of chABC generated epitopes in the retina after intravitreal	141
injections	
5.2.4. RGC cell loss in the chABC and BDNF-treated retinas	141
5.3. Discussion	147
5.3.1. Quantification of RGC dendritic morphology	
5.3.1.1. Dendritic morphology in experimental glaucoma	
5.3.1.2. Dendritic morphology after chondroitinase ABC injection	
5.3.1.2.1. Chondroitinase ABC-promoted plasticity	
5.3.1.3. Dendritic morphology after BDNF injection	
5.3.1.4. Dendritic morphology after the combined injection of chABC and BDNF	152
5.3.1.5. Dendritic morphology after chABC injection into a non-glaucomatous retina	
5.3.2. The presence of chABC generated epitopes in the retina after intravitreal	
injections. Distribution of CSPGs in the eye	
5.3.3. Fast Sholl	155
5.4. Summary	156

Chapter 6: Chondroitin sulphate proteoglycans (CSPGs) in you	
6.1. Introduction	
6.2. Results	
6.2.1. Western blotting	162
6.2.2. Immunohistochemistry	163
6.3. Discussion	
6.4. Chapter summary	171
hapter 7: General discussion	172
7.1. Summary	
7.2. Future work	
7.3. Conclusion	
REFERENCES	178

.

#### Acknowledgements

I would like to express profound gratitude to my supervisors, Prof James E. Morgan, Dr Jonathan T. Erichsen and Dr Julie Albon, for their guidance and expertise during my PhD.

I am also grateful to Prof Alun Davies for giving me an opportunity to do research in his lab in the Department of Biosciences and Dr Humberto Gutierrez for his assistance during my work in this lab.

I also want to express my appreciation to Dr Debbie Tudor, Dr Alex Tumlinson, Dr Boris Povazay, Prof Wolfgang Drexler, Dr Gillian Smith, Dr Nick White, Dr Ankush Prashar, Ketan Kapoor, Vedran Kajic, Alicia Charlton, Lilian Kisiswa and Stephen Cross for their support in some practical aspects of my work.

At last but not least, I would like to acknowledge everyone from VNMB group for their constant support.

#### **Contributions**

The majority of work in this thesis is my own, however the following parts of the work were undertaken in collaborations. I would like to acknowledge everyone who has contributed to my work.

#### **Protocols**

- > The protocols for biolistic transfection (section 2.1) of retinal explant culture were optimised in collaboration with Humberto Gutierrez.
- ➤ Calibration of Tonolab rebound tonometer was performed in collaboration with Dr Ankush Prashar (sections 2.2.2 & 4.2.1).
- ➤ OCT data processing and postprocessing procedure was performed Dr Alex Tumlinson, Ketan Kapoor and Vedran Kajic (section 2.2.4.3). Vedran Kajic performed a manual segmentation (section 2.2.4.3).
- Ex vivo FD-OCT imaging (section 2.3.1) was performed by Alicia Charlton, Dr Boris Povazay and supervised by Prof Wolfgang Drexler.
- > The protocol for croyosections of the anterior chamber (section 2.3.4) was provided and performed by Dr Gill Smith.
- ➤ The protocols for biochemical and immunohistochemical analyses of GAGs in a rat retina (section 2.4) were optimised in collaboration with Dr Debbie Tudor. The experiments described in Chapter 6 were performed in collaboration with Dr Debbie Tudor.

#### **Figures**

- ➤ Dr Gillian Smith provided photographs for Figure 4.5C, excluding the indications of AC=anterior chamber, TM=trabecular meshwork and MB=microbeads.
- > Dr Alex Tumlinson provided Figures 4.9 and the OCT images for Figure 4.12.
- > Stephen Cross contributed to Figures 4.9 by providing data for the rats CR425, CR426 and CR427 and to Figure 4.12 by providing data for the rat CR427.
- ➤ Ketan Kapoor contributed to Figures 4.9 abd 4.11 by post-processing the OCT images.
- ➤ Alicia Charlton, Dr Boris Povazay and Prof Wolfgang Drexler provided the OCT images for Figures 4.12 and 4.13.

#### **Abstract**

Glaucoma is the second leading cause of vision loss in the world. In the commonest form of the disease, chronic open angle glaucoma, increased intraocular pressure (IOP) is associated with accelerated death of retinal ganglion cells (RGCs) and consequent loss of visual field. Currently, there is no treatment to recover lost vision. If surviving tissue could be regenerated on the basis of its plasticity in glaucomatous eye, visual impairment associated with glaucoma might be potentially reversed. The project was to determine if RGC remodelling in glaucoma might be driven by combined IOP reduction and manipulation of retinal perineuronal nets to form a neural substrate for the recovery of vision loss in glaucoma

The purpose of the initial part of the study was to establish an *in vitro* model of glaucoma such as retinal explant culture to analyse morphological changes of RGCs over a period of time. Biolistic transfection of retinal explant culture has been optimised to study remodelling of adult RGCs *in vitro*. Broad-spectrum caspase inhibitor enhanced RGC survival and axonal regrowth while exogenous BDNF enhanced the number of growth cones on the axons of RGCs.

The main part of the project was conducted using two rat glaucoma models, induced by either injection of hypertonic saline into the episcleral veins to sclerose the trabecular meshwork or paramagnetic microbeads into the anterior chamber (a novel technique). Optical coherence tomography (OCT) imaging enabled the observation of progressive glaucomatous changes *in vivo* and estimation of retinal nerve fibre layer thickness (RNFL). A significant reduction in RNFL thickness 17-32 days following induction of intraocular pressure was observed.

To investigate the possibility that the dendritic changes of RGCs in glaucoma could be reversed, chondroitinase ABC was injected into the rats' eyes to promote RGCs regeneration in glaucoma by enzymatic digestion of PNN. The treatment of glaucomatous retinas with chondroitinase ABC resulted in a significant change in morphological parameters of RGCs compared to RGCs of non-treated glaucomatous eyes, suggesting that chABC promoted recovery of RGC dendritic tree in adult glaucomatous eyes.

Our study confirmed the existence of a perineuronal net in the rat retina and indicated that molecular weight distribution and immunohistochemical tissue localisation of glycosaminoglycans varied in young, old and glaucomatous rat retinas. Chondroitinase sulphate proteoglycans were mainly localised to the photoreceptor layer, while aggrecan core protein to the inner retina. Aggrecan was highly degraded in young, old and glaucomatous retinas.

#### **Abbreviations**

AM acetoxymethyl ester
ANOVA analysis of variance

ARVO Association for Research in Vision and Ophthalmology

ATPase adenosine triphosphatase

BCIP 5-bromo-4-chloroindol-3-yl phosphate

BDNF brain derived neurotrophic factor

Boc-D-FMK broad-spectrum, irreversible caspase inhibitor

BSS Balanced Salt Solution

CNTF ciliary neurotrophic factor

COP-1 copolymer-1

CS chondroitin sulphate

CS-PGs chondroitin sulphate proteoglycans

3D three-dimensional

3D UHR-OCT Three Dimensional Ultrahigh Resolution OCT

DiI 1,1'-diocta-decyl-3,3,3',3'-tetramethylindocarbocyanine

perchlorate

DMEM Dulbecco's Modified Eagle's Medium

DNA deoxyribonucleic acid

EAE autoimmune encephalomyelitis

ECM extracellular matrix

EGFP expression plasmid for green fluorescent protein

EGS European Glaucoma Society

ERFP expression plasmid for red fluorescent protein

ERG electroretinography

EYFP expression plasmid for yellow fluorescent protein

FBS fetal bovine serum

FD-OCT frequency domain optical coherence tomography

FGF-2 fibroblast growth factor

FWHM full width at half maximum

GAGs glycosaminoglycans

GDNF glial cell line-derived neurotrophic factor

GON glaucomatous optic neuropathy
HBSS Hank's Buffered Salt Solution

HPM hydroxypropylmethylcellulose

IGF-I insulin-like growth factor
ILM inner limiting membrane

ImageJ Image Processing and Analysis in Java

IOP intraocular pressure
IP intraperitoneally

IPM interphotoreceptor matrix
LGN lateral geniculate nucleus
Mab monoclonal antibodies

MATLAB MATrix LABoratory

MBP myelin basic protein

MEM Minimum Essential Medium

MMP matrix metalloproteases

M-Pathways Magnocellular Pathways
NPCs neural progenitor cells

NBT Nitro Blue Tetrazolium

N-CAM neural cell adhesion molecule

NF- κB nuclear factor-κB

Ng-CAM neuron-glia cell adhesion molecule

NGF nerve growth factor

NT-3 neurotrophin-3
NT-4 neurotrophin-4
NTR neurotrophin

OBL ocular blood flow

OHTS Hypertension Treatment Study

ONH optic nerve head

PBS phosphate buffered saline

PFA paraformaldehyde

PGA prostaglandin analogs

PI propidium iodide

PI3-kinase phosphatidyl inositol-3-kinase

PIL Personal License

PMSF phenylmethylsulphonylfluoride

PNNs Perineuronal nets

P-Pathways Parvocellular Pathways

PPL Personal Project License

RGB red, green, and blue

RGCs retinal ganglion cells

rhBDNF recombinant human brain-derived neurotrophic factor

RNA ribonucleic acid

RNFL retinal fibre layer

RPE retinal pigment epithelium

SD standard deviation

SDS-PAGE sodium dodecyl sulphate polyacrylamide gel electrophoresis

SEM standard errors of the mean

SLD multiplexed two-superluminescent-diode

SPSS v.16 Statistical Package for the Social Sciences version 16

SS-OCT Thorlabs Swept Source OCT

T-588 R(-)-1-(benzo[b]thiophen-5-yl)-2-[2-(N,N-diethylamino)

ethoxy]ethanol hydrochloride

TNF-α tumour necrosis factor alpha

Trk tropomyosin-related kinase

WHO World Health Organization

## **List of Figures**

Figure 1.1. Confocal image showing the morphologic features (small soma and
dendritic arbour) that characterize the normal midget cell, with arrowhead indicating
intraretinal axon segment (A). Morphologic features that characterize the soma,
dendritic field, and intraretinal axon segment (arrowhead) of a parasol cell in the
,
normal retina (B). Scale bar: 10 μm (A), 25 μm (B) (Weber et al., 1998)
Figure 1.2. Small bistratified cell (A). Wide field ganglion cell, classified as diffuse
because their dendrites branch throughout the inner plexiform layer (IPL) (B). Scale
bar: 100 µm (Yamada et al., 2004).
Figure 1.3. Confocal image showing the morphologic features that characterize
midget cell (A) and parasol cell (B) from glaucomatous eyes. Although the soma size
of the midget cell (A) is comparable to the soma size of the normal midget cell in
Figure 1.2, its dendritic arbour is reduced and its axon is very thin compared with that
of other midget cells of similar soma size. Arrowhead indicates intraretinal axon
segment, while arrow indicates dendritic abnormalities. Scale bar, 10 µm (A) and 25
μm (B) (Weber et al., 1998)15
Figure 1.4. DiI-labelled RGCs in control (A) and experimental (B) eyes after 10
weeks post IOP elevation. Scale bar: 75 μm (Ahmed et al., 2001a)25
Figure 1.5. Neurotrophin-receptor interactions. Each neurotrophin binds to p75NTR
but not to the Trk receptors. After maturation of the proneurotrophins through
proteolysis, each mature neurotrophin can bind and activate p75NTR, but shows more
specific interactions with the three Trk receptors. NGF recognises TrkA, BDNF and
NT4 activate TrkB, and NT3 binds TrkC (Reichardt 2006)27
Figure 2.1. The Helios Gene gun (copied from www.bio-rad.com)
Figure 2.2. Sample delivery. The helium pulse sweeps the microcarriers from the
inside wall of the sample cartridge (copied from www.bio-rad.com)
Figure 2.3. Tonolab rebound tonometer (copied from
http://www.tiolat.fi/images.htm)
Figure 2.4. Surgical set-up used during the microinjection procedure. Rats were
anaesthetised in a chamber before surgery. Anaesthesia was maintained via an
inhalation mask (A). Photographs of magnetic beads before (left eppendorf) and after
agitating (right eppendorf). Since the beads tended to settle under the influence of
gravity, they were agitated using a vortex stirrer for approximately 10 seconds prior to
injection (B)46
Figure 2.5. A photograph of a custom-built OCT system (A) and schematics of the
1050-nm encoded frequency domain OCT system (B). The broadband source is
interfaced to a fiber-optic inferometer where the first arm is sent to an adjustable
reference mirror in a free-space portion including dispersion compensation and an
attenuator. The patient module consists of collimation and focusing optics and a 2-D
scanner. On its way back, the light from the sample arm is recombined with the
reference light, producing a spectral interference pattern that is sent to an all-reflective
imaging spectrometer with a reflective planar grating. Processing of the signal from
the InGaAs camera is performed with a standard industrial personal computer, while
- The state of the
an independent didital cidnal procecot il is di camiac tha pocition delicenomotore one
an independent digital signal processor (DSP) serves the position galvanometers and
synchronizes the acquisition (copied and cited from Povazay et al., 2007)49
synchronizes the acquisition (copied and cited from Povazay et al., 2007)
synchronizes the acquisition (copied and cited from Povazay et al., 2007)49

position to align the focusing beam with the optic disc. The rat had a mask for
isoflurane inhalation (C). An OCT image of a retina with an optic nerve head
displayed on the monitor (D)50
Figure 3.1. Fluorescent images of wholemount retinal explants stained with
propidium iodide (A, C, E) and calcein (B, D, F) cultured in HBSS (control) (A, B),
MEM (C, D) and Neurobasal-A (E, F) for 1 day. Scale bars: 50 μm66
Figure 3.2. Mean values of propidium iodide (PI) (A) and calcein AM (B)
fluorescence intensity from retinal explants, based on a single experiment. Diagonal
bars indicate fluorescence intensity in explants cultured in HBSS, grey in MEM and
black in Neurobasal-A medium. Error bars indicate standard deviation (SD)67
Figure 3.3. Positive staining of retinal explants with calcein AM (A) and
counterstaining with propidium iodide (B) shows good survival after 3 days in culture.
Scale bars: $500 \ \mu m$
Figure 3.4. Expression of YFP and RFP in mouse RGCs, 2 days post transfection.
Confocal image of RGCs transfected with expression plasmids for YFP (labelled
green) and RFP (labelled red). Some cells were labelled with pYFP and pRFP
(labelled orange). Scale bar: 100 µm70
Figure 3.5. Expression of YFP in mouse RGCs, 1 day post transfection. Confocal
images of RGCs transfected with expression plasmids for YFP (labelled yellow). The
arrow indicates an axon. Scale bars: 100 µm70
Figure 3.6. Fluorescent images of wholemount retinal explants stained with calcein
AM, cultured in HBSS (A), Neurobasal-A with B27 and N2 supplements (B, C) and
Neurobasal-A with B27 and horse serum (D, E) for 2 days. Intense green fluorescence
was detected in the non-shot samples (B, D), in contrast to the virtually absent
fluorescence in the samples that were shot with DNA-coated gold particles (C, E).
The images were taken from the centre of the wholemount preparations. Scale bars:
200μm72
Figure 3.7. Mean values of calcein AM fluorescence intensity in retinal explants,
based on a single experiment. Diagonal bars indicate fluorescence intensity in
explants cultured in HBSS, grey bars indicate fluorescence intensity in explants that
were not shot with DNA-coated gold particles, incubated in Neurobasal-A medium
with serum (N+serum) or Neurobasal-A medium (N) and black bars indicate
fluorescence intensity in explants that were shot with DNA-coated gold particles,
incubated in Neurobasal-A medium with serum (N+serum) or Neurobasal-A medium
(N). The Error bars indicate standard deviation (SD)73
Figure 3.8. Confocal images of RGCs from fixed retinal explants labelled with DiI-
coated tungsten particles. Retinal explants were cultured in Neurobasal-A medium
(with B27 supplement, horse serum, L-glutamine and penicillin/streptomycin) for
approximately 15 minutes before labelling. The somas, dendritic fields and axons are
visible. Scale bars: 100 µm74
Figure 3.9. Average numbers of surviving RGCs per explant in control and caspase
inhibitor-treated explants. A significant increase in the number of RGCs was
observed in retinas cultured with caspase inhibitor than in control explants after 2
days in culture. Analyses are based on 31 explants per group. Error bars represent
standard error (SEM). * p<0.0576
Figure 3.10. RGC transfected with YFP-expressing plasmid, cultured in caspase
inhibitor-supplemented medium. Scale: 100 µm76
Figure 3.11. Growth cones on axons in RGCs cultured in caspase inhibitor-
supplemented medium after 2 days in culture. Scale, 20 µm77

Figure 3.12. Number of axons within the distance of 500 µm from the optic disc in
control and caspase inhibitor-treated explants. RGCs in caspase inhibitor-treated
explants displayed a significant increase in the number of axons within 500 µm of an
an optic disc compared to control explants after 2 days in culture. Analyses are based
on 31 explants per group. Error bars indicate standard error (SEM). * p<0.0577
Figure 3.13. Confocal images of the optic discs from retinas transfected with YFP-
expressing plasmid. Axons can be seen in the proximity of the optic discs in control
and caspase inhibitor-treated explant after two days in culture. Scale: 100.µm79
Figure 3.14. An axon in the proximity of the optic disc after 2 days (A) and the same
axon after 3 days (B) in culture. The measured distance to the optic disc was reduced
by approximately 40µm after 3 days compared to 2 days in culture. Axonal sprouting
was observed after 2 days (C) but not after 3 days in culture (D). Scale: 20 µm79
Figure 3.15. Ratio of axons with growth cones to all analysed axons (18 for controls
and 10 for BDNF-treated axons). A significant increase in the number of growth
,
cones was observed in explants cultured with BDNF compared to controls after 2 days
in culture. Error bars indicate standard error. * p<0.05
Figure 3.16. Growth cones on axons in RGCs from explants cultured in control and
BDNF-supplemented medium after 2 days in culture. Scale, 20 µm80
Figure 3.17. Number of axons within the distance of 500 µm from the optic disc in
control (not exposed to caspase inhibitor) and BDNF-treated explants Analyses are
based on 13 explants per group. Error bars indicate standard error80
Figure 3.18. Incubation of rabbit retina. Photograph (A) and schematic diagram (B)
of the hybrid interphase/perfusion chamber (copied from Koizumi et al., 2007)83
Figure 4.1. Calibration of the Tonolab rebound tonometer in a cannulated rat eye.
The relationship between IOP in the anterior chamber (measured using pressure
transducer) and IOP reading obtained with the rebound tonometer. The measurements
were taken at 1mm (Figures 4.1 A & B) and 3mm (Figure 4.1 C) distance from
tonometer probe to cornea. The parameters for these curves are presented in Table
4.1
Figure 4.2. Intraocular pressures (IOP) following a single injection of hypertonic
saline in rat CR308 (A) and three injections rat CR303 (B). The arrows indicate times
of injections. Error bars: standard deviations. Open symbols: glaucoma; closed
symbols: control
Figure 4.3. The mean intraocular pressure (IOP) in the experimental rats injected with
hypertonic saline during the experimental period. Open symbols: glaucoma; closed
symbols: control. Error bars: standard error of the mean
Figure 4.4. An image showing location of the magnet relative to the rat eye during
redirection of magnetic beads with the magnet. The arrow indicates the magnet. Scale
bar, 1 cm101
Figure 4.5. Rat anterior segment showing the distribution of paramagnetic beads
immediately post injection with using a magnet (A) and without a magnet (B). The
arrows indicate beads in the anterior chamber angle. (C) Cryosection of the anterior
chamber injected with magnetic beads showing complete occlusion of the iridocorneal
angle. AC=anterior chamber; TM=trabecular meshwork; MB=microbeads. Inset
image shows higher magnification image of the angle with altered contrast to
highlight the microbead distribution (indicated by arrows)
· · · · · · · · · · · · · · · · · · ·
Figure 4.6. Intraocular pressures (IOP) following single bead injections with using a
magnet to direct beads to the anterior chamber angle in (A) rat CR352 and (B) rat
CR355. Error bars: standard deviations. Open symbols: injected eye; closed symbols:

control eye. Intraocular pressures (IOP) following single bead injection without using
a magnet in rat CR461 (C)
Figure 4.7. The mean intraocular pressure (IOP) in the experimental rats injected with
magnetic beads during the first 42 days after injection. Open symbols: injected eyes;
closed symbols: control eyes. Error bars: standard error of the mean
Figure 4.8. Schematic figure showing the location of the 12 sample areas that were
imaged in the superior, inferior, temporal and nasal part of a retina within the
distances of 1, 2 and 3mm from the optic disc (O). Double arrows indicate the
distances of 1000 µm between the imaged areas (A). Sample images of RGCL stained
with Hoechst from control (B) and injected (C) eye from a rat injected with magnetic
beads. Cells were counted using ImageJ plugin, Cell Counter. Pink dots indicate how
the cells were picked out for counting. Scale bars, 100 µm109
Figure 4.9. (A) A plot showing experimental subjects, dates of bead injection and
OCT imaging. Rats were imaged once before injection and once (CR401, CR402,
CR404, CR426) or twice (CR391, CR392, CR393, CR425, CR427) after injection.
(B) Plots showing summarized RNFL thickness trends in control (left column) and
experimental eyes (right column) before bead injection, 7-10 days after injection and
17-32 days after injection. Plain and dashed lines represent mean and standard
deviation, respectively. The RNFL thicknesses were measured at different angular
orientation from ONH (t, temporal; s, superior; n, nasal; i, inferior). (Thanks to Alex
Tumlinson and Stephen Cross).
Figure 4.10. Changes in mean RNFL thickness in OCT scans caused by magnetic
bead injection. Closed symbols: control eyes, open symbols: experimental eyes. N=3
before injection; n=9 7-10 days after injection and n=11 (2 rats had the thickness
measured twice within 17-32 days period) 17-32 days after injection. Data are
represented as the mean ± SEM. ** P<0.01 (Independent Samples T-Test)113
Figure 4.11. OCT images showing extreme case of glaucoma progression in rat
CR427 before bead injection, 3 and 4 weeks after injection. Left column, control eye.
Right column, injected eye. Below the images, IOP profile of the rat CR427 following
bead injection (OCT Images courtesy of Alex Tumlinson and Stephen Cross) 114
Figure 4.12. Summary chart showing IOP profiles, 3D volumes, enface images and
depth profiles for the normal rat and the rats: CR314, CR305, CR300 and CR308. The
red lines: IOPs in the injected (glaucomatous) eyes. The blue lines: IOPs in the
contralateral eyes. Error bars: standard deviations. (Thanks to Alicia Charlton, Dr
Boris Povazay and Prof Wolfgang Drexler)116
Figure 4.13. OCT images (A) & (B) were consistent with histological images (B)-(F).
The extensive damage in the retina from the experimental eye from the rat CR308 was
observed in the OCT image (A) as well as in vertical sections stained with Hoechst
(B) and imaged with DIC method (C). There was no damage in the normal eye from
the rat CR308 (D-F). GCL, ganglion cell layer; IPL, inner plexiform layer; INL, inner
nuclear layer; OPL, outer plexiform layer; ONL, outer nuclear layer117
Figure 5.1. A horizontal bar plot showing a plan of the experiment
Figure 5.2. The mean intraocular pressure (IOP) in the experimental rats whose
glaucomatous or control (or both glaucomatous and control) retinas were included in
the study (n=32) during the first 43 days after injection. Open symbols: injected eyes;
closed symbols: control eyes. Error bars: standard error of the mean130
Figure 5.3. Dil labelled RGCs from control and glaucomatous eyes
Figure 5.4. Dil labelled RGCs from glaucomatous eyes injected with chABC, BDNF,
chABC+BDNF and RGC from control eye injected with chABC134

Figure 5.5. Correlation between the total estimated intersections per cell obtained by the Fast Sholl and the total length in micrometers of the dendritic arbours per cell as estimated by independent neurite tracing. Twenty individual neurons were sampled across the range of morphologies and the total number of estimated intersections derived according to the method described in the results section (vertical axis). Total dendritic length was measured by direct tracing of the dendrites (horizontal axis). The resulting linear equation can subsequently be used as a standard curve to calculate the total (metric) length in micrometers of dendritic arbours in experimental samples of neurons. 135 Figure 5.6. (A) Sholl analysis of RGC dendrites from control (white symbols) and glaucomatous retinas (black symbols) showing reduction in the number of intersections relative to the distance from cell soma for RGCs from glaucomatous retinas. The radial distances were calculated and the corresponding 10 um intervals assigned to each branching and/or terminal point. Error bars indicate SEM. (B) A typical IOP plot for a magnetic bead model. Intraocular pressures (IOP) following single bead injections in rat CR341. The arrow indicates time of injections. Error bars: standard deviations. Open symbols: control; closed symbols: glaucoma. N indicates the number of analysed cells. Dil labelled RGCs from (C) normal eve and (B) Figure 5.7. Sholl analysis of RGC dendrites from control retinas (white symbols), glaucoma (black symbols), chABC-injected glaucomatous retinas (grey symbols) (A), BDNF-injected glaucomatous retinas (grey symbols) (B), chABC+BDNF-injected glaucomatous retinas (grey symbols) (C) and chABC-injected negative control retinas (grey symbols) (D). The radial distances were calculated and the corresponding 10 µm intervals assigned to each branching and/or terminal point. Error bars indicate Figure 5.8. The total dendritic length was compared among the groups. White bars indicate mean values for control retinas, black for glaucoma, grey for chABC-injected glaucomatous retinas (A), diagonal stripes for BDNF-injected glaucomatous retinas (B), grid for chABC+BDNF-injected glaucomatous retinas (C) and horizontal lines for chABC-injected negative control retinas (D). Error bars indicate SEM. \* p<0.05, Figure 5.9. The number of branching points was compared among the groups. White bars indicate mean values for control retinas, black for glaucoma, grey for chABCinjected glaucomatous retinas (A), diagonal stripes for BDNF-injected glaucomatous retinas (B), grid for chABC+BDNF-injected glaucomatous retinas (C) and horizontal lines for chABC-injected negative control retinas (D). Error bars indicate SEM. \* Figure 5.10. The dendritic field areas were compared among the groups. White bars indicate mean values for control retinas, black for glaucoma, grey for chABC-injected glaucomatous retinas (A), diagonal stripes for BDNF-injected glaucomatous retinas (B), grid for chABC+BDNF-injected glaucomatous retinas (C) and horizontal lines for chABC-injected negative control retinas (D). Error bars indicate SEM. \* p<0.05, Figure 5.11. Rat retinal sections from a control adult rat eye injected intravitreally with chondroitinase ABC. Section incubated with a mixture of antibodies specific for chondroitin-0-sulphate (1B5), chondroitin-4-sulphate (2B6) and chondroitin-6sulphate (3B3) demonstrated immunostaining throughout the retina that was detectable 24 hours following the intravitreal injection of chABC into the rat eye (A). Section digested with chondroitinase ABC directly on the slide prior to incubation

with the antibodies 1B5, 2B6 and 3B3 showed a strong immunostaining throughout
the retina that was the strongest in the photoreceptor layer (B). Section incubated
without primary antibodies did not show immunostaining (C). Scale, 100 µm 142
Figure 6.1. Diagrammatic representation of the structural epitopes and catabolic
neoepitopes on aggrecan (native and deglycosylated) and link protein (copied from
Haye et al., 2008)
Figure 6.2. Western blot analysis of GAGs from old, young (3 weeks old) and old
glaucomatous rat retinas. 6B4 recognises aggrecan and aggrecan metabolites. Bands
from old normal retinas were stained more intensely than those from old
glaucomatous eyes. The weakest staining intensity was present in a track with bands
from young retinas. Molecular weight standards are shown on the left hand side of the
gel. Non-specific bands, 50 and 25 kDa, are marked by red oval lines165
Figure 6.3. Western blot analysis of GAGs from old, young (3 weeks old), and old
glaucomatous rat retinas. 2B6 recognises chondroitinase-generated chondroitin-4-
sulphate (C4S). Molecular weight standards are shown on the left hand side of the gel.
Non-specific bands, 50 and 25 kDa, are marked by red oval lines166
Figure 6.4. Rat retinal sections from 8 weeks old, old normal and old glaucomatous
eyes (both over 6 months old) were incubated with antibodies specific for
chondroitin-0-sulphate (1B5), chondroitin-4-sulphate (2B6), chondroitin-6-sulphate
(3B3) and aggrecan core protein IgD domain (6B4). The (+) notation indicates that
the sections were predigested with chondroitinase ABC to expose the stub epitopes
prior to incubation with 1B5, 2B6 and 3B3 antibodies
Figure 6.5. Rat retinal sections from 8 weeks old, old normal and old glaucomatous
eyes (both over 6 months old) were incubated were incubated with antibodies specific
for (7D1), (BC-4), (BC-13) and no primary antibodies (No 1°)

## List of Tables

Table 2.1. Media used during optimisation of retinal dissection protocol	34
Table 2.2. Media used during retinal culture.	35
Table 4.1. Parameters for calibration of Tonolab rebound tonometer in cannu	ulated rat
eyes. a Distance from tonometer probe to cornea	95
Table 4.2. The left column shows the number of days post injection and	the right
column shows the number of rats that had IOPs measured during these d	lays. The
values in the table are related to Figure 4.3.	99
Table 4.3. Cell density, mean number of cells counted per field and cell lo	oss in the
RGCL for control and glaucomatous retinas. Cell densities and cell co	ounts are
expressed as means (cells per mm <sup>2</sup> $\pm$ SEM and cells $\pm$ SEM, respectively). C	ell loss is
expressed as a percentage relative to the contralateral (control) retina $\pm$ SEM.	108
Table 5.1. Summary of the total dendritic length, the number of branching p	oints and
the dendritic fields were estimated and compared among the groups. S	Statistical
analyses were performed using Mann-Whitney Test in SPSS 16.0 to d	letermine
significant differences between the groups	145

**Chapter 1: Introduction** 

#### 1.1. Glaucoma

#### 1.1.1. Background

Glaucoma is a gradually progressive neuropathy that involves excavation of the optic disc and loss of retinal ganglion cells (RGCs) (Pease et al., 2000), leading to visual impairment and blindness. The disease is a leading clinical problem worldwide, being the second most common cause of blindness (Quigley, 1996; Thylefors et al., 1995). According to the World Health Organization (WHO), about 37 million people worldwide in 2002 were blind, with more than 82% of all blind people being 50 years or older (Resnikoff et al., 2004). Risk factors for glaucoma are usually associated with relatively high intraocular pressure (IOP), age and a genetic predisposition. Although lowering IOP often slows the development and the progression of the disease, it is not always possible to lower IOP to a harmless level (Libby et al., 2005). Furthermore, even lowering IOP does not always prevent the progression of the disease (AGIS-Investigators, 2000).

In the normal eye, aqueous humour is produced by the ciliary body and then flows into the posterior chamber and through the pupil into the anterior chamber. Aqueous leaves the eye through the trabecular meshwork, flowing into Schlemm's canal and into episcleral veins. The balance between aqueous production inside the eye and its drainage out of the eye determines the intraocular pressure, which normally falls within a range of 10-21mmHg. However, it can be as low as 0mmHg in hypotomy and can be over 70mmHg in severe glaucoma. A pressure of 20-30mmHg generally leads to progressive damage over many years, while a pressure of 40-50mmHg contributes to a rapid loss of vision (Khaw et al., 2004a).

#### 1.1.2. Forms of glaucoma

The clinical forms of glaucoma have been classified as primary and secondary glaucomas. In primary glaucomas, the initiating event begins in the anterior chamber angle or conventional outflow pathway, without an apparent impact from other disorders. These types of glaucoma are bilateral and usually have a genetic basis (Ritch et al., 1989). The secondary glaucomas occur as an effect of a recognised

predisposing condition. These conditions can be unilateral or bilateral, acquired or with a genetic basis (Ritch et al., 1989).

The primary glaucomas include primary open-angle glaucoma, primary-angle closure glaucoma, and primary congenital glaucoma. In primary open-angle glaucoma, there is an increased resistance to aqueous humour outflow in the trabecular meshwork or Schlemm's canal (Ritch et al., 1989). Primary-angle closure glaucoma is characterised by apposition of the lens to the back of the iris which prevents the flow of aqueous from the posterior chamber to the anterior chamber (Khaw et al., 2004a). Primary congenital glaucoma is caused by incomplete development of the anterior chamber angle (Ritch et al., 1989).

The aetiologic classification of secondary glaucoma is based on the underlying factors that cause the elevated intraocular pressure. According to this classification, secondary glaucomas can be divided into conditions associated with: developmental disorders, ocular disease, systemic diseases and drugs, inflammation and trauma, and ocular surgery (Ritch et al., 1989).

#### 1.1.3. Diagnostic aspects

The basic diagnostic evaluation of glaucoma consists of intraocular pressure measurement (tonometry) as well as morphological and functional studies of the eye. The main pathological findings in glaucoma are neuroretinal rim loss (which reflects loss of retinal ganglion cells), increased excavation of the papilla, nasal displacement of the vessels of the papilla, sharp bending of the vessels, and haemorrhages at the periphery of the papilla (Dietlein et al., 2009).

#### 1.1.4. Research approaches to treatment

Current treatment for glaucoma is focussed on the reduction of IOP, which has been shown to be effective in preventing disease progression in ocular hypertension, primary open angle glaucoma and normal tension glaucoma. Glaucoma can be treated using pharmacological, laser and surgical intervention (Khaw et al., 2004b). Although there are treatments for lowering IOP, a lot of damage can occur before a patient

presents and, in some cases, damage can be so extensive that the patients' ability to carry out everyday activities are compromised. To date, treatments can only arrest glaucoma, although some groups are investigating ways to repair the damage. Present research in glaucoma management is focussed on three approaches: the development of new strategies to lower IOP, the administration of agents that can rescue damaged RGCs (neuroprotection) and optic nerve regeneration (Dahlmann-Noor et al., 2010).

Neuroprotection has been defined as treating disease by preventing neuronal death or deterioration (Levin 1999). With reference to glaucoma, neuroprotection is an intervention aimed at preventing the optic nerve damage and RGC death. This can be achieved by affecting cellular factors derived from the optic nerve itself or by eliminating extracellular risk factors (for instance, reducing IOP). However, the effectiveness of neuroprotective agents in the treatment of glaucoma has not been demonstrated (Sena et al., 2010). Recent clinical trials examining the safety and efficacy of oral memantine (Allergan) for glaucoma treatment did not show any significant benefit when compared to placebo-treated patients (Bessero, 2010).

Stem cell transplantation is currently being investigated as a potential therapeutic approach. An adult retinal explant organotypic tissue culture system has been studied as an *in vitro* intraocular stem cell transplantation model (Johnson and Martin, 2008). The transplantation of oligodendrocyte precursor cells and mesenchymal stem cells was shown to have a neuroprotective effect in a rat glaucoma model (Bull et al., 2009; Johnson et al., 2010). Apart from stem cell treatments that aim at prolonging RGC survival by providing neurotrophic factors, some stem and precursor cell studies investigate whether transplanted cells differentiate into RGC-like phenotypes, raising the possibility of improving vision. Similarly to stem cells, a spontaneously immortalised Müller cell line can migrate and differentiate into various retinal cell types (Lawrence et al., 2007; Limb et al., 2002). The migration of Müller cells into the RGC layer, following their transplantation into glaucomatous eyes, was promoted by modulating extracellular matrix with chondroitinase ABC and by controlling microglial reactivity with anti-inflammatory therapy (Bull et al., 2008; Singhal et al., 2008).

Another potential treatment approach is endogenous expression of neurotrophic factors. Transfection of growth factor genes into RGCs using viral vectors leads to a sustained increase in the endogenous expression of neurotrophic factors. Adenoassociated virus mediated expression of brain-derived neurotrophic factor (BDNF) (Martin et al., 2003) and ciliary neurotrophic factor (CNTF) (Leaver et al., 2006; Pease et al., 2009) demonstrated a protective effect of neurotrophic factor gene therapy in a model of glaucoma. Intravitreal injection of BDNF and glial cell line-derived neurotrophic factor (GDNF), followed by electroporation, also enhanced survival of RGCs (Ishikawa et al., 2005; Mo et al., 2002).

Direct injection of neurotrophic factors, such as BDNF, CNTF, NT-4, fibroblast growth factor (FGF-2) and neurturin, into the vitreous or optic nerve lesion sites prolonged RGC survival *in vivo*, and their exogenous application prolonged RGC survival *in vitro* (Parrilla-Reverter et al., 2009). Neuroprotectants, including nipradilol and T-588, were also effective against RGC damage in a glaucoma model (Karim et al., 2009; Maeda et al., 2004).

In addition to enhancing RGC survival, several growth factors have also been shown to promote axonal regrowth. Intravitreal injections of CNTF *in vivo* stimulated axonal regeneration (Cui and Harvey, 2000). Intravitreal injections of AAV to deliver FGF-2 to RGCs enhanced axonal regrowth after axotomy (Sapieha et al., 2003). Neural-tube-derived embryonic stem cells from chicken supported regeneration of RGC axons within the rat optic nerve, involving astrocytic expression of the matrix metalloproteases (MMP)-2 and -14, digestion of chondroitin sulphate proteoglycans and secretion of trophic factors (Charalambous et al., 2008).

#### 1.1.5. Current treatments

#### 1.1.5.1. Effect of IOP reduction

The Early Manifest Glaucoma Trial (Leske et al., 2003), Ocular Hypertension Treatment Study (Kass et al., 2002) and Advanced Glaucoma Intervention Study (AGIS-Investigators, 2000) imply that there is a positive association between IOP level and the severity of glaucomatous injury. Moreover, they support the therapeutic

efficacy of lowering IOP in reducing the rate of progression of glaucomatous field loss (AGIS-Investigators, 2000; Collaborative Normal-Tension Glaucoma Study, 1998; Gordon et al., 2002; Kass et al., 2002; Leske et al., 2003; Nouri-Mahdavi et al., 2004). Nevertheless, lowering of IOP by either surgery or drug therapy might not thoroughly prevent progression of visual field loss in all patients, which can even progress more rapidly in those with greater initial injury (Harbin et al., 1976; Leske et al., 2003; Schwartz et al., 2004).

#### 1.1.5.2. Pharmacotherapy

There are two approaches to the medical reduction of intraocular pressure. The first approach is a reduction of the production of aqueous humor using beta-blockers (inhibition of the beta-mediated stimulation of Na+/K+-ATPase), carbonic anhydrase inhibitors or sympathomimetic drugs (activation of the alpha-mediated inhibition of Na+/K+-ATPase). Another method to reduce IOP is by increasing the outflow of aqueous humor with cholinergic/parasympathomimetic drugs and prostaglandin derivatives (trabecular meshwork), sympathomimetic drugs (uveoscleral outflow) or prostaglandin derivatives (uveoscleral outflow). According to the European Glaucoma Society (EGS) guidelines, prostaglandin analogs, beta-blockers, alpha-2 agonists, and topical carbonic anhydrase inhibitors are the recommended drugs (Dietlein et al., 2009). Topical prostaglandin analogs (PGA) are among the more effective medications for lowering intraocular pressure, with reductions of 33% (van der Valk et al., 2005) and a 15% to 20% failure rate (Hedman et al., 2002).

Many types of treatment for glaucoma that do not lower the intraocular pressure are being investigated for prospective use mostly in patients with normal-pressure glaucoma. However, there is not sufficient evidence to support their use (Sycha et al., 2003). Potential treatments include calcium antagonists (nimodipine, nifedipine) administered in low doses to patients with vasospastic manifestations (Tomita et al., 1999) and mineralocorticosteroids (fludrocortisone) given in low doses to patients with marked arterial hypotension (Gugleta et al., 1999).

#### 1.1.5.3. Surgery and laser techniques

Indications for surgical intervention include a progression of optic neuropathy or visual field defects in a patient with chronic open-angle glaucoma despite the administration of two or three topical treatments (Burr et al., 2005). A surgery might also be recommended if local therapy is required immediately but is not tolerated due to systemic or local side effects, or if the regular use of eye drops is not possible. Surgical procedures for glaucoma include trabeculectomy, goniotomy, implant surgery and iridectomy (Dietlein et al., 2009).

The purpose of cyclophotocoagulation is to decrease the inflow of aqueous humor by destroying the non-pigmented epithelial cells of the ciliary body that produce it. The ciliary body is coagulated with a laser, either from inside the eye, under endoscopic visualisation, or through the sclera without opening the globe (Dietlein et al., 2009). There are conflicting opinions about the value of this treatment among surgical ophthalmologists (Becker and Funk, 2001; Krott et al., 1997).

#### 1.1.6. Mechanisms of RGC death in glaucoma

Previous evidence identifies apoptosis as a potential final pathway of RGC death in glaucoma (Kerrigan et al., 1997; Quigley, 1999; Quigley et al., 1995) and indicates that both pro- and anti-apoptotic (pro-survival) pathways are activated in experimental glaucoma (Levkovitch-Verbin et al., 2007). Apoptosis is a programmed cell death, characterised by chromatin condensation, cellular shrinkage, blebbing of the plasma membrane, DNA fragmentation, and ultimately intracellular fragmentation associated with the formation of apoptotic bodies (Kerr et al., 1972; Wyllie et al., 1984). Finally, cells undergo phagocytosis without inflammation, mediated by macrophages or surrounding tissue (Quigley et al., 1995). A number of mechanisms have been suggested to initiate RGC apoptosis in glaucoma, including neurotrophic factor deprivation, hypoperfusion, glial cell activation, glutamate excitoxicity and an abnormal immune response (Kuehn et al., 2005).

#### 1.1.6.1. Neurotrophic factor deprivation

Since axonal transport is essential to the normal functioning of neurons, retrograde transport of neurotrophins produced in the target organ may be necessary for RGC survival (Kuehn et al., 2005). According to the present hypothesis, the retrograde delivery of neurotrophic substances to RGCs is inhibited by pressure-induced axonal transport obstruction at the optic nerve head, resulting in apoptosis (Johnson et al., 2000). However, it has been shown that neurotrophic factors such as BDNF can also be produced by RGCs, and their local intraretinal release influences the survival of RGCs in the rat (Spalding et al., 2005; von Bartheld et al., 1996; Wang et al., 2002). Neurotrophins involved in developmental apoptosis include: BDNF, nerve growth factor (NGF), neurotrophin-3, neurotrophin-4/5, neurotrophin-6 and neurotrophin-7. These neurotrophic factors can bind to two transmembrane receptor families, which may directly interact with each other. These include the Trk receptors within the tyrosine kinase family and the extracellular domain of the p75 neurotrophin receptor (Guerin et al., 2006).

A number of studies support the idea that neurotrophic deprivation is a cause of RGC death. BDNF delivery into the retina is significantly reduced in animal models of glaucoma (Kuehn et al., 2005; Pease et al., 2000; Quigley et al., 2000), while administration of BDNF into the rat eye with experimentally elevated IOP has been found to increase the number of rescued RGCs (Ko et al., 2001; Kuehn et al., 2005). In addition, the injection of ciliary neurotrophic factor (CNTF) in axotomised adult rat optic nerves caused partial survival of RGCs (Ji et al., 2004; van Adel et al., 2003).

#### 1.1.6.2. Hypoperfusion

Two theories explaining glaucomatous optic neuropathy (GON) have been described: the mechanical and the vascular (Fechtner and Weinreb, 1994). The mechanical theory suggests that GON is a direct consequence of elevated IOP, causing damage to the lamina cribrosa and neural axons (Yan et al., 1994). According to the vascular theory of glaucoma, GON is caused by an insufficient blood supply to the optic nerve head due to vascular risk factors reducing ocular blood flow (OBL), including elevated IOP (Flammer et al., 2002). Since blood flow to the anterior optic nerve

depends on perfusion pressure, increased IOP might obstruct the vascular supply to the optic nerve by contributing to elevated pressure in the optic nerve. Optic nerve ischaemia might also occur due to insufficient autoregulation of blood flow within the optic nerve in glaucoma (Flammer et al., 2002).

#### 1.1.6.3. Glial cell activation

Another important factor contributing to RGC death in glaucoma is activation of glial cells. There are three types of glial cells in the mammalian retina including astrocytes, microglia and Müller cells (Kuehn et al., 2005). Retinal glial cells become activated in glaucoma, leading to the increased retinal expression of glial fibrillar acidic protein, an early event in the pathogenesis of glaucoma (Elizabeth et al., 2004; Wang et al., 2000; Woldemussie et al., 2004). Since glial cells support neuronal functions, it is suggested that RGC death caused by the activation of glial cells might occur due to the reduced levels of glial support. Nevertheless, it might be possible that the activation of glial cells leads to the release of substances detrimental to RGCs, including cytokines, reactive oxygen species or nitric oxide (Tezel and Wax, 2000). It has been shown that mixed retinal glia cultures exposed to increased hydrostatic pressure release tumour necrosis factor alpha (TNF-α) (Tezel and Wax, 2000), an inducer of apoptotic cell death through TNF- $\alpha$  receptor-1 (p55) occupancy in a caspase-mediated pathway (Tezel et al., 2001; Tezel and Wax, 2000). According to the results obtained from immunohistochemical studies, TNF-α is produced by retinal glia in glaucoma and its receptor is present on RGCs (Tezel et al., 2001).

Apoptosis mediated by glial cells could also be caused by the enhanced synthesis of nitric oxide which affects synaptic plasticity, neurotransmitter release and regulation of vascular tone. Increased amounts of nitric oxide can cause cell death in RGCs and other various cell types (Dawson and Dawson, 1996; Morgan et al., 1999). In a rat model of experimentally induced glaucoma, excessive levels of the enzymes responsible for the production of nitric oxide have been observed in the optic nerve head (Shareef et al., 1999). RGC damage seemed to be reduced by the inhibited synthesis of nitric oxide in this model (Neufeld et al., 1999). However, in a different rat model, induced by hypertonic saline injection into the episcleral veins, inhibition of these enzymes did not protect RGCs (Morrison et al., 2005; Pang et al., 2005).

There is evidence from immunohistochemical studies that elevated levels of nitric oxide synthase are present in the human glaucomatous nerve head (Neufeld et al., 1997).

#### 1.1.6.4. Glutamate toxicity

Glutamate is a main excitatory neurotransmitter in the retina, produced by presynaptic cells. The release of large amounts of glutamate leads to neuronal death in the process of excitotoxicity (Caprioli et al., 1996). Although increased glutamate levels have been observed in human patients suffering from glaucoma as well as in a primate model of glaucoma (Dreyer, 1998), it has not been confirmed by some other studies (Honkanen et al., 2003; Wamsley et al., 2005). Therefore, the role of glutamate toxicity in glaucoma remains uncertain. Recent studies have demonstrated resistance of RGCs to glutamate toxicity in the presence of neurotrophic factors (Ullian et al., 2004), in contrast to the sensitivity of retinal amacrine cells to increased glutamate levels. It was suggested that the reduced numbers of RGCs followed by the glutamate administration might have been caused by a loss of amacrine cells and a lack of neurotrophic support for RGCs (Kuehn et al., 2005).

#### 1.1.6.5. Abnormal immune response

A number of studies have suggested a role for humoral immune response in the pathogenesis of glaucoma (Schori et al., 2001; Wax, 2000). Autoantibodies directed against retinal antigens as well as optic nerve head proteoglycans have been observed in the sera of glaucoma patients (Tezel et al., 1999). Since one of the functions of proteoglycans is the creation of a spatial network for the support of the optic nerve and blood vessels, an immune response to proteoglycans might weaken the extracellular matrix supporting the lamina cribrosa, inducing or enhancing cupping of optic nerve head (Kuehn et al., 2005).

There are also reports that immunisation with copolymer-1 (COP-1) enhanced activity of T lymphocytes, which had neuroprotective effects on RGCs in animals subjected to optic nerve injury, glutamate excitotoxicity, and chronically elevated IOP (Kipnis et al., 2000; Schori et al., 2001; Schori et al., 2002). COP-1, a synthetic amino acid

polymer, was shown to suppress autoimmune encephalomyelitis (EAE) induced by myelin basic protein (MBP) (Teitelbaum et al., 1971). Although the precise mechanism of neuroprotection induced by T cells is unknown, it has been suggested that an immune response to the degeneration of the optic nerve leads to the secondary degeneration of additional RGCs. However, the survival of surrounding cells could be caused by the presence of neurotrophins at the site of injury. Neurotrophic factors such as nerve growth factor, BDNF, neurotrophins 3, 4, and 5, are released by T cells accumulated at the site of injury and presented with specific antigen (Schwartz and Budenz, 2004). In addition, T cells activated by the use of low-dosage γ-irradiation were found to have neuroprotective effects after glutamate excitotoxicity or optic nerve injury (Kipnis et al., 2004). Ultimately neuroprotection, caused possibly by the T cell-mediated immune response was observed after bone marrow transplantation and high-dose irradiation in a mouse model of hereditary pigmentary glaucoma (Anderson et al., 2005).

#### 1.1.7. Morphology and function of RGCs

Several types of RGCs have been identified based on soma size and the architecture of the dendritic field in the primate retina: midget, parasol, small bistratified and wide-field cells (Dacey, 1993; Dacey and Petersen, 1992; Kolb et al., 1992; Perry and Cowey, 1981; Rodieck et al., 1985; Watanabe and Rodieck, 1989; Weber et al., 1998; Yamada et al., 2005).

Midget cells represent approximately 80% of the total population of ganglion cells in the primate retina. They are characterised by medium-sized somas and small- or medium-sized dendritic trees that are frequently formed from a single dendrite, which then forms a solid, bushy dendritic arbour (Figure 1.1A). Midget cells project to the four dorsal, parvocellular layers of the lateral geniculate nucleus (LGN) (Dacey, 1993; Watanabe and Rodieck, 1989; Rodieck et al., 1985; Dacey & Petersen, 1992; Weber et al., 1998).

Parasol cells represent approximately 10% of the ganglion cells in the primate retina, with the largest somas and dendritic fields in the ganglion cell layer (Figure 1.1B).

Their dendritic trees are frequently comprised of three or four thick primary dendrites forming an extremely symmetrical arbour. The axons of these neurons are generally larger compared to the axons of midget cells and project to the two ventral magnocellular layers of the LGN. In contrast to midget cells, parasol cells are characterised by large receptive fields with rapidly conducting axons, and they are most responsive to achromatic stimuli of high temporal and low spatial frequency (Rodieck et al., 1985; Dacey & Petersen, 1992; Weber et al., 1998).

Bistratified cells, similarly to midget cells, project to the parvocellular geniculate layers (Dacey, 1994) (Figure 1.2.A). Wide-field cells, heterogeneous cells with large dendritic arbours (Peterson and Dacey, 2000) (Figure 1.2B), project to the lateral geniculate nucleus, the superior colliculus, or the pretectum (Dacey et al., 2003).

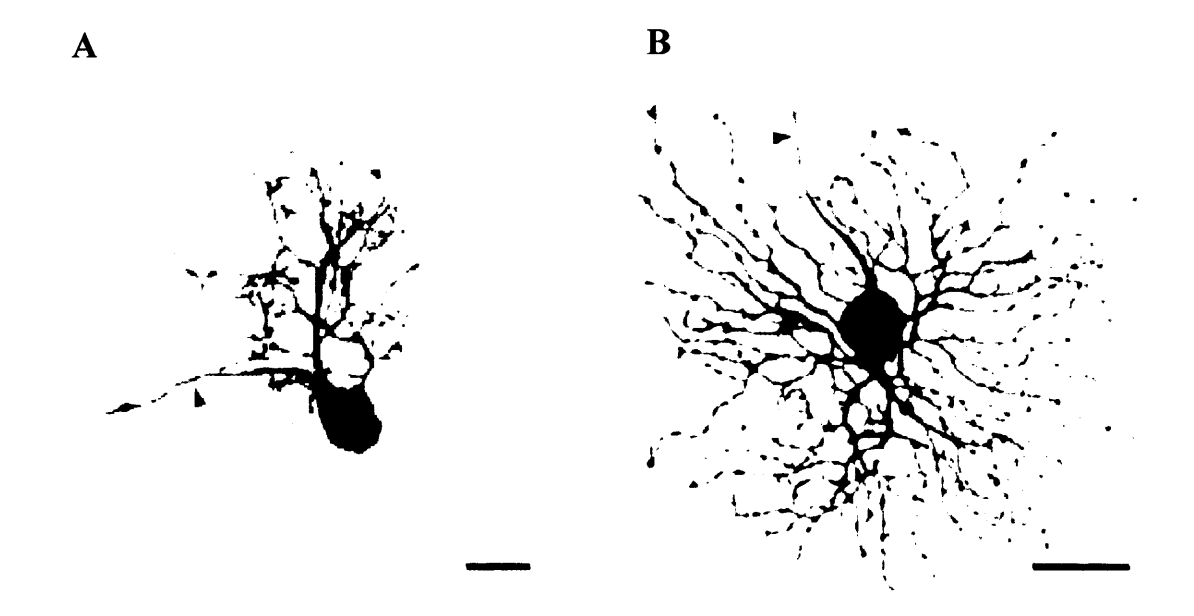
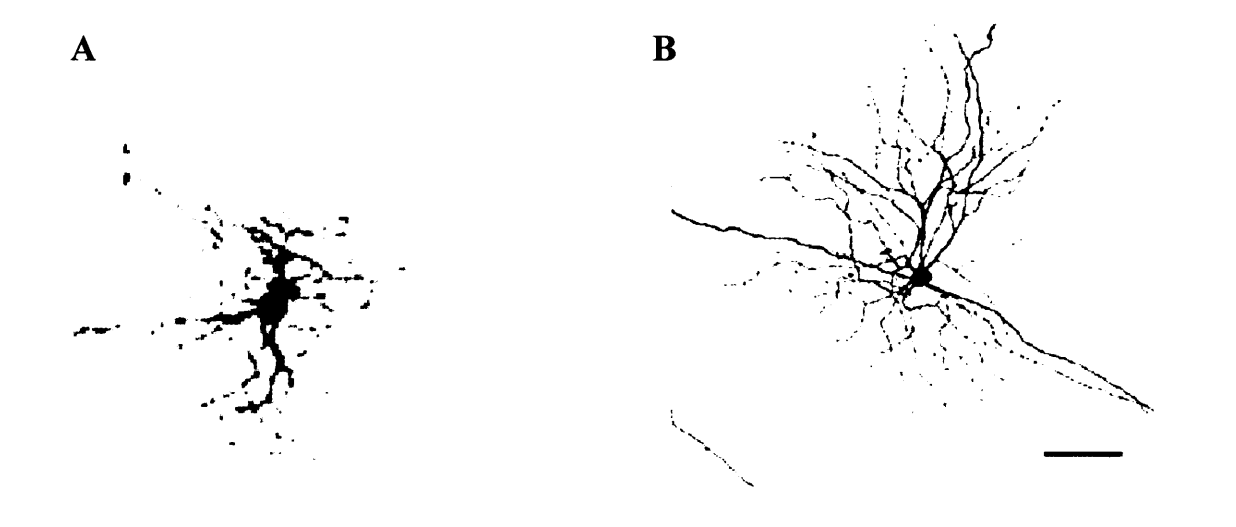


Figure 1.1. Confocal image showing the morphologic features (small soma and dendritic arbour) that characterize the normal midget cell, with *arrowhead* indicating intraretinal axon segment (A). Morphologic features that characterize the soma, dendritic field, and intraretinal axon segment (*arrowhead*) of a parasol cell in the normal retina (B). Scale bar:  $10 \mu m$  (A),  $25 \mu m$  (B) (Weber et al., 1998).



**Figure 1.2.** Small bistratified cell (A). Wide field ganglion cell, classified as diffuse because their dendrites branch throughout the inner plexiform layer (IPL) (B). Scale bar: 100 μm (Yamada et al., 2004).

#### 1.1.7.1. Morphology and function of RGC in glaucoma

Weber et al. (1998) have observed that the earliest structural signs of glaucomatous neuropathy in RGCs, induced by the elevated IOP, involved changes at the level of the dendritic arbour, including a thinning of the proximal and distal dendrites, sudden reductions in dendritic process diameter at branch points, and reduced complexity of the cell's dendritic tree (Figure 1.3). The changes at the level of the dendritic arbour preceded the reduction in axon diameter, while soma size was reduced simultaneously or later. These data clearly indicate a progressive process of RGC degeneration in glaucoma (Weber et al., 1998).

Some studies examining changes in axon diameter (Quigley et al., 1988), soma size (Glovinsky et al., 1991; Glovinsky et al., 1993) and neurofilament content (Vickers et al., 1995) in ganglion cells from glaucomatous eyes suggested that the most detrimental changes occur in large ganglion cells compared to other cell types. Data demonstrating the differential effects of chronically elevated IOP on neurons in the magnocellular and parvocellular layers of the LGN suggest that these large cells could be primarily parasol cells (Chaturvedi et al., 1993). This supports the hypothesis that the P- and M-pathways of the primate visual system are affected differentially by the disease, which might significantly contribute to the development of more sensitive psychophysical tests for the early detection of glaucoma (Ruiz-Ederra and Verkman, 2006). However, Weber et al. (1998) observed only subtle differences in the patterns and degrees of degenerative changes between midget and parasol cells in response to chronic elevation in IOP.

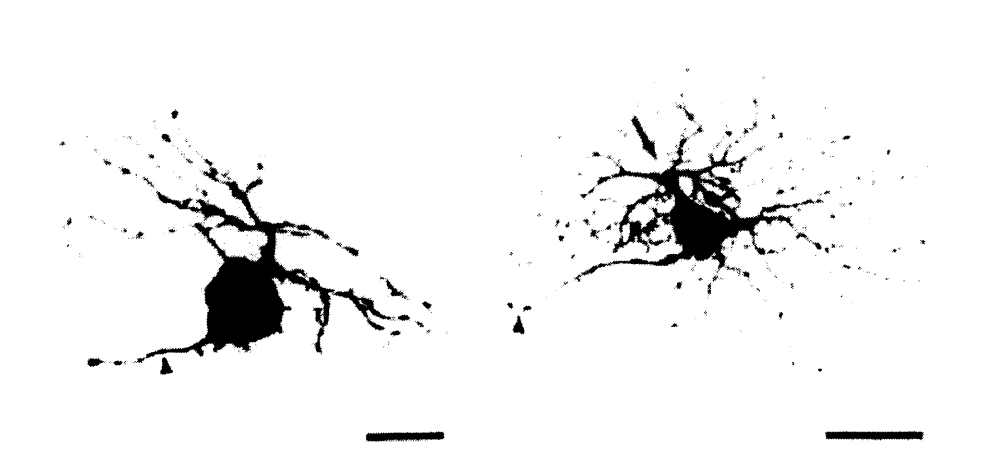


Figure 1.3. Confocal image showing the morphologic features that characterize midget cell (A) and parasol cell (B) from glaucomatous eyes. Although the soma size of the midget cell (A) is comparable to the soma size of the normal midget cell in Figure 1.2, its dendritic arbour is reduced and its axon is very thin compared with that of other midget cells of similar soma size. Arrowhead indicates intraretinal axon segment, while arrow indicates dendritic abnormalities. Scale bar,  $10 \mu m$  (A) and  $25 \mu m$  (B) (Weber et al., 1998).

#### 1.1.8. Models of experimental glaucoma

Our understanding of how the retina and optic nerve head respond in human glaucoma has been limited by the lack of non-invasive methods for assessing cellular responses in humans. Therefore, cellular function has to be investigated using appropriate animal models. Most commonly used animal models of glaucoma are created by experimentally induced elevation of IOP, the only risk factor against which all glaucoma therapy is currently focussed. However, visual field progression occurs in some patients despite a clinically acceptable decline in IOP (Morrison et al., 2005). Although these models can be regarded as models of pressure-induced optic nerve damage rather than glaucoma models, it might be anticipated that knowledge of the mechanisms by which enhanced IOP causes optic nerve damage will be useful for understanding optic nerve damage in human glaucoma. This knowledge might then be applied to develop and examine specific therapies to preserve vision in glaucoma patients (Morrison et al., 2005).

There are two types of chronically elevated IOP models, spontaneous and experimentally induced (Morrison et al., 2005). Naturally occurring models do not require experimental manipulations that might induce responses that could be wrongly recognised as responses to pressure (Morrison et al., 2005). Another benefit is that the onset of IOP occurs and builds up slowly. However, since the pressure elevation is usually bilateral in these models (Libby et al., 2005) they lack the built-in control of a normotensive contralateral eye. Moreover, it might be difficult to predict the time of pressure elevation, thus not allowing for the determination of early events in the damage process. In contrast to spontaneous models, experimental models provide the fellow eye as a control due to the unilateral elevation of IOP. Also, the timing of the IOP increase is usually straightforward to predict after the experimental manipulation, which enables determination of the sequence of events of retina and optic nerve damage as a result of increased IOP (Morrison et al., 2005).

There are three important issues that have to be considered with animal models of experimentally pressure-induced optic nerve damage. Firstly, developing techniques for measuring IOP should accurately reflect the level of pressure to which the optic nerve head and retina are exposed. Secondly, optic nerve damage is usually determined histologically and electrophysiologically and, in the case of non-human primates, by psychophysical methods. Finally, the best way to achieve a chronic increase in IOP is to obstruct aqueous humour outflow (Morrison et al., 2005).

#### 1.1.8.1. Mouse model of glaucoma

Chronically elevated IOP in the mouse eye that contributes to the damage or loss of RGC and optic nerve axons can be induced either experimentally (Aihara et al., 2003; Grozdanic et al., 2003; Mabuchi et al., 2003; Ruiz-Ederra and Verkman, 2006) or can occur spontaneously in certain strains (Sheldon et al., 1995).

Various mouse models with genetic changes relevant to glaucoma have been studied, including models with dysgenesis of the anterior segment, those lacking specific receptors and those with targeted mutations of signalling or structural proteins (Lindsey and Weinreb, 2005).

Although experimental rat models of elevated IOP are extremely valuable in understanding the mechanisms that occur in glaucoma, IOP is increased rapidly to detrimental levels and RGC usually die faster than in natural or inherited glaucoma (Libby et al., 2005). Therefore, inherited mouse glaucoma models have been developed with spontaneously occurring secondary glaucoma and sequential RGC damage. These include the DBA/2NNia, DBA/2J and AKXD-28/Ty inbred mouse strains (Anderson et al., 2008; Anderson et al., 2001; John et al., 1998; Sheldon et al., 1995). One of these models, DBA/2J, is characterised by an increase in IOP starting at approximately 6 months of age and the presence of peripheral anterior synechiae, iris atrophy, and pigment dispersion. Changes in the iris and the anterior chamber angle cause aqueous outflow obstruction and induce secondary glaucoma in this model (John et al., 1998). However, there might be differences in the mechanism of neural damage compared to clinical glaucoma since the mouse lacks a lamina cribrosa (May and Lutjen-Drecoll, 2002).

IOP can be measured in mouse using various methods, including insertion of a glass-tipped micropipette into the anterior chamber that is connected to a pressure transducer (Aihara et al., 2002; John et al., 1997), the servo-null method (Avila et al., 2001), Goldmann tonometer (Cohan and Bohr, 2001), rebound tonometer (Danias et al., 2003), TonoPen (Reitsamer et al., 2004) and modified Schiotz indentation tonometer (Gross et al., 2003). Due to the small size of the mouse eye, reliable measurements can be difficult to obtain. Additionally, eye displacement or transient pressure changes related to one method might not allow for obtaining valuable measurements using another method. Thus, validation of the results might be difficult to obtain. Another drawback of inherited glaucoma models is that they are more expensive and time-consuming to study than experimentally induced models (Libby et al., 2005).

#### 1.1.8.2. Non-human primate model of IOP-induced optic nerve damage

The most commonly used models at present are non-human primates and rodents. Because of the close anatomic similarities between the structure of human and non-human primate optic nerve, the best-established models of pressure-induced optic nerve damage have been developed in non-human primates. The primate optic nerve, as in the human, is composed of a nerve fiber layer as well as prelaminar, laminar, and retrolaminar regions (Anderson, 1969; Anderson, 1970).

The methods used for inducing elevated IOP in primates include laser photocoagulation of the trabecular meshwork (Gaasterland et al., 1978) and injection of various particles into the anterior chamber, including ghost red blood cells (Quigley and Addicks, 1980) as well as latex microspheres (Weber and Zelenak, 2001). In non-human primates, IOP can be measured using a modified Goldmann tonometer (Kaufman and Davis, 1980), TonoPen tonometer (Peterson et al., 1996) or pneumatonometer (Toris et al., 2000). Most frequently, IOP measurements are performed with the use of a general anaesthetic, which was reported to be the least likely to artifactually lower IOP (Erickson-Lamy et al., 1984). Nevertheless, due to the cumulative harmful effects which anaesthetics might have on the primates and their physiology, topical anaesthesia has been recently utilised, enabling accurate measurement of the IOP in the awake animal (Toris et al., 2003). Compared with applying general anaesthetics, this approach allows for more straightforward detection of subtle changes in IOP and more reproducible measurements of IOP response (Morrison et al., 2005).

Optic nerve and retinal damage in the monkey are assessed histologically. Axon loss can also be assessed by analysing the nerve fiber layer in the retina using fundus photography (Quigley, 1986). Additionally, this method allows clinical evidence of optic nerve head cupping to be obtained. Cupping can be also identified with the use of laser scanning ophthalmoscopy (Burgoyne et al., 2002).

One of the drawbacks of using primates is associated with difficulties in inducing a moderate increase of IOP that mimics the IOP observed in human open angle glaucoma. The interpretation of the consequential optic nerve damage can be complicated by the obstructed retinal blood flow in the case of a high elevation of pressure. However, this can be overcome by administration of topical pressure-lowering agents (Pena et al., 2001). Another drawback of using the monkey is related to obtaining accurate measurements of IOP in awake animals which must be trained for this purpose (Toris et al., 2003). Problems caused by general anaesthetics have

already been mentioned (Morrison et al., 2005). Additionally, monkeys are expensive to purchase and to maintain and can be potentially risky for the health of animal care workers. Owing to the cost of these animals, it might be difficult to provide the large numbers of monkeys necessary for experiments aimed at studying cellular functions in the optic nerve head and retina in relation to IOP (Morrison et al., 2005).

## 1.1.8.3. Rat model of IOP-induced optic nerve damage

Due to the several disadvantages of using non-human primate models, there is a need for a more cost-effective, easier to handle model of pressure-induced optic nerve damage. A suitable model should enable identification of the cellular mechanisms of optic nerve damage and the development of potential treatments for glaucoma (Morrison, 2005). Experimental rat models are relatively inexpensive to purchase and maintain, allowing for a large number of animals to be used per experiment and therefore for obtaining more valid results (Morrison et al., 1995). They are also easy to handle, enabling frequent measuring of IOP in the awake state. In addition, the biology of a rat's central nervous system and optic nerve damage are well described, allowing for straightforward assessment of changes caused by the variations in IOP. Eventually, the data obtained from the work with a rat model can be further investigated in more focussed experiments in primate models, linking basic studies and human glaucoma (Morrison 1995).

There are several anatomic similarities and differences between the rat and primate optic nerve. In both species, axons in the optic nerve head are unmyelinated, though myelination in primates commences at the posterior sclera, while in rats roughly 0.5mm posterior to the sclera (Morrison et al., 1995). The rat's lamina cribrosa is less developed than in the primate, with single collagen bundles forming a lamina-cribrosa like structure (Albrecht May, 2008). Due to the thinner sclera in the rat compared with the primate, it is likely that the chronic elevation of IOP resulting from experimental aqueous humour outflow obstruction has more impact on the rat's optic nerve than the primate nerve (Morrison et al., 1995). Finally, because of a similar close ultrastructural relationship between optic nerve head astrocytes and axons in rats and primates, rat models are considered to be very relevant for evaluating cellular mechanisms of axonal injury from increased IOP (Morrison et al., 2005).

There are different methods for the induction of chronic experimental IOP increase in rats. Significant elevation of IOP, caused by enhanced resistance to aqueous humour outflow, can be induced by scarring of the eye angle. This can be performed by injection of hypertonic saline into aqueous humour outflow pathway (Morrison et al., 1997) or by laser treatment of the eye angle (Woldemussie et al., 2001). Another technique, in contrast to the methods mentioned above, generates less optic nerve and RGC damage over time. This method that provides a different mechanism of pressure elevation is cautery of episcleral veins, (Shareef et al., 1995). A more recently introduced method is the injection of various substances such as latex or polystyrene microspheres (Sappington et al., 2010; Urcola et al., 2006) into the eye anterior chamber that leads to the obstruction of trabecular meshwork channel. This method tends to be less technically challenging from the other methods that induce chronic IOP.

IOP is most commonly measured in glaucomatous rats using the TonoPen tonometer due to its ready availability, its high reliability and no requirement for special modification. Moreover, circadian fluctuations in IOP can be assessed with the TonoPen in conscious animals (Moore et al., 1996). Other instruments include the pneumatonometer (Shareef et al., 1995), modifications of the Goldmann tonometer (Cohan and Bohr, 2001) and the rebound tonometer (Goldblum and Mittag, 2002). The Goldmann tonometer can be used in anaesthetized rats, while modification of this tonometer allowed for measuring IOP in conscious, unsedated rats (Cohan and Bohr, 2001).

Pressure-induced damage can be determined by counting axons using light or electron microscopy in optic nerve cross sections which are then compared to control sections (e.g. from the other eye) (Chauhan et al., 2002; Levkovitch-Verbin et al., 2002). Another method, a qualitative damage scale (Chauhan et al., 2006), allows for easy and rapid estimation of many optic nerves. By counting cells in the retinal ganglion cell layer of the retina (Schlamp et al., 2001), or by staining cells with dye exposed to the superior colliculus or the optic nerve (Sawada and Neufeld, 1999), damage can be assessed by estimating the loss of retinal ganglion cells (Schlamp et al., 2001). Due to the lower number of axons and RGCs in the rat eye compared to the primate, these methods are easier to carry out in rats (Cepurna et al., 2005). Apart from studying

cellular and physiologic mechanisms of glaucomatous optic nerve damage, rat models can be also used to evaluate potential neuroprotective strategies (Morrison, 2005)

## **1.1.8.4.** *In vitro* systems

In vivo experimentation, though necessary, might sometimes be affected by various uncontrollable factors. Therefore, in vitro systems are often used to perform highly controlled preliminary studies. The in vitro systems used in glaucoma research include retinal explant organ culture and primary RGC culture.

## 1.1.8.4.1. Retinal explant culture

Retinal explant cultures serve as a model of glaucoma since the explanation of the retina requires the severing of all axons within the optic nerve and the consequential degeneration of RGCs. This system is particularly useful for experiments that require the presence of the whole retinal tissue but cannot be conducted *in vivo* due to limitations involving tissue access, confounding systemic factors, or control over microenvironment. Nevertheless, this *in vitro* system is not as complex as animal models and thus *in vitro* experiments must be supported by *in vivo* studies (Johnson and Tomarev, 2010).

## 1.1.8.4.2. Retinal ganglion cell culture

Retinal ganglion cell culture is useful in studying the response of RGCs to specific conditions in isolation from the rest of the eye. RGCs may be obtained by the chemical or enzymatic treatment of freshly isolated rodent retina to produce a dissociated primary culture (Otori, 2008).

The RGC-5 cell line is an immortalised cell line derived from the rat that express Thy1, Brn3C, Trk-A, and various neurotrophic factors (Agarwal et al., 2007; Krishnamoorthy et al., 2001). However, this cell line differs in many aspects from true RGCs, therefore results obtained with the cell line must be interpreted with caution (Frassetto et al., 2006). RGC-5 cells are more similar to glial cells in culture than to primary RGCs and do not express the range of electrophysiological ion channels that

are attributed to RGCs. In addition, RGC-5 cells responded to the broad-spectrum protein kinase inhibitor staurosporine in a different way than RGCs (Frassetto et al., 2006).

## 1.2. Neuroplasticity

In neuroscience, plasticity has been described as the ability of the nervous system to modify its organisation and eventually its function (Guterman, 2007; Kolb et al., 2003) or, more distinctively, as the capacity to rearrange patterns and systems of connections (Guterman, 2007; Stiles, 2000). Donald Hebb (1949) assumed that synaptic efficacy could be selectively modified by experience, while Konorski (1948) linked neural plasticity to the ability of an organism to undergo habit, extinction and conditioning formation. There are two types of plasticity: synaptic and anatomical plasticity. Synaptic plasticity is defined as activity-dependent changes in the efficacy of synaptic transmission across synapses, while anatomical plasticity (also known as structural plasticity or remodelling) is defined as the change in anatomical arrangement of neural connections with the formation of new synapses (Galtrey et al., 2007). Plasticity has an important function in the alteration of connections during development whereas, in the adult central nervous system (CNS), plasticity occurs at a lower level in response to experience, age or injury (Galtrey et al., 2007). Plasticity at the single synapse level has been shown by demonstrating the capability of synaptic transmission to change as a function of other simultaneous inputs received by the post-synaptic neuron (Kandel, 1970; Kandel and Schwartz, 1982). In addition to synaptic plasticity, neural plasticity might be linked to other mechanisms such as modulation of neuronal excitability or experience-dependent neurogenesis (Giese et al., 2001; Karten et al., 2005; Shors et al., 2001). Acknowledgment of the highly plastic nature of the CNS, and the fact that it changes constantly during life, is a fairly novel development. Until very recently, most neuroscientists considered that the nervous system modifies at particular sites only using very few mechanisms (Wolpaw and Carp, 2006). Although there is poor recovery after injury in adult mammalian CNS, partial functional recovery has been observed, suggesting the presence of at least some neuronal plasticity. However, it is still poorly understood what functional mechanisms and anatomical features are associated with CNS plasticity (Ahmed et al., 2001a). Structural reorganisation of soma, axons or dendrites as well as atrophy or

hypertrophy of somata in neurons has been observed after lesions (Eysel and Wolfhard, 1984; Steward and Vinsant, 1978). Lesion-induced dendritic plasticity has been detected in the fetal, adult and aged CNS (Buell and Coleman, 1979; Buell and Coleman, 1981). Apart from humans, plasticity has been detected in various mammals, including cats, rabbits, rats and mice (Peichl and Bolz, 1984; Rothblat and Schwartz, 1979; Valverde, 1967).

## 1.2.1. Neuroplasticity and diseases of the CNS

Imbalanced plasticity of neuronal networks in the brain involved in perceptual, cognitive, and motor behaviour might be associated with deficits in the integration of efferent and afferent processes in schizophrenia (Guterman, 2007). Injuries of the CNS, such as stroke, traumatic brain injury and spinal cord injury, can lead to devastating and permanent failure of function. At present, there are no approved medicines with the capacity to restore lost higher and sensimotor functions. Therefore, it is necessary to understand how to overcome mechanisms that inhibit regeneration as well as mechanisms that increase neuronal plasticity to design new therapeutics for the treatment of CNS injuries (Wieloch and Nikolich, 2006).

## 1.2.2. Regulators of neuroplasticity

Loss of function during stroke is caused by neuronal death in the infarcted tissue, as well as, cell dysfunction in the areas neighbouring the infarct. Three distinct, subsequent mechanisms are involved in functional recovery. This includes reversal of diaschisis and activation of cell repair, followed by functional cell plasticity involved in changing the characteristics of existing neuronal pathways, and finally neuroanatomical plasticity leading to the development of new connections. The first two phases are involved in normal learning, the powerful force throughout functional recovery (Wieloch and Nikolich, 2006). Spontaneous functional recovery after stroke can be increased by external interventions. Activators of the noradrenergic, dopaminergic and cholinergic systems stimulate functional plasticity (Floel et al., 2005; Sawaki et al., 2002; Wieloch and Nikolich, 2006), while growth factors and attenuators of axonal growth inhibition enhance neuroanatomical plasticity (Sugiura et al., 2005; Wang et al., 2004). Physical therapy increases recovery during the chronic

phase, and might be improved by adjuvant treatments (Wieloch and Nikolich, 2006; Will et al., 2004).

## 1.2.3. Neuroplasticity in the retina

During the prenatal period, when the mammalian visual nervous system selforganises, spontaneous activity is a main force driving this process (Shatz, 1996). This activity is inherent to the visual system and enhances a distribution of neurons and connections that normally does not occur in the adult visual system. However, retinal plasticity has been observed also in the adult visual nervous system. Retinal lesion leads to a reorganisation of the cortical receptive field distribution. In particular, cortical neurons selective to visual stimuli in the area of the visual field corresponding to the scotoma become selective to stimuli originating in other parts of the retina (Andrade et al., 2001).

Some studies imply an association between the lesion-induced increase in the soma size of RGCs and soma density in the visual system. Experiments conducted in the visual system of developing rats suggest that RGCs soma size is dependent on the available space in the retina and is also influenced by the target tissue. Reductions of RGC density in the retina have been observed after tectal lesions induced by vacuum aspiration or kainic acid injection and to the increase of soma size of the surviving RGCs (Bahr et al., 1992; Carpenter et al., 1986). Another study showed that RGCs were removed rapidly without affecting bipolar or amacrine cells following the transection of rat optic nerve at birth, implying that cutting the optic nerve affects only RGCs (Beazley et al., 1987). Similar changes have been detected in studies of other vertebrate species. Alterations in dendritic morphology, although smaller in older animals, were observed in RGCs lying adjacent to regions of degeneration after retinal lesions in postnatal cats (Eysel et al., 1985). Another example is the increased soma size of the remaining RGCs after a reduction in the RGC density at the area centralis after transection of the optic nerve in postnatal cats (Rapaport and Stone, 1983). Kirby and Chalupa (1986) showed crowding of RGCs in the remaining eye of the embryonic cat after enucleation. The authors concluded that the spaces left by dying cells enabled an increase in soma size and dendritic field of the remaining RGCs. Similarly, Ahmed et al. (2001a) showed an increase in soma size of RGCs and an expansion of their

dendritic fields after an increase in IOP (Figure 1.4). One explanation for the increase in dendritic trees of the surviving RGCs could be the presence of free synaptic endings of bipolar and amacrine cells which might stimulate hypertrophy of the remaining RGCs. Synaptic connections might then be formed by these cells onto these remaining cell dendrites (Ahmed et al., 2001a). In contrast to the studies showing an increase in dendritic field and soma, other investigators observed dendritic pruning and RGC soma shrinkage in rat and primate experimental glaucoma (Morgan et al., 2006).

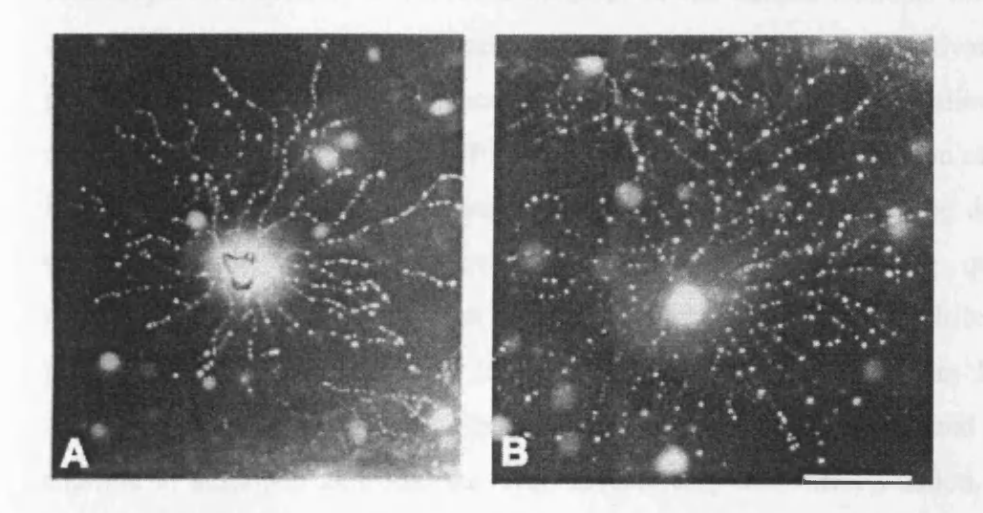


Figure 1.4. Dil-labelled RGCs in control (A) and experimental (B) eyes after 10 weeks post IOP elevation. Scale bar:  $75 \mu m$  (Ahmed et al., 2001a).

Apart from RGCs, morphological plasticity has been observed in other cells of the adult mammalian retina. Significant reduction in the type A horizontal cell dendrites, which sprouted into the inner retina, has been observed in cat and rabbit after a sublethal doses of kainic acid (Peichl and Bolz, 1984). Another example is the elongated processes of rod and horizontal bipolar cells in adult cat retina following experimentally induced retinal detachment (Lewis et al., 1998).

#### 1.2.4. Neurotrophins

Reduction of IOP leads to improved axonal function, and consequently to the increased retrograde transport of neurotrophins to the cell body (Herzog and von

Bartheld, 1998). Neurotrophins, due to their autocrine, endocrine and paracrine properties, can regulate survival, differentiation and regeneration of neurons (Herzog and von Bartheld, 1998). Neurotrophins are a family of closely related proteins that were originally identified as promoters of neuronal survival, but have since been demonstrated to regulate neuronal survival, development and function in both the peripheral and central nervous system. Four neurotrophins are expressed in mammals, including NGF, brain-derived neurotrophic factor (BDNF), neurotrophin-3 (NT-3) and neurotrophin-4 (NT-4). Each activates at least one of the tropomyosin-related kinase (Trk) family of receptor tyrosine kinases (TrkA, TrkB, TrkC) and p75 neurotrophin receptor (p75 NTR), a member of the tumour necrosis factor receptor superfamily (Figure 1.5.). Activation of Trk receptors results in activation of Ras, phosphatidyl inositol-3 (PI3)-kinase, phospholipase C-y 1 and signalling pathways regulated through these proteins. P75NTR activation leads to activation of the nuclear factor-κB (NF- κB), Jun kinase and other signalling pathways. During development, the number of surviving neurons is controlled by restraining quantities of neurotrophins. Moreover, the neurotrophins control axon growth, dendrite growth and pruning, cell fate decisions and the expression of proteins important for neuronal function. In the adult CNS, neurotrophins regulate synaptic function and plasticity in addition to sustained neuronal survival, morphology and differentiation. Thus, their constant presence is essential. Additionally, mutations in neurotrophins or their receptors have been associated with many human genetic diseases (Reichardt, 2006).

In the visual system, neurotrophins are involved in the development and maintenance of RGCs. BDNF has frequently appeared as a very important neurotrophic factor that affects development of vertebrate RGCs, including survival, morphological differentiation of axons and dendrites, synapse formation, and regeneration (Bahr, 2000; Frost et al., 2001; Isenmann et al., 2003; von Bartheld, 1998). Although BDNF does not modulate programmed cell death of RGCs *in vivo* (Cellerino et al., 1998; Pollock et al., 2003; Rohrer et al., 2001), it has been shown to act as a potent survival factor for axotomised and injured RGCs (Di Polo et al., 1998; Mansour-Robaey et al., 1994). In addition, BDNF can increase the extension and regeneration of retinal neurons *in vitro* (Goldberg et al., 2002; Lom and Cohen-Cory, 1999; Takano et al., 2002).

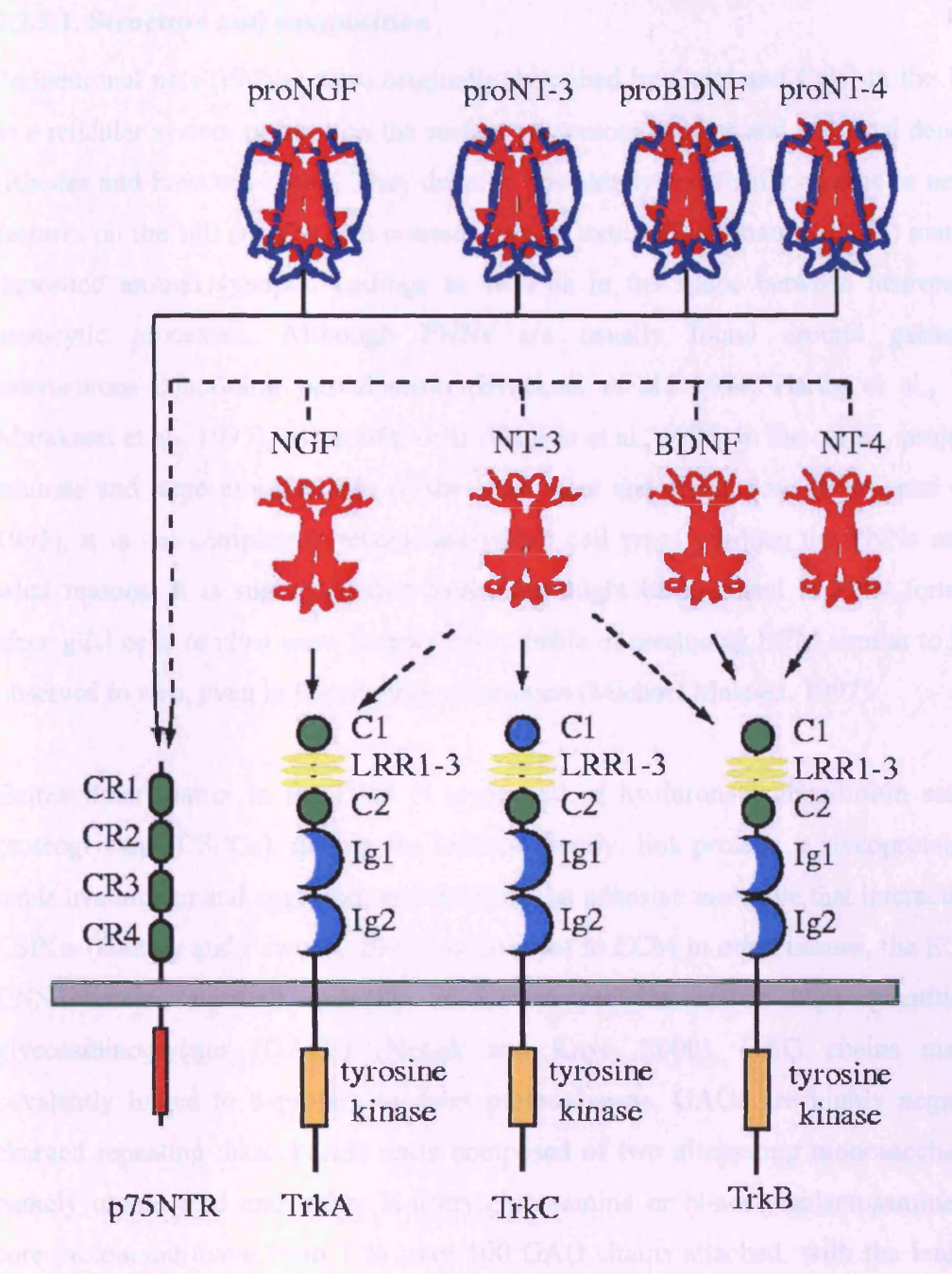


**Figure 1.5.** Neurotrophin-receptor interactions. Each neurotrophin binds to p75NTR but not to the Trk receptors. After maturation of the proneurotrophins through proteolysis, each mature neurotrophin can bind and activate p75NTR, but shows more specific interactions with the three Trk receptors. NGF recognises TrkA, BDNF and NT4 activate TrkB, and NT3 binds TrkC (Reichardt 2006).

#### 1.2.5. Perineuronal nets

## 1.2.5.1. Structure and composition

Perineuronal nets (PNNs) were originally described by Golgi and Cajal in the 1890s as a reticular system present on the surface of neuronal bodies and proximal dendrites (Rhodes and Fawcett, 2004). They develop postnatally and finally emerge as net-like features on the cell surface as a consequence of extracellular matrix (ECM) materials deposited around synaptic endings as well as in the space between neurons and astrocytic processes. Although PNNs are usually found around gabanergic interneurons containing parvalbumin (Bruckner et al., 1994; Hartig et al., 1992; Murakami et al., 1995), pyramidal cells (Hausen et al., 1996) in the cortex, projection neurons and large motoneurons of the brain stem and spinal cord (Murakami et al., 1995), it is not completely recognised which cell types produce the PNNs and for what reasons. It is suggested that astrocytes might be involved in PNN formation since glial cells *in vitro* were found to be capable of producing ECM similar to PNNs observed *in vivo*, even in the absence of neurons (Michael Maleski, 1997).

Extracellular matrix in the CNS is composed of hyaluronan; chondroitin sulphate proteoglycans (CSPGs), mainly the lectican family; link protein, a glycoprotein that binds hyaluronan and aggrecan; and tenascin, an adhesive molecule that interacts with CSPGs (Galtrey and Fawcett, 2007). In contrast to ECM in other tissues, the ECM in CNS contains a small quantity of fibrous proteins and a high quantities of glycosaminoglycans (GAGs) (Novak and Kaye, 2000). GAG chains may be covalently linked to a protein to form proteoglycans. GAGs are highly negatively charged repeating disaccharide units composed of two alternating monosaccharides, namely uronic acid and either N-acetylglucosamine or N-acetylgalactosamine. The core protein can have from 1 to over 100 GAG chains attached, with the length of GAG chains varying from 10 to 400 000 kDa (Rhodes and Fawcett, 2004). Based on their glycosaminoglycans chains, proteoglycans are classified into four main groups: chondroitin sulphate, dermatan sulphate, keratin sulphate and heparin sulphate (Inatani and Tanihara, 2002). There are several types of CSPGs, including large aggregating proteoglycans such as aggrecan (Paulsson et al., 1987) and versican (Krusius et al., 1987); the brain specific proteoglycans neurocan (Grumet et al., 1993)

and brevican (Yamada et al., 1994); NG2 (Levine and Card, 1987; Stallcup and Beasley, 1987) and phosphacan/DSD-1 (Grumet et al., 1993; Grumet et al., 1994).

CSPGs in the ECM play an important role in determining the functional responses of cells to their environment during development, cell migration, maturation differentiation and survival and tissue homeostasis (Oohira et al., 2004). Many of the functional properties of CSPGs are attributed to the attached CS-GAG chains. CS-GAGs bind various growth factors and growth inhibitory factors (Galtrey et al., 2007). CS-PGs are particularly strongly expressed in the embryonic brain (Oakley and Tosney, 1991; Snow et al., 1990).

## 1.2.5.2. Functional roles of PNNs in plasticity

There are several possibilities for the function of PNNs: synaptic stabilisation and limitation of synaptic plasticity (Hockfield et al., 1990), neuroprotection (Morawski et al., 2004) or support of ion homeostasis in the region of very active neurons (Härtig et al., 1999).

The assumption that PNNs have a role in the maintenance of tissue architecture and maturation of synapses on motorneurons originated from the observation of the late development of PNNs, and their association with only certain types of neurons (Celio and Blumcke, 1994; Kalb and Hockfield, 1990; Margolis and Margolis, 1993). The late postnatal appearance of PNNs in the visual cortex has been found to overlap with the end of a critical period (Sur et al., 1988; Zaremba et al., 1989), the developmental phase during which synapses are still susceptible to experience (Daw and Wyatt, 1976). Although synaptic plasticity is significantly reduced at the end of the critical period, visually deprived rats preserved some plasticity of the visual cortex (Cynader et al., 1976). Since previous studies observed alterations in CSPGs expression in the visual cortex in visually deprived rats (Guimaraes et al., 1990; Hockfield et al., 1990; Zaremba et al., 1989), CSPGs and PNNs are involved in maintaining synaptic stability and preventing plasticity in the mature animal (Rhodes and Fawcett, 2004). The above studies have been supported by (Pizzorusso et al., 2002), who demonstrated restoration of synaptic plasticity after the treatment of mature rat visual cortex with bacterial enzyme chondroitinase ABC, which degraded CSPGs present in the PNNs.

Synaptic plasticity is normally observed only in animals reared in the dark or during a critical period in development.

Chondroitinase has been applied to models of CNS injury *in vivo*. Bradbury et al. (2002) demonstrated degradation of chondroitin sulphate glycosaminoglycans (CS-GAG) around the lesion site and axonal regeneration after treatment of the lesioned adult rat dorsal column with chondroitinase. Additionally, his studies showed an associated increase in the expression of the growth associated protein (GAP)-43 in lesioned neurons, restoration of post-synaptic activity below the lesion and functional recovery. Further studies also support the positive effects of chondroitinase ABC (ChABC) on axonal regeneration after injury (Krekoski et al., 2001; Tropea et al., 2003; Yick et al., 2003; Zuo et al., 2002).

Tropea et al. (2003) studied effects of the combined treatment with ChABC and BDNF on injured RGCs. Delivery of brain-derived BDNF was performed to enhance the intrinsic ability of RGCs to re-elongate their axons, while the treatment with chABC was conducted to reduce the neurite growth-inhibitory properties of the adult chondroitin sulphate proteoglycans. The results showed that the combined treatment had effects on axon growth and synapse formation by the sprouting axons, implying the potential of this approach in therapies for the repair of the damaged adult CNS (Tropea et al., 2003).

Taken together, the above studies strongly support the potential to restore neuronal growth and plasticity to the adult CNS (Rhodes and Fawcett, 2004).

## 1.3. Hypothesis

This project addresses the hypothesis that the changes in the dendritic tree of RGCs in the experimental glaucoma model can be reversed by the reduction of IOP followed by the enzymatic digestion of CSPGs to disrupt the perineuronal net. The action of the enzyme chABC might be enhanced by the action of neuroprotective agents such as BDNF.

## 1.4. Project aims

The main aims of this project are:

- > To identify changes in RGC morphology and quantify RGC loss after the induction of ocular hypertension in a rodent model of experimental glaucoma.
- > To determine if RGC remodelling in glaucoma might be driven by combined IOP reduction and manipulation of retinal perineuronal nets/retinal neurotrophin levels. (Proteoglycan perineuronal net will be disrupted by intravitral injection of chABC and the levels of neurotrophins increased by intravitreal injection of BDNF).
- > To investigate and compare the presence of CS-GAGs, the key components of the ECM in the CNS, and aggrecan core protein epitopes in young, old and glaucomatous rat retinas.

## **Chapter 2: Materials and Methods**

## 2.1. Ex vivo – retinal explant culture

## 2.1.1. Experimental animals

Experiments were performed either on adult mice with mixed background, strains C57BL/6Crl and C3H/HeJ, or adult male Norwegian Brown rats (*Rattus norvegicus*). Mice, obtained from Ingenium Pharmaceuticals, Germany, were killed by cervical dislocation. Rats, obtained from Harlan, UK, were euthanised by over-exposure to CO2, and death was confirmed by cervical dislocation. Eyes were enucleated immediately post-mortem.

#### 2.1.2. Retinal dissection

To optimise the protocol for retinal dissection, different approaches were tested. Initially, dissection of the retina was performed under non-sterile conditions. To eliminate contamination problems, dissection was then performed using aseptic technique within a Microflow laminar flow hood. Surgical instruments were autoclaved at 120 °C for 20 minutes and immersed in 70% ethanol directly before dissection.

Initially, dissection was carried out on a petri-dish covered with Sylgard 184 silicone elastomer (Dow Corning, UK) and, in later experiments, directly on a petri-dish. The freshly enucleated eyes were immersed in medium. A number of media were tested to optimise the dissection protocol to ensure retinal viability. These can be seen in Table 2.1. A slit was cut in the sclera close to the cornea and the anterior chamber was dissected. The retina was then carefully isolated from the retinal pigment epithelium (RPE) remaining in the eyecup, and the vitreous still attached to the retina was carefully removed either on a culture plate (initially) or during dissection (later). The retina was flattened using a brush or by cutting slits in the retina. In later experiments, a brush was not used for dissection to minimise mechanical damage during the procedure. In preliminary experiments, the isolated retina was placed with vitreous side up on a culture dish covered with pieces of glass or on a black Millipore filter (AABP02500) to prevent folding. Since this approach did not prevent folding of the

retina, in subsequent experiments, the tissue was placed with ganglion cell side up on 0.4 µm Millicell culture plate inserts (Millipore). Excess media was aspirated.

Finally, the following protocol was optimised for retinal dissection. The whole procedure was carried out with as little disruption and manipulation as possible to avoid mechanical damage. Dissection was performed using aseptic technique within a Microflow laminar flow hood. Surgical instruments were immersed in 70% ethanol directly before dissection. The freshly enucleated eyes were immersed in a refrigerated HBSS (Gibco, UK) medium. A slit was cut in the sclera close to the cornea and the anterior chamber was dissected. The retina was then carefully isolated from the retinal pigment epithelium remaining in the eyecup, and the vitreous still attached to the retina was carefully removed. The retina was placed with ganglion cell side up on  $0.4~\mu m$  Millicell culture plate inserts (Millipore) and excess media was aspirated.

Medium	Serum	Supplement	Other
DMEM	heat-inactivated	2mM	100 U/ml
(Dulbecco's	FBS (lab stock)	L-glutamine	penicillin/streptomycin
Modified Eagle			
Medium) (lab			
stock)			
50% MEM	25% heat-	_	25% HBSS (Gibco)
(Minimum	inactivated horse		6.5 mg/ml glucose
Essential Medium)	serum (lab stock)		100 U/ml
(Gibco)			penicillin/streptomycin
oxygenated Ames'	_	_	_
(Sigma)			

Table 2.1. Media used during optimisation of retinal dissection protocol.

## 2.1.3. Culture conditions

The isolated retinas were cultured in 5% CO2 at 37°C in various media as indicated in Table 2.2 for at least one hour prior to ballistic labelling. Media were changed daily or

every other day. The culture conditions and media tested were those previously described by other investigators (Gutierrez et al., 2005; Koizumi et al., 2007; Sun et al., 2002; Wang et al., 2002; Xin et al., 2007). Eventually, the following protocol was established: the retina was cultured in 5% CO2 at 37°C in Neurobasal-A (Gibco, UK) medium containing 0.8 mM L-glutamine, 2% B27 and 1% N2 supplements (Gibco, UK) and 100 U/ml penicillin/streptomycin before diolistic labelling. The medium was exchanged daily.

Medium	Serum	Supplement	Other
DMEM	heat-inactivated FBS	2mM L-glutamine	100 U/ml
			penicillin/streptomycin
50% MEM	25% heat-inactivated	_	25% HBSS
	horse serum		6.5 mg/ml glucose
			100 U/ml
			penicillin/streptomycin
Oxygenated Ames'	_	-	_
Ames'	1% heat-inactivated	1% N2 supplement	_
	horse serum	(Gibco)	
		0.3 mg/ml	
		L-glutamine	
Neurobasal-A	2% heat-inactivated	2mM L-glutamine	100 U/ml
(Gibco)	horse serum	2% B27 supplement	penicillin/streptomycin
		(Gibco)	
Neurobasal-A	_	2mM L-glutamine	100 U/ml
		2% B27 supplement	penicillin/streptomycin
		1% N2 supplement	
Neurobasal-A	_	0.8mM L-glutamine	100 U/ml
		2% B27 supplement	penicillin/streptomycin
		1% N2 supplement	

Table 2.2. Media used during retinal culture.

## 2.1.4. Cell viability assays

Cell viability of retinal culture was assessed using propidium iodide (PI) (Sigma, UK) as a marker of necrosis and the vital dye calcein AM (Invitrogen, UK). Propidium iodide (3,8-Diamino-5-[3-(diethylmethylammonio)propyl]-6-phenylphenanthridinium diiodide), which binds to double-stranded DNA, labels the nuclei of non-viable cells but can not cross the membrane of viable cells (Smith et al., 2007). Calcein acetoxymethyl ester (AM) is retained in cells with intact membranes but cannot stain dead cells. In live cells, following acetoxymethyl ester hydrolysis by intracellular esterases, the nonfluorescent calcein AM is converted to a green-fluorescent calcein (Caspi et al., 2007; Decherchi et al., 1997).

For cell viability assays, retina was isolated as described in section 2.1.2 and the wholemount retinas were cultured in duplicates either in HBSS (control), 50% MEM (formulated as described in section 2.1.3.), Neurobasal-A containing 2% B27 supplement, 1% N2 supplement, 0.8mM L-glutamine and 100 U/ml penicillin/streptomycin or Neurobasal-A containing 2% B27 supplement, 2% horse serum, 2mM L-glutamine and 100 U/ml penicillin/streptomycin. The retinas, after 1 and 3 days of culture, were incubated with propidium iodide and calcein AM for approximately 40 minutes (section 3.2.1).

For comparison of the effects of biolistic transfection on tissue survival, retinas were cultured in HBSS (control), Neurobasal-A medium without serum (supplemented as above) or Neurobasal-A medium with serum (supplemented as above). The explants, after 2 days of culture, were incubated with calcein (5 µl was added to the surface of the tissue submerged in 1 ml medium) for approximately 40 minutes (section 3.2.2).

## 2.1.4.1. Image capture of labelled RGCs

The retinas were imaged using a Zeiss Axiovert200 inverted fluorescent microscope and LSM510 software.

The average fluorescence (RGB) intensity of propidium iodide and calcein signal were measured using ImageJ (Image Processing and Analysis in Java) plugin

(Measure RGB) program and were shown as mean RGB values for the entire image. The intensities were obtained, based on a standard 256 intensity level scale. Based on the mean RGB values, standard deviations were obtained with the program. The camera settings were fixed to permit direct comparison between preparations.

## 2.1.4.2. Statistical analysis

Retinal explants were compared to determine if there was a significant difference between the explants maintained under different conditions of culture and transfection. The data were tested for normality using SPSS 16.0. The non-parametric data described in section 3.2.5 were then analysed using Mann-Whitney Test in SPSS 16.0.

## 2.1.5. Gene gun processes

The Helios gene gun (BioRad, UK) enables rapid and direct gene transfer into cells (Figure 2.1.). It can be applied to study gene therapy, DNA vaccination and *in vivo* transformation of plants. An adjustable low-pressure helium pulse is used to deliver the DNA- or RNA-coated gold or tungsten microcarriers directly into the target cells or tissue (Figure 2.2.). The tubing preparation station and the tubing centre included in the system allow the preparation of up to 50 sample cartridges with coated microcarriers at once. The cartridges are loaded into the holder, which is then inserted into the device ready for labelling. In this study, the gene gun was used to deliver both plasmid DNA and fluorescent dyes (DiI) to the RGCs within isolated retina.



Figure 2.1. The Helios Gene gun (copied from www.bio-rad.com).

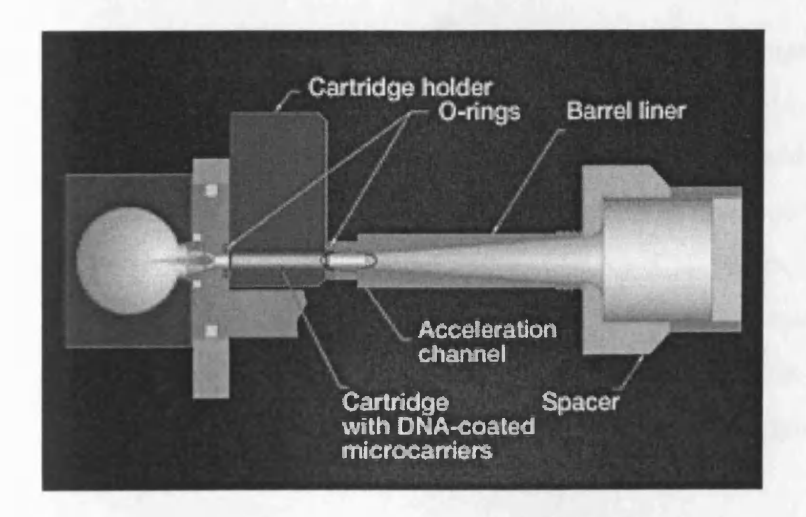


**Figure 2.2.** Sample delivery. The helium pulse sweeps the microcarriers from the inside wall of the sample cartridge (copied from www.bio-rad.com).

#### 2.1.5.1. Biolistic labelling

After at least 1 hour incubation in 5% CO2 at 37°C, the retina on the insert was put on a clean petri-dish, and RGCs were labelled by the biolistic delivery of gold particles (1.6 μm diameter; BioRad) coated with either expression plasmid (Clontech, UK) for yellow fluorescent protein (EYFP), red fluorescent protein (ERFP) or green fluorescent protein (EGFP) with a κB reporter plasmid and ERFP into the wholemount retina using the hand-held gene gun. The coated gold particles (BioRad, UK) were propelled into the cultured tissue at a helium pressure that varied from 100 to 150 psi. In order to protect the tissue from the shock wave, a 70 μm nylon mesh screen (lab stock) or a 3 μm filter in later experiments, was placed between the gun and the culture. The preparation was quickly transferred to the insert in the culture medium and excess medium was aspirated such that the remaining medium just covered the retinal surface.

#### 2.1.5.2. Diolistic labelling

In contrast to the GFP labelling techniques based on viral transfection requiring several hours for fluorescent protein to be expressed in transfected cells, the diolistic technique enables rapid labelling of cells in various neuronal tissues (Gan et al., 2000). In order to observe labelled RGCs in wholemount preparations of retina,

RGCs were labelled by the ballistic delivery of 1.7 μm tungsten microparticles coated with lipophilic dye - DiI beads (Molecular Probes, UK) (1,1'-diocta-decyl-3,3,3',3'-tetramethylindocarbocyanine perchlorate) using the hand-held gene gun (Helios Gene-gun, BioRad). In order to prevent clusters of dye-coated particles from landing on the preparation, cell culture inserts (Becton Dickinson Labware) with 3 μm pore size were interposed between the gene gun and the target tissue. The tungsten particles were propelled into the tissue at a pressure of 100-150 psi. After shooting, the retinal preparations were fixed with 4% paraformaldehyde in 0.1 M phosphate buffer (pH 7.4).

## 2.1.5.3. Image capture of labelled RGCs

Approximately 0.5 hour after diolistic or 24-48 hours after biolistic labelling, the wholemount retinas were imaged using a Zeiss Axioplan laser scanning confocal microscope and LSM510 software.

# 2.1.6. Effects of BDNF and caspase inhibitors on neuronal survival and axonal growth cones formation

Retinas were isolated from Brown Norwegian male rats 8-12 weeks of age and cultured on 0.4 μm Millicell culture plate inserts in Neurobasal-A medium containing 2% B27 supplement, 1% N2 supplement, 0.8 mM L-glutamine and 100 U/ml penicillin/streptomycin at 37°C in 5% CO2. A Helios gene gun system was used for particle-mediated transfer of an YFP-expressing plasmid to RGCs as described in section 2.1.5.1. Retinal explants were treated with 250nM broad-spectrum, irreversible caspase inhibitor (Boc-D-FMK) or with 100 ng/ml recombinant human brain-derived neurotrophic factor (rhBDNF). The morphology of RGCs in the treated and the control explants was observed by confocal microscopy (Zeiss Axioplan laser scanning confocal microscope and LSM510 software).

## 2.2. In vivo - experimental glaucoma models

## 2.2.1. Introduction to animal techniques

All experimental procedures complied with Home Office (UK) regulations concerning the Animals (Scientific procedures) Act 1986 and ARVO Statement for the Use of Animals in Ophthalmic and Vision Research. Experiments were performed according to personal license number (PIL) 30/7912, and under project license number (PPL) 30/2470.

The animal models used were based on the episcleral drainage vessel sclerosis rodent model of glaucoma (Jia et al., 2000; Morrison et al., 1997; Morrison et al., 1998) (section 2.2.3) and injection of ferro-magnetic microspheres into the anterior chamber (section 2.2.4). Six to 8 month old male ex-breeder Brown Norway rats (Rattus Norwegicus) were housed at 21°C on 24 hour 40-60 lux and provided with standard laboratory diet and water ad libitum. Animals were handled for at least 1 week before commencing the experimental procedure. Their weights were recorded as an index of health.

## 2.2.2. Calibration of the Tonolab rebound tonometer in cannulated rat eye

The Tonolab rebound tonometer (Tiolat, Oy, Finland) (Figure 2.3) used in the study has been developed for measuring rodent IOP, especially in glaucoma research (Wang et al., 2005). This device projects a very light probe towards the cornea and calculates IOP based on the probe's rebound kinetics. An IOP value corresponding to a weighted average of 6 readings, rounded to the nearest integer, is displayed at each point when tonometry measurements are taken. These weighted average IOP values are referred to below as single readings.



Figure 2.3. Tonolab rebound tonometer (copied from http://www.tiolat.fi/images.htm).

Calibration experiments were performed using enucleated eyes from Norwegian Brown rats. Directly after enucleation, eyes were mounted on a stand and a 30-gauge needle was inserted through the cornea into the anterior chamber. The needle was attached via polyethylene tubing to a 3-way connector, which was attached to a burette containing Balanced Salt Solution (Aqsia, Bausch & Lomb, U.K.), a pressure transducer with a full scale reading 0 to 2.5 psi (Omega PX800-002GV, Omega Corp., USA), and a custom-manufactured screw-gauge syringe. The pressure in the system could be varied with the screw-gauge syringe or by altering the level of fluid in the burette. With the cannulated eye and screw-gauge syringe isolated from the system, the pressure transducer was calibrated by recording its output voltage as a function of fluid height in the burette (since 1mmH20 = 0.0735 mmHg, pressure in mmBSS was converted to mmHg using a conversion factor of 0.0735, under the assumption that mmBSS = mmH20). Then the burette was isolated and the pressure in the eye was varied using the screw-gauge. IOP was increased with the screw-gauge syringe from 10 mmHg up to 60 mmHg and then back to 10 mmHg, in steps of approximately 5 mmHg. The IOP was measured at each step using the rebound tonometer and recorded alongside the IOP measured by the pressure inducer.

To test the effect of small changes in the position of the tonometer relative to the eye, calibration was obtained with the tonometer positioned at varying distances from the cornea, i.e. 1mm and 3mm (Chapter 3). The calibration of tonometer was performed in collaboration with Dr Ankush Prashar.

## 2.2.3. Hypertonic saline model

## 2.2.3.1. Induction of glaucoma

#### 2.2.3.1.1. Microneedle assembly

Disposable microneedles were made from 10 µl borosilicate glass pipettes (Sigma-Aldrich, UK) pulled using a pipette puller (David Kopf Instruments, USA). The rough microneedle tips were bevelled to avoid excessive tissue damage during injection and to allow for an easy injection into the vessel. The needle was lowered onto a flat rotating (14000 rpm) surface attached to an industrial rotator and covered with diamond lapping film (World Precision Instruments, UK). Microneedle diameter was

measured using a DMRA2 microscope (Leica, UK) and Leica QWin image analysis software. Microneedles with an outer diameter of 10-40  $\mu$ m were used, depending on the size of episcleral veins.

The narrow end of the microneedle was cut to approximately 3 mm segment. The segment was then inserted into the end of polyethylene tubing (Sandown Scientific, UK) with an outer diameter of 0.038 inches or 0.048 inches, and the 23G needle with the tip broken off was inserted into the other end of the tubing. Finally all the junctions were sealed with Superglue, UHU, or Araldite over-laid with high viscosity Superglue, followed by the additional sealing with heat-shrink tubing. A small plastic tab was positioned along the tubing and held with high viscosity Superglue to mark the bevel of the microneedle. After assembly, microneedles were stored in a plastic box or in a Petri-dish and then sterilised before use by applying 100% ethanol to the bevelled tip, followed by air-drying.

#### 2.2.3.1.2. Anaesthesia

Before injection, rats were anaesthetised via inhalation of 4% isoflurane (Baxter) with oxygen in a chamber. For the surgical procedure, they were transferred to a respirator connected to a supply of oxygenated isoflurane. Rats were monitored throughout the surgery to assess the level of anaesthesia, and the supply of isoflurane was adjusted appropriately. The operated eye was hydrated during surgery with 0.9% sterile saline drops.

## 2.2.3.1.3. Surgical procedure

The conjunctiva was incised under a surgical light microscope (Zeiss, USA). A small plastic ring (width <2.5 mm, with diameter matching the rat eye just posterior to the limbus) was inserted using forceps so that it lied just posterior to the episcleral plexus of veins, but anterior to the equator of the eye. The plastic ring was retained under its own elasticity so that it exerted gentle compression of the veins with minimal distortion of the globe. The ring was incomplete so that one sector (approximately 30-60 degrees) was open to identify and cannulate a single episcleral vein. The ring was

removed following injection of hypertonic saline (1.75M) into episcleral venous system of the left eye under general anaesthesia. A topical antibiotic chloramphenicol (Chauvin Pharmaceuticals Ltd, UK) was given post injection to reduce the risk of infection.

#### 2.2.3.2. IOP measurements

In order to minimise diurnal fluctuations in IOP, rats were housed in a constant low-light environment (40-60 lux). IOPs were measured at least 3 times before injection and daily to every 7 days, normally every 3 days after injection using a rebound tonometer (Tiolat, Oy, Finland) calibrated for use with a rat eye (Wang et al., 2005). All measurements were made in awake animals in which the cornea was anaesthetised using topical 0.4% oxybuprocaine hydrochloride eye drops (Chauvin, UK). IOP measurements were taken from the experimental (left) and contralateral (right) eye. The IOP was taken as the mean and standard deviation (SD) of 6 readings.

#### 2.2.3.3. Euthanasia

Animals were killed at variable intervals from 33 to 136 days following the induction of ocular hypertension (n=27). One rat, uninjected, was killed due to severe injury that did not respond to the treatment. Another rat died due to an overdose of isoflurane during the surgery.

All other rats received a lethal dose (approximately 1ml) of sodium pentobarbital (Euthatal) (n=28). In most cases, this was followed by transcardial perfusion (n=19). A rat was placed on the operating table with its back down and the pinch-response method was used to determine if the reflexes were absent. Once an animal was unresponsive to this stimulus, an incision with large scissors was made through the abdomen for the length of the diaphragm and the connective tissue at the bottom of diaphragm was cut through to allow access to the rib cage. Two horizontal cuts were made through the rib cage and the thoracic cavity was opened up. It was clamped spread open to expose the heart and provide drainage for blood and fluids. While holding the beating heart steady with forceps, a needle was inserted directly into the left ventricle and extended straight up about 5 mm. The needle, connected to a Cole

Parmer (USA) perfusion pump, was held in position by clamping in place near the point of entry. A cut in the right atrium was made and blood was flushed out using 0.9% saline. When blood had been cleared from the body, saline was changed to 4% paraformaldehyde (PFA) in 0.1 M phosphate buffer (pH 7.4). Perfusion was stopped shortly after reflex movements ceased and the needle was removed from the heart. Approximately 200ml of PFA was used for each rat. The eyes were removed and stored in 4% PFA at 4°C.

## 2.2.4. Magnetic bead model

## 2.2.4.1. Induction of glaucoma

Sixty one male breeder Brown Norway rats were housed in a constant low-light environment (40-60 lux) to minimise diurnal fluctuations in IOP, with food and water provided ad libitum. IOPs were measured 3 times before injection and every 2-3 days after injection using a TonoLab rebound tonometer (Tiolat, Oy, Finland) calibrated for use with the rat eye (Wang et al., 2005). All measurements were made in awake animals in which the cornea was anaesthetised using topical 0.4% oxybuprocaine hydrochloride eye drops (Chauvin, UK). The IOP was taken as the mean and standard deviation (SD) of 5 readings.

In each animal, the IOP was elevated in the left eye by injecting a sterile BSS, Alcon Corp.) containing 30 mg/ml ferro-magnetic microspheres (CHI Scientific, Inc., USA, bead diameter 5 microns) into the anterior chamber. All injections were made under Isoflurane anaesthesia (as described in section 2.3.1.2), with topical chloramphenicol (0.5%) administered pre and post injection (Cusi, UK). Microspheres were sterilised by γ-irradiation with a Gammacell 1000 Elite (Nordon International Inc. 22 TBq Caesium Source). Approximately 10 to 20 μl was injected into the anterior chamber of the left eye, delivering approximately 0.3 to 0.6 mg of beads. The right eye acted as an unoperated control. Injections were made using a sterile 32 (Hamilton) or 33-gauge (WPI Corporation) needle parallel to the iris under general anaesthesia. The 33-gauge needles were bevelled on 3 sides to facilitate injection through the cornea. A tunnelled injection was made with the needle running parallel to the anterior surface of the iris to minimise the risk of iris trauma. Since the beads tended to settle under the

influence of gravity (Figure 2.4 A & B), the syringe and needle were agitated using a vortex stirrer for approximately 10 seconds prior to injection to resuspend the beads in BSS. The minimum period between subsequent injections was 1 week in accordance with Home Office license requirements (UK).





**Figure 2.4.** Surgical set-up used during the microinjection procedure. Rats were anaesthetised in a chamber before surgery. Anaesthesia was maintained via an inhalation mask (A). Photographs of magnetic beads before (left eppendorf) and after agitating (right eppendorf). Since the beads tended to settle under the influence of gravity, they were agitated using a vortex stirrer for approximately 10 seconds prior to injection (B).

Once the injection of beads was completed, the needle was kept in position and the beads then drawn away from the injection site using a small hand held magnet (0.45 Tesla, 2.5 cm long) which prevented the egress of beads from the injection track. The magnet was then used to distribute the microspheres around the iridocorneal angle to reduce the outflow of aqueous humour via the trabecular meshwork (Figure 4.4). Four rats were injected with 10 µl or 20 µl of magnetic microspheres without directing them to the iridocorneal angle using a magnet. One rat received a vehicle injection of 10 µl BSS into the anterior chamber. Immediate increases in IOP could be minimised by leakage of aqueous around the injection cannula once the beads had been drawn away from the injections site. Injections of microspheres were performed up to three times in the left eye, depending on the required level and duration of the IOP elevation. Rats were killed by an overdose of CO<sub>2</sub> and the retinas were dissected out for a short-term culture in Neurobasal-A medium (Invitrogen, UK) (section 2.1.3) for subsequent studies. The cells in RGC layer were then immediately labelled by gene gunning with fluorescent dye DiI (section 2.5.1.2).

An elevated IOP was defined as 5 mmHg or greater elevation compared with the contralateral control eye. A sustained IOP was defined as 5 mmHg or greater elevation compared with the contralateral control eye on at least 7 consecutive days.

Anterior segment images of the beads distribution were taken as required with a Nikon Coolpix 4500 camera attached to a Haag Streit slitlamp.

## 2.2.4.2. Chondroitinase ABC and BDNF injections into a glaucomatous rat eye

The injections were performed after a 3-4 weeks period of IOP elevation that was followed by a 1 week period of decreased IOP. All injections were made under isoflurane anaesthesia, with topical chloramphenicol (0.5%) administered pre and post injection (Cusi, UK). Before anaesthesia, the experimental eye was treated with phenylephrine hydrochloride or 1% tropicamide (Chauvin Pharmaceuticals, UK) to dilate the pupil. Either 3µl of 10mU/eye chondroitinase ABC (from Proteus vulgaris; protease free; Seikagaku, Tokyo, Japan), 1 µl of 1µg/ml recombinant human BDNF (R&D systems, UK) or both agents (during the same procedure) were injected into the vitreous of a glaucomatous, left rat eye. The right eye acted as an unoperated control.

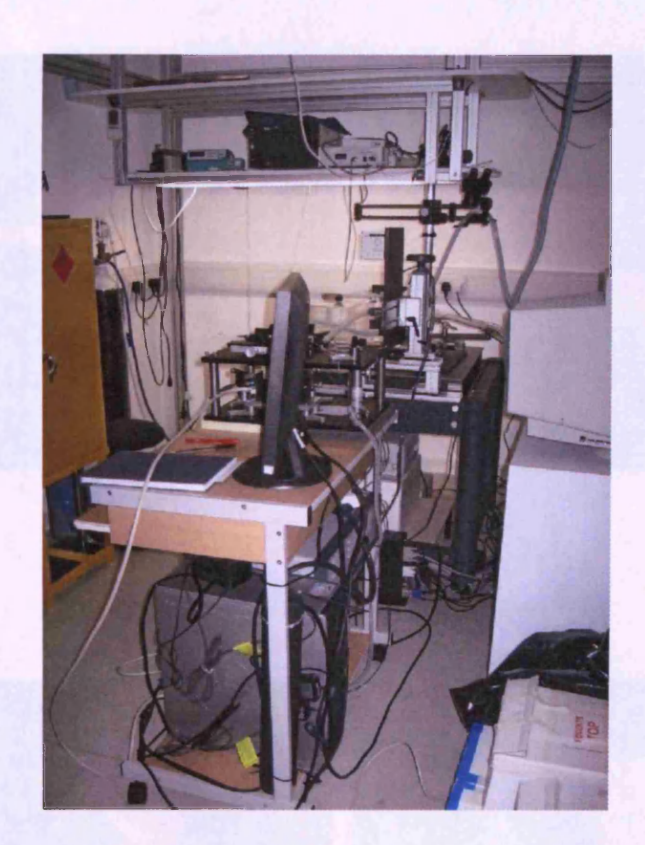
Alternatively,  $3\mu l$  of 10mU/eye chondroitinase ABC was injected into the normal rat eye. A thin sheet of transparent polypropylene was placed on the eye to allow the observation of the optic disc during the injections. A drop of sodium hyaluronate-Healonid (Pharmacia) was placed on the eye to prevent movement of the polypropylene. The needle tip was directed to the vitreous, above the optic disc. After injection, the needle was kept inside for a few seconds to enable the solution to settle in the vitreous and then slowly withdrawn. The animals were kept for two weeks after injection before being killed.

## 2.2.4.3. FD-OCT in vivo imaging

A frequency domain optical coherence tomography (FD-OCT) (Choma et al., 2003; de Boer et al., 2003; Fercher et al., 1995; Gerd and Michael Walter, 1998; Leitgeb et al., 2003; Nassif et al., 2004), also referred to as spectral or Fourier domain OCT system, was used to image rat retinas *in vivo*. The system enables high-speed, high sensitivity and depth-resolved measurements of the retina due to analysis of the interference pattern in the optical frequency spectrum. FD-OCT is based on all-reflective high-speed In-GaAs spectrometer, operating in the 1050 nm wavelength region with 70 nm bandwidth (~7 μm effective axial resolution) (Povazay et al., 2007a) (Figure 2.5).

## **Animal preparation**

Rats were first anaesthetised with 0.3 ml ketamine hydrochloride (Pfizer) injected intraperitoneally (IP) and eyes were then dilated with tropicamide (1%) (Bausch and Lomb) applied topically as drops. Approximately 7 minutes after ketamine injection, a rat was transferred to a stand where anaesthesia was maintained with isoflurane (1%) with oxygen inhaled via a mask and placed in a custom-made holder to minimize body and eye motion (Figure 2.6). The design of the holder was gradually developed during the experiments. The goniometric stage on which rats were placed was rotated to allow the optic disc to be clearly viewed with an ophthalmoscope. The optic disc was placed at the centre of field view by the sample arm optics to match the orientation of the OCT instrumentation. Narrow field scans were collected to focus on details of the optic disc whereas wider field scans were collected to the extent that the optics of the collection system would allow.



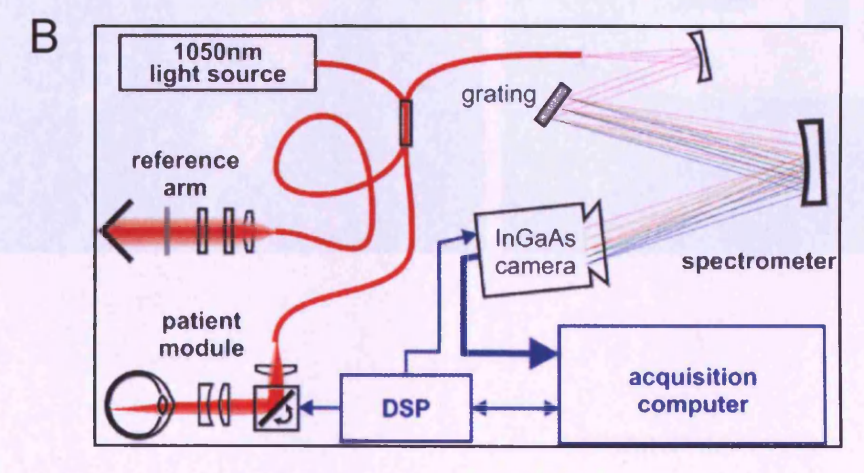
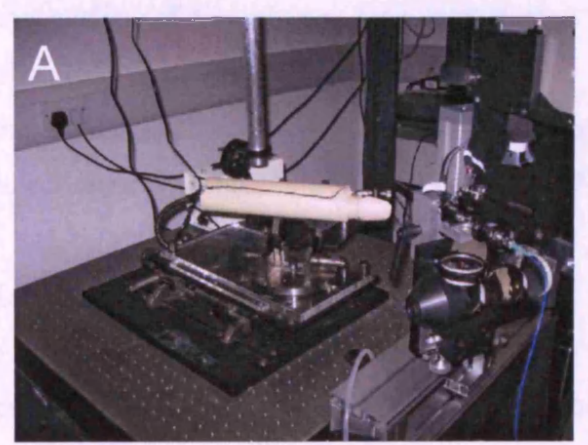
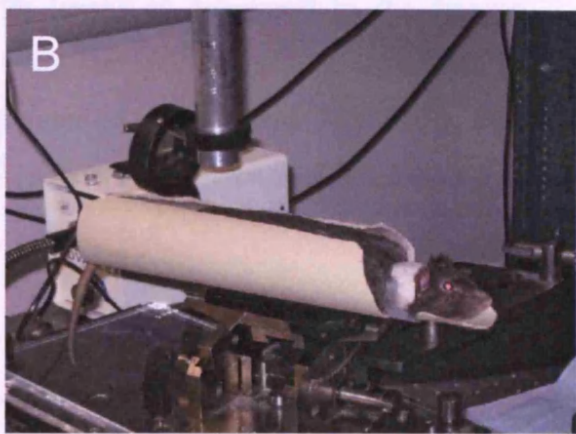
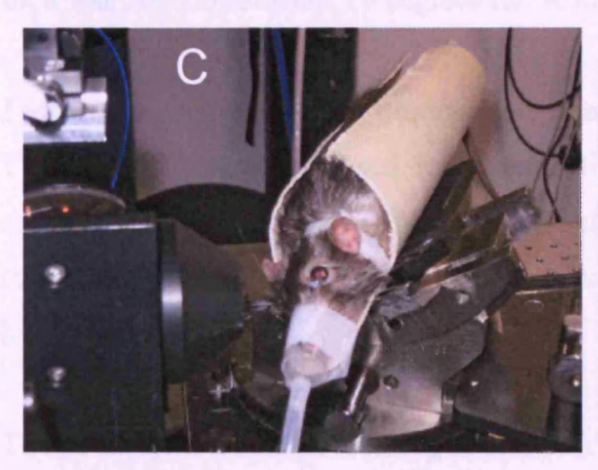


Figure 2.5. A photograph of a custom-built OCT system (A) and schematics of the 1050-nm encoded frequency domain OCT system (B). The broadband source is interfaced to a fiber-optic inferometer where the first arm is sent to an adjustable reference mirror in a free-space portion including dispersion compensation and an attenuator. The patient module consists of collimation and focusing optics and a 2-D scanner. On its way back, the light from the sample arm is recombined with the reference light, producing a spectral interference pattern that is sent to an all-reflective imaging spectrometer with a reflective planar grating. Processing of the signal from the InGaAs camera is performed with a standard industrial personal computer, while an independent digital signal processor (DSP) serves the position galvanometers and synchronizes the acquisition (copied and cited from Povazay et al., 2007).









**Figure 2.6.** Photographs of a custom-built set-up for OCT imaging *in vivo*. A goniometric stage with a holder (A). An experimental rat placed in a holder to minimize body and eye motion (B). Imaging of the rat that has been rotated to a position to align the focusing beam with the optic disc. The rat had a mask for isoflurane inhalation (C). An OCT image of a retina with an optic nerve head displayed on the monitor (D).

Initially, during the entire procedure, BSS was applied to both eyes to prevent them from drying out. Later, zero-power, glass contact lenses were filled with ophthalmic saline and placed on the imaged eyes to prevent loss of corneal surface quality since the quality of the images was improved with lenses as compared to the images obtained from hydrated eyes. Rat eyes were imaged once before inducing experimental glaucoma by bead injection and then once (n=4 rats) 7-10 days after injection (Figure 4.9A).

## Image acquisition system

A spectrometer based OCT engine utilizing a 70nm bandwidth (FWHM) light source centred at 1050 nm, was mated to a custom built ophthalmic sample arm. The beam at the exit pupil of the sample arm was approximately collimated (the sample arm allows +/- 8 Diopters of adjustment via Bidal system) at 0.5 mm 1/e^2 diameter. The non-contact system allowed a working distance of 2 cm. A typical volume acquisition used was 500 x 500 scans, 15 degrees full scan centred at optic nerve head (ONH).

## Postprocessing procedure - quantitative image analysis

The OCT data was processed for visualization using ImageJ. The steps involved: registration, filtering and reslicing. Manual segmentation was performed using custom-built Java code. Segmentation data was analysed and graphed using custom MATLAB code.

## The protocol for data processing in ImageJ:

- 1. Import stack into ImageJ
- 2. Manually delete maybe the first, second and final slice due to image artefacts.
- 3. makeRectangle(1, 46, 511, 551); <--- These dimensions apply to 512x512 images, and were different in 1024x1024 images
- 4. run("Crop");
- 5. run("8-bit"); <--- by making the image '8-bit', any changes in contrast and brightness can be applied to the image and saved.
- 6. run("Brightness/Contrast..."); Manually adjust brightness/contrast
- 7. run("Remove Outliers...", "radius=0.5 threshold=0 which=Dark stack");
- 8. run("Remove Outliers...", "radius=0.5 threshold=0 which=Bright stack");
- 9. run("Brightness/Contrast..."); Manually adjust brightness/contrast again

- 10. Select the middle slice as a reference point
- 11. run("StackReg ", "transformation=Translation"); <---StackReg
- 12. run("Reslice [/]...", "slice=1.000 start=Top avoid");
- 13. run("A trous filter stack", "k1=5 k2=2.2 k3=2.2 k4=0 k5=0 non std=1.50"); <---
- 14. run("Reslice [/]...", "slice=1.000 start=Top avoid");
- 15. run("Brightness/Contrast..."); Manually adjust brightness and contrast one final time.
- 16 Save as ...\_newfilt.tif

## Postprocessing procedure - segmentation

Segmentation of the different layers was performed by distinguishing the texture of different layers and their interfaces. The retinal fibre layer (RNFL) thickness was segmented at the scleral rim (the inner limiting membrane, ILM to the retinal pigment epithelium, RPE). The ILM was identified, when starting from the vitreous, by finding the first signal above a threshold and the strongest signals in every depth scan. The RPE was identified the same way when starting from the opposite side of the tomogram (scleral side). The retinal nerve fiber layer surface was easily identified in all images.

## Quantification of RNFL thickness

RNFL thickness was quantified from the OCT images of control and experimental eyes at different imaging times (Figure 4.9B). The mean was taken across the population of retinas. For the thickness comparison, the values for injected and control eyes were grouped according to the time of imaging (before injection, 7-10 days or 17-32 days post injection), and the mean values from each group were compared to the mean values from other groups.

#### **Statistics**

Differences in RNFL thickness were analysed by Independent Sample T-test in SPSS 16 for comparisons between different time points of imaging within the same group of eyes (control or experimental) or the same time points within different group of eyes. Data were expressed as the mean  $\pm$  SEM (Figure 4.10).

OCT data processing and postprocessing procedure was performed Dr Alex Tumlinson, Ketan Kapoor and Vedran Kajic. Vedran Kajic performed a manual segmentation. *Ex vivo* FD-OCT imaging was performed by Alicia Charlton, Dr Boris Povazay and supervised by Prof Wolfgang Drexler. I performed OCT imaging *in vivo* and data analysis of RNFL thickness.

# 2.3. Ex vivo evaluation of glaucomatous changes in experimental glaucoma models

## 2.3.1. Ex vivo FD-OCT imaging

Rats used for *ex vivo* OCT imaging were injected with hypertonic saline and perfused using 4% paraformaldehyde in 0.1 M phosphate buffer (section 2.3.1.5). The dissected posterior eye-cups containing retina were stored in fixative (4% paraformaldehyde) at 4°C until required for imaging. The samples were imaged by two optical coherence tomography systems, a 1300 nm Thorlabs Swept Source OCT (SS-OCT) and an 800 nm Three Dimensional Ultrahigh Resolution OCT (3D UHR-OCT). The left glaucomatous eyes were imaged using both OCT machines while the right control eyes only using the 800 nm UHR-OCT. Imaging parameters were determined according to the anatomical structures that were required to be visualised.

The OCT images from the rat CR308 were compared to the histological images of retinal sections from the same rat (Figure 4.13). Wax sections were prepared as described in section 2.4.2.2 and stained with Hoechst solution, as described in section 2.3.2.

## 2.3.2. Hoechst labelling

Hoechst solution, (bisbenzimide, Sigma-Aldrich), which labels cell nuclei by binding to DNA, was prepared by diluting a stock solution of 1 mg/ml bisbenzimide in PBS (1 µl of 1 mg/ml bisbenzimide in 1ml PBS). Frozen sections were stained with Hoechst solution for 10 minutes, washed 3 times in PBS for 5 minutes each, and then mounted in Hydromount aqueous non-fluorescing mounting medium (National Diagnostics

BDH, UK). The slides were then covered with aluminium foil and left to dry overnight. Hoechst stained sections were observed using a Leica AF6000 fluorescent microscope and imaged using Leica CTR6000 software.

#### 2.3.3. Diolistics and analysis of RGC morphology (magnetic bead model)

#### 2.3.3.1. Retinal dissection

Retinal dissection was performed as described in section 2.1.2 for the optimised protocol, except that antibiotics were not used for the short-term culture.

### 2.3.3.2. Preparation of dye-coated particles and diolistic labelling

Thirty milligrams of tungsten particles (~1.7 µm in diameter, Bio-Rad 165-2269) were spread on a clean glass slide. Three milligrams of 1,1'-dioctadecyl-3,3,3',3'tetramethylindocarbocyanine perchlorate (DiI, N-22880, Molecular Probes, UK) was dissolved in 100 µl of dichloromethane (methylene chloride, Sigma Diagnostics, UK) and applied over the tungsten particles on the glass slide. Dichloromethane quickly evaporated, and the tungsten particles were coated with DiI (Sun et al., 2002). After drying for 10-15 minutes, the dye-coated tungsten particles were scraped off with a clean razorblade onto a weighing boat. One end of the tubing (Bio-Rad) was sealed with parafilm and a 1-5 ml pipette tip was placed into the other end of the tubing. The powder was poured into the pipette tip and thus into the tubing. The open end of the tubing was then sealed, and the tube was shaken to get the powder to stick evenly across the whole tubing. Immediately before shooting, the "bullets" were cut into the appropriate lengths using the tube cutter (Bio-Rad) for use in the gene gun. A handheld gene gun (Helios Gene-gun, Bio-Rad) was used to propel the dye-coated particles into the wholemount retina. In order to prevent clusters of dye-coated particles from landing on the preparation, cell culture inserts (Becton Dickinson Labware, UK) with 3 µm pore size were interposed between the gene gun and the target tissue. The dye-coated particles were propelled into the tissue at a pressure of 70-150 psi. The retinal preparations were fixed with 4% paraformaldehyde in 0.1 M phosphate buffer (pH 7.4) for at least 40 minutes before the subsequent Hoechst staining (section 2.1.6.3).

Images of the DiI-labelled RGC stacks from the slides with wholemount retinas were obtained using a Zeiss LSM510 laser scanning confocal microscope and LSM510 software.

#### 2.3.3.3. Analysis of morphological parameters

The imaged DiI-labelled dendritic trees of RGCs were subjected to quantitative morphological analysis. The Sholl analysis was performed using Fast Sholl Matlab-based program (Gutierrez and Davies, 2007). In addition, the program made it possible to estimate the total dendritic length and the number of branching points. For dendritic field size, a polygon was drawn by linking the tips of dendrites, and the area calculated with ImageJ. Statistical analysis was performed in commercial softwareSPSS (SPSS, ver. 16.0 for Windows) using Mann-Whitney Test or Independent Student T-Test, with a significance level of p<0.05.

### 2.3.3.4. Neuron nuclei imaging and counting

For the quantification of retinal ganglion cell loss, retinas were prepared as wholemounts (retinal ganglion cell side up) and stained with a Hoechst 33342 (Sigma, UK) solution of 1 mg/ml bisbenzimide in PBS for 20 minutes, washed 3 times in PBS for 5 minutes each and mounted in Prolong Gold antifade medium (Invitrogen, UK). The number of cells in the retinal ganglion cell layer was counted to provide an index of cell damage. Although amacrine cells would have been included in the analysis (Cowey and Perry, 1979; Munemasa et al., 2008; Perry, 1981), this has been validated in the mouse glaucoma model as a useful surrogate measure of retinal ganglion cell damage that avoids the variability associated with RGC labelling (Jakobs et al., 2005). Images of the RGCL (retinal ganglion cell layer) were obtained using a fluorescent microscope (Leica 6000B) linked to (Microbrightfield) and Stereo Investigator (Microbrightfield) software. Retinal specimens were placed on a motorized stage and the cells in the RGCL were imaged with a 20x objective in a total of 12 fields (each with an area of 217141.8 µm<sup>2</sup>) arranged in a grid centred on the optic nerve. The number of labelled cells in each image, after cropping the image to 113094.7 µm², was counted manually using the Cell Counter plug-in for ImageJ (NIH Image, NIH,

USA). Approximately 2.4% of the retina was evaluated for cell count. Standard morphologic criteria were applied for discriminating non-neuronal cells (endothelial and glial cells) from neuronal cells.

Statistical analysis was performed using commercial software SPSS ver. 16.0 for Windows). Normally distributed data were compared using One-way Anova. IOP measurements for single animals were expressed as mean  $\pm$  standard deviation (SD). Group values were expressed as means and standard errors of the mean (SEM).

#### 2.3.4. Croyosections of the anterior chamber

The eye-cups were transferred into 30% sucrose in 4% PFA for 24–48 hours before sectioning. Cryosections (10 µm thick, cut on a sliding microtome) of the anterior chambers prepared on gelatine-coated slides were stained with Harri's Haematoxylin which model and Eosin (H&E) (as described in section 2.1.6.2) and mounted under DPX (Raymond A Lamb) for DIC imaging. Section images were taken using a Leica DMRA2 brightfield microscope and Leica QWin v3 software.

# 2.4. Biochemical and immunohistochemical analyses of GAGs in a rat retina

Biochemical and immunohistochemical analyses of glycosaminoglycans (GAGs) in a rat retina were performed to identify differences in size and distribution of GAGs in young, old and glaucomatous retinas.

#### 2.4.1. Biochemical analysis

#### 2.4.1.1. Animals

Retinas used for biochemical analysis were obtained from 3 weeks old, old normal (including one chABC-injected eye) and old glaucomatous rat eyes (old eyes were over 6 months old). The adult normal eyes were contralateral to the glaucomatous eyes injected with magnetic beads.

#### 2.4.1.2. Guanidine extraction

After the rats were killed using CO2, retinas were dissected and placed directly into the extraction buffer consisting of: 4 M guanidinium chloride, 0.05 M sodium acetate containing 0.01 M Na2EDTA, 0.1 M 6-amino hexanoid (caproic) acid. Directly before use, inhibitors were added to the extraction buffer: 5 mM benzamidine-HCl and 0.5 mM phenylmethylsulphonylfluoride (PMSF). The extraction was carried out at 4°C for 48h with continuous rolling. After extraction, the samples were centrifuged and supernatant was retained and dialysed exhaustively against Milli-Q grade water using Spectro/Por Dialysis Membrane 25mm/16mm (Spectrum Laboratories, Inc.).

#### 2.4.1.3. Protein assay

Protein assay was performed using Quant-iT Protein Assay Kits (Invitrogen, UK) according to manufacturer instructions.

#### 2.4.1.4. SDS-PAGE

Sodium dodecyl sulphate polyacrylamide gel electrophoresis (SDS-PAGE) was used to separate proteins according to size. Proteinase-free chondroitinase ABC (Sigma) (0.01 unit/10  $\mu$ g of GAG) was added to each sample to digest CSPGs and generate chondroitin sulphate stub epitopes. Digestion was carried out overnight at 37°C. Samples were diluted with an equal volume of 2X sample buffer, 1M Tris Acetate, pH 8 (0.125 M Tris HCl, 4% SDS, 20% glycerol and 0.01% bromophenol blue pH 6.8) with 5%  $\beta$ -mercaptoethanol (Sigma). Samples were then boiled for 5 minutes to allow denaturation of the proteins prior to being loaded onto 4-12% Tris-glycine gels (Invitrogen) together with a marker (Bio-Rad, All Blue). Eighty  $\mu$ g GAG was loaded per lane. Samples were then subjected to electrophoresis in SDS-PAGE running buffer (192mM Glycine, 0.1% SDS and 25mM Trizma pH 8.3) at 120-150V.

#### 2.4.1.5. Western blotting

Following SDS-PAGE, proteins/proteoglycans were transferred onto nitrocellulose paper (Scheiler and Schuell Protran BA 83) in SDS-transfer buffer (25 mM Trizma, 192 mM Glycine, 20% Methanol, pH 8.1-8.4) at 100V for 1 hour using the Bio-Rad electrophoretic transfer system. That was followed by blocking the nitrocellulose membrane with 5% bovine Serum Albumine (BSA) (Sigma) in PBS on a rocking plate for 1 hour. After washes in PBS, the membrane was incubated overnight at room temperature with primary antibodies diluted in 1% BSA in PBS as follows: mAbs 2B6 (1: 100), 3B3 (1:10), 6B4 (1:100), 1B5 (1:100). PBS was then used to remove unbound primary antibodies, following addition of the secondary alkaline phosphatase (AP) conjugated mouse antibody (Promega) at 1:7500 dilution in 1% BSA in PBS for 1 hour at room temperature. Unbound secondary antibodies were then rinsed off with three 10 minutes washes in PBS. Finally, bands were visualised using the substrate of 10 ml AP buffer (100 mM NaCl, 5mM MgCl2 and 100 mM Tris base pH 9.55) with 66 μl Nitro Blue Tetrazolium (NBT) (Promega) and 33 μl 5-bromo-4-chloroindol-3-yl phosphate (BCIP) (Promega) at room temperature until colour had developed. The reaction was stopped by washing the membrane with water.

### 2.4.2. Immunohistochemistry

#### 2.4.2.1. Animals

Immunohistochemical analysis was conducted on retinal sections obtained from 8 weeks old, old normal and old glaucomatous rat eyes (old eyes were over 6 months old). The old normal eyes were contralateral to the glaucomatous eyes injected with hypertonic saline.

#### 2.4.2.2. Preparation of wax sections

Rat eyes were enucleated and the anterior chamber was cut away from the rat eye. The eyes were dehydrated through a series of increasing alcohol concentrations (v/v distilled water) as follows: 50% alcohol for 30 minutes, 70% alcohol for 1 hour, 90% alcohol for 1 hour, 100% alcohol for 1 hour and 100% alcohol for 30 minutes. Dehydrated tissue was then immersed in 50% v/v mixture absolute alcohol/xylene for

10 minutes and twice 100% xylene for 10 minutes. Then, most of the xylene was poured off and the eyes were warmed by placing in a wax oven for 10 minutes. Tissues were blotted on filter paper and placed into molten wax in clean pots in the oven for 30 minutes to remove xylene, then transferred to fresh molten wax and left overnight to ensure wax had impregnated the tissue. Finally, tissues were embedded in wax as described above and then refrigerated overnight. The wax blocks were removed from the mould, trimmed and then 7 µm serial sections were cut on a microtome (Microm HM330). Selected sections were placed into a cold water bath, then into a hot water bath (40°C), and finally transferred onto microscope slides with an adhesive coating (Histobond Lamb, UK). The slides were dried on a hot plate at 36°C and then incubated at 56°C in an oven overnight to allow the sections to adhere to the slides.

#### 2.4.2.3. Chondroitinase ABC digestion and immunostaining using DAB method

Wax sections were dewaxed by immersion in two changes of fresh xylene for 10 minutes each and rehydrated through a series of decreasing alcohol concentrations (v/v distilled water) twice for 5 minutes in 100% alcohol, 3 minutes in 90% alcohol and 3 minutes in 70% alcohol, followed by washing in cold running water for 5 minutes. The space around the sections was marked with a hydrophobic marker. Chondroitinase ABC (0.4U chABC/1ml buffer) (Sigma, UK) was pipetted onto the sections to digest GAGs. The slides were left at 37°C for 2 hours. After 2 hours, the slides were washed in PBS for 5 minutes and then blocked with 0.25% fish skin gelatine, 5% goat serum, 0.1% Triton X-100 in PBS for 1 hour at room temp. The block was removed and primary antibodies were added at 1:100 dilutions in PBS (2B6, 3B3, 1B5,) or at 1:10 dilution in PBS (6B4). Monoclonal antibodies 2B6, 3B3, 1B5 and 6B4 are specific to chondroitinase-generated chondroitin-4-sulphate (C4S), chondroitin-6-sulphate (C6S), chondroitin-0-sulphate (C0S) disaccharide epitopes and aggrecan core protein IgD domain, respectively. Following an overnight incubation at 4°C, the slides were washed 3 times for 5 minutes in PBS. Goat anti-mouse biotinylated secondary antibody diluted 1:100 in PBS was added to the slides and left at room temp for 1 h. After washing slides 3 times for 5 minutes in PBS, Vectastatin ABC reagent (antibiotin) (Vector, UK) was applied to slides for 30 minutes to detect immunolabelling. The slides were washed in PBS for 5 minutes, then DAB reagent

(peroxidise substrate solution) (Vector, UK) was used to visualise immunolabelling according to manufacturer's instructions except that nickel-brown solution was not added to give a brown colour. Development of colour reaction was carried out for a maximum of 10 minutes. The slides were washed in water, dehydrated through a series of alcohols, cleared in xylene and mounted in DPX.

In addition, immunohistochemistry was conducted on a single chABC-injected, non-glaucomatous retina to confirm the presence of the enzyme in a rat retina following an intravitreal injection. The protocol used was as described above except that the primary antibody dilutions (3B3, 1B5, 2B6) were pooled together.

**Chapter 3: Retinal explant culture** 

#### 3.1. Introduction

## Establishment of a retinal explant culture technique

Retinal explant cultures serve as a model of glaucoma because the explanation of the retina requires the severing of all axons within the optic nerve and the consequential degeneration of RGCs. This system is particularly useful for experiments that cannot be performed *in vivo* due to limitations involving tissue access, confounding systemic factors, or control over microenvironment. Although tissue culture systems cannot reproduce the complexity of the natural environment completely, they provide a system that is more controllable and stable than *in vivo* systems. The control over this *in vitro* system can be further enhanced by using defined, serum-free media formulations (Johnson and Tomarev, 2010).

One way of transfecting retinal explants is to deliver genes by particle bombardment, also known as "gene gun" delivery or "biolistics". This technique, first developed by Sanford, Klein and colleages as a method of gene transfer to plant cells, is a physical method of cell transfection in which high density particles coated with genes are accelerated to a high velocity by a gun apparatus to penetrate cell membranes (Klein et al., 1992; Sanford et al., 1987). A main advantage of this method, as compared to other transfection techniques, is that it is not dependent on target cell characteristics such as electrical potential, specific ligand receptors and /or the structural components on the cell surface (Uchida et al., 2009). This method has been useful in efficient transformation of various organisms and targets including mammalian cells (Zelenin et al., 1989), bacteria (Smith et al., 1992), fungi (Armaleo et al., 1990) and intracellular organelles (Johnston et al., 1988). In contrast to viral techniques, the biolistic transfection requires less advanced molecular biology facilities and is devoid of the side effects related to the use of recombinant viruses. In addition, the location of transfection can be determined by the specific areas of the tissue that are bombarded by gold particles. However, the biolistic transfection technique might contribute to the difficulties encountered in keeping the cultures alive due to mechanical stress resulting from the procedure. Therefore, the pressure wave should be minimised in order to avoid mechanical damage of the culture while maintaining enough particle acceleration for the desired degree of penetration (Lo et al., 1994).

#### Experimental design

The purpose of the present study was to optimise culture conditions for an adult rat retina, to allow retinal explants to be maintained over a period of time sufficient to express fluorescent proteins in retinal culture, which is a key factor determining good labelling (section 2.1 & 2.1.2). A subsequent aim was to optimise parameters for gene gun delivery technique into retinal ganglion cells (section 2.1.5). The expression of genes delivered to retinal ganglion cells by particle-mediated transfer enabled an investigation of the morphology of retinal ganglion cells and the effects of expressed proteins on morphological changes of the cells in the axotomised retina (section 2.1.5.1). Another method of cell labelling used in this study was the diolistic method, which enabled random RGC labelling with gene gun propelled lipophilic fluorescent dye, DiI, coated particles (section 2.1.5.2). As with the biolistic technique, the diolistic method enables the visualization of the dendritic field, the cell body, and the intraretinal axon of each labeled neuron (Qin et al., 2006). Both techniques, biolistic and diolistic, require viable tissue to label RGCs. However, the "shooting" with the diolistic technique can be done almost immediately after retinal explanation whereas biolistics requires at least 24 hours of culture before the labelled cells can be observed. In general, better labelling is obtained with the biolistic technique due to the expression of fluorescent proteins.

The initial step for optimisation of culture conditions was to assess the effects of various media formulations on the viability of retina in culture (sections 3.2.1 & 2.1.4). The viability of the retinal preparations incubated in two different media formulations was compared using propidium iodide and a vital dye calcein. Propidium iodide is a red marker of necrosis that labels the nuclei of non-viable cells but cannot cross the membrane of viable cells (Smith et al., 2007). Calcein is retained in cells with intact membranes, where the nonfluorescent calcein is converted to a green-fluorescent calcein (Caspi et al., 2007; Decherchi et al., 1997).

Since the initial results showing transfected RGCs were difficult to reproduce (section 3.2.2), it was likely that the process of transfection might affect the survival of retinas. To understand the effects of biolistic transfection on the culture survival, the retinas were shot with gold particles (1.6  $\mu$ m diameter, 0.2  $\mu$ g plasmid / cartridge, 20 mg gold for 20 cartridges) at 150 psi using a filter with 70  $\mu$ m pore size to protect the tissue

from the shock wave and the viability of the non-shot retinal explants was compared to the viability of the explants propelled with plasmid DNA-coated gold particles 2 days post shooting, using the vital dye, calcein (sections 3.2.3 & 2.1.4).

Once the culture conditions and biolistic transfection were optimised, it was possible to study the effects of various factors on neuronal survival and the number of axonal growth cones, as described in sections 3.2.5 & 2.1.6. Statistical analyses were performed using Mann-Whitney Test in SPSS 16.0.

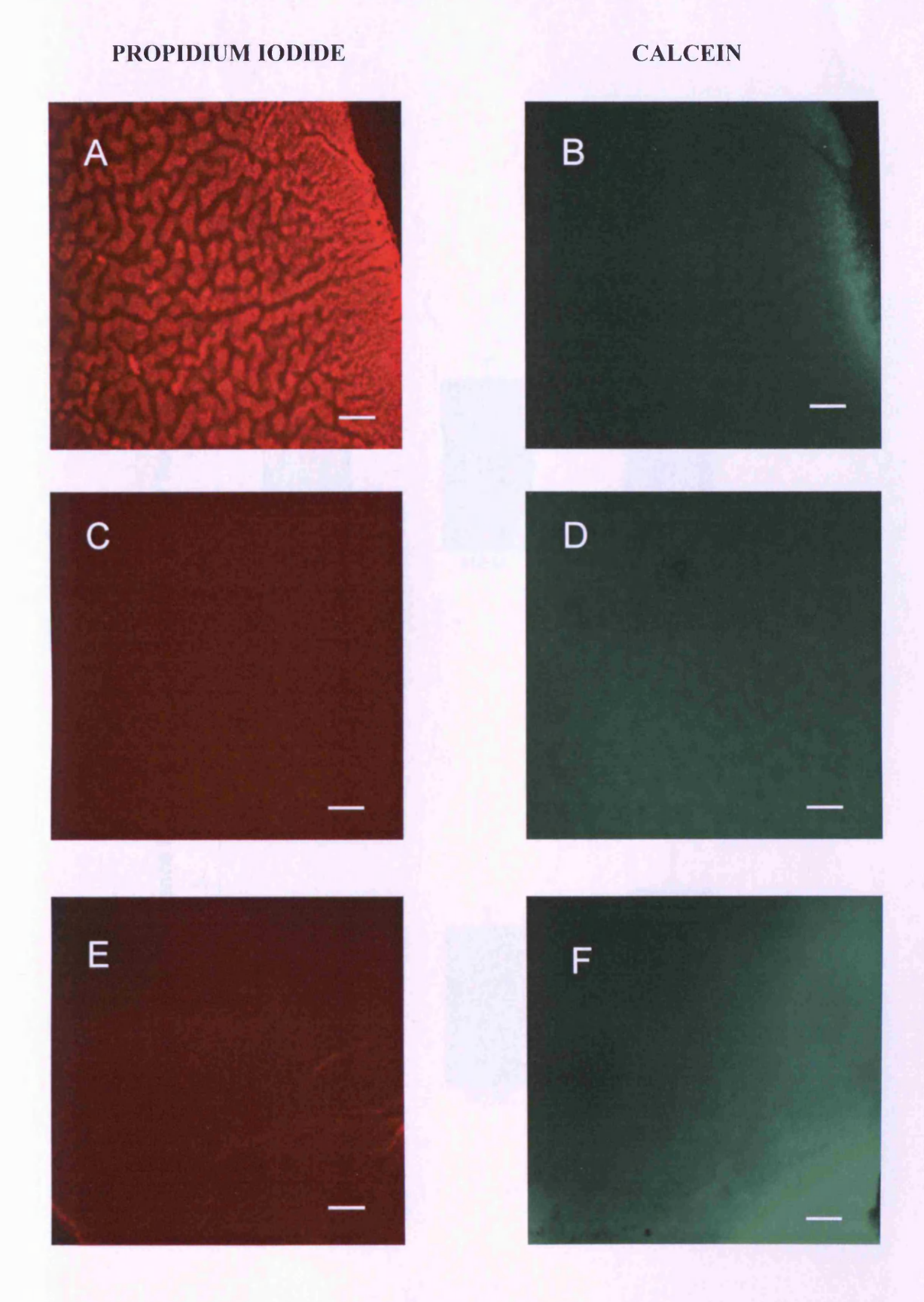
### 3.2. Results

# 3.2.1. Assessment of retinal explant viability with calcein AM and propidium iodide

Retinal wholemount preparations were cultured for 1 day in duplicate in 50% Dulbecco's Minimal Essential Medium (as described in the section 2.1.3, according to Gutierrez et al., 2005) or Neurobasal-A containing 2% B27 supplement, 1% N2 supplement, 0.8mM L-glutamine and 100U/ml penicillin/streptomycin (according to Wang et al., 2002) or in Hank's Balanced Salt Solution (HBSS) for control. The retinas were stained with propidium idodide and calcein AM to asses the viability of tissue. The results were based on a single experiment (Figure 3.1).

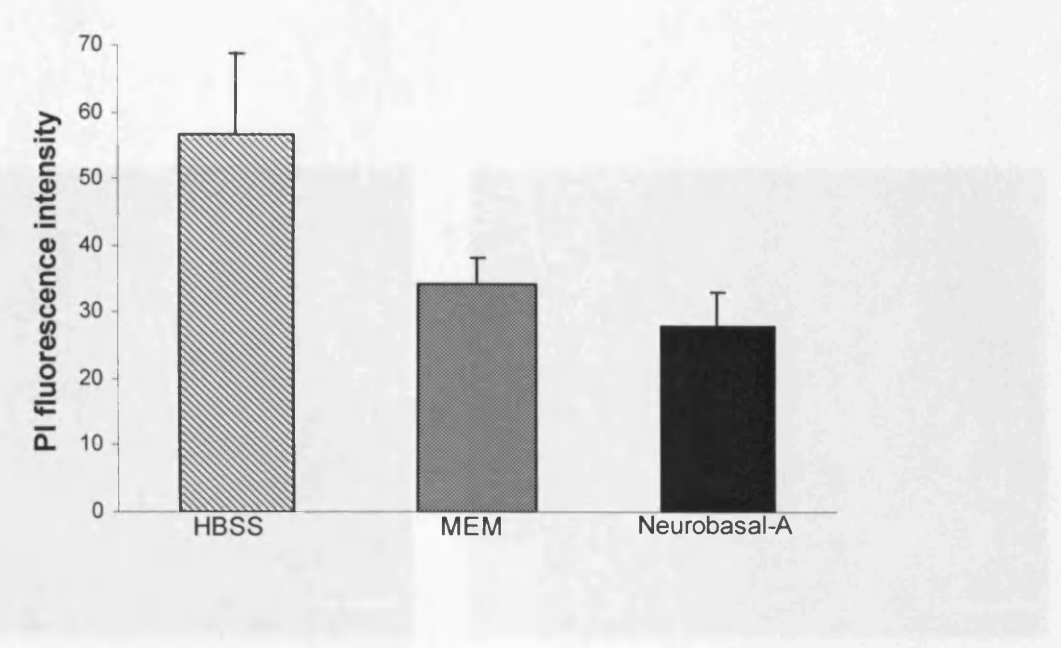
The mean values of calcein and propidium iodide labelling intensity in explants were compared to determine differences in the viability of tissue cultured in different media. The method of measuring intensity (RGB±SD) is described in Methods Chapter 2, section 2.1.4.1. The intensities of red propidium iodide staining were 56.50±12.19, 34.19±3.86 and 27.94±5.24 in retinas incubated in HBSS, Dulbecco's Minimal Essential Medium and Neurobasal-A medium, respectively (Figures 3.1A, C, E & 3.2A). The fluorescent intensities of calcein staining were 24.27±3.2, 31.51±3.53 and 38.45±17.70 in retinas incubated in HBSS, Dulbecco's Minimal Essential Medium and Neurobasal-A medium, respectively (Figures 3.1B, D, F & 3.2B).

After 3 days in culture, intensive staining with calcein AM (67.43±10.33) and low counterstaining with propidium iodide (28.55±1.95) were observed in retinal explants, indicating the good viability of the specimens (Figure 3.3).



**Figure 3.1.** Fluorescent images of wholemount retinal explants stained with propidium iodide (A, C, E) and calcein (B, D, F) cultured in HBSS (control) (A, B), MEM (C, D) and Neurobasal-A (E, F) for 1 day. Scale bars: 50 μm.







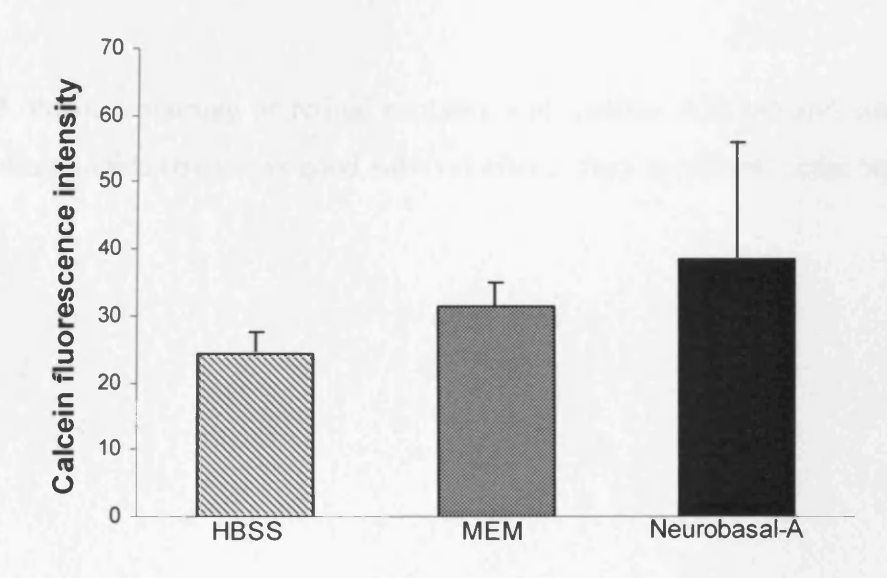


**Figure 3.2.** Mean values of propidium iodide (PI) (A) and calcein AM (B) fluorescence intensity from retinal explants, based on a single experiment. Diagonal bars indicate fluorescence intensity in explants cultured in HBSS, grey in MEM and black in Neurobasal-A medium. Error bars indicate standard deviation (SD).

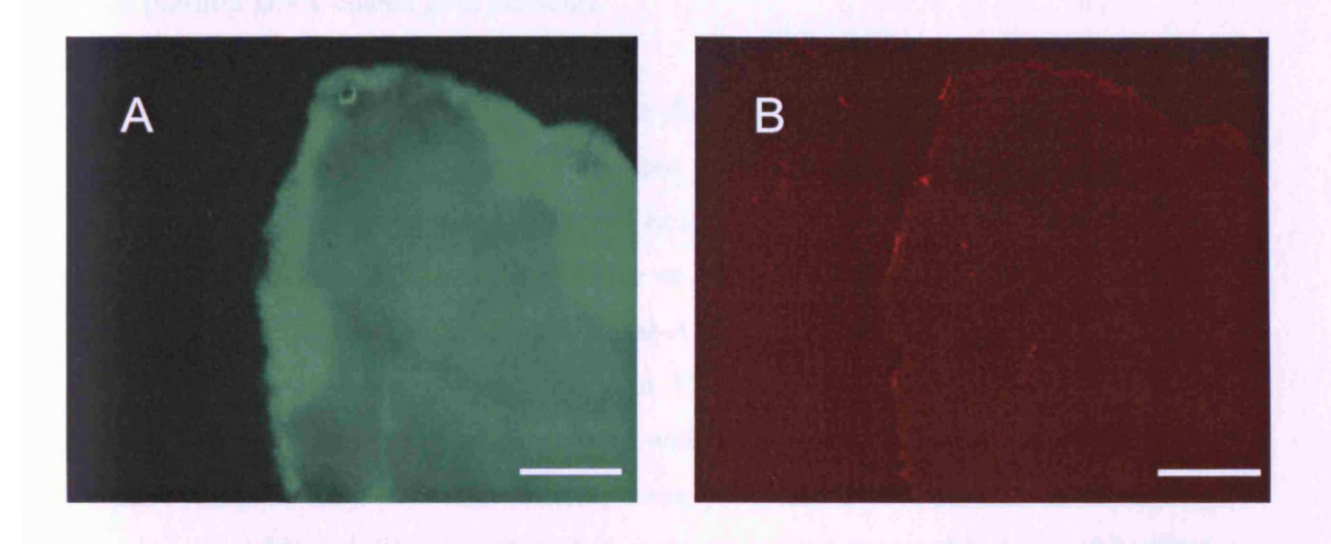


Figure 3.3. Positive staining of retinal explants with calcein AM (A) and counterstaining with propidium iodide (B) shows good survival after 3 days in culture. Scale bars: 500 μm.

#### 3.2.2. Evaluation of the biolistic transfection technique

Since assays (section 3.2.1) demonstrated the viability of explants after 3 days in culture (Figure 3.3), the applicability of the particle-mediated gene delivery to the tissue was assessed. In the present study, the success of plasmid delivery was examined by the observation of fluorescent protein expression after biolistic transfer of plasmid DNA-coated gold particles.

Since mice were more needily available for the experiments than rats, the initial experiments with biolistic transfection were performed using mouse retinal explants. Mice retinas were isolated (as described in section 2.1.2) and mounted ganglion cell side up on a black Millipore filter paper or on 0.4 µm Millicell culture plate insert (Millipore) and incubated in Neurobasal-A (as described in section 2.1.3). After approximately 1-2 hours of incubation at 37°C, the retinas were transfected by the biolistic delivery of gold particles coated with a pYFP only (Figure 3.4) or pYFP and pRFP (Figure 3.5). The microcarriers were propelled into the retina at a delivery pressure of 150 psi. Fluorescent protein expression was observed in 1 out of 2 retinas at 2 days post transfection (Figure 3.4) or in 1 out of 4 retinas at 1 day post transfection (Figure 3.5). In Figure 3.4, dendritic fields with somas were clearly visible in 4 cells (3 labelled red, 1 yellow and 1 green), while in 3 cells (2 labelled yellow and 1 green) only somas were visible. Axons were not visible in any of these cells. A neuron with a cell body, a medium-sized dendritic field and an axon was observed in Figure 3.5 B. Although the preliminary results showed the presence of some transfected RGCs, it was difficult to reproduce these results, suggesting that further optimisation of the technique was required.

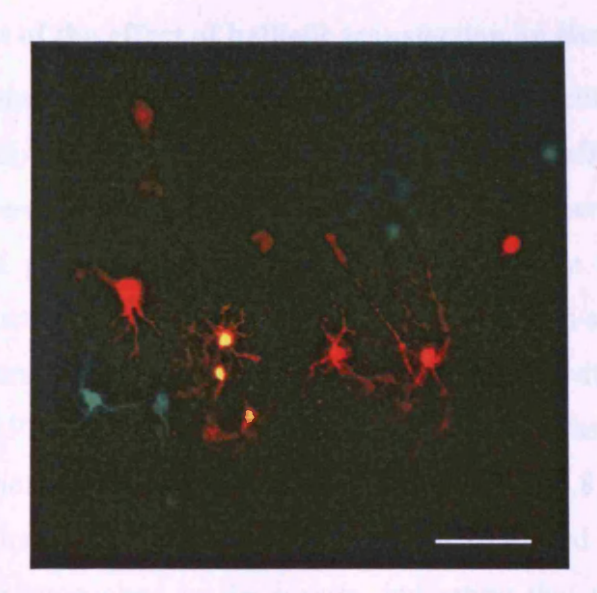


Figure 3.4. Expression of YFP and RFP in mouse RGCs, 2 days post transfection. Confocal image of RGCs transfected with expression plasmids for YFP (labelled green) and RFP (labelled red). Some cells were labelled with pYFP and pRFP (labelled orange). Scale bar:  $100 \, \mu m$ .

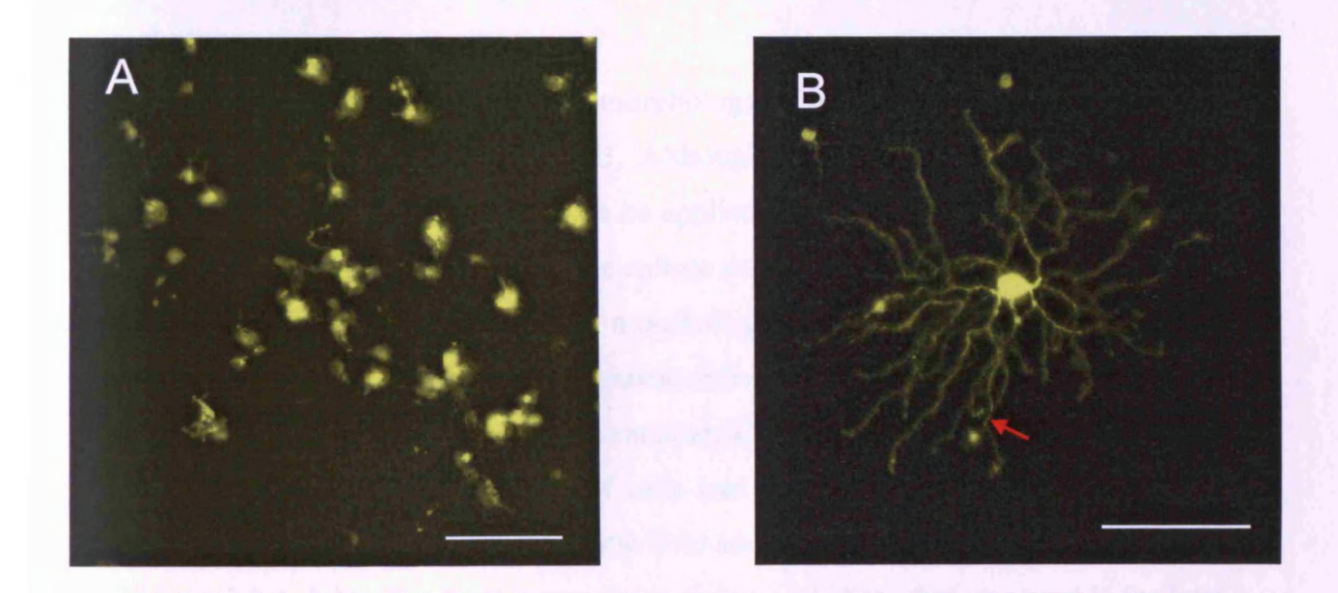


Figure 3.5. Expression of YFP in mouse RGCs, 1 day post transfection. Confocal images of RGCs transfected with expression plasmids for YFP (labelled yellow). The arrow indicates an axon. Scale bars: 100 μm.

#### 3.2.3. Assessment of the effect of ballistic transfection on tissue survival

Since the initial results showing transfected RGCs were difficult to reproduce (section 3.2.2), it was likely that the process of transfection might affect the survival of the retinas. The fluorescent intensity of calcein staining varied between the samples shot with DNA-coated gold particles using a gene gun and the non-shot samples, the fluorescent intensity of calcein being higher in the non-shot preparations, and displaying an intense green fluorescence (Neurobasal-A with serum, 47.06±4.60; Neurobasal-A, 35.91±7.52) (Figures 3.6 B, D & 3.7), in contrast to lower fluorescence intensity in the shot explants (Neurobasal-A with serum, 21.81±2.37; Neurobasal-A, 16.58±3.02) (Figures 3.6 C, E & 3.7). The explants incubated in HBSS (17.29±1.04) were found to be unattached to the inserts, indicating that tissue had died. These observations suggested that the viability of the culture was disrupted by the biolistic particle-mediated gene transfer, which was probably due to the mechanical shock associated with the procedure. The results were based on a single experiment.

# 3.2.4. Assessment of the morphology of labelled RGCs using the diolistic technique

In addition to ballistic labelling, the morphology of RGCs can be assessed in tissue labelled with a lipophilic dye — DiI. Although this strategy can not be used in combination with gene delivery, it can be applied to test the effects of various growth factors and other reagents added to the culture medium on the RGCs morphology and remodelling. In order to observe the morphology of labelled RGCs in fixed retinal explants, retina was labelled by the ballistic delivery of tungsten particles coated with DiI followed by fixation in 4% paraformaldehyde. The DiI staining of retinal culture demonstrated that the morphology of cells had been preserved during the diolistic labelling procedure. Cell soma, dendritic field and axon were all visible after labelling (Figures 3.8 A & B). The final protocol for diolistic labelling that was used in the later experiments (chapter 5) is described in section 2.3.3.2.

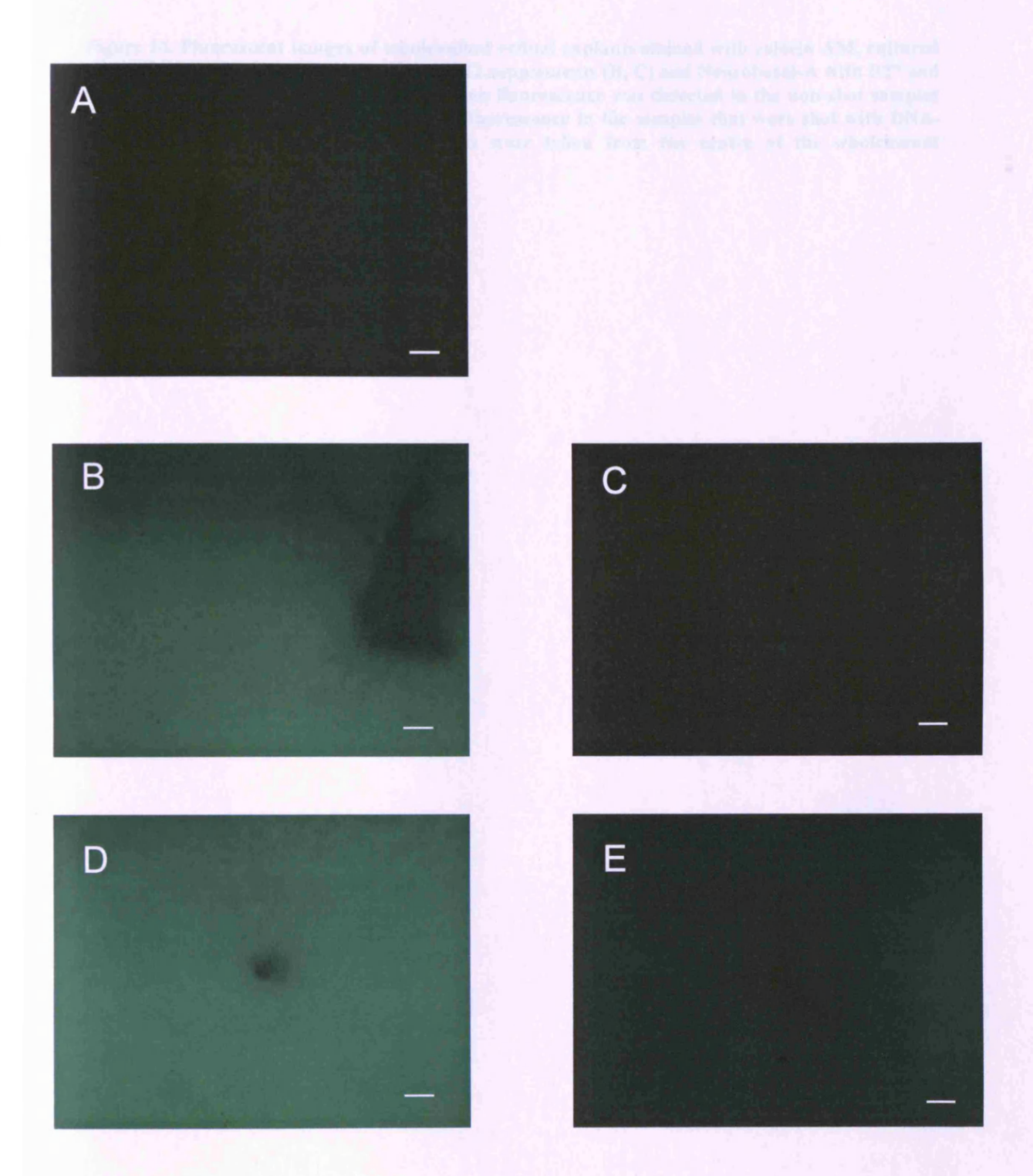
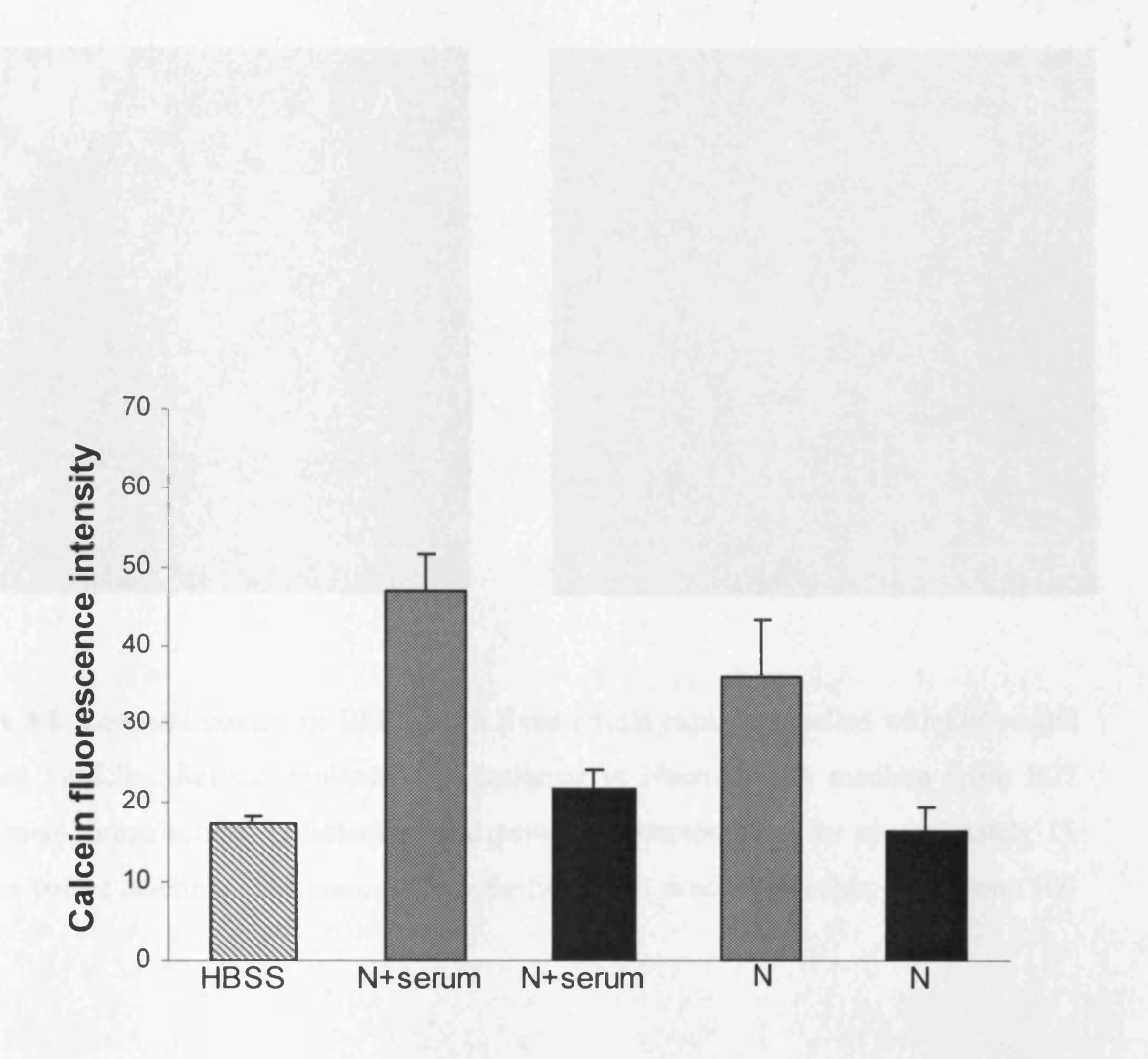


Figure 3.6. Fluorescent images of wholemount retinal explants stained with calcein AM, cultured in HBSS (A), Neurobasal-A with B27 and N2 supplements (B, C) and Neurobasal-A with B27 and horse serum (D, E) for 2 days. Intense green fluorescence was detected in the non-transfected samples (B, D), in contrast to the virtually absent fluorescence in the transfected samples (C, E). The gold particles were propelled into explants at a pressure 200 psi. The images were taken from the centre of the wholemount preparations. Scale bars: 200μm.

Figure 14. Fluorescent images of wholemount retinal explants stained with calcein AM, cultured in HBSS (A), Neurobasal-A with B27 and N2 supplements (B, C) and Neurobasal-A with B27 and horse serum (D, E) for 2 days. Intense green fluorescence was detected in the non-shot samples (B, D), in contrast to the virtually absent fluorescence in the samples that were shot with DNA-coated gold particles (C, E). The images were taken from the centre of the wholemount preparations. Scale bars: 200 µm.

Figure 3.6



**Figure 3.7.** Mean values of calcein AM fluorescence intensity in retinal explants, based on a single experiment. Diagonal bars indicate fluorescence intensity in explants cultured in HBSS, grey bars indicate fluorescence intensity in explants that were not shot with DNA-coated gold particles, incubated in Neurobasal-A medium with serum (N+serum) or Neurobasal-A medium (N) and black bars indicate fluorescence intensity in explants that were shot with DNA-coated gold particles, incubated in Neurobasal-A medium with serum (N+serum) or Neurobasal-A medium (N). The Error bars indicate standard deviation (SD).

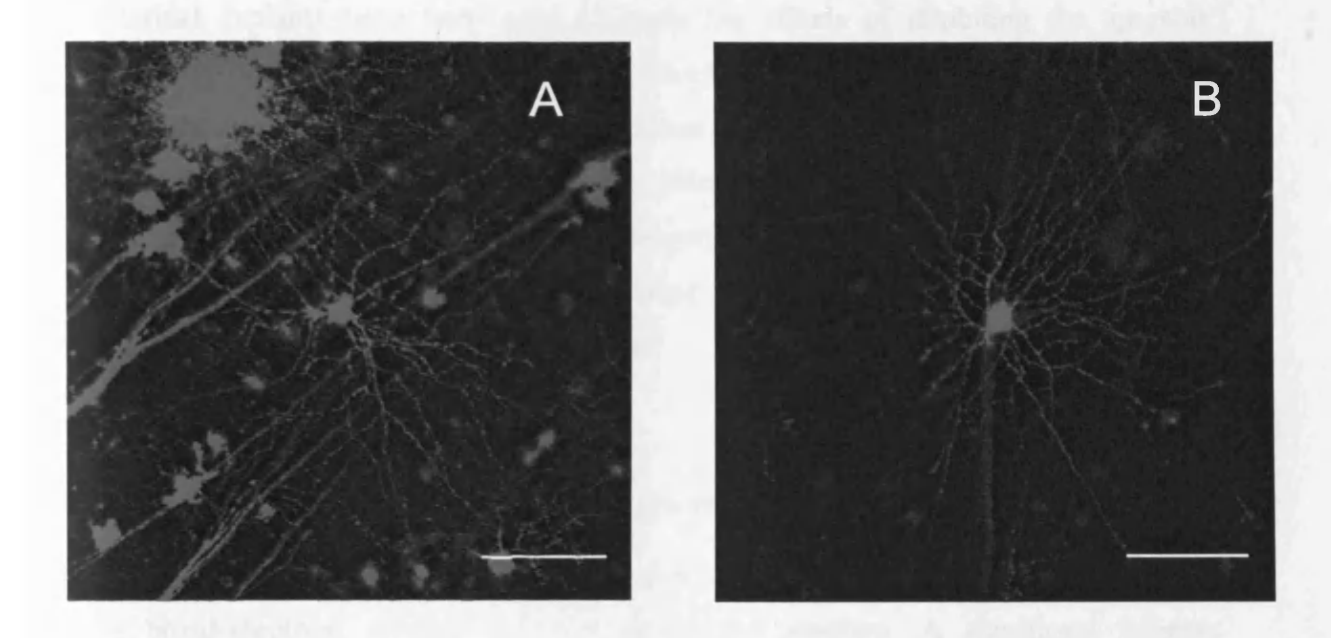


Figure 3.8. Confocal images of RGCs from fixed retinal explants labelled with DiI-coated tungsten particles. Retinal explants were cultured in Neurobasal-A medium (with B27 supplement, horse serum, L-glutamine and penicillin/streptomycin) for approximately 15 minutes before labelling. The somas, dendritic fields and axons are visible. Scale bars:  $100 \, \mu m$ .

# 3.2.5. Effects of caspase inhibitors and BDNF on neuronal survival and the number of axonal growth cones after axotomy

Retinal explants have been used to study the effects of inhibiting the apoptotic pathway on retinal ganglion cell death (Kermer et al., 2000). In the present study, biolistic transfection of retinal explant cultures as a model to study RGC survival and axonal growth cones formation in living retinal ganglion cells was used. The effects of caspase inhibitors and BDNF on neuronal survival and the number of axonal growth cones after axotomy were tested. Retinas were isolated from Brown Norwegian male rats at 8-12 weeks of age.

### 3.2.5.1. Effects of caspase inhibitor on the survival of transfected RGCs

Thirty one explants per group were cultured in the medium supplemented with either a broad-spectrum caspase inhibitor or control medium. A significant increase (P<0.05) in the number of RGCs was observed in retinas cultured with caspase inhibitor compared to control explants after 2 days in culture (Figure 3.9). Figure 3.10 shows an example of RGC cultured in caspase inhibitor-supplemented medium.

# 3.2.5.2. Effects of caspase inhibitor on the number of axons in the proximity of the optic disc

Growth cones on axons were observed in RGCs cultured in caspase-inhibitor supplemented with medium after 2 days in culture (Figure 3.11). The production of a new growth cone, a structure essential for axonal extension, is required for regrowth after axotomy (Bray et al., 1978).

The number of axons per number of transfected RGCs within 500  $\mu$ m of the optic disc was estimated in 31 control and 31 caspase inhibitor-treated explants. RGCs in caspase inhibitor-treated explants displayed a significant increase (P<0.05) in the number of axons within 500  $\mu$ m of the optic disc compared to control explants after 2 days in culture (Figure 3.12).

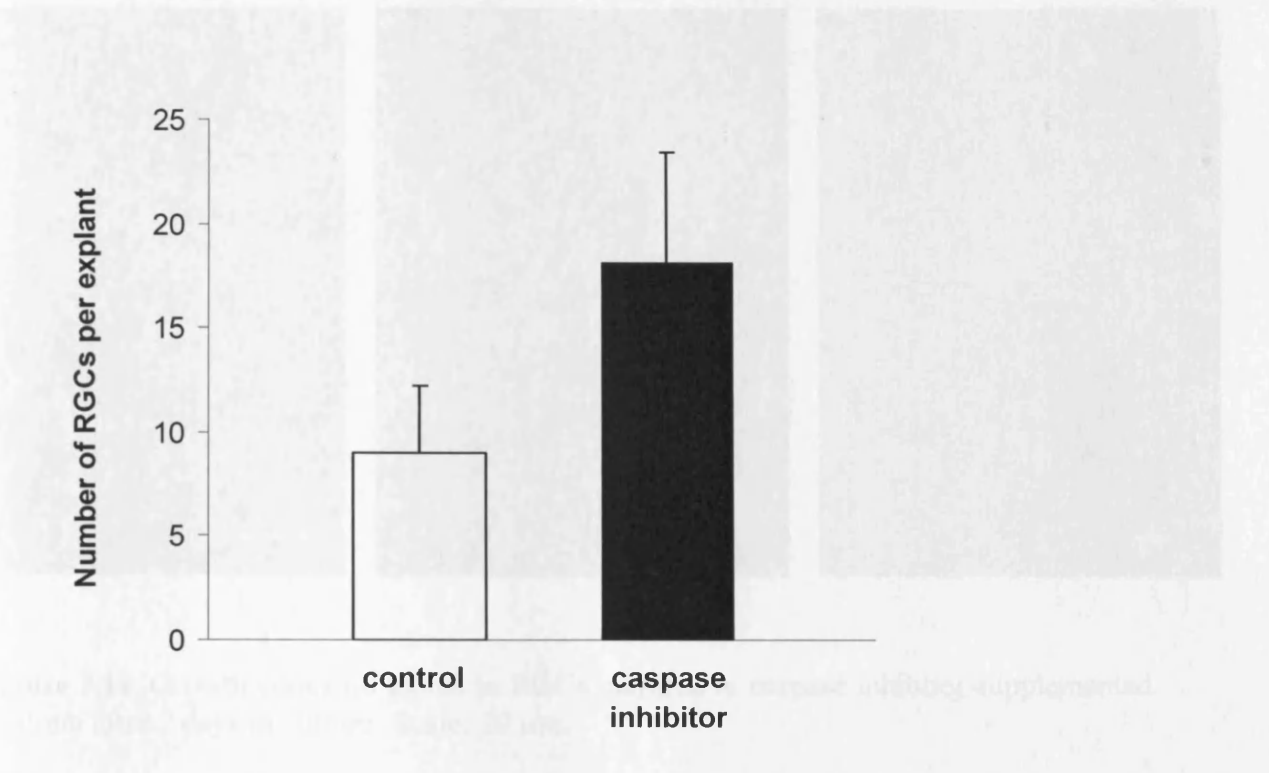


**Figure 3.9**. Average numbers of surviving RGCs per explant in control and caspase inhibitor-treated explants. A two-fold increase in the number of RGCs was observed in retinas cultured with caspase inhibitor than in control explants after 2 days in culture. Analyses are based on 31 explants per group. Error bars represent standard error (SEM).

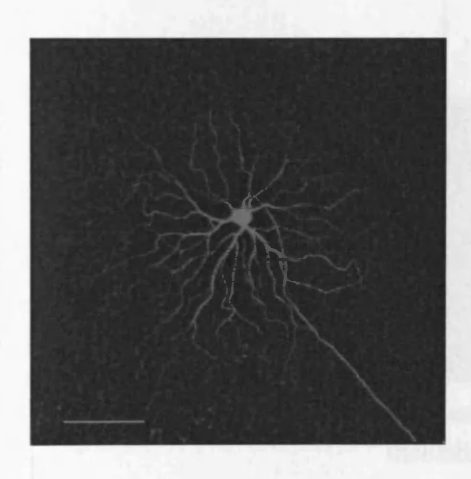


Figure 3.10. RGC transfected with YFP-expressing plasmid, cultured in caspase inhibitor-supplemented medium. Scale:  $100 \ \mu m$ .

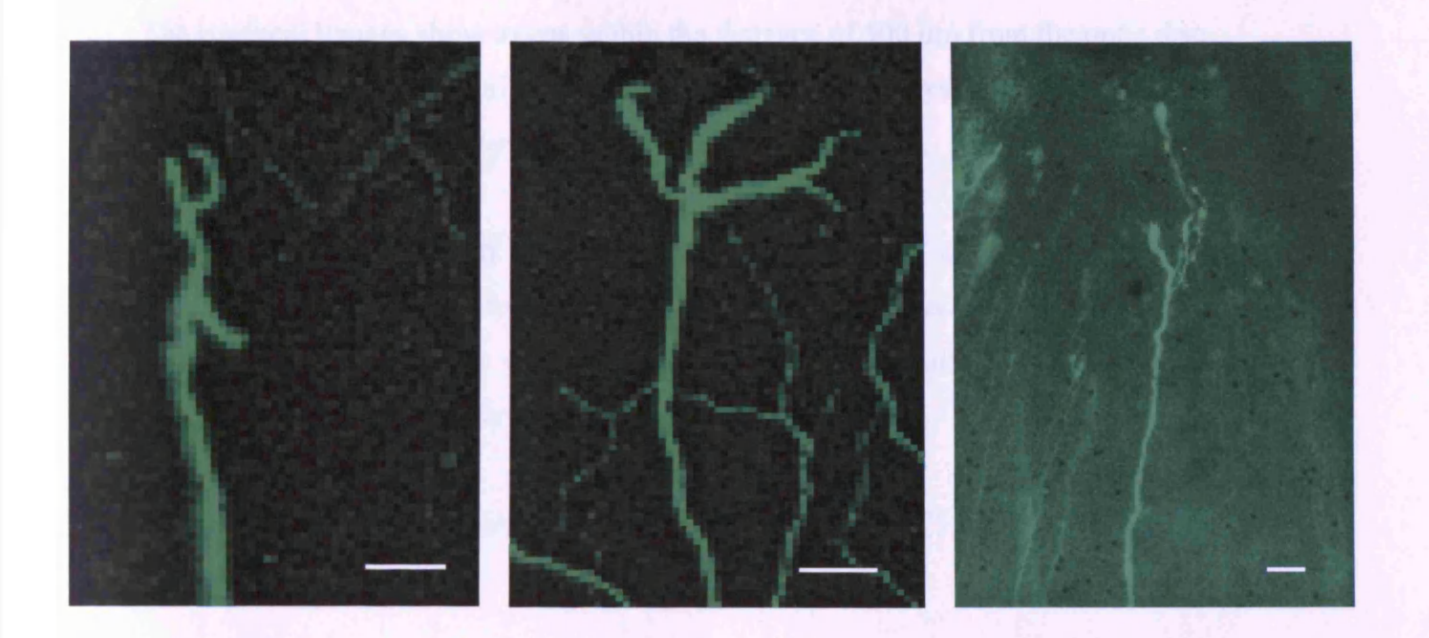


Figure 3.11. Growth cones on axons in RGCs cultured in caspase inhibitor-supplemented medium after 2 days in culture. Scale,  $20 \mu m$ .

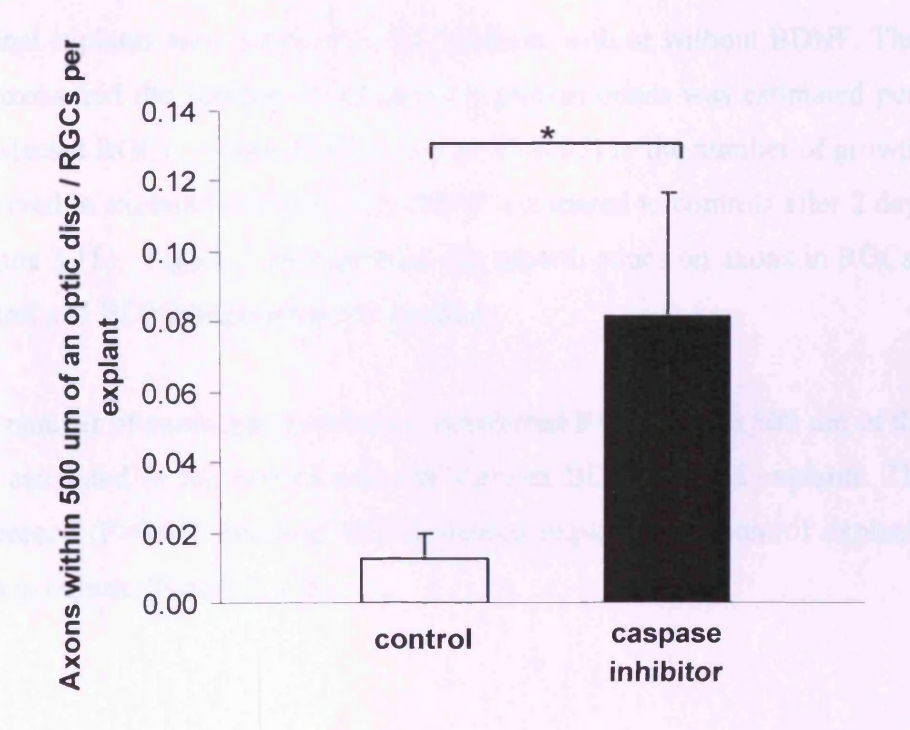


Figure 3.12. Number of axons within the distance of 500  $\mu$ m from the optic disc in control and caspase inhibitor-treated explants. RGCs in caspase inhibitor-treated explants displayed a significant increase in the number of axons within 500  $\mu$ m of an optic disc compared to control explants after 2 days in culture. Analyses are based on 31 explants per group. Error bars indicate standard error (SEM). \* p<0.05.

The confocal images show axons within the distance of 500 µm from the optic disc in control and caspase inhibitor-treated explants after 2 days in culture. The retinas were transfected with YFP-expressing plasmid (Figure 3.13).

Due to the observation of an increased number of axons near the optic disc, the distance from the axon tip to the optic disc was measured after 2 and 3 days in culture. The distance to the optic disc was reduced by approximately  $40\mu m$  after 3 days compared to 2 days in culture (Figure 3.14 A & B).

Axonal sprouting was observed after 2 days (Figure 3.14 C) but not after 3 days in culture (Figure 3.14 D).

# 3.2.5.3. The number of axonal growth cones and the number of axons in the proximity of the optic disc in BDNF-treated explants

Retinal explants were cultured in the medium with or without BDNF. The number of all axons and the number of axons with growth cones was estimated per number of transfected RGCs. A significant increase (P<0.05) in the number of growth cones was observed in explants cultured with BDNF compared to controls after 2 days in culture (Figure 3.15). Figure 3.16 illustrates the growth cones on axons in RGCs cultured in control and BDNF-supplemented medium.

The number of axons per number of transfected RGCs within 500  $\mu$ m of the optic disc was estimated in thirteen control and thirteen BDNF-treated explants. There was no difference (P>0.05) between BDNF-treated explants and control explants after two days in culture (Figure 3.17).

# optic discs

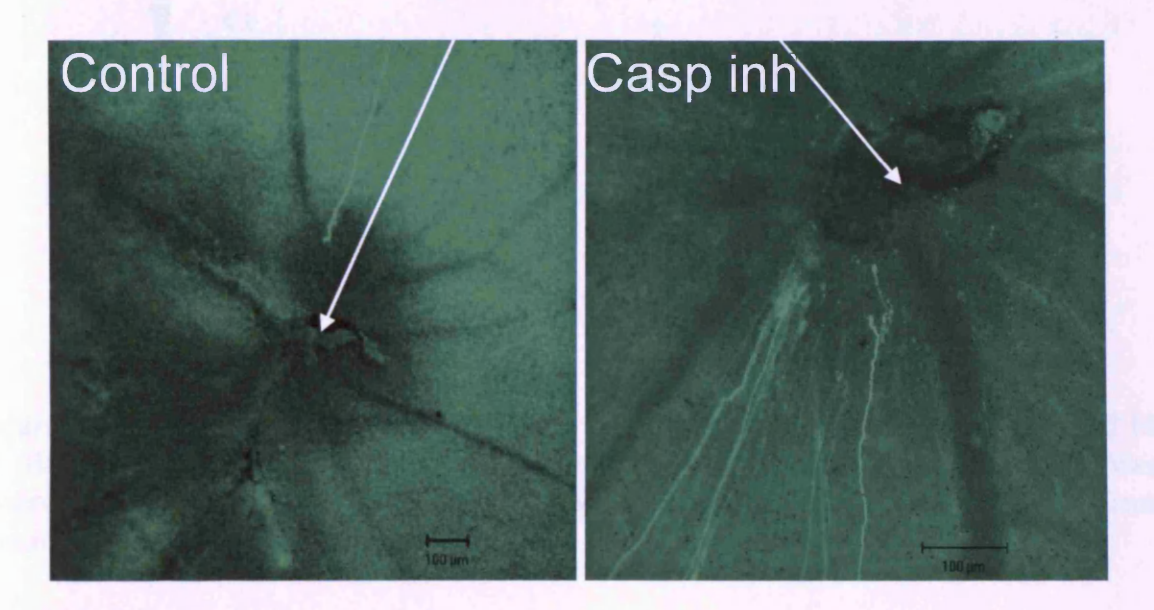


**Figure 3.13.** Confocal images of the optic discs from retinas transfected with YFP-expressing plasmid. Axons can be seen in the proximity of the optic discs in control and caspase inhibitor-treated explant after two days in culture. Scale:  $100 \mu m$ .

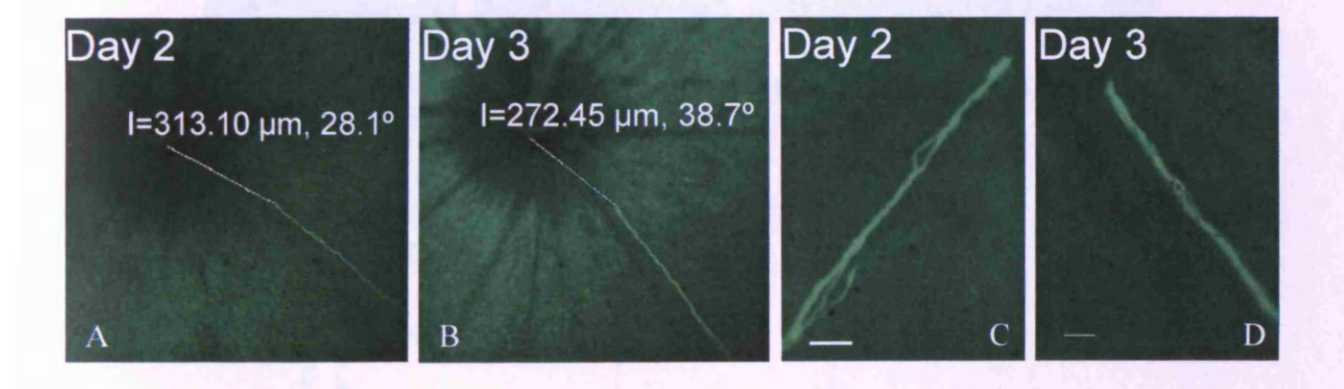


**Figure 3.14.** Axon in the proximity of the optic disc after 2 days (A) and the same axon after 3 days (B) in culture. The measured distance to the optic disc was reduced by approximately 40μm after 3 days compared to 2 days in culture. Axonal sprouting was observed after 2 days (C) but not after 3 days in culture (D). Scale: 20 μm.

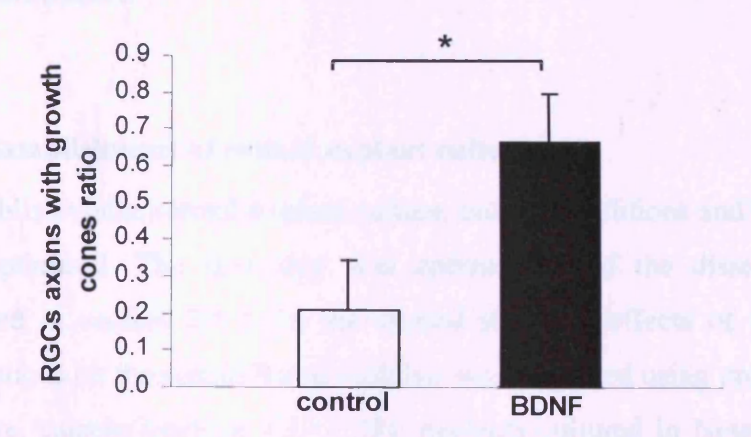


**Figure 3.15.** Ratio of axons with growth cones to all analysed axons (18 for controls and 10 for BDNF-treated axons). A significant increase in the number of growth cones was observed in explants cultured with BDNF compared to controls after 2 days in culture. Error bars indicate standard error. \* p<0.05.

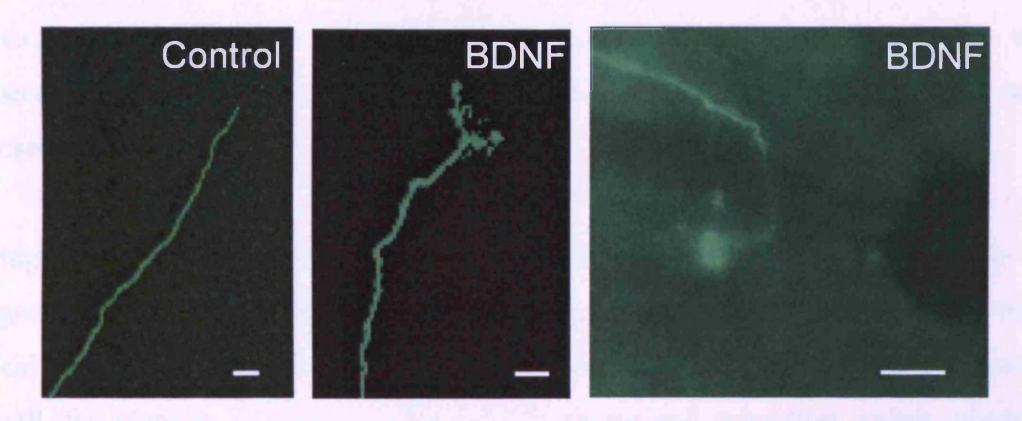
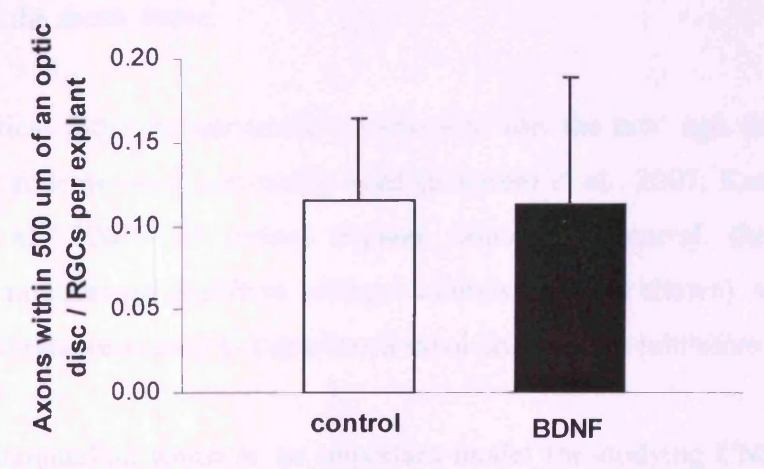


Figure 3.16. Growth cones on axons in RGCs from explants cultured in control and BDNF-supplemented medium after 2 days in culture. Scale, 20 μm.



**Figure 3.17.** Number of axons within the distance of 500 μm from the optic discs in control (not exposed to caspase inhibitor) and BDNF-treated explants. Analyses are based on 13 explants per group. Error bars indicate standard error.

#### 3.3. Discussion

### 3.3.1. Establishment of retinal explant culture

To establish viable retinal explant culture, culture conditions and biolistic transfection were optimised. The first step was optimisation of the dissection procedure, as described in section 2.1.2. In the second step, the effects of two different media formulations on the retinal tissue viability were assessed using propidium iodide and a vital dye, calcein (section 3.2.1). The explants cultured in Neurobasal-A had better viability than those incubated in Dulbecco's Minimal Essential Medium and control HBSS. Since the results showing the presence of some transfected RGCs were difficult to reproduce (section 3.2.2), the next step involved optimisation of the biolistic technique, including evaluation of the effects of biolistics on the viability of the explants. Viability assays using calcein demonstrated that retinal viability was reduced in the explants exposed to the biolistic procedure as compared to the non-exposed explants (section 3.2.3).

During the course of these experiments, it was established that the helium pressure for the gene gun and the pore size of the filter used to protect from the shock wave were critical to the survival and successful transfection (not all data have been shown). Overall, the viability of tissue (estimated by calcein and propidium iodide staining) was better when lower helium pressure (100 psi) with a 70  $\mu$ m filter was used. In addition to using lower pressure, a filter with 3  $\mu$ m pore size was introduced to protect tissues from the shock wave.

Another critical factor to successful transfection was the rats' age. In the literature, young adult rodents were commonly used (Koizumi et al., 2007; Kretz et al., 2004, Homma et al., 2007) for retinal explant culture. In general, the survival and transfection rate seemed higher in younger animals (data not shown), and therefore 8-12 weeks old rats were used in experiment involving caspase inhibitors and BDNF.

The adult mammalian retina is an important model for studying CNS function and diseases due to its easily accessible anatomical position, physiological properties and

highly organised structure. Organotypic retinal cultures, in contrast to dissociated cultures, can preserve cell-cell contacts and interactions between various cell populations (Xin et al., 2007). Two different approaches for culturing retinal tissue have been reported: explant and slice culture (Feigenspan et al., 1993; Gahwiler, 1981; Ogilvie et al., 1999). Feigenspan et al. (1993) used vertical slices of retina cultures on cover slips in a roller-tube system while Duenker et al. (2005) described a floating culture of whole-mount retina in a Petri dish (Duenker et al., 2005).

Retinal explant cultures of whole or partial retina were developed to maintain the tissue architecture characteristic of the retina *in situ* (Xin et al., 2007). Retinal explants, as other explanted tissues, preserve several histological and biochemical qualities of cells, allowing for long-term culture (Seigel, 1999). The explants retain the highest level of tissue preservation of all retinal cell culture systems and therefore have been used in *in vitro* studies requiring intact cell-cell associations (Xin et al., 2007).

Retinas are difficult to culture, primarily due to the high metabolism of the photoreceptors (Ames et al., 1992). Therefore, most studies have been performed using very young or neonatal retinas with low metabolic demands, since their photoreceptors are not yet functional.

In the literature, there are wide variations in the technical aspects of retinal explant culture, suggesting that there is no general agreement on the best procedure. Sun et al. (2002) cultured a wholemount retina from adult rats on a black Millipore filter in oxygenated Ames medium. A slightly different formulation of Ames' medium (with N2 supplement and horse serum) was used to culture adult rabbit retinas on Millipore Millicell culture inserts for up to six days (Koizumi et al., 2007). Two different types of culture chambers were used in their study (i.e. individual small dishes placed on a rocking plate and a large reservoir tank where the culture inserts were kept afloat on custom made stands), and the medium was agitated using a magnetic stirrer (Figure 3.19). The method described by Xin and colleagues (2007) applied HBSS for dissection of mouse retinal wholemounts, which were then cultured on poly-D-lysine/laminin coated glass coverslips in Neurobasal-A medium containing horse serum and B27 supplement. Wang et al. (2002) used DMEM plus N2 for retinal

explant culture and Neurobasal-A medium containing B27 and N2 supplements when prolonged culturing was necessary. DMEM with FCS and Fungizone were also used for mouse retinal culture for 4 weeks (Ogilvie et al., 1999).

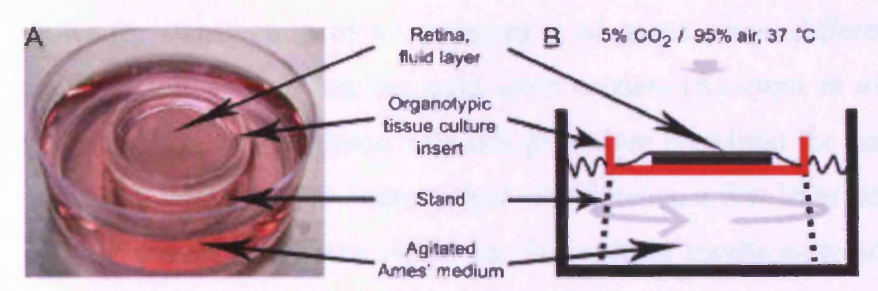


**Figure 3.18.** Incubation of rabbit retina. Photograph (A) and schematic diagram (B) of the hybrid interphase/perfusion chamber (copied from Koizumi et al., 2007).

Since the method for adult rat retinal explant culture had not been previously used in our laboratory, it was necessary to develop the technique for culturing retina over a period of time sufficient to study protein expression. To optimise this culture technique for adult rodent retina, various culture protocols, described previously by other investigators, were tested. In preliminary experiments, the effects of two different media formulations on the culture viability were compared. One of the tested media, 50% Dulbecco's Minimal Essential Medium, has been used to culture cortical slices from mouse cerebrum (Gutierrez et al., 2005).

Neurobasal-A is a serum-free medium that incorporates modification such as serum-free medium supplement B27, additional tropic factors and lower osmolarity to DMEM. The medium was formulated for the long-term viability of CNS neurons. It has resulted in excellent long-term viability of rat embryonic hippocampal neurons after 4 weeks in culture (Brewer et al., 1993). Adult hippocampal neurons were cultured for over 3 weeks in B27/Neurobasal culture medium during which they regenerated axons and dendrites (Brewer 1997). In addition, Neurobasal-A supplemented with B27 and horse serum allowed for maintenance of postnatal mouse retina for up to 14 days in culture (Xin et al., 2007). In our study, Neurobasal-A formulated, as described by Wang et al. (2002), was used. Using propidium iodide and calcein, the viability of explants incubated in Neurobasal-A and Dulbecco's Minimal Essential Medium media was estimated. In addition, a viability of explants cultured in Neurobasal-A for another 2 days was estimated (section 3.2.1).

The significant advantage of an organotypic retinal culture, when used with the biolistic technique, is that it enables expression of various genes without designing viral vectors or generating transgenic animals (Koizumi et al., 2007). Biolistic transfection is an efficient, rapid and flexible method of gene delivery to the retina. It allows for transfection of a combination of genes, since different plasmids can be coated simultaneously on the gold microcarriers (Koizumi et al., 2007). However, mechanical shock associated with this procedure may limit the survival of the culture (Lo et al., 1994). In two independent experiments, a few transfected cells at 1 and 2 day post-transfection were observed. Since these results were not reproducible, our next approach was to assess the effects of the particle-mediated gene transfer on the viability of the culture using the vital dye calcein. Retinal viability was found to be disrupted by ballistic transfection as compared to the viable explants not exposed to the procedure, probably due to the shock wave produced by the helium pressure, which was set at 150 psi. Another factor that might influence the survival of explants during the transfection procedure is the type of screen placed between the gun and the culture to protect the cells from the shock wave. A 70 µm nylon mesh screen, as described by Gutierrez et al. (2005), was used. Uchida et al. (2009) found that an optimal helium pressure was 75 to 100 psi for effective gene gun transfection, however damage increased considerably at helium pressure over 150 psi. The results indicated that physical cell damage was mainly the effect of collision of the gold particles with the cells during particle bombardment (Uchida et al., 2009). Considering our findings, the next strategy involved manipulation of the delivery pressure and using a screen with a lower pore size. The final protocol for biolistic transfection, used for experiments involving caspase inhibitors and BDNF, was 100 psi with a 3 µm screen (section 3.2.5).

The morphology of RGCs was assessed in fixed tissue labelled with DiI (section 3.2.4). The diolistic technique allows for fast labelling of numerous cells with a wide variety of colours (Gan et al., 2000). DiI labelling of RGCs from normal rat retina showed a well preserved neuronal structure.

# 3.3.2. Effects of caspase inhibitors and BDNF on neuronal survival and the number of axonal growth cones

In our study, a broad-spectrum caspase inhibitor increased the survival of RGCs and the number of axons in the proximity of the optic disc after axotomy (sections 3.2.5.1 & 3.2.5.2.). However, it was not established whether the increase in the number of axons was due to the rescue of dying axons or due to axonal regrowth. Exogenous BDNF enhanced the number of growth cones on the axons of RGCs, but BDNF administration, in the absence of caspase inhibition, did not have an effect on the number of axons in the proximity of the optic disc (section 3.2.5.3). However, due to the lack of controls, ie freshly isolated retina, this could not be confirmed.

Our observations showing that a caspase inhibitor increased the survival of RGCs in culture are consistent with previous studies. In addition, a number of studies suggested the effects of caspase inhibitors on axonal regrowth. A decreased amount of RGC death was observed in retinal explant cultured with a caspase-3 inhibitor (Manabe et al., 2002). Caspase inhibitors-1, -3, -8 and -9 and neurotrophic factors such as BDNF and CNTF were reported to have an effect on RGCs survival and neurite regrowth in explant culture (Oshitari and Adachi-Usami et al., 2003). The most effective in RGC rescue and neurite regrowth was the combination of CNTF and caspase-9 inhibitor (Oshitari and Adachi-Usami et al., 2003). These results suggested that neurite regrowth can be supported by caspase inhibitors by preventing RGCs apoptosis and allowing the rescued RGCs to regenerate neurites (Oshitari and Adachi-Usami et al., 2003). Another study found that BDNF and NT-4 (but not NT-3 or CNTF) significantly increased the outgrowth of early embryonic and adult regenerating retinal ganglion cell axons, however the effect was more subtle in adult explants (Avwenagha et al., 2003).

Other growth factors such as insulin-like growth factor (IGF-I) considerably enhanced survival and neurite outgrowth from adult rat RGCs in retinal explants via a wortmannin-dependent mechanism. The downregulation of IGF-I resulted in the final upregulation of caspase-3 leading to RGC apoptosis after optic nerve injury (Homma et al., 2007).

Apart from retinal explants, the effects of caspase inhibitors and neurotrophic factors on RGCs survival and regrowth were estimated in other *in vitro* systems as well as *in vivo*. BDNF was found to affect survival of cultured RGCs isolated from the perinatal rat retina (Johnson et al., 1986). Caspase inhibitors, when administered intraocularly at the time of the optic nerve transection, protected about 30-35% RGCs from death (Chaudhary et al., 1999).

## 3.4. Summary

The *in vitro* model of an organotypic retinal culture is relevant to glaucoma, since the process of explanation requires RGCs axotomy, resulting in severe axonal damage. The advantage of this model is that the conditions can be controlled more precisely than in *in vivo* glaucoma models. The ability to control the *in vitro* environment offers an opportunity to test the effects of long-term application of substances on retina as well as to study hypotheses that can not be tested *in vivo* (Johnson and Tomarev, 2010).

When used with biolistic transfection, this model allows for expression of proteins in the retina and the subsequent observation of changes in RGCs morphology during the experimental period. We found that the most critical parameters for the successful transfection were the helium pressure, the pore size of a filter between the tissue and a gene gun, and the age of animals.

The optimisation of an adult rat retinal explant culture technique together with biolistic transfection enabled the assessment of the effects of caspase inhibitors and BDNF on neuronal survival and axonal growth cones formation. A broad-spectrum caspase inhibitor enhanced the survival of adult RGCs and the number of axons in the proximity of the optic disc, while exogenous BDNF enhanced the number of growth cones on the RGC axons.

Chapter 4: Experimental glaucoma: profiling intraocular pressure, cell loss and optic nerve head damage in experimental glaucoma

#### 4.1. Introduction

#### 4.1.1. IOP profiles and cell loss

Considerable advances have been made in our understanding of the pathophysiology of glaucoma, helped in part by the availability of cost effective models of disease based on rodents, such as the rat and mouse (John, 2005; Morrison et al., 2008). While spontaneous genetic models of glaucoma exist (John et al., 1999), the use of models in which the precise onset of glaucoma can be determined is important for grading diseases and for the evaluation of novel therapies.

A variety of methods have been developed for the elevation of intraocular pressure (IOP), each with advantages and disadvantages. For example, cautery of episcleral vessels (Laquis et al., 1998; Naskar et al., 2002; Shareef et al., 1995; Urcola et al., 2006), perhaps the simplest method, runs the risk that it might comprise venous drainage of the choroid and therefore induce retinal effects unrelated to the elevation of IOP. Other methods, such as episcleral vein sclerosis with hypertonic saline (method described in results section 4.22) (Morgan et al., 2006; Morrison et al., 1997; Nissirios et al., 2008) limit the outflow of aqueous at the level of the trabecular meshwork to produce stable and moderate elevations of IOP with a low risk of choroidal damage (Morrison, 2005). However, the injections can be technically challenging. As a result of these considerations, alternative methods have been sought to induce experimental glaucoma in rodents. Laser occlusion of the episcleral vessels (Chiu et al., 2007; Levkovitch-Verbin et al., 2002; Martin et al., 2002; Pease et al., 2008; Siu et al., 2002; WoldeMussie et al., 2001) can be effective but works best with albino animals and requires use of a laser facility. More recently, methods based on obstruction of the trabecular meshwork with microscopic beads have been used (Urcola et al., 2006), following successful application of this technique in primates (Weber and Zelenak, 2001). The injection of microbeads into the anterior chamber is straightforward, does not require specialist equipment and can be applied to a range of species with only minor modification. Furthermore, the IOP elevation can be modulated with subsequent injections. Unfortunately, the principal disadvantage is that beads can be difficult to retain following injection, and as a result, they can locate to the pupil and compromise visualisation of the retina.

To address these issues, a novel technique for the induction of ocular hypertension using paramagnetic microbeads has been developed (see section 4.4). These beads have the advantage that they can be directed specifically to the iridocorneal angle in the rodent eye to optimise occlusion of the trabecular meshwork and facilitate visualisation of the fundus. Subsequent injections of beads can be given, as required, to further modulate the elevation in IOP.

# 4.1.2. OCT imaging studies: *in vivo* detection and monitoring of retinal damage in experimental glaucoma

The death of retinal ganglion cells axons is associated with thinning of the retinal nerve fiber layer (RNFL). RNFL thickness increases at the opening in the sclera, i.e. the optic disc. The edge of the disc carries axons that form the neuroretinal rim, while the centre of the disc is devoid of axons, forming a cup-shaped cavity recognised clinically as the optic disc cup (Elliot, 1917). The shape of the cup changes as a result of the degree of axonal loss in glaucoma; thinning of the neuroretinal rim occurs and the cup volume increases (Jonas et al., 1999).

According to recent studies, significant structural damage in the optic nerve head (ONH) and retinal nerve fiber layer (RNFL) may precede visual field loss. The Hypertension Treatment Study (OHTS) showed that disc changes preceded visual field abnormalities in more than 50% of patients diagnosed with glaucoma (Gordon et al., 2002). Therefore, many studies have focussed on the development of methods for improving the quantification of the RNFL. Over the last ten years, ONH and RNFL imaging has become widely used to diagnose early glaucoma and the disease progression (Li et al., 2010). The imaging technologies used to measure topographic parameters of the ONH and RNFL include confocal scanning laser ophthalmoscopy, scanning laser polarimetry and optical coherence tomography (OCT) (Ervin et al., 2002; Mohammadi et al., 2004; Zangwill et al., 2005).

OCT was proposed as a powerful, noninvasive, cross-sectional imaging technique in 1991 (Huang et al., 1991; Huang et al., 2010) In contrast to the methods described above, clinical OCT apparatus provides high-resolution cross-sectional images of the retinal nerve at the margin of the optic disc (Cense et al., 2004; Jaffe and Caprioli,

2004). In this method, RNFL is measured relative to a reference plane, normally located at the margin of the optic disc. Although this geometric estimate of RNFL is improved compared to confocal or polarimetric techniques, it might be affected by optic disc tilt and deformations (Povazay et al., 2007b).

More recently, three-dimensional (3D) quantification of the RNFL became possible due to the development of very sensitive (Choma et al., 2003) fast frequency domain (spectral) OCT (FD-OCT) techniques (Cense et al., 2004; Leitgeb et al., 2004; Wojtkowski et al., 2004) coupled with ultrahigh-resolution OCT (Drexler, 2004). The imaging using this technique provides clear delineation of the RNFL relative to the scleral rim, an invariant retinal landmark (Povazay et al., 2007b). High-speed, ultrahigh-resolution OCT using spectral–Fourier domain detection offers several advantages for imaging the rat retina. The ultrahigh image resolution enables visualization of individual retinal layers while high-speed imaging enables acquisition of 3D-OCT data and high-definition OCT images (Srinivasan et al., 2006). Another important advantage of *in vivo* OCT imaging is that it allows an estimation of progressive glaucomatous changes within the same animals without the need for sacrificing them (i.e. within animal longitudinal studies).

The purpose of using OCT was to evaluate the changes in the RNFL thickness and optic nerve head in experimental glaucoma using frequency-domain optical coherence tomography imaging, operating either at 1050 nm (*in vivo* imaging) or 800 nm (*ex vivo* imaging). For *in vivo* imaging, the images were obtained from nine rats that were imaged before induction of experimental glaucoma by bead injection and up to two times after the induction of experimental glaucoma. 1050 nm was used for *in vivo* imaging because it performs better than 800nm in the event that the optical clarity of the anterior segment is compromised, as observed in the magnetic bead model, particularly in animals with high IOPs. For *ex vivo* imaging, the dissected retinas were imaged post mortem. In this case, ocular hypertension had been previously induced by injection of hypertonic saline.

### 4.1.3. Experimental design

Calibration of a rebound tonometer is required for accurate measurement of IOP in rat eyes. Therefore, the Tonolab rebound tonometer was calibrated in cannulated rat eyes (see section 2.2.2). Following calibration, the tonometer was used to monitor IOP in awake rats following topical ocular anaesthesia (Wang et al., 2005). Elevated IOP, an important risk factor for glaucoma, was initially achieved by an injection of hypertonic saline into the limbal episcleral drainage vessels (see sections 2.2.3 & 4.2.2). However, due to some technical issues related to the generation of this model, we subsequently developed a novel technique for the induction of ocular hypertension using paramagnetic microbeads (see sections 2.2.4.1 & 4.2.3). It has been suggested that the injection of microbeads would be the best and simplest way to induce experimental glaucoma (Urcola et al., 2006; Weber and Zelenak, 2001). However, to preserve the clarity of the optic axis and to optimise location of the beads to the iridocorneal angle, magnetic beads were used. The size of the beads was selected based on the dimensions of the trabecular meshwork. Therefore, a bead diameter of 5µm was selected since this seemed most likely to occlude the spaces reported in the rodent trabecular meshwork (Smith et al., 2001).

IOP measurements were made using a Tonolab rebound tonometer under topical anaesthesia, which allowed non-invasive determination of IOP (Wang et al. 2005). The use of a topical anaesthetic prevents any hypotensive (Jia et al., 2000) or neuroprotective (Fujikawa, 1995; Ozden and Isenmann, 2004) effects that might have been observed with general anaesthesia. Rats were housed in constant low-level light to stabilise the circadian variation in IOP that would normal maximise during the dark phase (Johnson et al., 2007).

The IOP profiles were generated for both glaucoma models (4.2.2 & 4.2.3.1). For the magnetic bead model, retinas were prepared as wholemounts and stained with Hoechst (see section 2.3.2). The mean densities of cells in the retinal ganglion cell layer (RGCL) in control and glaucomatous retinas were compared to estimate cell loss (see section 4.2.3.2). In addition, RGCs were counted in the rats injected with BSS and those in which magnetic beads were not redirected. These controls were produced

to assess the effect of BSS injection and the effect of using a magnet on the IOP elevation in the magnetic bead model.

A frequency domain optical coherence tomography (FD-OCT) (Choma et al., 2003; de Boer et al., 2003; Fercher et al., 1995; Gerd and Michael Walter, 1998; Leitgeb et al., 2003; Nassif et al., 2004) was used to image rat retinas in vivo (section 4.2.4.1 & 2.2.4.3). The system enables high-speed, high sensitivity and depth-resolved measurements of the retina due to analysis of the interference pattern in the optical frequency spectrum. The OCT data were processed for visualization using ImageJ. The steps involved: registration, filtering and reslicing. Manual segmentation was performed using custom-built Java code. Segmentation data were analysed and graphed using custom MATLAB code. Segmentation of the different layers was performed by distinguishing the texture of different layers and their interfaces. The retinal fibre layer (RNFL) thickness was segmented at the scleral rim (the inner limiting membrane, ILM, to the retinal pigment epithelium, RPE). The RNFL surface was easily identified in all images, and RNFL thickness was quantified from the OCT images of control and experimental eyes at different imaging times (before injection, 7-10 days or 17-32 days post injection). Progressive glaucomatous changes in an experimental rat eye were observed before bead injection, 3 weeks and 4 weeks after injection in OCT images. The cell loss and IOP profiles were estimated for 6 and 9 imaged rats, respectively.

The level of damage in experimental glaucoma induced by the injection of hypertonic saline was estimated by Optical Coherence Tomography *ex vivo* imaging (see section 2.3.1 & 4.2.4.2). The samples were imaged *ex vivo* by two optical coherence tomography systems, a 1300 nm Thorlabs Swept Source OCT (SS-OCT) and an 800 nm Three Dimensional Ultrahigh Resolution OCT (3D UHR-OCT). Three different types of retinal images were collected: 3D UHR OCT, enface OCT and UHR OCT depth profiles (cross sections of rat optic nerve head). The retinas were grouped from normal to advanced glaucoma according to the increasing integral IOP values. In addition, the OCT images from the rat CR308 were compared to the histological images of post mortem retinal sections from the same rat.

### 4.2. Results

### 4.2.1. Calibration of the Tonolab rebound tonometer in cannulated rat eyes

Figure 4.1 shows the calibration curves obtained when the tonometer was tested on freshly enucleated, cannulated rat eyes. The measurements were taken at 1mm (Figures 4.1 A & B) and 3mm (Figure 4.1 C) probe-to-cornea distances. The R-squared values showed good linearity (R2 = 0.90) at 3mm, suggesting that the rebound tonometer readings were proportional to the true IOP in rat eyes measured by a pressure transducer. However, the relationship between the true and measured IOP was less accurate (R2 = 0.67 - 0.88) when the tonometer was at 1mm distance from the cornea. Table 4.1 shows different parameters for calibration of the Tonolab rebound tonometer in cannulated rat eyes.

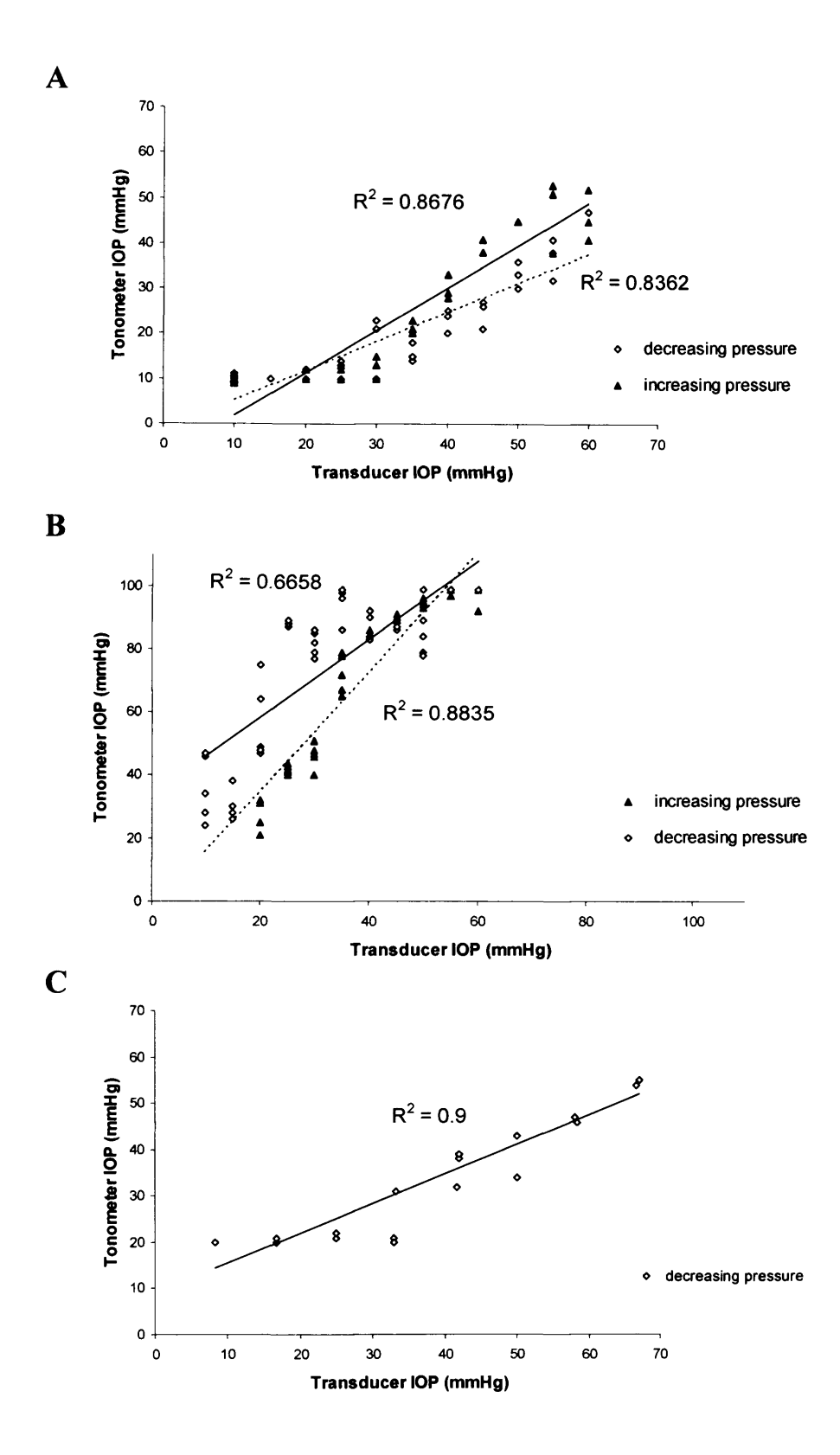
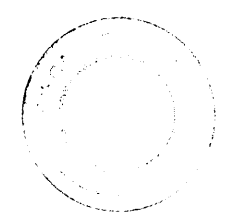


**Figure 4.1.** Calibration of the Tonolab rebound tonometer in a cannulated rat eye. The relationship between IOP in the anterior chamber (measured using pressure transducer) and IOP reading obtained with the rebound tonometer. The measurements were taken at 1mm (Figures 4.1 A & B) and 3mm (Figure 4.1 C) distance from tonometer probe to cornea. The parameters for these curves are presented in Table 4.1.

Calibration experiment	Eye	Distance (mm) <sup>a</sup>	R <sup>2</sup>	Pressure	
1	1	1	0.84	decreasing	
1	2	1	0.87	increasing	
2	3	1	0.67	increasing	
2	4	1	0.88	decreasing	
3	5	3	0.90	decreasing	

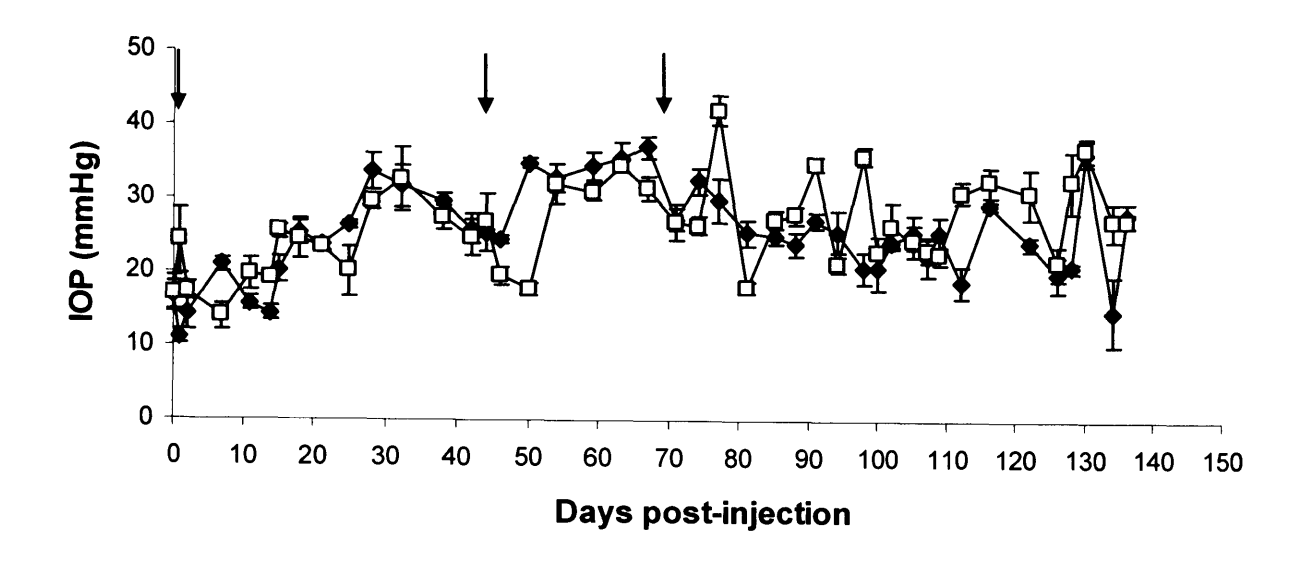
**Table 4.1.** Parameters for calibration of Tonolab rebound tonometer in cannulated rat eyes. a Distance from tonometer probe to cornea.

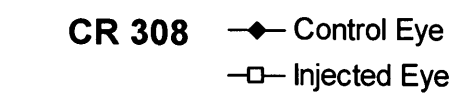


### 4.2.2. Intraocular pressure elevation in the hyperonic saline model

The IOP profiles following hypertonic saline injection could be classified either as a sustained increase in IOP (Figure 4.2B, 33% of eyes) or a fluctuating increase (Figure 4.2A, 7.4% of eyes). A sustained IOP increase (defined as an elevation in IOP 5 mmHg greater than the contralateral eye on at least 7 consecutive days) was obtained in 33% of rats. A fluctuating IOP increase (positive integral IOP increase) was obtained in 7.4% of rats. Overall, IOP increase was obtained in 40.4% of rats. Because of this low conversion rate, other methods were sought to increase IOP in a more consistent fashion (see section 4.2.3).

The mean IOP for all animals (n=27) was 24.9±1.2 mmHg in the injected eyes and 24.7±0.6 mmHg in the contralateral untreated eyes. The mean and peak IOP increases were 0.2±1.1 mmHg and 18.5±2.5 mmHg, respectively, with a mean integral IOP change of -34.5±71.0 mmHg days. For the rats with sustained IOP increases, the mean IOP was 30.0±2.7 mmHg in the experimental eyes and 25.2±1.2 mmHg in the contralateral untreated eyes. The average and peak IOP increases for the sustained IOP increases were 8.7±3.5 mmHg and 31.7±2.6 mmHg, respectively, with a mean integral IOP increase of 128.7±186.1 mmHg days. The mean duration for the sustained IOP increase after a single injection was 17.8±3.4 days with a maximum duration of 40 days. Figure 4.3 shows the mean intraocular pressure (IOP) in experimental and contralateral eyes in the experimental rats injected with hypertonic saline during the whole experimental period. Table 4.2 is related to Figure 4.3 and shows the number of rats (right column) that had IOP measured during a certain number of days post-injection (left column). The mean number of days post-injection was 71.4±7.0, with the maximum duration of 150 days.





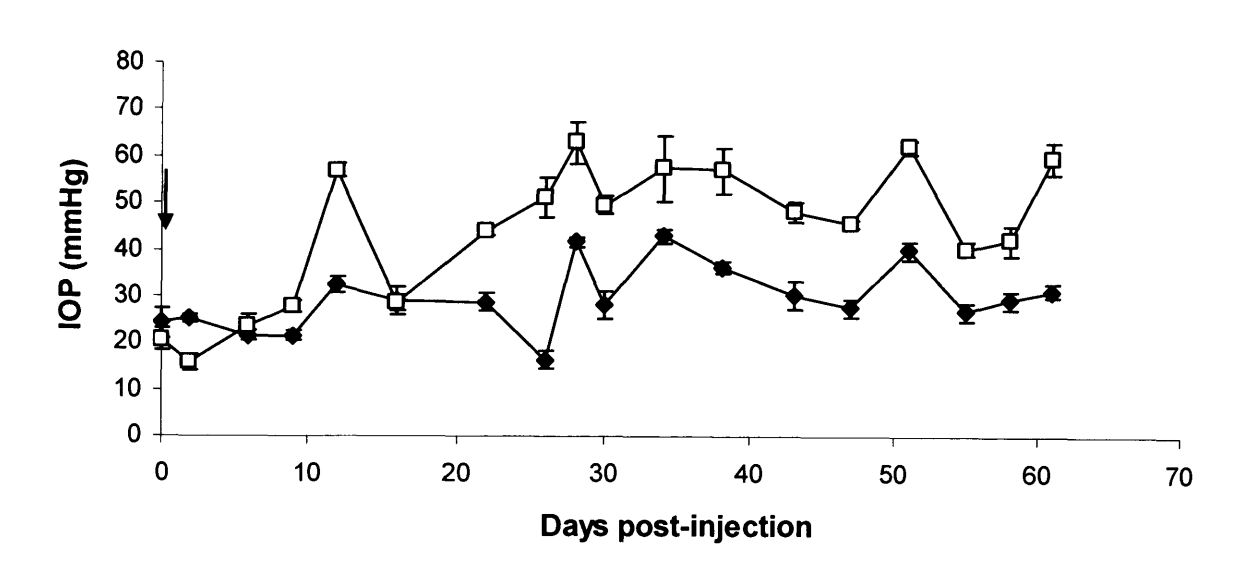


**Figure 4.2.** Intraocular pressures (IOP) following a single injection of hypertonic saline in rat CR308 (A) and three injections rat CR303 (B). The arrows indicate times of injections. Error bars: standard deviations. Open symbols: glaucoma; closed symbols: control.

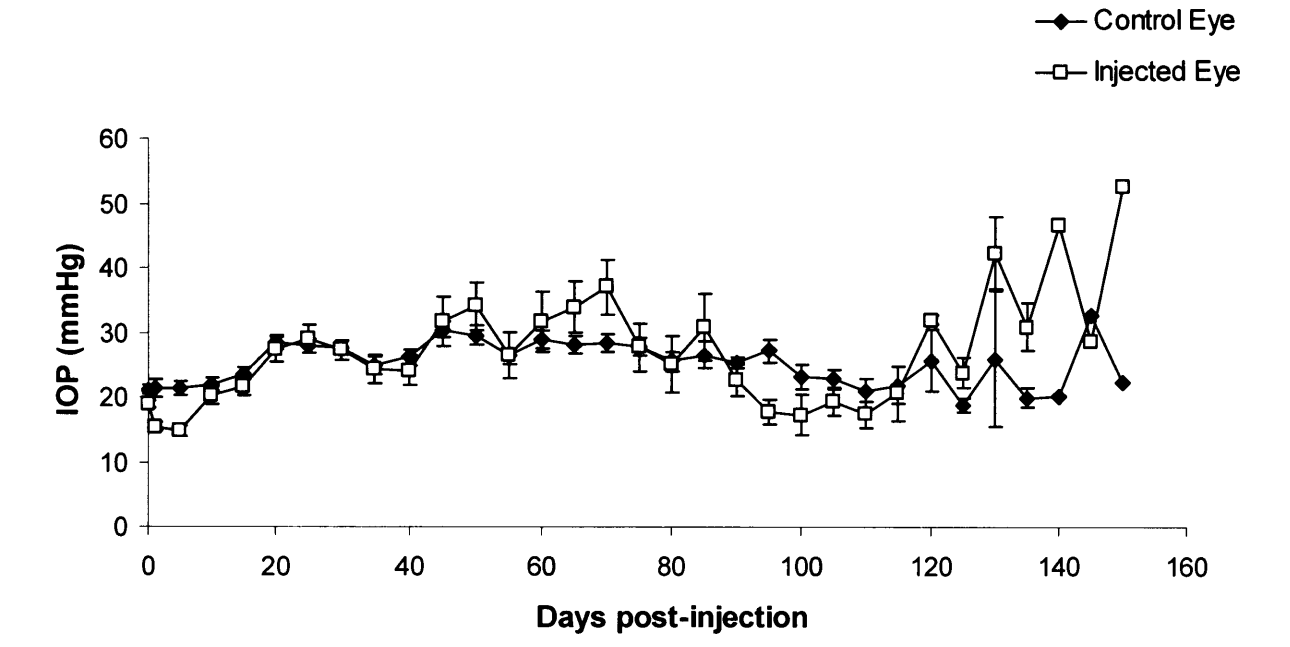


**Figure 4.3.** The mean intraocular pressure (IOP) in the experimental rats injected with hypertonic saline during the experimental period. Open symbols: glaucoma; closed symbols: control. Error bars: standard error of the mean.

Days post-injection	Number of rats
1-25	27
30	26
35	25
40	23
45-50	16
55-60	15
65	14
70-85	10
90	8
95-105	7
110	6
115	4
120	3
125-135	2
140-150	1

**Table 4.2.** The left column shows the number of days post injection and the right column shows the number of rats that had IOPs measured during these days. The values in the table are related to Figure 4.3.

### 4.2.3. Intraocular pressure elevation and cell loss in the magnetic bead model

### 4.2.3.1. Intraocular pressure elevation

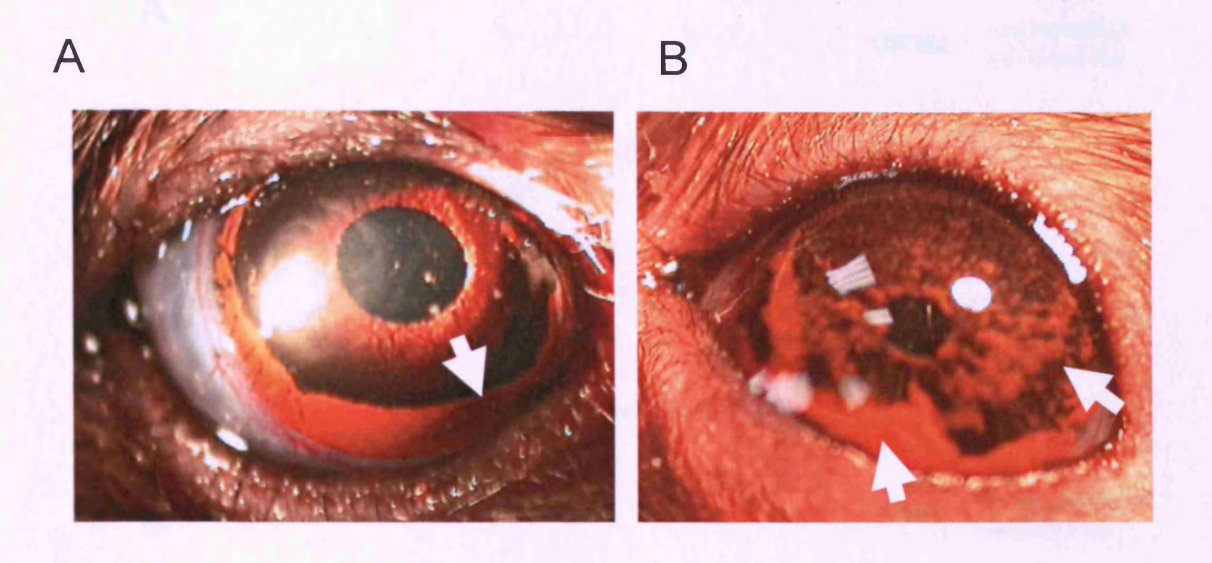
Since the induction of glaucoma with the hypertonic saline resulted in a low proportion of rats with an IOP increase, other methods were sought to increase IOP in a more consistent fashion. To address this issue, we developed a novel technique for the induction of ocular hypertension using paramagnetic microbeads.

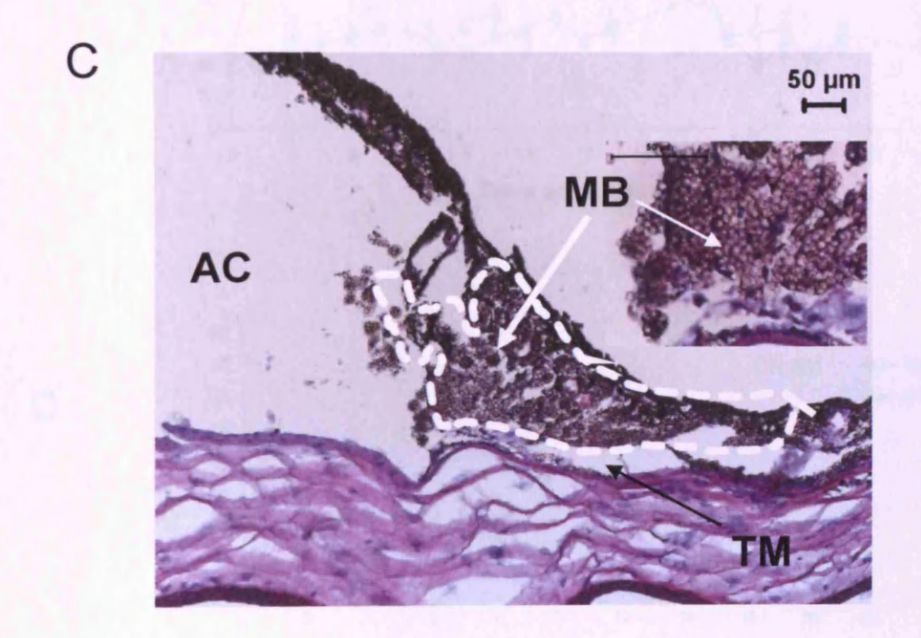
Microbead injections were made in 61 rats (section 2.2.4). Figure 4.4 demonstrates directing the microspheres to the iridocorneal angle with an external magnet. The typical bead distribution following injection and redirection with an external magnet is shown in Figure 4.5A and without redirection with an external magnet in Figure 4.5B. With sufficient anterior chamber depth, the beads could easily be directed to provide uniform occlusion of the iridocorneal angle, a process facilitated by retention of the cannula tip in the anterior chamber during bead redistribution. Histological examination of the anterior segment of the eye following a single intraocular bead injection confirmed sequestration of the beads within the trabecular meshwork (Figure 4.5C).

Microbead injections occupy the iridocorneal angle. Mirobeads were well tolerated and did not provoke a uveitic response. Localised iris haemorrhages were noted if the tip of the injection cannula damaged superficial vessels, but these were small and resolved within a few days. The IOP profiles following injection could be classified either as a sustained increase in IOP (Figure 4.6A, 64% of eyes) or a fluctuating increase (Figure 4.6B, 36% of eyes). A sustained IOP increase (defined as an elevation in IOP 5 mmHg greater than the contralateral eye on at least 7 consecutive days) was obtained in 64% of rats. The mean duration for the IOP increase after a single injection was 12.8±0.9 days with a maximum duration of 27 days.

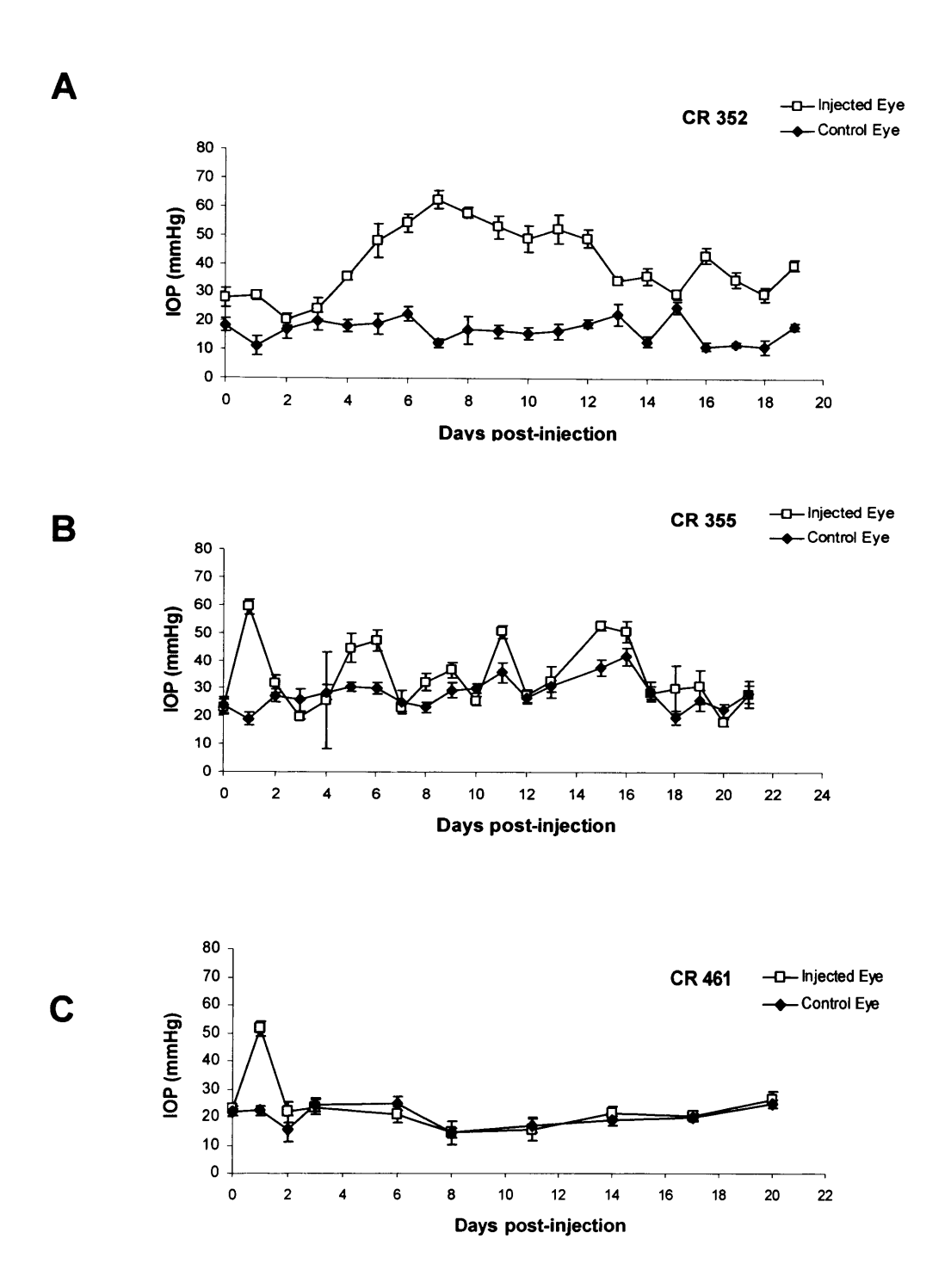


Figure 4.4. An image showing location of the magnet relative to the rat eye during redirection of magnetic beads with the magnet. The arrow indicates the magnet. Scale bar, 1 cm.





**Figure 4.5.** Rat anterior segment showing the distribution of paramagnetic beads immediately post injection with using a magnet (A) and without a magnet (B). The arrows indicate beads in the anterior chamber angle. (C) Cryosection of the anterior chamber injected with magnetic beads showing complete occlusion of the iridocorneal angle. AC=anterior chamber; TM=trabecular meshwork; MB=microbeads. Inset image shows higher magnification image of the angle with altered contrast to highlight the microbead distribution (indicated by arrows).



**Figure 4.6.** Intraocular pressures (IOP) following single bead injections with using a magnet to direct beads to the anterior chamber angle in (A) rat CR352 and (B) rat CR355. Error bars: standard deviations. Open symbols: injected eye; closed symbols: control eye. Intraocular pressures (IOP) following single bead injection without using a magnet in rat CR461 (C).

Up to 3 injections were made in any single animal. Fifty-one animals received injections with 20 μl, four with 10 μl and six with 15 μl. Injections were repeated to prevent the IOP falling to within 5 mmHg of the contralateral control eye. The typical injection period was 2-4 weeks (minimum 1 week). To compare the effects of different bead volumes on IOP profiles, eight additional rats were injected with 10ul bead volumes. (Those rats were not included in the group analysis for IOP profiles and cell loss). Eyes injected with 10μl (N=12) or 20μl of beads (N=51) did not demonstrate a significant difference in either the mean IOP increase (6.0±1.5 vs 6.2±1.2 mmHg) or peak IOP (31.05±2.0 mmHg vs 35.8±1.2 mmHg).

Since the IOP increase did not show a consistent relationship with injection volume, the results from all the animals have been pooled. The mean IOP for all the animals was 29.4±0.9 mmHg for injected eyes and 23.6±0.4 mmHg in the contralateral untreated eyes (P<0.001). The mean and peak IOP increases were 5.8±1.0mmHg and 35.7±1.0 mmHg, respectively, with a mean integral IOP increase of 118.0±57.4 mmHg days. The mean duration of an experimental period for all animals was 74±5.4 days, ranging from 11 to 178 days.

For rats with sustained IOP increases, the mean IOP was 32.5±1.0 mmHg in the experimental eyes and 23.0±0.5 mmHg in the contralateral untreated eyes. The average and peak IOP increases were 9.5±1.1 mmHg and 37.8±1.0 mmHg, respectively, with a mean integral IOP increase of 323.1±55.3 mmHg days. The mean duration of an experimental period for rats with sustained IOP increases was 68±7.1 days, ranging from 11 to 178 days. The mean duration for the sustained IOP increase after a single injection was 12.8±0.9 days with a maximum duration of 27 days. Figure 4.7 shows the mean intraocular pressure (IOP) in experimental and contralateral eyes in all experimental rats during the first 42 days after injection.

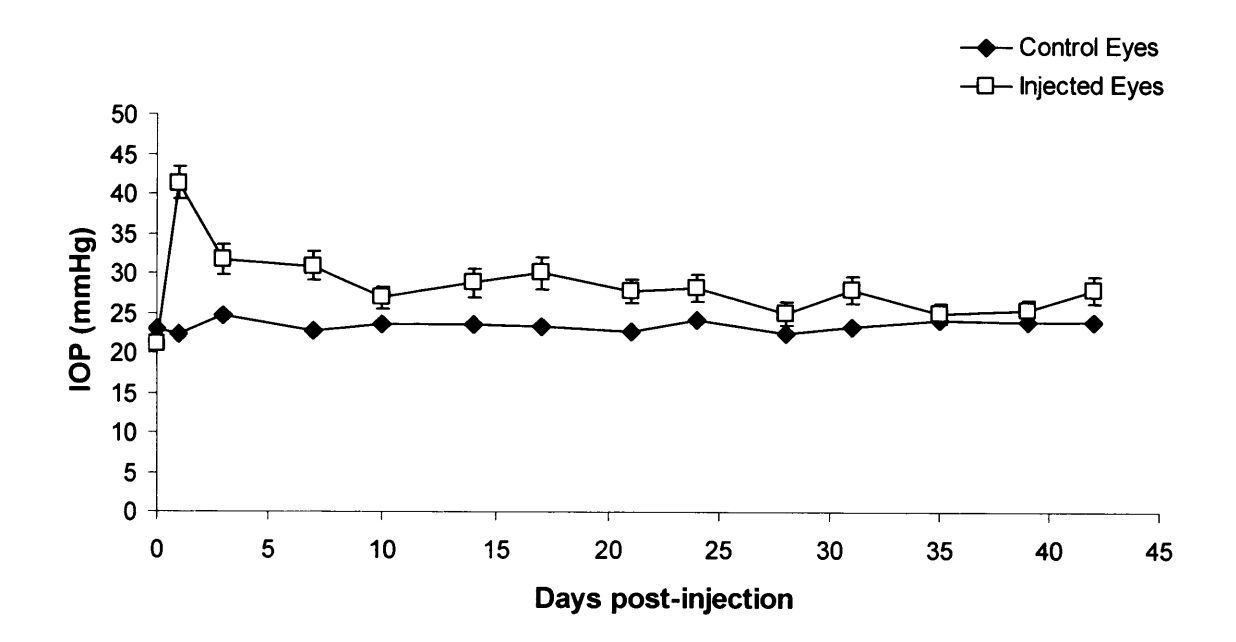


**Figure 4.7.** The mean intraocular pressure (IOP) in the experimental rats injected with magnetic beads during the first 42 days after injection. Open symbols: injected eyes; closed symbols: control eyes. Error bars: standard error of the mean.

To investigate the effect of using a magnet on the IOP elevation in a magnetic bead model, rats were injected with magnetic beads without directing them to the iridocorneal angle using a magnet. Two rats were injected once with 10 µl and two rats with 20 µl. One of the rats injected with 20 µl was killed soon after the injection due to severe haemorrhage and therefore was not included in the analysis of IOP profile. Following injection, the majority of beads settled on the inferior part of the anterior chamber, near the injection site (Figure 4.5B). The remaining beads were spread around the anterior chamber. Figure 4.6C shows the IOP profile for one of the injected rats. The mean IOP for the 3 injected rats was 27.0±1.6 mmHg for injected eyes and 24.3±2.3 mmHg in the contralateral untreated eyes. The mean and peak IOP increases were 2.7±1.7 mmHg and 24.1±2.7 mmHg, respectively, with a mean integral IOP increase of -0.6±33.6 mmHg days. The mean number of days with IOP increase above 5 mmHg was 2.33±0.3 days. The duration of the experimental period post injection was 20 days for all animals.

A vehicle control was produced to assess the effect of BSS injection on IOP elevation. Using the same technique as for the bead injection, a single rat received a vehicle injection of 10 μl BSS into the anterior chamber. The mean IOP for this rat was 26.6±9.9 (SD) mmHg for the injected eye and 22.4±4.7 (SD) mmHg in the contralateral untreated eye. The mean and peak IOP changes were -4.2±7.2 (SD) mmHg and 4.8 mmHg, respectively. An IOP increase above 5 mmHg was not detected in the time before sacrifice.

### 4.2.3.2. Neuron quantification in the RGCL

Retinas were dissected out and prepared as wholemount preparations. The mean density of cells in the RGCL in control retinas was 4080±99 cells/mm² and 2593±139 cells/mm² in glaucomatous retinas, accounting for 36.4±2.4% cell loss (P=0.002) (Table 4.3). Figure 4.8 shows the location of the imaged fields that were used for counting RGCs and sample images of the RGCL stained with Hoechst from control and injected eye. The RGCL neuronal populations were sampled in 21 animals with a mean IOP elevation of 7.7±1.4 mmHg and mean integral IOP increase of 194.5±87.5 mmHg days. In a linear regression analysis, the relationship was not significant

between the degree of cell loss relative to the contralateral control eye for the duration of IOP increase (r2= 0.18, P=0.56), peak or mean IOP increase or area under the IOP curve. A consistent difference in retinal regions was not observed when samples were taken at 1, 2 or 3 mm from the optic disc for the degree of loss (P=0.983 in One-way ANOVA).

Little change in RGC counts following bead injections was observed without magnetic redirection. When the RGC counts for animals receiving 10 or 20 μl injections were pooled, the mean density of cells in the RGCL in control eyes was 3725.9±87.7 cells/mm² compared with 3685.0±190.4 cells/mm² in bead injected eyes. For the rat injected with BSS, cell density in the RGCL in contralateral control eye was 3655.6 cells/mm², compared with 3925.5 cells/mm² in control retina injected with saline.

Discrete (<100um) retinal haemorrhages were observed in a peripapillary distribution in 5 of the 61 eyes. Comparison of the IOP profiles, either on the basis of peak IOP or integral IOP increase did not reveal a significant difference between eyes with or without haemorrhages (P>0.05).

Eccentricity	Cell density in	Cell count	Cell density in	Cell count per	% Cell loss
	control retinas	per field in	glaucomatous	field in	
	(cell/mm²)	control	retinas	glaucomatous	
		retinas	(cell/mm²)	retinas	
lmm	4170 ± 104	471 ± 12	2701 ± 128	305 ± 14	$35.2 \pm 2.5$
2mm	$4327 \pm 98$	489 ± 11	2699 ± 144	305 ± 16	$37.6 \pm 2.3$
3mm	3745 ± 96	423 ± 11	2381 ± 145	269 ± 16	$36.4 \pm 2.6$
Mean	4080 ± 99	461 ± 11	2593 ± 139	293 ± 16	$36.4 \pm 2.4$

Table 4.3

Cell density, mean number of cells counted per field and cell loss in the RGCL for control and glaucomatous retinas. Cell densities and cell counts are expressed as means (cells per mm<sup>2</sup>  $\pm$  SEM and cells  $\pm$  SEM, respectively). Cell loss is expressed as a percentage relative to the contralateral (control) retina  $\pm$  SEM.

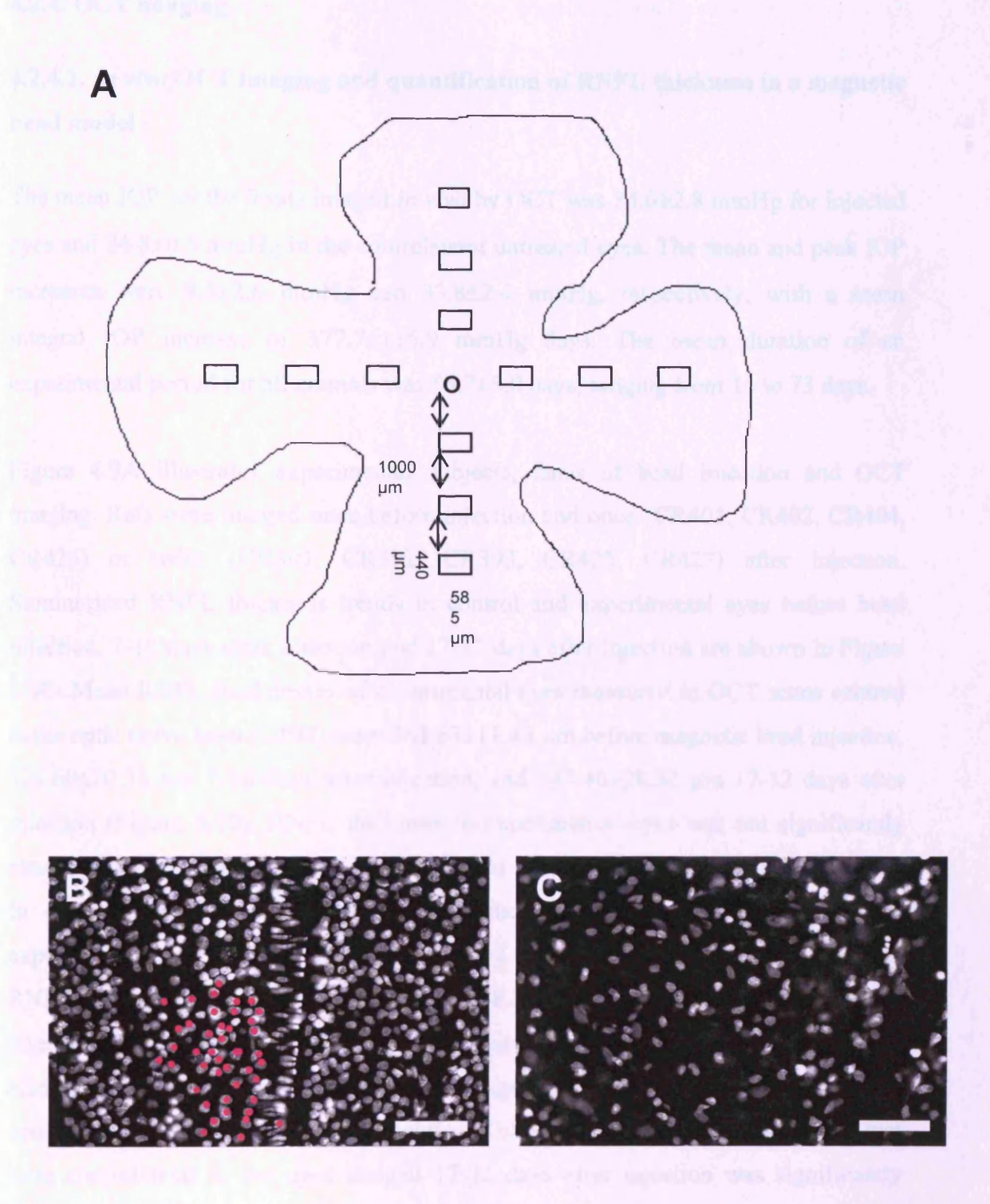


Figure 4.8. Schematic figure showing the location of the 12 sample areas that were imaged in the superior, inferior, temporal and nasal part of a retina within the distances of 1, 2 and 3mm from the optic disc (O). Double arrows indicate the distances of 1000  $\mu$ m between the imaged areas (A). Sample images of RGCL stained with Hoechst from control (B) and injected (C) eye from a rat injected with magnetic beads. Cells were counted using ImageJ plugin, Cell Counter. Pink dots indicate how the cells were picked out for counting. Scale bars, 100  $\mu$ m.

### 4.2.4. OCT imaging

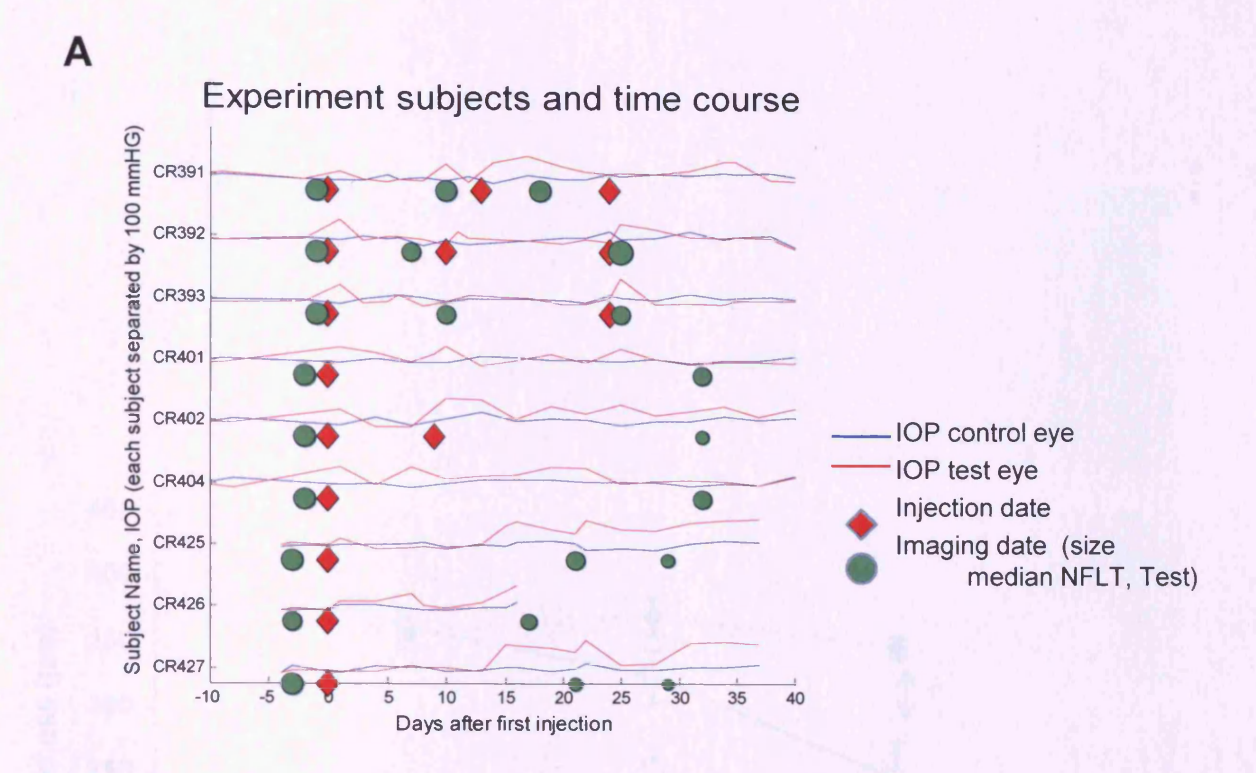
## 4.2.4.1. *In vivo* OCT imaging and quantification of RNFL thickness in a magnetic bead model

The mean IOP for the 9 rats imaged *in vivo* by OCT was 34.0±2.8 mmHg for injected eyes and 24.8±0.5 mmHg in the contralateral untreated eyes. The mean and peak IOP increases were 9.3±2.6 mmHg and 33.8±2.4 mmHg, respectively, with a mean integral IOP increase of 377.7±115.9 mmHg days. The mean duration of an experimental period for all animals was 56.7±8.0 days, ranging from 15 to 73 days.

Figure 4.9A illustrates experimental subjects, dates of bead injection and OCT imaging. Rats were imaged once before injection and once (CR401, CR402, CR404, CR426) or twice (CR391, CR392, CR393, CR425, CR427) after injection. Summarized RNFL thickness trends in control and experimental eyes before bead injection, 7-10 days after injection and 17-32 days after injection are shown in Figure 4.9B. Mean RNFL thicknesses of experimental eyes measured in OCT scans centred at the optic nerve head (ONH) were 363.63±11.43 µm before magnetic bead injection, 325.60±20.38 µm 7-10 days after injection, and 247.40±28.32 µm 17-32 days after injection (Figure 4.10). RNFL thickness in experimental eyes was not significantly changed 7-10 days after injection compared to the RNFL thickness before injection. In contrast, there was a significant difference between the RFNL thickness of experimental eyes before injection and 17-32 days after injection (P<0.01). Mean RNFL thicknesses of control eyes were 358.28±11.41 µm before magnetic bead injection, 371.23±14.22 μm 7-10 days after injection and 347.13±8.58μm 17-32 days after injection. There were no significant changes in RFNL thickness in the untreated control eyes during the experimental period. The RFNL thickness of control eyes that were contralateral to the eyes imaged 17-32 days after injection was significantly different compared to the RFNL thickness of experimental eyes imaged 17-32 days after injection (P<0.01).

The average cell loss, estimated in the 5 out of 9 OCT imaged rats, was 35.79±13.97%.

Figure 4.11 demonstrates progressive glaucomatous changes in an experimental rat eye before bead injection, 3 weeks and 4 weeks after injection in OCT images. A cupping of the optic nerve head was clearly visible 3 weeks post injection and progressed to a very deep cupping 4 weeks post injection. Retinal layers were discernible before injection and 3 weeks after injection but not 4 weeks after injection. In contrast to the changes in the experimental eye, there were no glaucomatous changes in the control eye. High IOP elevation was observed in the injected eye of this experimental rat (Figure 4.11, below the images).



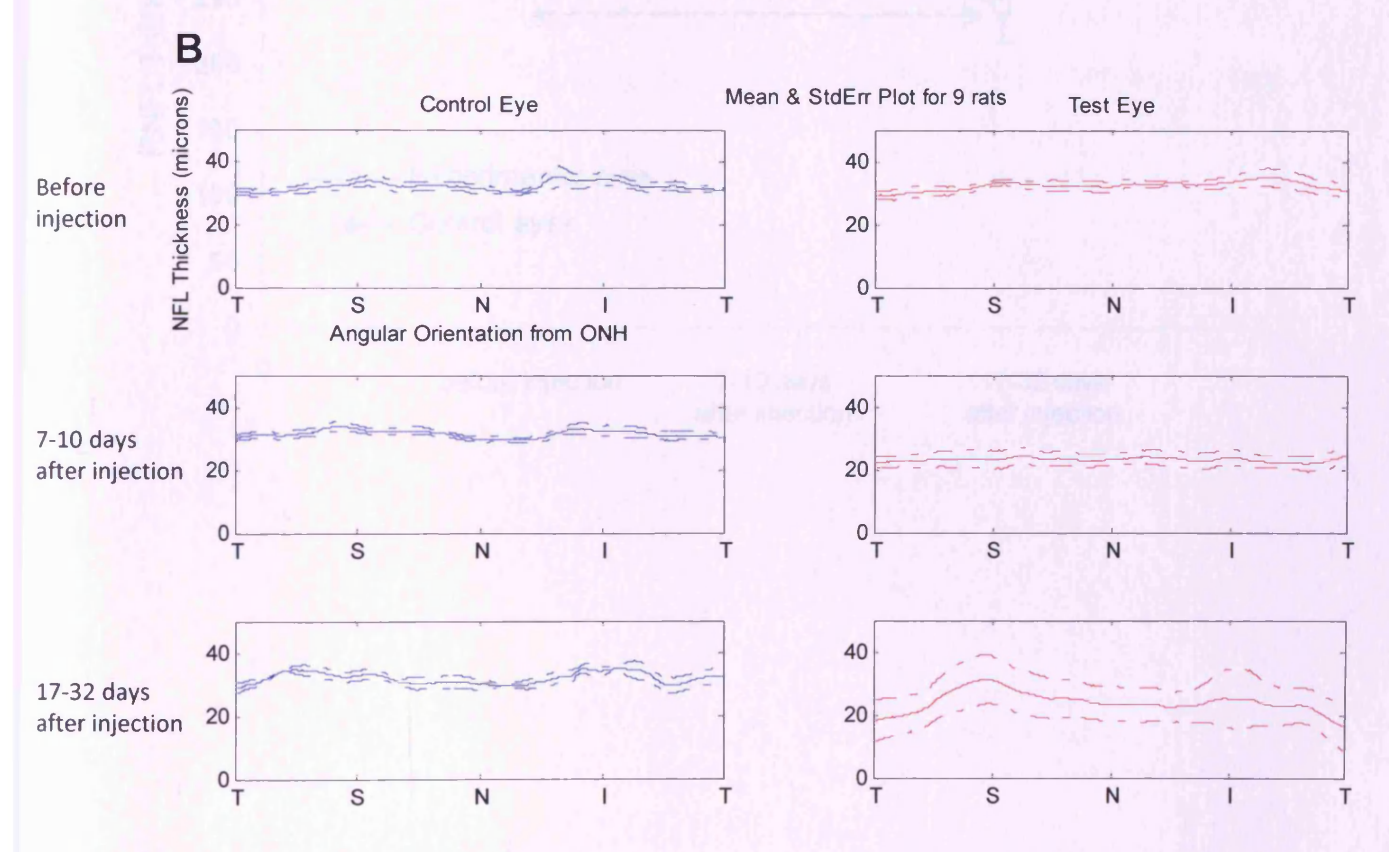
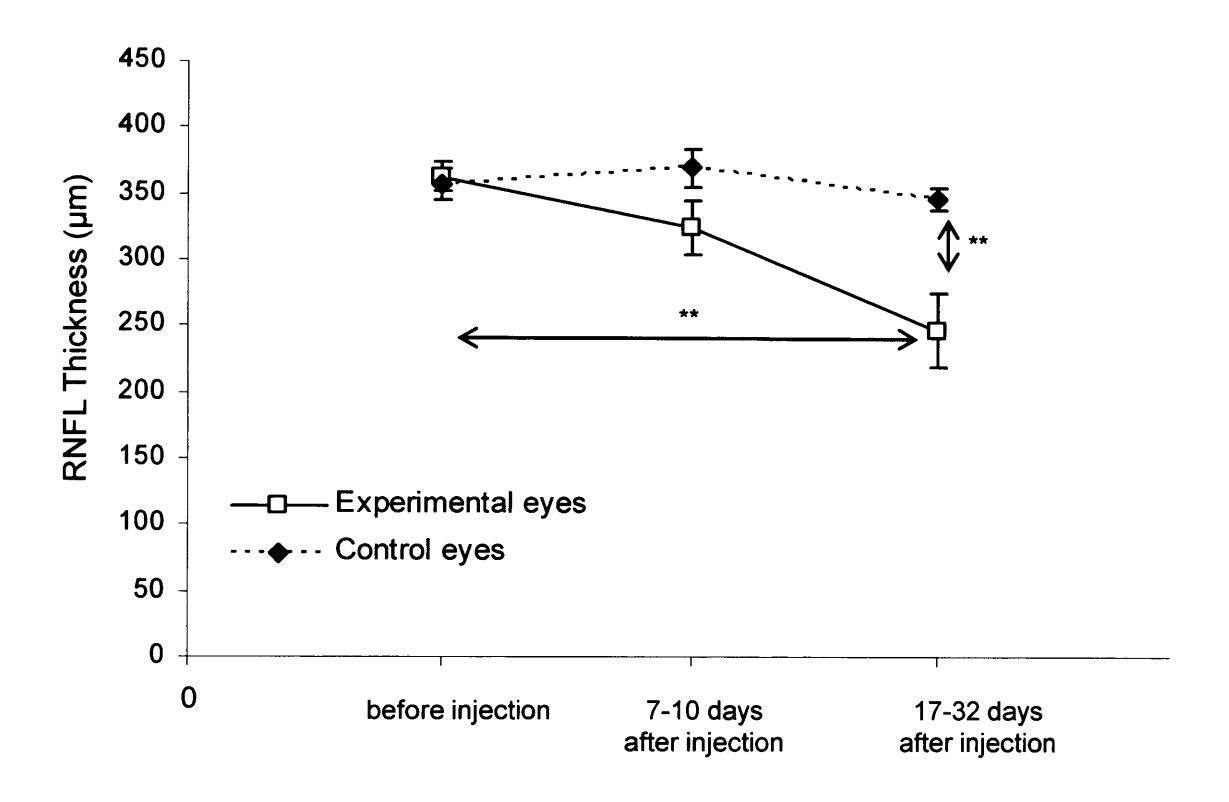
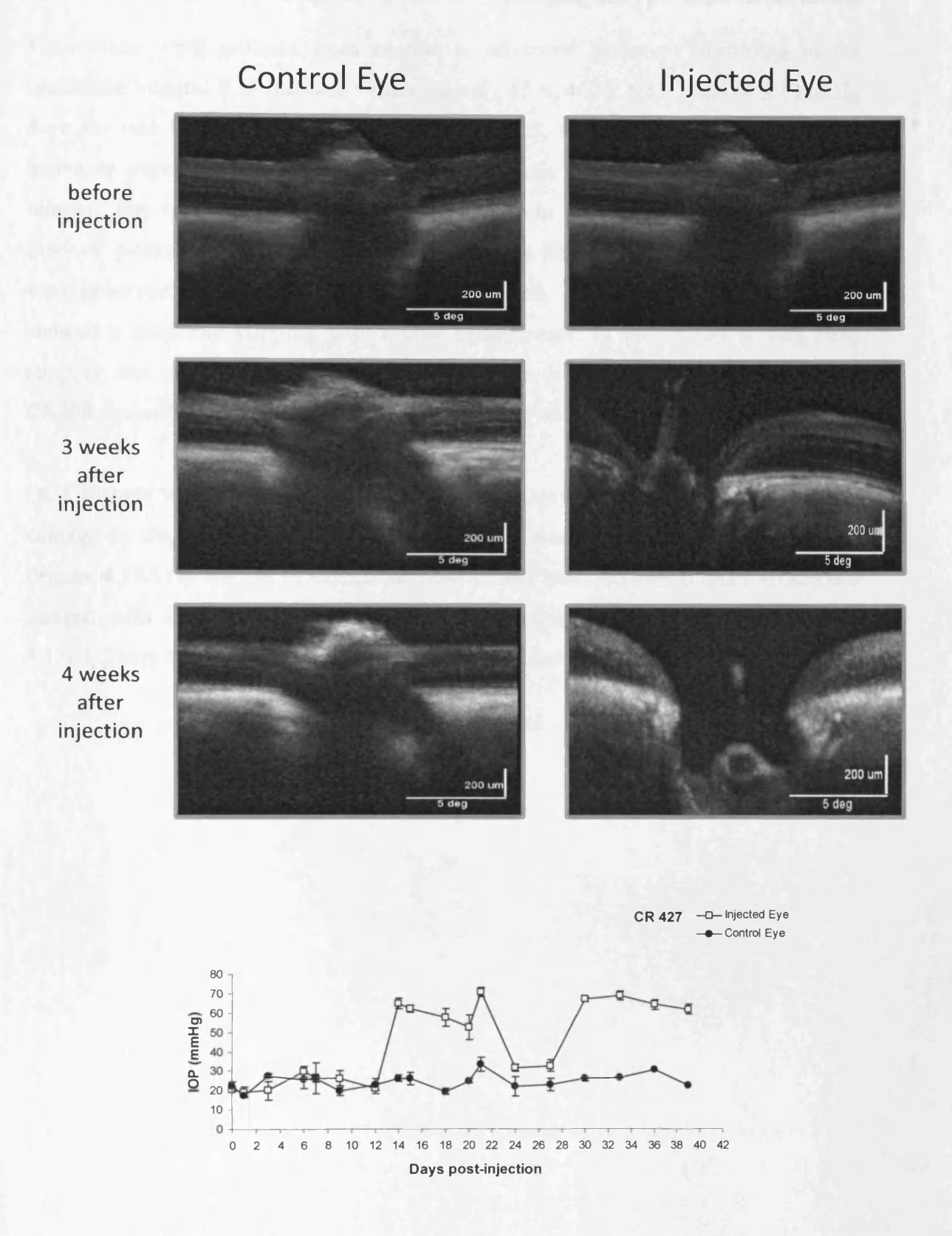


Figure 4.9. (A) A plot showing experimental subjects, dates of bead injection and OCT imaging. Rats were imaged once before injection and once (CR401, CR402, CR404, CR426) or twice (CR391, CR392, CR393, CR425, CR427) after injection. (B) Plots showing summarized RNFL thickness trends in control (left column) and experimental eyes (right column) before bead injection, 7-10 days after injection and 17-32 days after injection. Plain and dashed lines represent mean and standard deviation, respectively. The RNFL thicknesses were measured at different angular orientation from ONH (t, temporal; s, superior; n, nasal; i, inferior). (Thanks to Alex Tumlinson and Stephen Cross).



**Figure 4.10**. Changes in mean RNFL thickness in OCT scans caused by magnetic bead injection. Closed symbols: injected eyes, open symbols: control eyes. N=3 before injection; n=9 7-10 days after injection and n=11 (2 rats had the thickness measured twice within 17-32 days period) 17-32 days after injection. Data are represented as the mean  $\pm$  SEM. \*\* P<0.01 (Independent Samples T-Test).



**Figure 4.11.** OCT images showing extreme case of glaucoma progression in rat CR427 before bead injection, 3 and 4 weeks after injection. Left column, control eye. Right column, injected eye. Below the images, IOP profile of the rat CR427 following bead injection (OCT Images courtesy of Alex Tumlinson and Stephen Cross).

## 4.2.4.2. Evaluation of damage by ex vivo OCT imaging in hypertonic saline model

The retinas were grouped from normal to advanced glaucoma according to the increasing integral IOP increase values, namely 65.4, 400.2, 621.7 and 903.1 mmHg days for rats CR314, CR305, CR300 and CR308, respectively. The integral IOP increases were related to the level of glaucomatous damage observed in the OCT images. The retinas from the normal rat and from rat CR314 did not show any obvious glaucomatous damage (Figure 4.12). The RNFL and contour of the retina were observed, and the layers were well delineated. The retina from the rat CR305 showed a moderate cupping with retinal detachments. In rat CR300, a very deep cupping was observed, and the retinal layers were difficult to recognise. The retina CR308 showed extensive damage through all layers with excessive cupping.

OCT images were consistent with histological images (Figure 4.13). The extensive damage in the retina from the experimental eye was observed in the OCT image (Figure 4.13A) as well as in vertical sections stained with Hoechst (Figure 4.13B) and imaged with Differential Interference Contrast (Nomarski) (DIC) method (Figure 4.13C). There was no damage in the normal eye (Figure 4.13D-F).

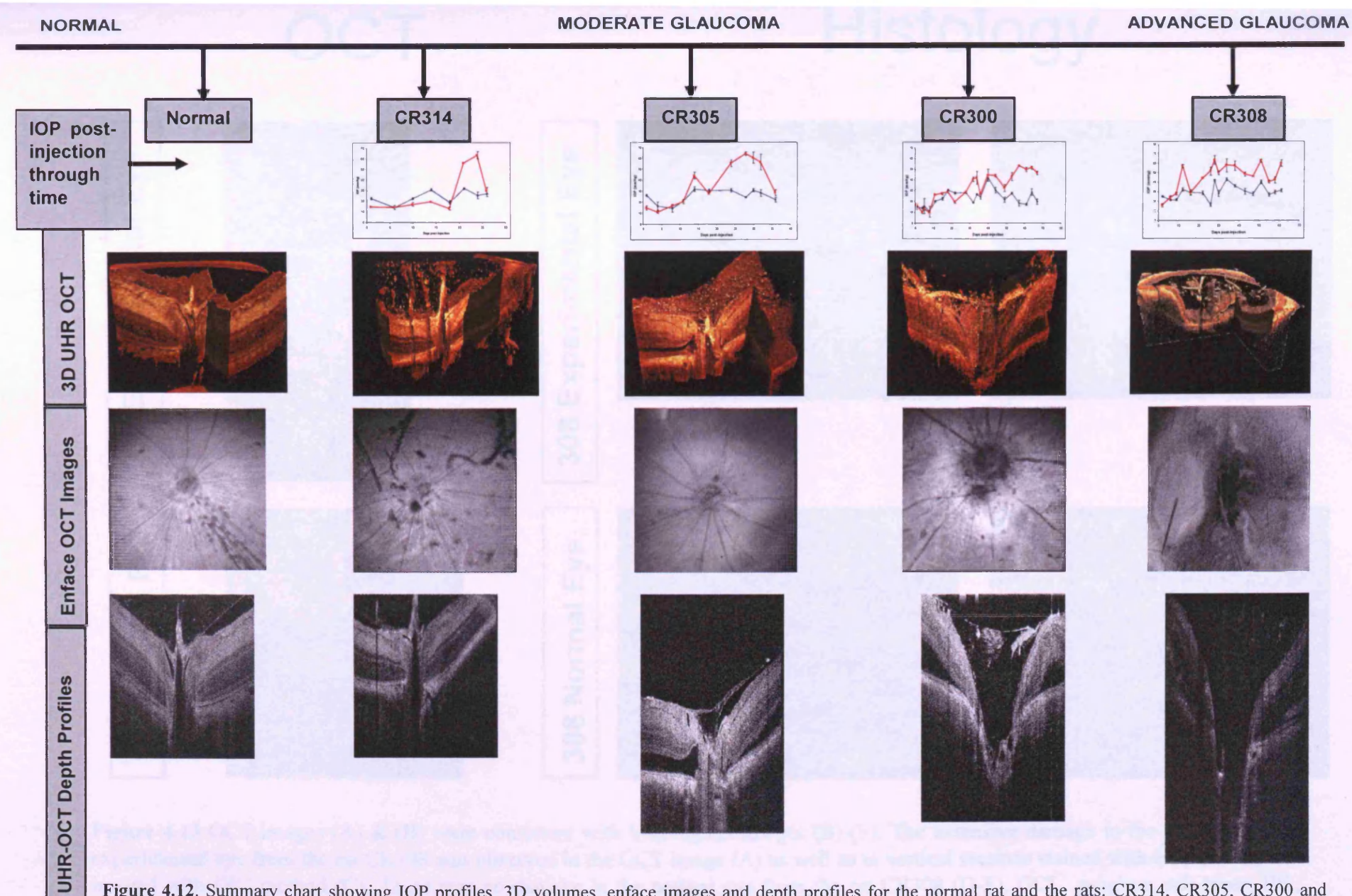


**Figure 4.12**. Summary chart showing IOP profiles, 3D volumes, enface images and depth profiles for the normal rat and the rats: CR314, CR305, CR300 and CR308. The red lines: IOPs in the injected (glaucomatous) eyes. The blue lines: IOPs in the contralateral eyes. Error bars: standard deviations. (Thanks to Alicia Charlton, Dr Boris Povazay and Prof Wolfgang Drexler).

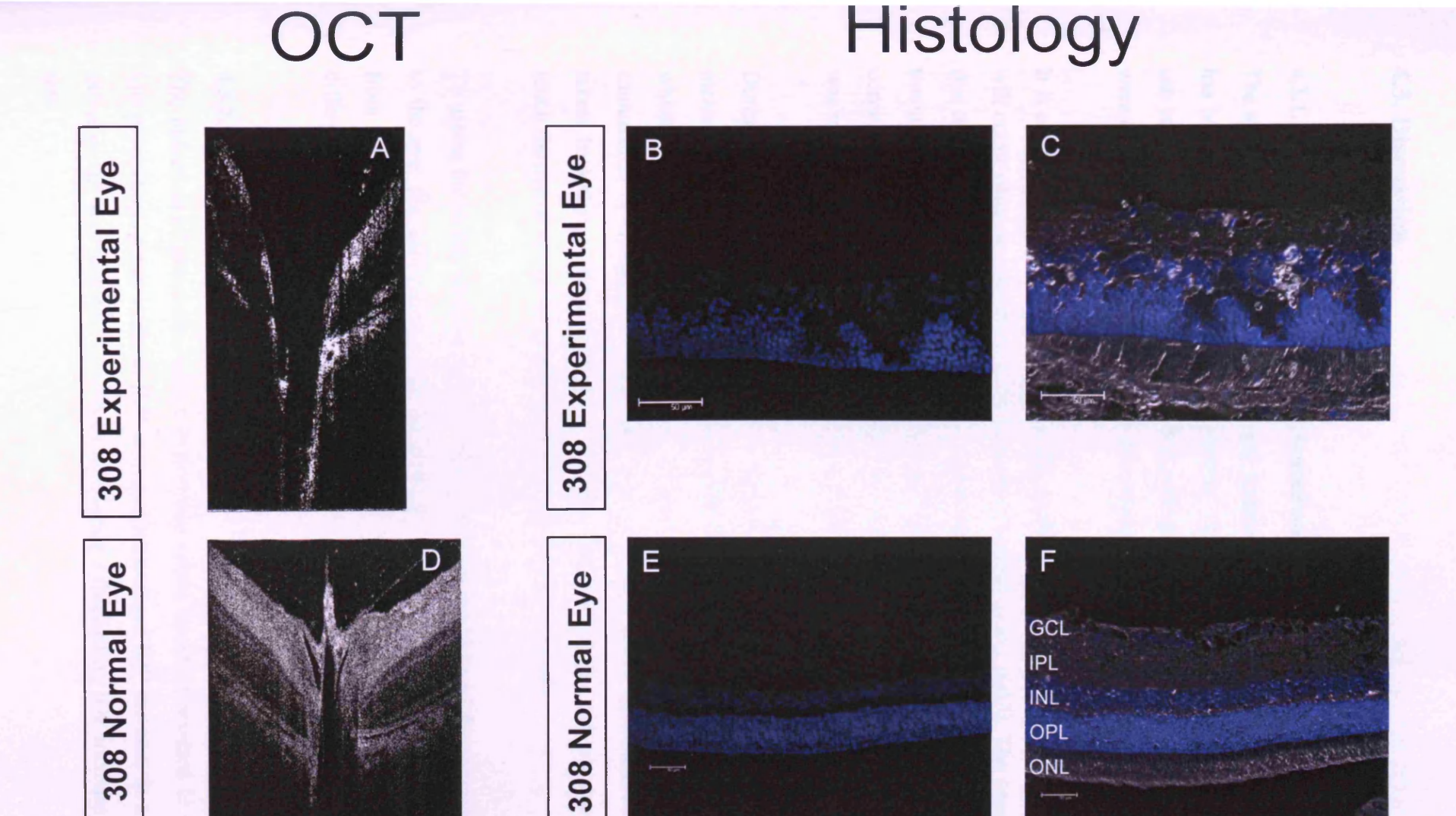


Figure 4.13 OCT images (A) & (B) were consistent with histological images (B)-(F). The extensive damage in the retina from the experimental eye from the rat CR308 was observed in the OCT image (A) as well as in vertical sections stained with Hoechst (B) and imaged with DIC method (C). There was no damage in the normal eye from the rat CR308 (D-F). GCL, ganglion cell layer; IPL, inner plexiform layer; INL, inner nuclear layer; OPL, outer plexiform layer; ONL, outer nuclear layer.

### 4.3. Discussion

#### 4.3.1. Evaluation of the Tonolab rebound tonometer

The applicability of a Tonolab rebound tonometer in measuring IOP in rats and mice has been evaluated by Wang et al. (2005). The study demonstrated that the Tonolab can precisely and reproducibly monitor IOP in rodents since the measured IOP values were comparable to the actual pressure in the eye.

It is considered likely that changes in the position of the tonometer relative to the eye will occur when measuring rats IOP in vivo (Prashar et al., 2007). The results showed that the relationship between the true and measured IOP was more accurate when the tonometer was at 3mm (R2 = 0.9) than at 1mm (R2 = 0.67 - 0.88) distance from the cornea. Calibrations obtained from chicken eyes suggested that the rebound tonometer was robust to varying probe-to-cornea distances over 3 to 5 mm (Prashar et al., 2007).

During the calibration procedure, a number of problems related to taking tonometer measurements were encountered. The initial problem was the cannulation of the eye, which often caused leakage. The leakage occurred either immediately after cannulation or during the calibration procedure, not allowing measurements to be taken. In addition, error messages occurred when the probe did not move, did not touch the eye or when the probe speed was too low or too high.

To assess the effect of other types of changes in the position of the tonometer relative to the eye, the calibration could be obtained with the tonometer laterally displaced from the centre of the cornea, and directed towards the centre of the cornea but at different angles to the visual axis (Prashar et al., 2007).

### 4.3.2. Hypertonic saline model

The induction of glaucoma with a hypertonic saline injection resulted in a relatively low proportion of rats with an IOP increase; a sustained IOP increase in a hypertonic saline model was obtained in 33% of rats, while a fluctuating IOP increase in 7.4% of rats.

Hypertonic saline injection into aqueous humor outflow pathways to produce scarring of the tissue is a commonly used method for producing chronic experimental IOP elevation in rats (Morrison et al., 1997). A plastic ring is placed around the equator of the eye to restrict the injection to the limbus, resulting in a saline flow into Schlemm's canal and across the trabecular meshwork. This leads to scarring of the meshwork and the anterior chamber angle due to inflammation. The level of the pressure rise is determined by the extent of scarring (Morrison et al., 2005).

The efficiency of the intraocular pressure induction depends on the extent and density of the resulting scarring of the anterior chamber angle. This is influenced by the anatomy of the limbal plexus and the effectiveness with which the ring confines the hypertonic saline to the limbus. Sustained IOP elevation usually occurs 7-10 days after injection, most probably when the scarring process matures and the inflammation drops, allowing continuation of normal production of aqueous humor (Morrison et al., 2005). Some investigators routinely perform a second injection in all animals (Chauhan et al., 2002) while others only do so if an IOP elevation does not occur within the first 2 weeks (Hanninen et al., 2002; Morrison et al., 1997). In the present study, the second injection was performed after an average 29.4±2.6 days.

The mean duration of sustained elevation was 17.8±3.4 days with a maximum duration of 40 days (53 days with 1 measurement of an IOP decrease within the period of increased IOP) with an elevated pressure when a rat was sacrificed. We have not attempted to maintain IOP elevation for a longer period due to the time-limitation of our experiments. Durations of elevated IOP with this method as long as 12 weeks have been reported (Hanninen et al., 2002; McKinnon et al., 2002). The IOP can potentially remain elevated for over 12 weeks if the rat is allowed to survive (Morrison et al., 2005). An important factor determining the duration of IOP elevation is the concentration of saline. 1.75 M saline was used in our experiments according to Morrison et al. (1997). The injection of a saline concentration more than 2.0 M generated a marked elevation that could remain highly elevated in a number of eyes for up to several months (Johnson et al., 2000; Morrison et al., 1997).

It has been reported that for the hypertonic saline model, the extent of pressure elevation ranged between 1.3 x to 2 x normal (Chauhan et al., 2002; Hanninen et al., 2002; McKinnon et al., 2002; Morrison et al., 1997; Morrison et al., 1998; Schlamp et al., 2001). Although in the present study, our mean IOP in injected eyes was the same as the mean IOP in contralateral eyes due to the low percentage of the animals with IOP elevation, the mean pressure elevation in rats with sustained IOP increase was 1.2 x normal. That was similar to the 1.3 x normal described by other investigators (Chauhan et al., 2002; Morrison et al., 1997; Morrison et al., 1998; Schlamp et al., 2001).

Following an initial period of successful experiments producing elevated IOP, several problems were encountered with the induction of increased IOP, resulting in only 40.7% of rats with an IOP increase (sustained and fluctuating). It is possible that the use of a different ring (obtained from the Morrison's lab) in the later experiments caused problems when trying to elevate IOP. If the ring was too tight the pressure from the ring may have forced aqueous to exit the eye resulting in an IOP decrease. However, if the ring was too loose, it might have confined the injection to the limbus insufficiently, not allowing for saline flow into Schlemm's canal and across the trabecular meshwork. It is likely that the size of aqueous drainage veins of our rats was different from that of the rats from the Morrison's lab. In addition, variability in vessel sizes was observed; in general the larger the animal, the larger the vessels.

Considering all the difficulties encountered during the experimental work with Morrison's model, it was decided to develop an alternative, less technically challenging glaucoma model based on the injection of magnetic beads into the anterior chamber.

### 4.3.3. Magnetic bead model

A simple and effective method for the elevation of IOP in the rat was described. The technique is technically undemanding and provides a measure of control over the distribution of beads within the anterior segment. The beads can be drawn away from the visual axis and distributed around the iridocorneal angle to optimise occlusion of the trabecular meshwork and facilitate visualisation of the retina and optic disc. A

sustained IOP increase was obtained in 64% of rats and a fluctuating increase in 36% of rats.

The principal finding of the present study is that fewer injections may be required to achieve a sustained increase in IOP compared with injections using non-magnetic beads. The data presented by others showed that the injection of latex microspheres. in combination with hydroxypropylmethylcellulose (HPM), or when given alone, required 6-9 weekly injections to achieve a sustained elevation in IOP (Urcola et al., 2006). Similarly, 8-10 injections were necessary to produce a sustained IOP elevation that lasted up to 2 weeks in the primate (Weber and Zelenak et al., 2001); for more prolonged IOP elevation in the primate, as many as 20 bead injections were required to maintain significant occlusion of the iridocorneal angle. In the present study, a sustained IOP increase in 64% of animals following up to 3 injections was achieved, lasting on average 12.8±0.9 days. The mean IOP in injected eyes in our model, 29.4±0.9 mmHg, was similar to the mean IOP seen in eyes injected with latex microspheres (28.1±0.7 mmHg) (Urcola et al., 2006). It was noted that the increase in IOP was not consistently related to the volume of the bead injection. One likely explanation is that the egress of aqueous seen following removal of the needle tended to normalise the IOP regardless of the injection volume. The present study used beads of approximately 5µm diameter which was smaller than the 10µm beads used in previous studies (Urcola et al., 2006; Weber and Zelenak et al., 2001). Recently, the use of 15µm beads has been reported to achieve sustained IOP elevations of up to 8 weeks based on 2 injections in rats suggesting that the use of larger beads may be important in the long term induction of ocular hypertension (Sappington et al., 2010). In preliminary experiments, the use of beads in the range 1-2 µm did not produce a consistent increase in IOP and had the disadvantage that the beads were more difficult to guide in the anterior chamber. A critical technical point is that the carrier fluid in which the beads are packaged to minimise the introduction of potentially toxic agents into the anterior chamber was removed, using similar method to Weber and Zelenak et al. (2001). For animals in which beads were not redirected, a significant, sustained elevation in IOP was not observed. Furthermore, we did not facilitate the egress of carrier solution that was possible with magnetic redirection since this would have resulted in the loss of beads from the anterior chamber. Even in the animals injected

with 20µl of beads, a significant reduction in RGCL cell density was not observed compared with animals with a sustained elevation in IOP as a result of redirecting the beads. Taken together, these observations suggest that the loss of cells in the RGCL results from the effects of sustained IOP increase, rather than from any transitory increase in IOP as a result of injection. The lack of RGCL cell loss in the animal injected with BSS alone is consistent with this conclusion.

The degree of cell loss in our model is similar to that reported for other models. The use of (non magnetic) microbead occlusion in a rat glaucoma model produced a level of RGC loss (23.1±2.1%) (Urcola et al., 2006) similar to that seen in the present study (36.4±2.4%). Comparable RGC loss (40%) has also been reported with the hypertonic saline model (Hanninen et al., 2002; Morrison, 1998; Morrison et al., 1997) and the episcleral vein cautery model (30%-40 %) (Ahmed et al., 2001a; Ahmed et al., 2001b; Naskar et al., 2002; Neufeld et al., 1999). A consistent variation in the degree of cell loss as a function of retinal eccentricity in the sampled range 1-3 mm was not observed. A similar diffuse pattern of cell loss has been reported in the episcleral (hypertonic saline) vein occlusion model (Garrett et al., 1991). By contrast, clustered RGC loss has been reported in the rat vein cautery model (Mittag et al., 2000). Other studies have reported greater cell loss in the central compared with peripheral regions, but in animals with longer durations of IOP elevation (Laquis et al., 1998; Neufeld et al., 1999; Urcola et al., 2006). In addition, there was no significant relationship between the degree of cell loss relative to the contralateral control eye for the duration of IOP increase, peak or mean IOP increase or the IOP integral. Chauhan et al (2002) observed a strong negative correlation between peak AIOP and the proportion of surviving axons and between  $\Delta$ IOP integral and the proportion of surviving axons.

### 4.3.4. OCT imaging

The use of OCT imaging validated the bead and hypertonic saline glaucoma models, revealing thickening of the retinal fibre layer over time *in vivo* and optic nerve head cupping *in vivo* and *ex vivo*.

The objective of the study described in section 4.2.4.1 was to evaluate rat retinal fibre layer thickness changes over time in a magnetic bead glaucoma model. A protocol

(section 2.2.4.3) for rat eye imaging, including preparation procedures such as methods of anaesthesia and positioning of the rat for imaging, has been successfully established. A spectral (Fourier domain) OCT system enabled visualisation of major intraretinal layers including retinal nuclear fibre layer (RNFL) and therefore evaluation of RFNL thickness. The RNFL thickness in experimental eyes was not significantly changed 1 week after injection compared to the RNFL thickness before injection. However, RNFL thicknesses of experimental eyes before injection and 17-32 days after injection were significantly different. Also, there was a significant difference in RFNL thickness between experimental eyes imaged 17-32 days after injection and control eyes that were contralateral to the eyes imaged 17-32 days after injection. The observation of progressive changes in an extreme case of glaucoma revealed a progressive cupping of the optic nerve head 3 and 4 weeks post injection. In addition, the outer retinal layers looked normal, and the thinning of the RNFL agreed with the calculated cell loss.

RNFL thickness changes in a rat model of optic nerve crush have been estimated using an OCT system with a modified commercial time-domain OCT and a multiplexed two-superluminescent-diode (SLD) light source with 890 nm wavelength and a bandwith of 150 nm. In this model, no changes in RNFL thickness were observed 1 week after the injury, but significant and progressive changes were evident after the second week. Consistent with our studies, there were no significant changes in the untreated control eyes during the experimental period (Nagata et al., 2009). Srinivasan et al. (2006) used a spectral-domain OCT to estimate RNFL thickness (which was approximately 30 µm) in normal Long-Evans rats. The RNFL thickness was also estimated in vivo by scanning laser ophthalmoscopy (SLO) that correlated well with the thickness assessed by histology. However, this method did not allow estimating absolute thickness or demonstrating cross-sectional images of RNFL (Kawaguchi et al., 2006). Therefore, OCT is more useful than SLO for RNFL thickness measurements. Using time-domain OCT, retinal thickness was measured to estimate retinal degeneration in mouse (Li et al., 2001). OCT imaging in the rodent eye is more challenging than in the human eye due to its smaller size and the thinner retina of the animal eye. The RNFL thickness measurements estimated by frequencydomain OCT imaging were highly reproducible in patients with glaucoma and normal subjects (González-García et al., 2009; Vizzeri et al., 2009).

The objective of the study described in section 4.2.4.2 was to assess the damage in the retina by ex vivo OCT imaging and characterise the relationship between retinal damage and IOP elevation. There was an association between integral IOP increase and the glaucomatous damage (optic disc cupping and deterioration of retinal layers) visible in OCT images. Optic disc cupping, a hallmark of glaucoma, has been demonstrated in optic nerve sections in monkeys (Quigley et al., 1984) and rats with IOP elevation (Sawada and Neufeld, 1999). In rats, both cupping (as measured by scanning laser tomography) and electroretinography (ERG) changes were strongly linked to the peak IOP and integral IOP increase in the experimental eye as compared to the control eye (Chauhan et al., 2002).

### 4.4. Summary

In summary, the results from two different glaucoma models were presented. More satisfactory and reproducible data were obtained from the magnetic bead model, with 64% of eyes showing sustained IOP increase, compared to hypertonic saline model with only 33% of eyes with a sustained IOP increase.

Injecting magnetic beads into the rodent eye is a simple method for the induction of experimental glaucoma. It has the principal advantages over non-magnetic microbead models that the visual axis is not obscured following injection and that complete occlusion of the iridocorneal angle can be achieved with a single injection. It is anticipated that it could be adapted with little modification for use in other species.

Optical coherence imaging enabled the observation of progressive glaucomatous changes *in vivo* and estimation of RNFL thickness before and after induction of elevated intraocular pressure. A significant reduction in RNFL thickness following induction of intraocular pressure was observed. In addition, OCT imaging was useful in the quantitative evaluation of glaucomatous damage *ex vivo*.

# Chapter 5: Dendrite morphology of RGCs in the control, glaucomatous and chABC/BDNF treated retinas

#### 5.1. Introduction

Retinal ganglion cell dendrite remodelling and shrinkage is a feature of several experimental models of glaucoma (Morgan et al., 2006). To investigate the possibility that this could be reversed and act as a neural substrate for the recovery of vision in glaucoma, the perineuronal net (PNN) was modified in eyes in which the intraocular pressure (IOP) had been returned to its preglaucomatous level. It was assumed that digestion of the PNN would enhance the ability of retinal ganglion cell (RGC) dendrites to regenerate following removal of the effect of elevated IOP. Since chondroitinase ABC influences plasticity by enzymatic digestion of the PNN (Kwok et al., 2008), the enzyme was injected intravitreally to promote retinal ganglion cells (RGCs) regeneration in glaucoma. In addition, the effects of brain-derived neurotrophic (BDNF) factor on the preservation of the dendritic field complexity using the magnetic bead model of glaucoma were investigated.

The first aim of the present study was to explore the changes in RGCs in a rat magnetic bead model of glaucoma by comparing RGC dendrite morphology in control and glaucomatous retinas. The second aim was to explore the changes in RGC morphology in glaucomatous retinas which had been injected with digestive enzyme chondroitinase ABC, neurotrophic factor BDNF or a combination of these two agents.

#### Experimental design

A plan of the experiment (described in Methods Chapter in section 2.2.4.2) is summarised in Figure 5.1. Bead injection into the left rat eyes is described in sections 2.2.4.1 and 4.4.1. The injections of either 3μl of 10mU/eye chondroitinase ABC, 1 μl of 1μg/ml recombinant human BDNF or both agents (during the same procedure) into the vitreous of a glaucomatous, left rat eye were performed after a 3-4 weeks period of IOP elevation that was followed by a 1 week period of decreased IOP. Alternatively, 3μl of 10mU/eye chondroitinase ABC was injected into the normal rat eye. The right eye acted as an unoperated control. The animals were kept for two weeks after injection before being sacrificed. Subsequently, a retina was dissected and a gene gun was used to propel DiI-coated tungsten particles into wholemount rat retinal explants (Diolistics). Images of completely stained RGCs were collected by confocal microscopy (as described in section 2.3.2.1). Using the diolistic method,

cells in the ganglion cell layer, both retinal ganglion cells and displaced amacrine cells, are stained randomly by the contact with tungsten particles. Ganglion cells were distinguished by the presence of an axon (Sun et al., 2002). The imaged cells were analysed using a Fast Sholl method (Gutierrez and Davies, 2007). RGC dendrite morphology in control and glaucomatous retinas was compared to the glaucomatous retinas injected with chABC, BDNF, chABC+BDNF and non-glaucomatous retinas injected with chABC. In addition, some retinas were stained with a fluorescent dye Hoechst and the images of retinal ganglion cell layer were collected from 12 retinal areas. RGCs were counted manually using ImageJ plugin Cell Counter. The number of RGCs in glaucomatous retinas injected with chABC or BDNF was compared to the number of RGCs in control retinas. Since not all retinas from the injected rats were labelled in a way that enabled analyses of RGC morphology (some retinas were under-labelled or over-labelled), the number of glaucomatous and control retinas used in the study varied slightly (section 5.2.1).

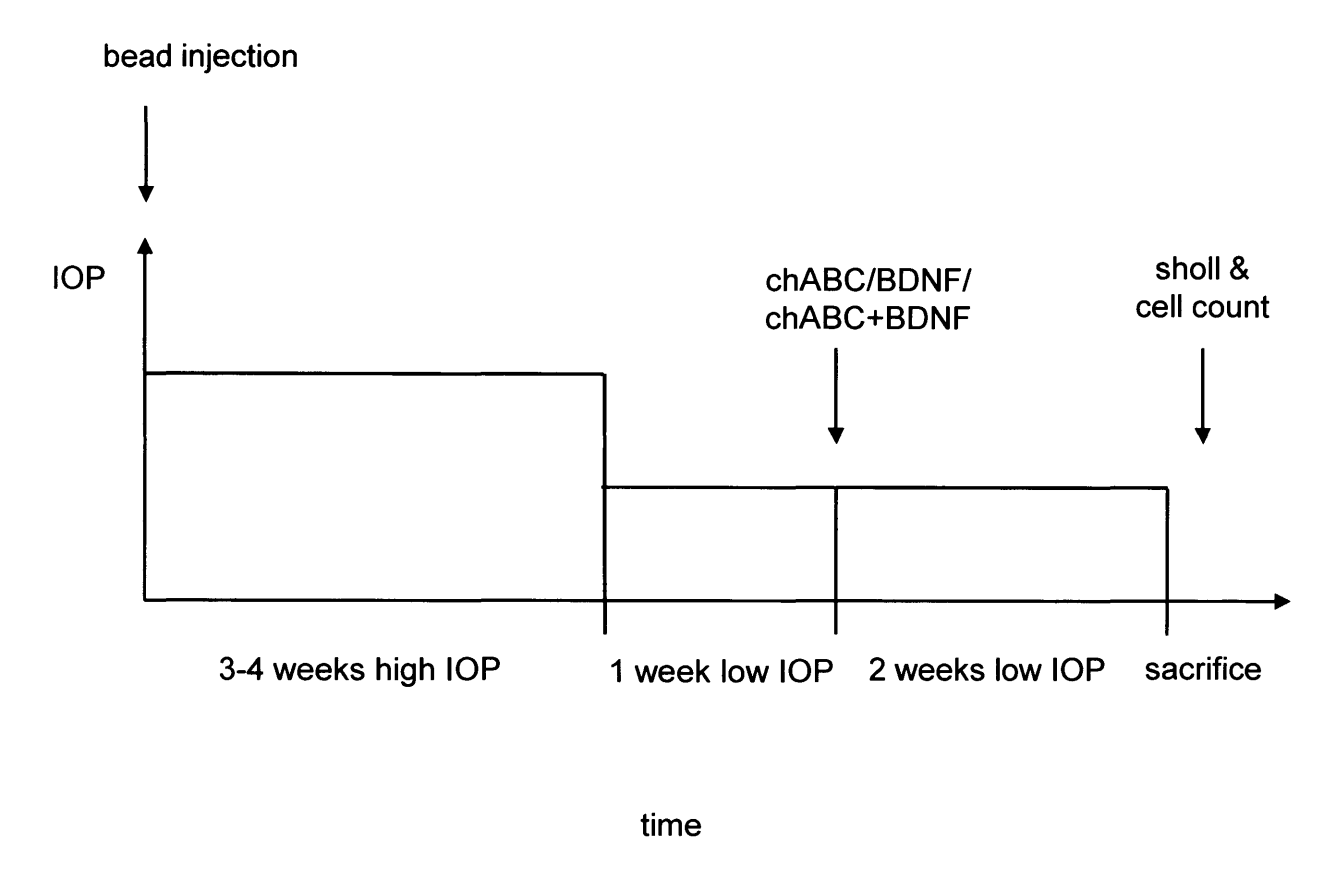


Figure 5.1. A horizontal bar plot showing a plan of the experiment.

#### 5.2 Results

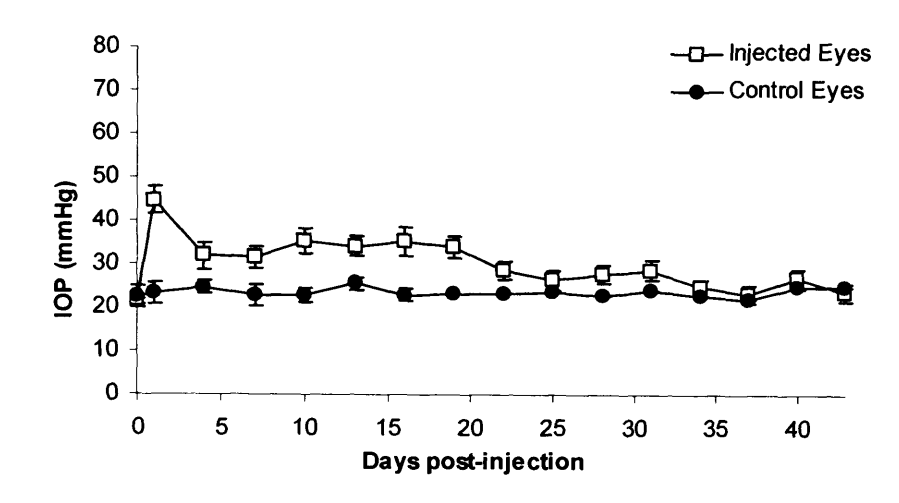
#### 5.2.1. IOP profiles

The IOP profile following first 43 days post-injection is shown in Figure 5.2. Thirty-two rats, whose glaucomatous or control (or both glaucomatous and control) retinas contributed to the study, were used to generate the IOP profiles. The mean IOPs for the rats (n=23) with glaucomatous retinas (including eyes injected with chABC, BDNF or chABC+BDNF) that were used to estimate dendrite morphology were 30.56±1.53 mmHg for injected eyes and 24.27±0.57 mmHg in the contralateral untreated eyes. The mean and peak IOP increases were 6.29±1.43 mmHg and 34.17±1.39 mmHg, respectively, with a mean integral IOP increase of 191.94±49.94 mmHg days. The mean duration of the experimental post-injection period was 58.83±4.02 days.

The mean IOPs for the rats (n=25) whose control retinas were used to estimate dendrite morphology were 29.96±1.36 mmHg for injected eyes and 23.74±0.60 mmHg in the contralateral untreated eyes. The mean and peak IOP increases were 6.22±1.45 mmHg and 35.88±1.52 mmHg, respectively, with a mean integral IOP increase of 177.43±47.49 mmHg days. The mean duration of the post-injection experimental period was 56.96±4.35 days.

The average number of cells analysed per retina was 5.17±0.62.

Α



В

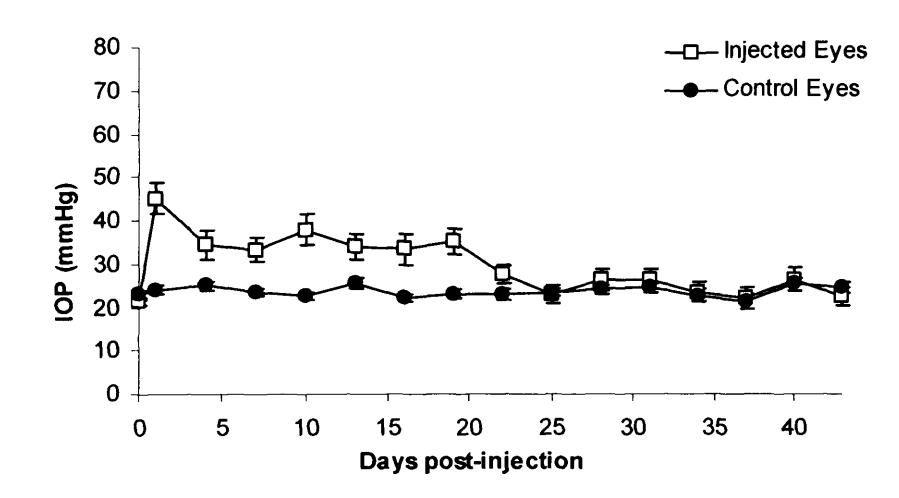


**Figure 5.2.** The mean intraocular pressure (IOP) in the experimental rats whose glaucomatous or/and control retinas were included in the study (n=32) (A) and rats whose glaucomatous retinas were used in the study (n=23) (B) injected with magnetic beads during the first 43 days after injection. Open symbols: injected eyes; closed symbols: control eyes. Error bars: standard error of the mean.

#### 5.2.2. Quantification of dendrite morphology

The injection of magnetic beads into the rat anterior chamber resulted in an induction of ocular hypertension (Figures 5.2 and section 4.2.3.1.). The diolistic method provided extensive labelling of RGCs. However, excessive labelling can reduce the number of cells in which the dendritic tree can be isolated and precisely reconstructed (Morgan et al., 2006). For this reason, only the cells with a dendritic tree clearly distinguishable from those of adjacent cells were analysed. The examples of DiI labelled RGCs from control and glaucomatous eyes are shown in Figure 5.3 while DiI labelled RGCs from glaucomatous eyes injected with chABC, BDNF, chABC+BDNF and RGC from control eye injected with chABC are shown in Figure 5.4.

RGCs (numbers shown in Table 5.1) from control (n=25 eyes), glaucomatous (n=9 eyes), chABC-injected glaucomatous (n=4 eyes), BDNF-injected glaucomatous (n=5 eyes), chABC+BDNF-injected glaucomatous (n=5 eyes) and non-glaucomatous chABC-injected retinas (n=3 eyes) were imaged and their dendritic trees analysed. The sholl plots, the total dendritic length, the number of branching points and the dendritic fields were estimated and compared among the groups as described below and in section 2.3.2.1.3, and are shown in Table 5.1.

The total number of intersections (i.e., the area under the Sholl curve) is directly proportional to the total metric length of the neuritic arbour (Gutierrez and Davies, 2007). The total number of intersections per cell and the number of bifurcations were estimated by the Fast Sholl program. The total neurite length of 20 neurons was measured by manual tracing of dendrites in NeuronJ. As shown in Figure 5.5., the corresponding linear regression shows a strong correlation (R2 = 0.972, P < 0.01) between actual length and the total number of intersections as estimated by Fast Sholl method. The resulting linear equation was subsequently used as a standard curve to derive the total (metric) length in micrometers of dendritic trees in experimental neurons. This calibration method was based on the method described by Gutierrez and Davies, 2007.

Statistical comparisons between the groups were performed in SPSS 16 using Mann-Whitney Test (for data that were not normally distributed) unless otherwise stated, with a significance level of p<0.05 (see Table 5.1, pg 144). The Sholl plots and bars in figures 5.6A, 5.7-5.10 represent mean values  $\pm$  SEM.

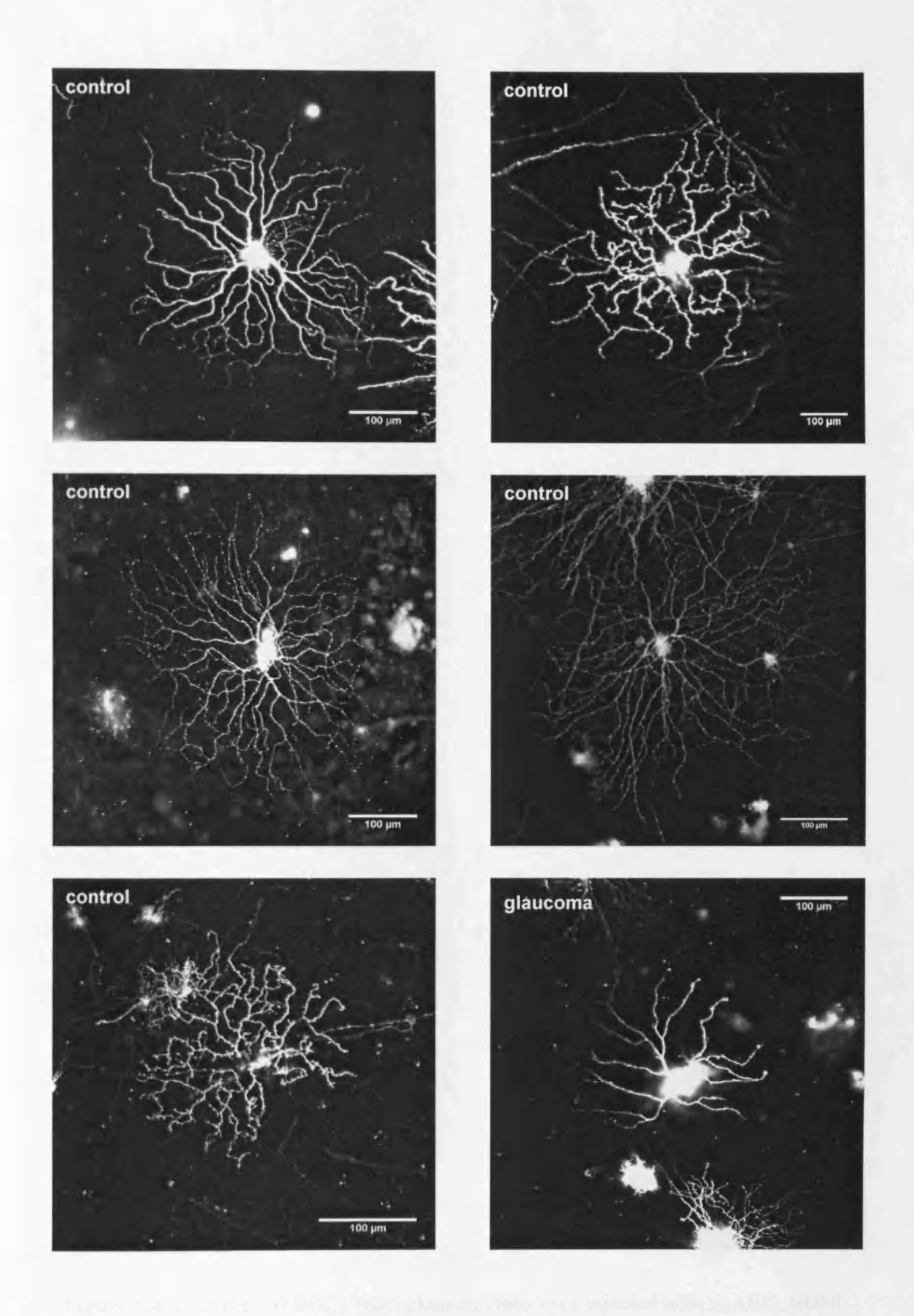
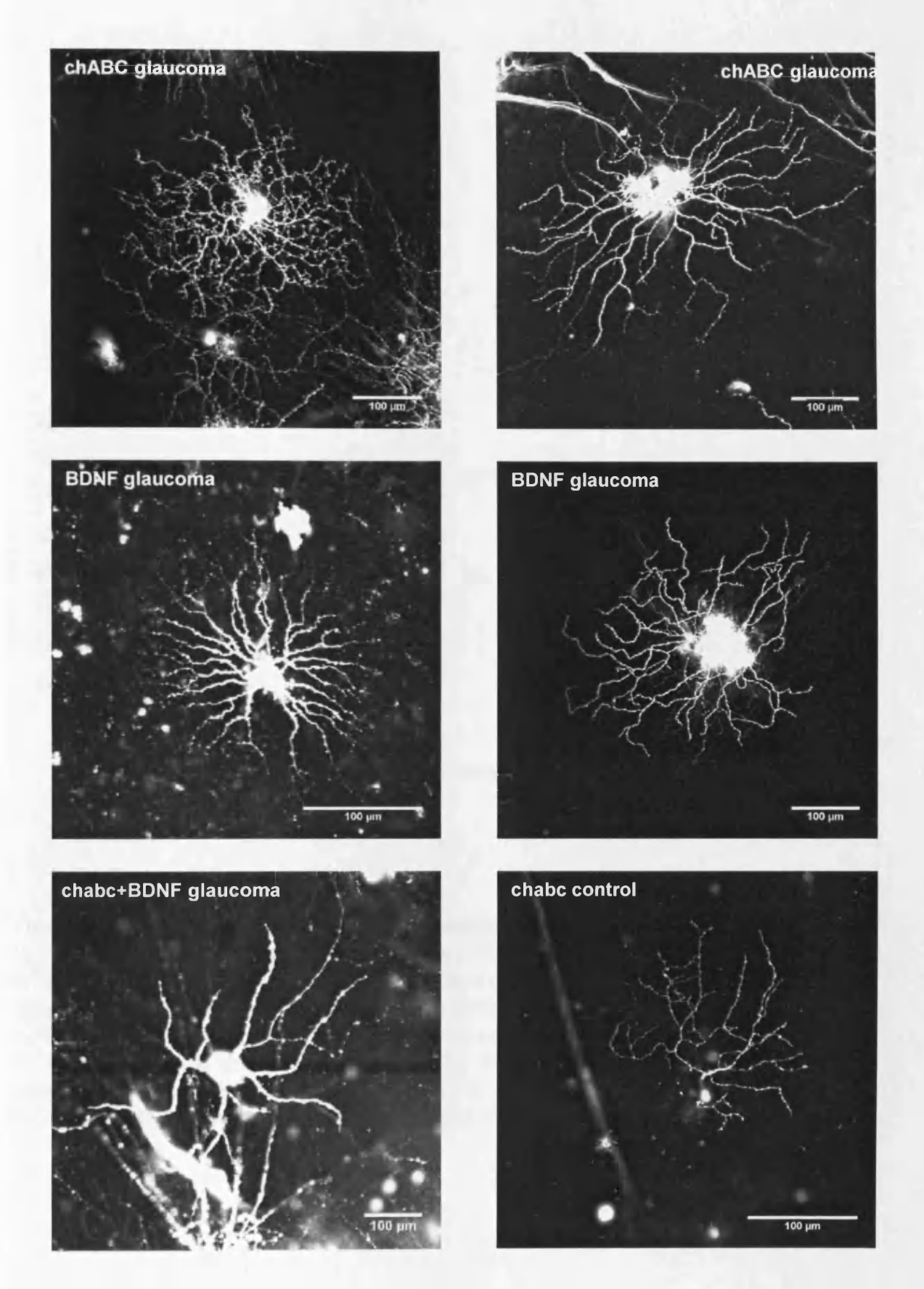


Figure 5.3. Dil labelled RGCs from control and glaucomatous eyes.



**Figure 5.4.** Dil labelled RGCs from glaucomatous eyes injected with chABC, BDNF, chABC+BDNF and RGC from control eye injected with chABC.

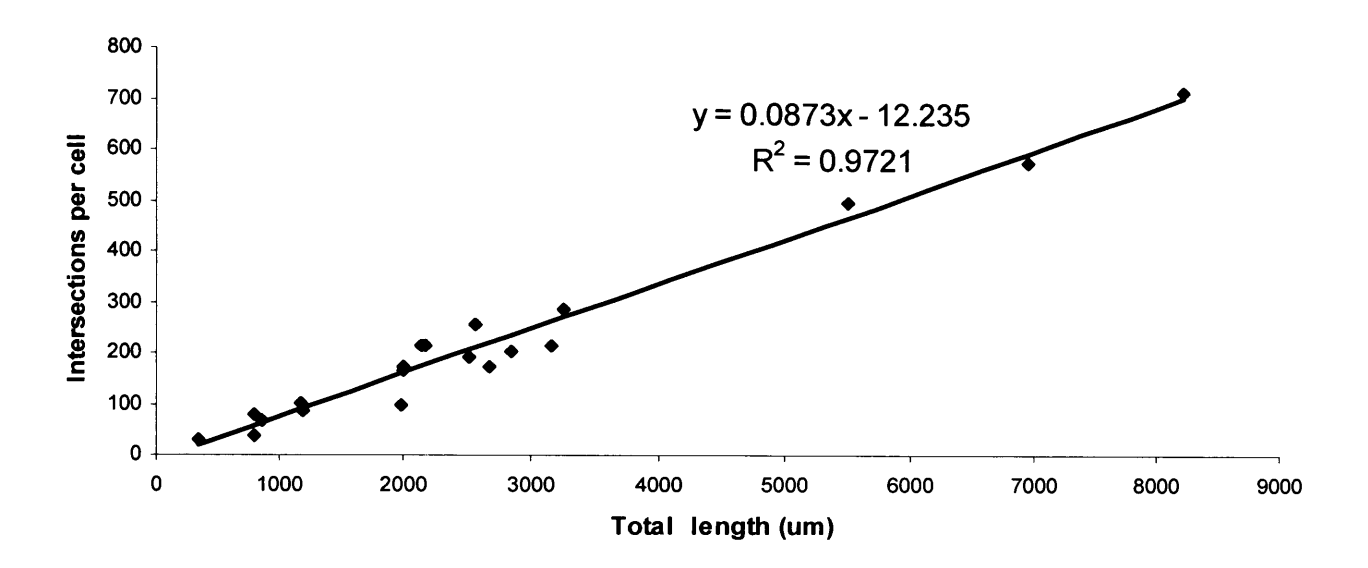


Figure 5.5. Correlation between the total estimated intersections per cell obtained by the Fast Sholl and the total length in micrometers of the dendritic arbours per cell as estimated by independent neurite tracing. Twenty individual neurons were sampled across the range of morphologies and the total number of estimated intersections derived according to the method described in the results section (vertical axis). Total dendritic length was measured by direct tracing of the dendrites (horizontal axis). The resulting linear equation can subsequently be used as a standard curve to calculate the total (metric) length in micrometers of dendritic arbours in experimental samples of neurons.

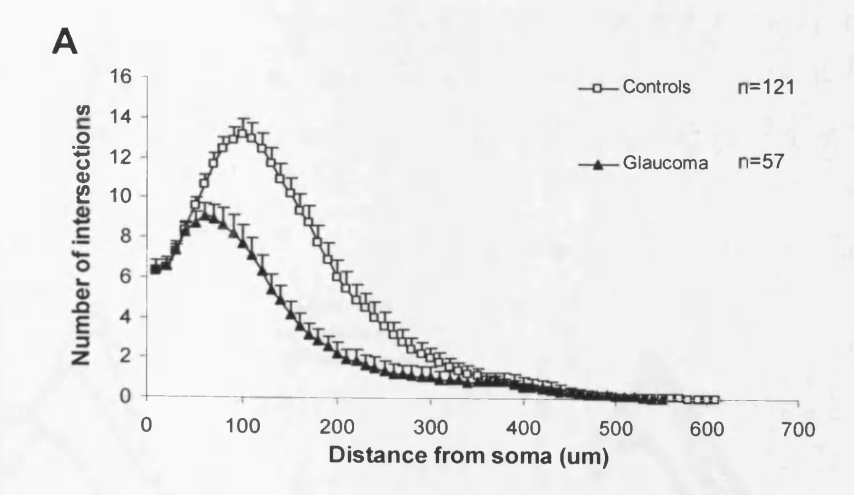
#### 5.2.2.1. Dendrite morphology in glaucoma vs. control

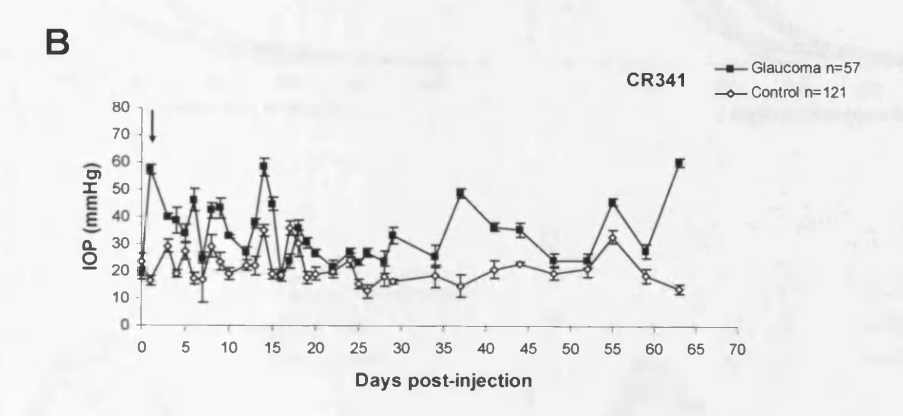
A typical IOP plot for a magnetic bead model is shown in Figure 5.6B. In Figures 5.6C&D, sample cells are shown from normal and glaucomatous retinas, respectively, indicating pruning of the dendritic tree with reduction in the complexity of the dendritic tree and overall dendritic area. The mean reduction in dendritic tree area for RGCs from the glaucomatous retinas was 33.0% compared with control retinas  $(76435.70\pm14171.26~\mu m^2~vs.~114028.60\pm11122.86~\mu m^2)$  (Figure 5.10). Sholl analysis revealed a 39.5% reduction in the number of intersections in glaucomatous retinas compared to control retinas (148.13±17.49 vs. 245.17±15.94, P<0.001). The maximum number of intersections for control RGCs was 13.21 at 100 µm distance from soma while, for glaucomatous RGCs, 9.07 at 60 µm distance from soma. Beyond these distances, the number of intersections decreased until the last measured point, at 610 µm distance from soma for control and at 540 µm distance from soma for glaucomatous RGCs (Figure 5.6A). The total dendritic length, proportional to the number of intersections, was significantly decreased in glaucoma compared to controls (1807.12±198.99 µm vs. 2948.47±182.60 µm, P<0.001) (Figure 5.8). The number of branching points was also significantly reduced in glaucoma compared to controls (11.96±1.85 vs. 28.88±1.74, P<0.001) (Figure 5.9).

### 5.2.2.2. Dendrite morphology in the treated retinas vs. glaucomatous and control retinas

#### **5.2.2.2.1. Sholl plots**

Figure 5.7 shows Sholl analysis of RGC dendrites from control, glaucomatous, and either chABC-injected glaucomatous (Figure 5.7A), BDNF-injected glaucomatous (Figure 5.7B), chABC+BDNF-injected glaucomatous retinas (Figure 5.7C) and non-glaucomatous chABC-injected (Figure 5.7D).





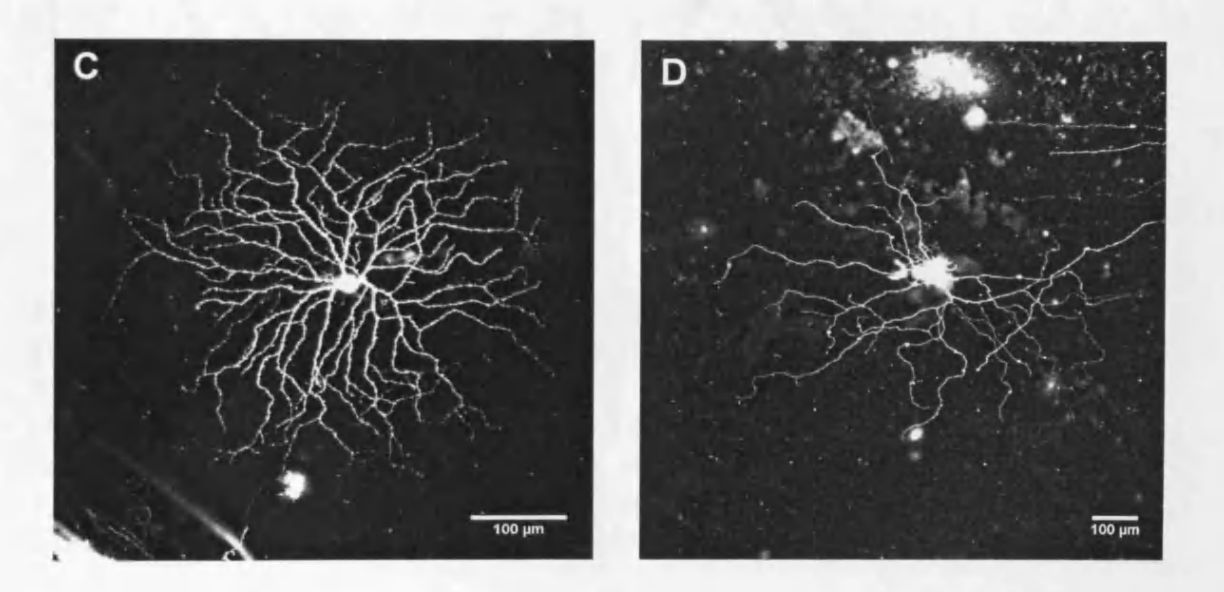
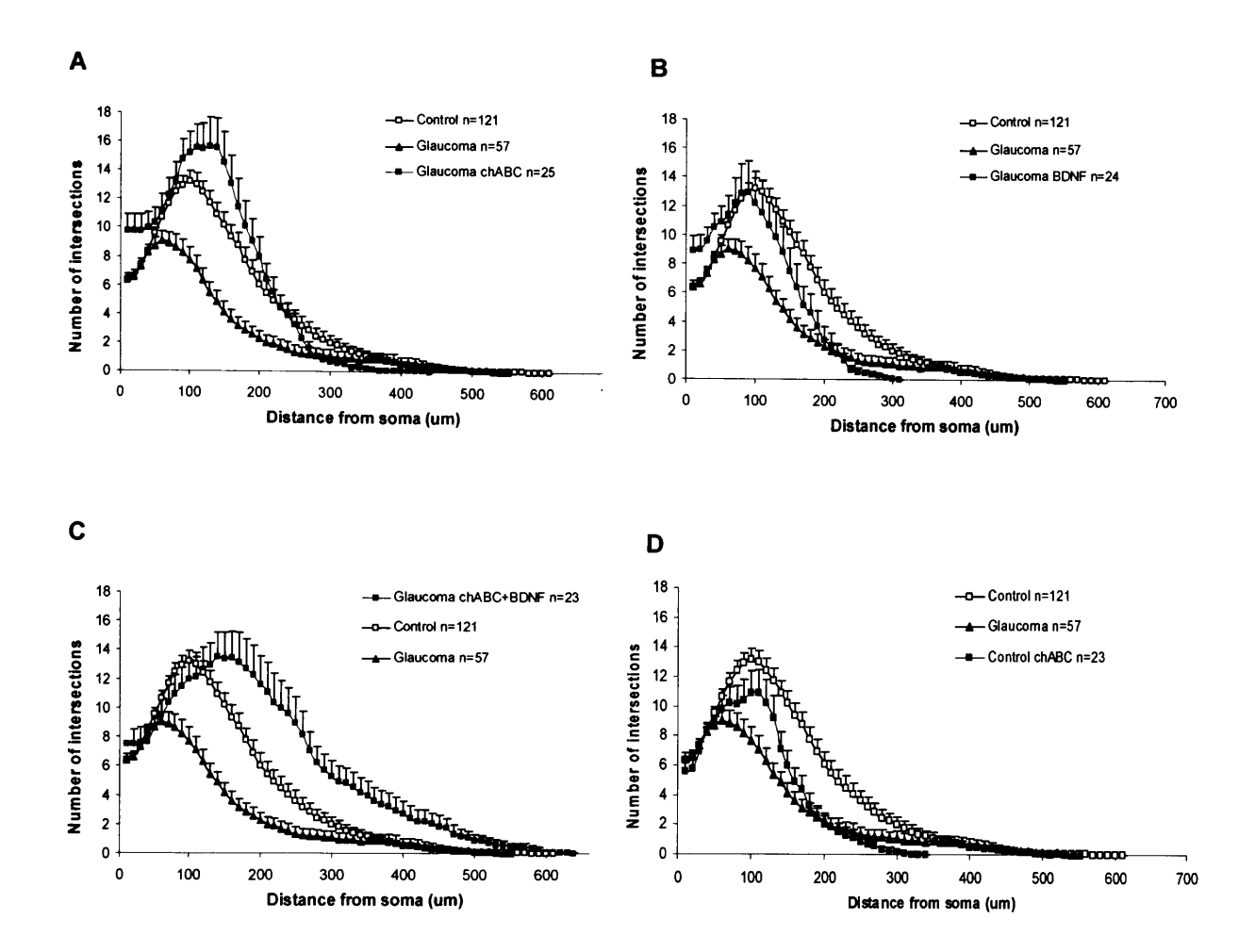


Figure 5.6. (A) Sholl analysis of RGC dendrites from control (white symbols) and glaucomatous retinas (black symbols) showing reduction in the number of intersections relative to the distance from cell soma for RGCs from glaucomatous retinas. The radial distances were calculated and the corresponding 10  $\mu$ m intervals assigned to each branching and/or terminal point. Error bars indicate SEM. (B) A typical IOP plot for a magnetic bead model. Intraocular pressures (IOP) following single bead injections in rat CR341. The arrow indicates time of injections. Error bars: standard deviations. Open symbols: control; closed symbols: glaucoma. N indicates the number of analysed cells. Dil labelled RGCs from (C) normal eye and (B) glaucomatous eye.



**Figure 5.7.** Sholl analysis of RGC dendrites from control retinas (white symbols), glaucoma (black symbols), chABC-injected glaucomatous retinas (grey symbols) (A), BDNF-injected glaucomatous retinas (grey symbols) (B), chABC+BDNF-injected glaucomatous retinas (grey symbols) (C) and chABC-injected negative control retinas (grey symbols) (D). The radial distances were calculated and the corresponding 10 μm intervals assigned to each branching and/or terminal point. Error bars indicate SEM. N indicates the number of analysed cells.

#### 5.2.2.2. Dendrite morphology in chABC-injected glaucomatous eyes

Intravitreal injection of  $10 \text{mU/3}\mu l$  chABC after a 3-4 week period of IOP elevation resulted in a significant increase of the total dendritic length in chABC-injected glaucomatous retinas compared to untreated glaucomatous retinas (3199.94±326.97 µm vs.  $1807.11\pm198.99$  µm, P<0.001) (Figure 5.8A). In addition, the number of branching points was significantly increased in chABC-injected eyes with glaucoma compared to glaucomatous retinas (27.04±5.56 vs.  $11.96\pm1.85$ , P<0.01) (Figure 5.9A). Both the total dendritic length and the number of branching points from chABC-treated glaucomatous eyes were not significantly different from control eyes (3199.94±326.97 µm vs.  $2948.47\pm182.60$  µm and  $27.04\pm5.56$  vs.  $28.88\pm1.74$ , respectively) (Figures 5.8A & 5.9A). A significant increase in the dendritic field area was observed in chABC-injected eyes with glaucoma compared to untreated glaucomatous retinas (95866.53±8838.97 µm² vs.  $76435.70\pm14171.26$  µm², P<0.01) (Figure 5.10A). However, the dendritic field area in these eyes was significantly reduced compared with controls (95866.53±8838.97 µm² vs.  $114028.60\pm11122.86$  µm², P<0.05) (Figure 5.10A).

#### 5.2.2.2.3. Dendrite morphology in BDNF-injected glaucomatous eyes

Intravitreal injection of 1µI of 1µg/µI BDNF after 3-4 weeks of IOP elevation led to a significant increase in the number of branching points in BDNF-injected eyes with glaucoma compared to glaucomatous retinas (26.29±4.35 vs. 11.96±1.85, P<0.001) and was not significantly different to that in controls (28.88±1.74) (Figure 5.9B). In contrast, other morphological features such as the total dendritic length and the dendritic field area were not significantly increased in BDNF-injected glaucomatous eyes compared to glaucoma (2306.53±298.03 µm vs. 1807.11±198.99 µm and 60029.35±9081.45 µm² vs. 76435.70±14171.26 µm², respectively). While the total dendritic length did not differ significantly from controls (2306.53±298.03 µm vs. 2948.47±182.60 µm), the dendritic field area was significantly lower than in controls (60029.35±9081.45 µm² vs. 114028.60±11122.86 µm², P<0.05) (Figures 5.8B & 5.10B).

#### 5.2.2.2.4. Dendrite morphology in chABC+BDNF-injected glaucomatous eyes

The combined treatment of 10mU/3µl chABC 1µl and 1µg/µl BDNF following the 3-4 week period of IOP elevation resulted in a significant increase in the total dendritic length in chABC+BDNF-injected glaucomatous retinas compared to glaucomatous  $(4306.19\pm481.49 \mu m \text{ vs. } 1807.12\pm198.99 \mu m, P<0.001)$  and control retinas (4306.19±481.49 μm vs. 2948.47±182.60 μm, P<0.001) (Figure 5.8C). In addition, the total length in chABC+BDNF-injected eyes was significantly higher than in BDNF-injected eyes (4306.19±481.49 µm vs. 2306.53±298.03 µm, P<0.01) (Figure 5.8B) but not significantly higher than in chABC-injected glaucomatous retinas (3199.94±326.97 µm) (Figure 5.8A). In addition, the dendritic field area in chABC+BDNF-injected glaucomatous retinas was significantly increased compared to glaucomatous retinas  $(264754.68\pm40080.85 \mu m^2 vs. 76435.70\pm14171.26 \mu m^2)$ P<0.001) and to controls (264754.68±40080.85  $\mu$ m<sup>2</sup> vs. 114028.60±11122.86  $\mu$ m<sup>2</sup>, P<0.001) (Figure 5.10C). In contrast, chABC+BDNF-injected glaucomatous retinas had a slightly reduced number of branching points compared to glaucomatous retinas (13.61±2.23 vs. 11.96±1.85), and there was a significant reduction compared to control retinas (13.61±2.23 vs. 28.88±1.74, P<0.001) (Figure 5.9C).

#### 5.2.2.2.5. Dendrite morphology in non-glaucomatous chABC-injected eyes

Intravitreal injection of  $10 \text{mU/3}\mu l$  chABC into the normal eyes led to a significant increase in the total dendritic length in RGCs of non-glaucomatous chABC-injected retinas compared to glaucomatous retinas (1929.95±196.74  $\mu m$  vs. 1807.12±198.99  $\mu m$ ) (Figure 5.8D). However, it was significantly lower than in controls (1929.95±196.74  $\mu m$  vs. 2948.47±182.60  $\mu m$ , P<0.05) and chABC-injected glaucomatous retinas (1929.95±196.74  $\mu m$  vs. 3199.94±326.97  $\mu m$ , P<0.001, Independent T-Test) (Figure 5.8A). The number of branching points was significantly higher in RGCs of non-glaucomatous chABC-injected retinas than in glaucomatous retinas (17.71±2.21 vs. 11.96±1.85, P<0.05) but significantly lower than in controls (17.71±2.21 vs. 28.88±1.74, P<0.05) and not significantly different from chABC-injected glaucomatous retinas (27.04±5.56) (Figure 5.9A). Dendritic field area was not significantly different in RGCs of non-glaucomatous chABC-injected retinas compared to glaucomatous retinas (58010.32±7907.45  $\mu m^2$  vs. 76435.70±14171.26

 $\mu$ m²) but was significantly lower than in controls (58010.32±7907.45  $\mu$ m² vs. 114028.60±11122.86  $\mu$ m², P<0.05) (Figure 5.10C) and significantly lower than in chABC-injected glaucomatous retinas (58010.32±7907.45  $\mu$ m² vs. 95866.53±8838.97  $\mu$ m², P<0.01) (Figure 5.10A).

#### 5.2.2.6. Summary of the results

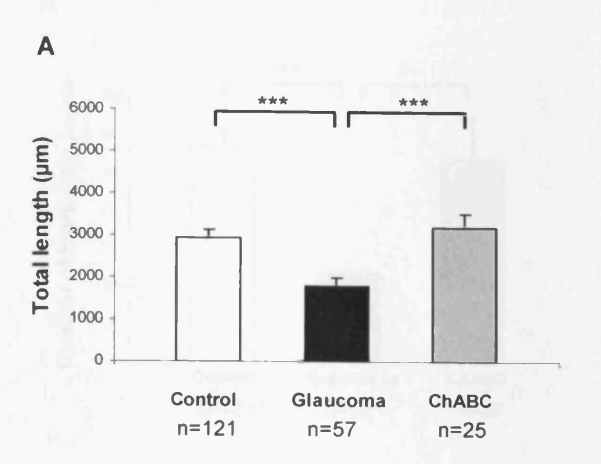
Table 5.1 summarises the morphological features identified in retinal ganglion cells from eyes subjected to different treatments.

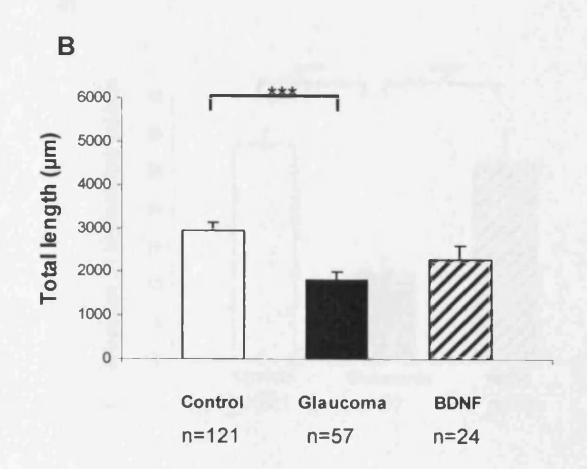
## 5.2.3. The presence of chABC generated epitopes in the retina after intravitreal injections

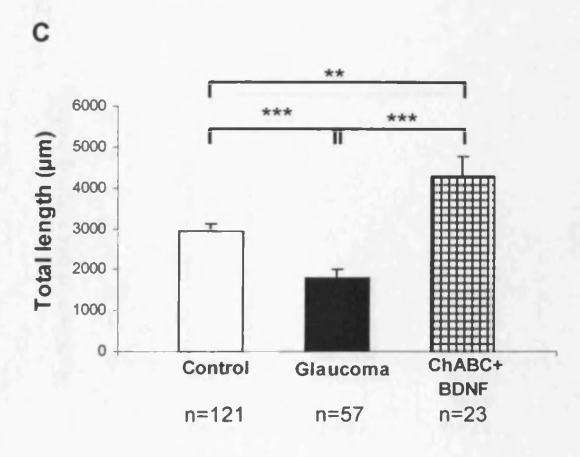
To confirm that the intravitreal injections of chABC digested chondroitin sulphate proteoglycans, immunohistochemistry was conducted (section 2.4.2.3) on a single, non-glaucomatous retina injected with chABC. Incubation of retinal sections with a mixture of monoclonal antibodies specific for chondroitinase ABC-generated chondroitin-6-sulphate (3B3), chondroitin-4-sulphate (2B6) and chondroitin-0-sulphate (1B5) disaccharide epitopes demonstrated immunostaining throughout the retina that was detectable 24 hours following the intravitreal injection of chABC into the rat eye (Figure 5.11A). The positive control section, which was also further digested by chABC directly on the slide, showed strong immunostaining throughout the retina that was the strongest in the photoreceptor layer (Figure 5.11B), indicating that not all epitopes had been exposed by the intravitreal injection. No immunostaining was detected in the section incubated without primary antibodies (Figure 5.11C).

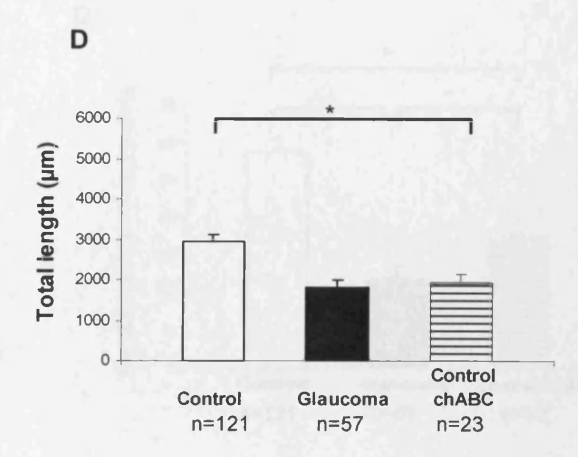
#### 5.2.4. RGC cell loss in the chABC and BDNF-treated retinas

In addition to examining changes in dendrite morphology following treatments with chABC and BDNF, RGCs of the treated glaucomatous and non-treated contralateral eyes from the same rats were counted to estimate the cell loss. RGC cell losses were 40.9%±11.4 for BDNF-injected rats and 35.8%±1.9 for chABC-injected rats compared to the 36.4±2.4% RGC loss in the non-treated glaucomatous eyes (section 4.4.2).

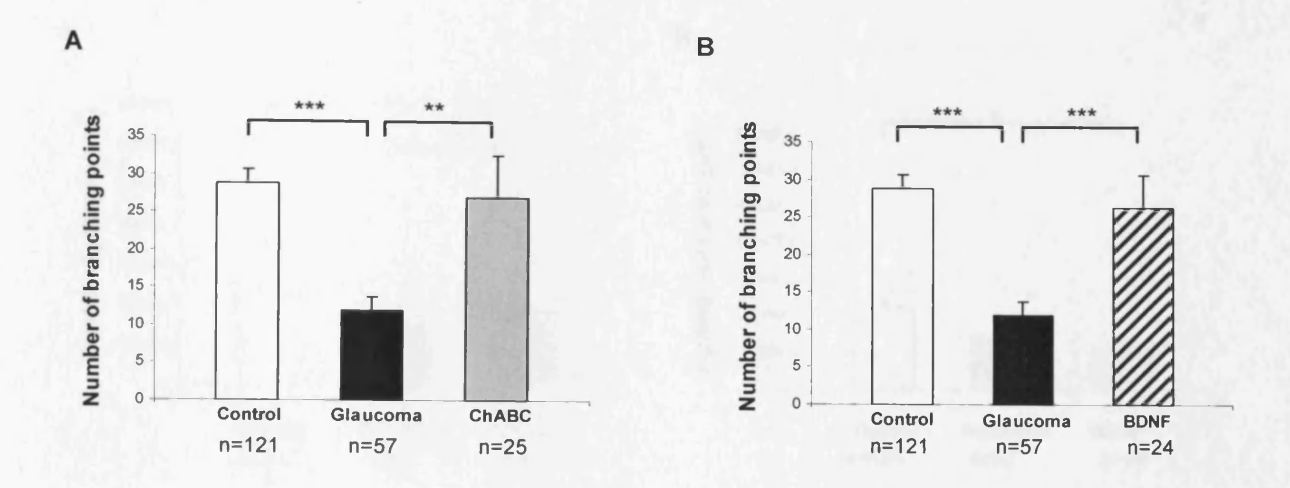








**Figure 5.8.** The total dendritic length was compared among the groups. White bars indicate mean values for control retinas, black for glaucoma, grey for chABC-injected glaucomatous retinas (A), diagonal stripes for BDNF-injected glaucomatous retinas (B), grid for chABC+BDNF-injected glaucomatous retinas (C) and horizontal lines for chABC-injected negative control retinas (D). Error bars indicate SEM. \* p<0.05, \*\* p<0.01, \*\*\*p<0.001. N indicates the number of analysed cells.



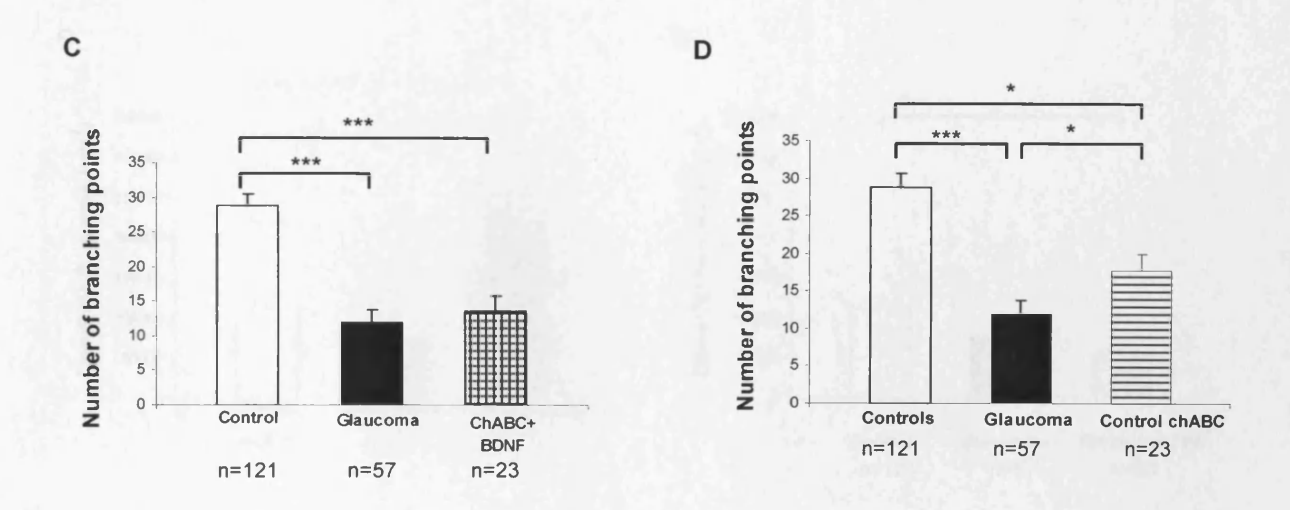


**Figure 5.9.** The number of branching points was compared among the groups. White bars indicate mean values for control retinas, black for glaucoma, grey for chABC-injected glaucomatous retinas (A), diagonal stripes for BDNF-injected glaucomatous retinas (B), grid for chABC+BDNF-injected glaucomatous retinas (C) and horizontal lines for chABC-injected negative control retinas (D). Error bars indicate SEM. \* p<0.05, \*\* p<0.01, \*\*\*p<0.001. N indicates the number of analysed cells.

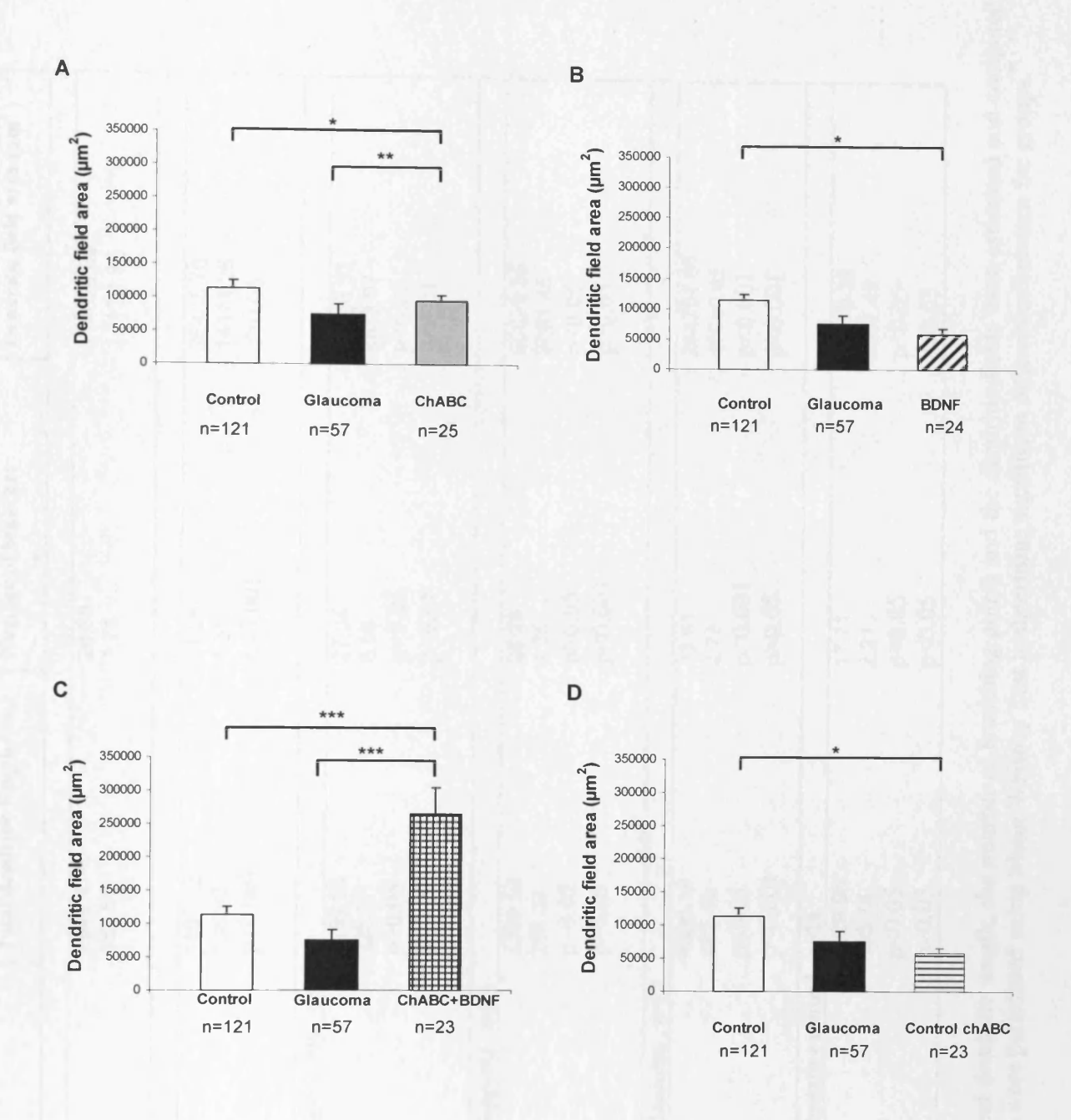


**Figure 5.10.** The dendritic field areas were compared among the groups. White bars indicate mean values for control retinas, black for glaucoma, grey for chABC-injected glaucomatous retinas (A), diagonal stripes for BDNF-injected glaucomatous retinas (B), grid for chABC+BDNF-injected glaucomatous retinas (C) and horizontal lines for chABC-injected negative control retinas (D). Error bars indicate SEM. \* p<0.05, \*\* p<0.01, \*\*\*p<0.001. N indicates the number of analysed cells.

	Total dendritic length (μm)	Number of branches	Dendritic field area (μm²)
Control n=121			
Mean	2948.47	28.88	114028.60
SEM	182.60	1.74	11122.86
Glaucoma n=57			
Mean	1807.12	11.96	76435.70
SEM	198.99	1.85	14171.26
Vs Control	p<0.001	p<0.001	p>0.05
ChABC-injected glauco	oma n=25		
Mean	3199.94	27.04	95866.53
SEM	326.97	5.56	8838.97
Vs Control	p>0.05	p>0.05	p<0.05
Vs Glaucoma	p<0.001	p<0.01	p<0.01
BDNF-injected glaucon	na n=24		
Mean	2306.53	26.29	60029.35
SEM	298.03	4.35	9081.45
Vs Control	p>0.05	p>0.05	p<0.05
Vs Glaucoma	p>0.05	p<0.001	p>0.05
ChABC+BDNF glaucon	ma n=23		
Mean	4306.19	13.61	264754.68
SEM	481.49	2.23	40080.85
Vs Control	p<0.01	p<0.001	p<0.001
Vs Glaucoma	p<0.001	p>0.05	p<0.001
ChABC-injected negati			
Mean	1929.95	17.71	58010.32
SEM	196.74	2.21	7907.45
Vs Control	p<0.05	p<0.05	p<0.05
Vs Glaucoma	p>0.05	p<0.05	p>0.05

**Table 5.1.** Summary of the total dendritic length, the number of branching points and the dendritic fields were estimated and compared among the groups. Statistical analyses were performed using Mann-Whitney Test to determine significant differences between the groups.

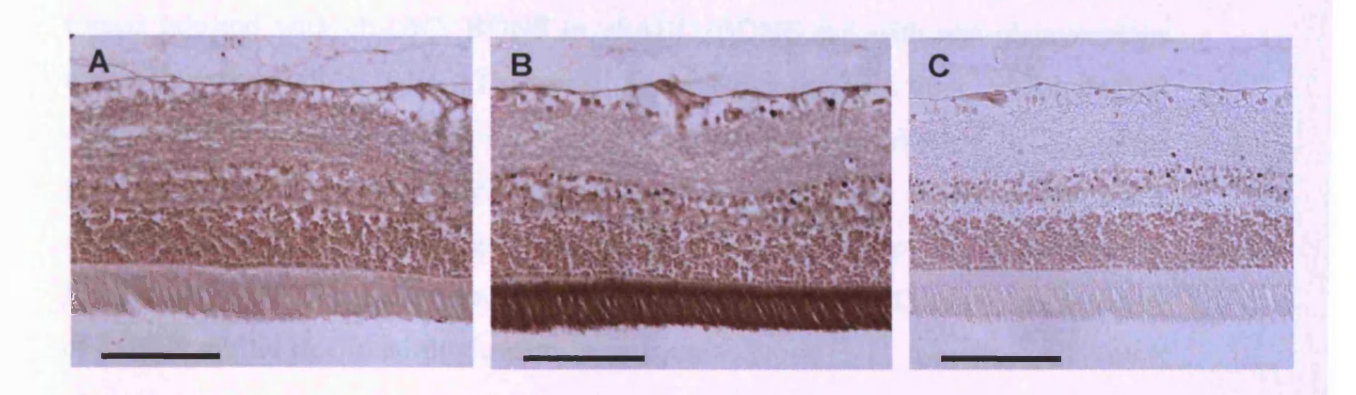


Figure 5.11. Rat retinal sections from a control adult rat eye injected intravitreally with chondroitinase ABC. Section incubated with a mixture of antibodies specific for chondroitin-0-sulphate (1B5), chondroitin-4-sulphate (2B6) and chondroitin-6-sulphate (3B3) demonstrated immunostaining throughout the retina that was detectable 24 hours following the intravitreal injection of chABC into the rat eye (A). Section digested with chondroitinase ABC directly on the slide prior to incubation with the antibodies 1B5, 2B6 and 3B3 showed a strong immunostaining throughout the retina that was the strongest in the photoreceptor layer (B). Section incubated without primary antibodies did not show immunostaining (C). Scale, 100 μm.

#### 5.3. Discussion

#### 5.3.1. Quantification of RGC dendritic morphology

The dendritic morphology of RGCs in control and glaucomatous retinas was quantified and compared to the dendritic morphology of RGCs in glaucomatous retinas injected with chABC, BDNF or chABC+BDNF and with non-glaucomatous retinas injected with chABC. The study showed, for the first time, morphological changes in RGCs in a magnetic bead model of glaucoma. The principal finding of the present study is that the treatment of glaucomatous retinas with chABC resulted in a significant change in all investigated morphological parameters of RGCs compared to RGCs of non-treated glaucomatous eyes, suggesting that chABC promoted recovery of RGC dendritic tree in adult glaucomatous eyes.

#### 5.3.1.1. Dendritic morphology in experimental glaucoma

Morphological changes in RGCs of glaucomatous eyes in comparison to contralateral control eyes were observed in a magnetic bead model of glaucoma. Marked pruning of the dendritic tree of labelled RGCs in glaucomatous retinas was observed as compared to normal. There was a statistically significant reduction in total dendritic length and the number of branching points in glaucomatous retinas compared to controls (p<0.001). Dendritic field area was modestly (by 33%) but not significantly reduced in glaucomatous RGCs compared to controls. The dendritic field of control RGCs, 114028.60±11122.86 μm², was larger compared to the dendritic field estimated by Sun et al (2002), ranging from 14306.63 to 75438.5 μm² for different RGC types (the dendritic field was calculated from the dendritic field diameter shown in Table 1). However, larger cells have been reported, with a dendritic field of a few hundred micrometres (Gan et al., 2000).

Morphological changes of RGCs in experimental rat glaucoma have been demonstrated (Morgan et al., 2006). The reduction in the dendritic field diameter for RGCs of the glaucomatous retinas compared to controls was 25.7% (P<0.001) (Morgan et al., 2006). The complexity of the dendritic field, as a number of dendritic

branches intersecting with each ring was reduced (Morgan et al., 2006). In experimental primate glaucoma, there was a reduction in the size of the RGC dendritic arborisation, with pruning of the terminal branches followed by a reduction in the size of the cell bodies and axons and eventual cell death (Weber et al., 1998). Similarly in cat retina, soma size, dendritic field, total dendritic length, and the number of branch bifurcations of dendrites was significantly reduced in glaucomatous eyes compared to normal eyes (Shou et al., 2003). These findings might be explained as the apparent selective loss of larger RGCs in glaucoma or by a reduction in RGC dendritic tree and cell soma area. The second explanation is in agreement with clinical psychophysical studies that failed to show selective damage to magnocellular or parvocellular retinogeniculate pathways in early glaucoma (Ansari et al., 2002; Graham et al., 1996).

In contrast to our findings and the above studies, Ahmed et al. (2001a) observed an increase in the soma and dendritic field diameter of dying RGCs in eyes with elevated IOP, suggesting the existence of plasticity in adult retina. These observations support the study performed on cat retina, demonstrating that the spaces vacated by dying cells allowed the remaining cells to increase their dendritic field and soma size (Kirby and Chalupa, 1986). Also, another study found that severe optic nerve damage caused 50% RGC death in adult rats and the surviving cells increased their cell size within 15 days (Rousseau et al., 1999). Ahmed et al. (2001a) suggested that the likely explanation for the increase in dendritic trees of the surviving RGCs might be the presence of free synaptic endings of bipolar and amacrine cells that could stimulate hypertrophy of the remaining ganglion cells. Consequently, there could be the formation of synaptic connections by these cells onto the remaining RGCs. However, there is no evidence to support this hypothesis (Ahmed et al, 2001a). The contrasting observations of the morphological neuronal changes in glaucoma in the studies showing an increase and the studies showing a reduction in the dendritic field and soma sizes might be due to the selectivity of measurement of individual labelled RGCs (Ahmed et al., 2001a).

It could be argued that the morphological changes observed in glaucoma were caused by severing of RGC axons during the retinal whole-mount preparation and by mechanical shock from the gene gun. Although this possibility cannot be ruled out completely, the degenerative changes described here for the glaucomatous retinas are highly representative and vary morphologically from normal retinas that were subjected to the same experimental approach. Moreover, 36.4±2.4% RGC death in glaucomatous eyes was observed for the magnetic bead model (Chapter 4.4.2). Overall, it is very unlikely that the morphological RGC changes in glaucoma were caused by factors other than an elevated IOP. However, considering the spiking IOPs in some rats (Chapter 4), there is a chance that some ischaemia was induced within the retina.

Another argument could be that the reduction in the dendritic field size is due to an inability to label distal processes of degenerating ganglion cells. However, the termination of label at the dendrite tips was consistent with a complete fill since DiI has been shown to label the complete dendritic field (Huxlin and Goodchild, 1997; Sun et al., 2002).

#### 5.3.1.2. Dendritic morphology after chondroitinase ABC injection

The primary goal of this study was to determine whether the bacterial enzyme chondroitinase ABC, by digestion of the perineuronal net, might promote retinal ganglion cell remodelling in experimental rat glaucoma. The results showed that the intravitreal injection of chABC resulted in a significant increase in the total dendritic length compared to the glaucomatous non-treated retinas. The total dendritic length in the glaucomatous eyes treated with chABC was not significantly different from control retinas. Also, the number of branching points was significantly higher in chABC-treated injured eyes than in non-treated glaucomatous eyes but not significantly different than in control eyes. Additionally, there was a significant increase in the dendritic field area in chABC-treated glaucomatous retinas compared to non-treated retinas from rats with glaucoma. However, the dendritic field area remained significantly lower in chABC-injected glaucomatous eyes than in control eyes. These data indicate that chABC promoted recovery of RGCs dendritic tree from adult rats with glaucoma. The recovered dendritic complexity was very similar to the complexity of control RGCs, though the recovery was still only partial.

#### 5.3.1.2.1. Chondroitinase ABC-promoted plasticity

A number of studies have established that the chondroitinase ABC promotes functional recovery in the injured CNS by degrading inhibitory chondroitin sulphate glycosaminoglycan chains. For example, the enzyme promoted axonal regeneration and the reactivation of plasticity (Crespo et al., 2007). ChABC was found to reactivate ocular dominance plasticity in the adult visual cortex (Pizzorusso et al., 2002; Pizzorusso et al., 2006) by removing the perineuronal chondroitin sulphate proteoglycans. Tropea et al. (2003) showed that, following injury, chABC injections into the partially denervated superior colliculus increased sprouting of the remaining retinal ganglion cell axons into the collicular scotoma. Sprouting was enhanced by combining BDNF with chABC (Tropea et al., 2003). In the rat cerebellum, degradation of CS-GAG chains by injections of chABC promoted an outgrowth of Purkinje axons (Corvetti and Rossi, 2005). Moreover, axon regeneration in the adult rat nigrostriatal tract was enhanced by the treatment with chABC (Moon et al., 2001). Following spinal cord injury, treatment with chABC resulted in regrowth of axons into the denervated territory and recovery of motor and bladder function in rats (Bradbury et al., 2002; Caggiano et al., 2005). ChABC also enhanced plasticity of intact systems within the brainstem and spinal cord after spinal cord injury (Barritt et al., 2006). Additionally, chABC digestion of the perineuronal nets promoted a functional change directly linked to anatomical evidence of sprouting by spinal cord afferents (Massey et al., 2006). A recent study has shown that the combined use of chABC, growth factors and neural stem/progenitor cells (NPCs) promoted functional repair and plasticity of the chronically injured spinal cord in adult rats (Karimi-Abdolrezaee et al., 2010). In organotypic culture, treatment with chABC increased the motility of dendritic spines (Chierzi et al., 2005). Since the spines are much more dynamic in the immature CNS than in the adult, they might indicate the occurrence of plasticity (Grutzendler et al., 2002). Another study showed that chABC improved functional recovery after peripheral nerve injury by promoting plasticity in the spinal cord. Thus, enhanced plasticity in the spinal cord allowed the CNS to compensate for inaccurate motor and sensory re-innervation of the periphery (Galtrey et al., 2007).

It has been shown that the chABC treatment did not cause detrimental effects on neuronal survival, alterations of visual acuity, or abnormalities of receptive field size

150

and spiking activity of visual cortical neurons (Pizzorusso et al., 2002). Similar conclusions related to the neuronal survival were drawn after comparing RGC loss from the non-treated glaucomatous rats with RGC loss from chABC-treated rats with glaucoma. The administration of chABC did not cause a significant change in the cell loss in the treated eyes compared to the non-treated glaucomatous eyes.

#### 5.3.1.3. Dendritic morphology after BDNF injection

It has been demonstrated that glaucoma-related optic nerve injury leads to the degeneration of retinal ganglion cells which begins with the dendritic tree, suggesting an opportunity for reversing glaucomatous neuropathy by applying various neuroprotectants (Weber et al., 1998). Brain-derived neurotrophic factor (BDNF) is one of the most promising neuroprotective trophic factors that has been studied (Chen and Weber, 2001; Weber and Harman, 2008). In addition to enhancing RGC survival, BDNF can also help to preserve dendritic integrity. Optic nerve injury in cats resulted in a significant reduction in the soma, dendritic field size and dendritic complexity indicated by a decrease in number of branches, total dendritic length, and dendritic surface area. Intravitreal treatment of the eye with BDNF at the time of injury resulted in enhanced preservation of soma and dendritic morphology. BDNF treatment resulted also in enhanced visual responses relative to no treatment (Weber and Harman, 2008).

The focus of the present study was to examine whether the surviving RGCs retained their normal dendritic morphology, an essential step towards maintaining neuronal function after glaucomatous injury. In this investigation, intravitreal injection of BDNF into the glaucomatous eye resulted in a significant increase in the number of dendrite bifurcations in the treated eyes with ocular hypertension compared to the non-treated eyes, supporting the previous study (Weber and Harman, 2008). However, other dendritic features, namely the total dendritic length and the dendritic field area, were not significantly different in the BDNF-treated glaucomatous eyes compared to the glaucomatous non-treated eyes. The fact that we observed a poorer effect of BDNF on the preservation of dendritic integrity than Weber & Harman (2008) might be due to the injection being made after a period of increased IOP and different injection dose. While rats in the study received a single, intravitreal injection of 1  $\mu$ l

of 1µg/µl BDNF after approximately 3-4 weeks of IOP elevation followed by the period of decreased IOP (approximately 1 week), Weber & Harman (2008) injected either 30 or 90 µl of 1µg/µl BDNF into the cat eyes immediately after optic nerve crush. The injected dose for the rats was consistent with studies investigating patterns of RGC survival following BDNF-administration in hypertensive eyes (Ko et al., 2001). It was reported that high doses of BDNF induced inflammation and reduced total RGC survival but saved the medium-sized, most severely affected neurons following nerve injury (Chen and Weber, 2001).

In the present study, BDNF injection did not reduce RGC death in the treated glaucomatous retinas ( $40.9\% \pm 11.4$ ) as compared to RGC death in the non-treated glaucomatous retinas ( $36.4 \pm 2.4\%$ , Chapter 4). This was expected since the BDNF was administered after the increase in IOP. In the episcleral vein cauterisation rat model, BDNF enhanced RGC survival in moderately chronic hypertensive eyes after being injected into 3 groups which received from one to three injections of BDNF on days 5, 19 and 33 (Ko et al., 2001). Another study demonstrated that BDNF alone showed only slight neuroprotection to RGCs after 4 weeks of ocular hypertension when injections of BDNF were received once a week on days 0, 7, 14 and 21 (Fu et al., 2009).

#### 5.3.1.4. Dendritic morphology after the combined injection of chABC and BDNF

Another objective of the experiments was to test the effects of the combined treatment with chABC and BDNF on the preservation and recovery of dendritic morphology in glaucoma. A previous study showed that the combined delivery of BDNF into the eye and injections of chABC into the superior colliculus produced synergistic effects (Tropea et al., 2003). This indicates that the combination of a neurotrophic factor that stimulates cellular responses essential for neurite growth with agents that change the brain parenchyma into a more permissive environment is particularly effective in triggering processes of plastic reorganisation that are essential for the return of function after CNS injury. The synergistic action of BDNF and chABC could be explained by the fact that the chABC-mediated degradation of CSPGs increased the accessibility of BDNF via enhanced diffusion of the neurotrophin in the tissue

parenchyma. These results suggest that chABC acts independently from BDNF, although it cannot be ruled out that BDNF signalling downstream of Trk activation is indirectly influenced by chABC (Tropea et al., 2003). TrkB accumulation and retrograde transport of BDNF is interrupted at the optic nerve in acute and chronic experimental glaucoma, suggesting that neurotrophin deprivation plays a role in the pathogenesis of RGC death in glaucoma (Pease et al., 2000).

A significant increase in the total dendritic length of the chABC+BDNF-injected glaucomatous retinas compared to non-treated glaucomatous and control retinas was observed in the present study. The combined treatment resulted in a significantly higher total length than by treatment with BDNF alone. However, the total length after the combined injection was not significantly different from the total length observed after chABC injection alone. This result suggests that the use of BDNF in isolation is insufficient to effect change. The PNN represents a substantial barrier for recovery which has to be addressed. Dendritic field area was also significantly increased in the chABC+BDNF injected retinas compared to the non-treated glaucomatous and control retinas. In contrast, the chABC+BDNF treatment did not result in an increased number of branching points compared to glaucomatous and control retinas. The possible explanation for the fact that, in contrast to the total dendritic length, the number of bifurcations was not significantly increased in the chABC+BDNF-treated glaucomatous retinas compared to the non-treated glaucomatous and control retinas could be that the population of the analysed neurons was relatively small (23 cells). Since several morphological subtypes of rat RGCs have been classified (Sun et al., 2002), it is possible that not all subtypes of RGCs were included in the analysis.

### 5.3.1.5. Dendritic morphology after chABC injection into a non-glaucomatous retina

The last part of this chapter was to examine the effects of chABC injection on the dendritic morphology in a normal rat eye. Therefore, applying the same experimental conditions as for the chABC injection into the glaucomatous eye, chABC was injected into a normal eye. The results showed that the total dendritic length, the number of

branching points and the dendritic field area were significantly lower in the non-glaucomatous chABC-injected retinas than in control non-treated retinas. The number of bifurcations was the only morphological feature that was significantly increased in the control chABC-injected retinas compared to the glaucomatous retinas. These data were not consistent with the data obtained from chABC-injected glaucomatous eyes, where the morphological features varied significantly from the glaucomatous eyes. There is a possibility that due to more scarring present in glaucoma, it could be more difficult to digest PNN in glaucomatous than in control retinas.

### 5.3.2. The presence of chABC generated epitopes in the retina after intravitreal injections. Distribution of CSPGs in the eye

Immunohistochemical analysis confirmed the presence of chABC generated epitopes, (chondroitin-6-sulphate, chondroitin-4-sulphate and chondroitin-0-sulphate) in the retina 24 hours after intravitreal injections, meaning that chondroitinase ABC was present in the retina following intravitreal injection. Based on that, it was assumed that chABC injections resulted in the presence of chABC in all injected retinas. Further digestion of the retinal section with chABC resulted in intense immunostaining throughout the retina; strongest in the photoreceptor layer, indicating that not all epitopes had been exposed by the intravitreal injection.

Previous studies demonstrated the distribution of chondroitin sulphate proteoglycans in two regions of the retina: nerve fibers, including the optic nerve, and the interphotoreceptor matrix (IPM), including the surface of retinal pigment epithelium (RPE) cells (Inatani and Tanihara, 2002). Antibody to CSPGs derived with bovine nasal cartridge was specific to the sclera, anterior uveal tract and endoneurium of the optic nerve (Poole et al., 1982) while an antibody to brain-derived chondroitin sulphate proteoglycans was immunoreactive with rat retinal ganglion cells (Aquino et al., 1984). In addition, proteoglycans were present in large quantities in the IPM and on the apical surface of RPE cells (Varner et al., 1987). The presence of CSPGs was indicated by the staining of filaments with Cupronic-Blue in human trabecular meshwork, and the staining, derived mainly from RPE cells, was eliminated by treatment with chABC (Tawara et al., 1989). Immunohistochemical analysis showed positive immunoreactivity with the antibodies against chondroitin-6-sulphate but not

against chondroitin-0-sulphate or the chondroitin-4-sulphate in the IPM of human, rat, mice and bovine retinas (Hollyfield et al., 1999). Only in the Brown Norway rat retina IPM labelling with chondroitin-6-sulphate was observed in the absence of chABC predigestion. In contrast to immunohistochemical analysis, Western blot analysis indicated the presence of some positive immunoreactivity against chondroitin-4-sulphate in IPM extracts from mouse and rat (Hollyfield et al., 1999).

#### 5.3.3. Fast Sholl

Sholl analysis (Sholl, 1953) is a broadly applied method for quantifying the characteristic scaling properties of dendritic arbors in vivo and neuritic arbors in vitro (Caserta et al., 1995; Davies et al., 1993; Duan et al., 2003; Gastinger et al., 2008; Gutierrez et al., 2004; Gutierrez et al., 2005; Haas et al., 2006; Inatani and Tanihara, 2002; Ip et al., 2002; Isaacs et al., 1998; Kheirandish et al., 2005; Libersat and Duch, 2002; Lowndes et al., 1990; Mizrahi and Libersat, 2002; Neale et al., 1993; Pante et al., 2005; Ristanovic et al., 2006; Robinson and Kolb, 1997; Shi et al., 2004; Spires et al., 2004; Wood et al., 2004; Zagrebelsky et al., 2005). This analysis shows the distribution of neuritic segments at regular intervals from the soma. Although this method has been useful in quantifying neuronal morphology, it has the disadvantage of being a very time-consuming method that requires grouping the neurite intersection points in a series of concentric circles centred on the cell soma. This leads to restrictions on the number of neurons that can be conveniently analysed. Fast Sholl is an alternative method for obtaining the complete Sholl profile of a population of neurons from a reduced set of sampled points (bifurcations and terminal points). This allows for simpler and faster analysis, permitting larger size of samples to be analysed, with a consequently more reliable statistical treatment of the data (Gutierrez and Davies, 2007).

In the Sholl analysis, the cumulative number of intersection points depends on the number of concentric circles, thus the larger number of concentric rings, the more precise the analysis but the greater analysis workload involved. In contrast to this type of Sholl analysis method, the total information in the Fast Sholl method is included in a set of counted points, bifurcation and terminal points. Therefore, the method allows an accurate estimation of the entire number of intersections without the direct

counting used in the conventional Sholl analysis. In addition, the total length of the dendritic tree can be calculated from the obtained data set using a standard curve (Gutierrez and Davies, 2007).

The precision of the Fast Sholl method in estimating the pattern of intersections rests on the larger number of samples. For individual meandering processes that intersect the same circle more than once (or even extend back towards the cell body), this method can lead to a minor underestimation of the number of intersections for those processes and, consequently, adding an error to the analysis. However, analysing larger numbers of neurons prevents the significance of the statistical impact of such relatively rare events on the overall growth pattern (Gutierrez and Davies, 2007). Since the number of analysed neurons from the treated retinas was considerably low, ranging from 23 to 25 RGCs, the possibility of an error resulting from the underestimation of the number of intersections for this particular type of processes cannot be ruled out. This problem might be resolved by including additional samples in the analysis.

Although automated systems for Sholl analysis are available, they require extremely good quality images, with high contrast and no background noise (Gutierrez and Davies, 2007). This is difficult to obtain using 'Diolistic' labelling method without separate manual tracing and extensive editing. Although Fast Sholl method permits marking and counting of the bifurcations and terminal points without the requirement for manual tracing, some cells had to be traced (either from stack projection or from the stack of images) when the quality of images was poor or when it was difficult to distinguish the dendritic tree from adjacent cells. Overall, this method proved to be useful and efficient in quantifying the morphological features of RGC dendrites.

#### 5.4. Summary

In summary, the results showed the significant changes in the total dendritic length and the number of branching points in glaucomatous retinas compared to controls in the magnetic bead model of glaucoma. Of all types of intravitreal injections studied, only RGCs of chABC-treated retinas displayed a highly significant increase with respect to all the morphological parameters measured compared to the RGCs of

glaucomatous eyes. The preliminary data suggest that chABC injection might be useful in the recovery of neuronal damage in glaucoma. This represents an important potential therapy for glaucoma and other neurogenerative diseases. However, the results from the injection of chABC alone suggest that it should be used with caution. Since CSPGs are found mainly in the interphotoreceptor matrix (Hollyfield et al., 1999), it is possible that the use of chABC may increase the risk of retinal damage, e.g. retinal detachment.

With respect to all types of tested agents and their combinations, a more detailed, more statistically robust analysis is needed, including testing the effects of different doses and times of injections.

•

÷

157

Chapter 6: Chondroitin sulphate proteoglycans (CSPGs) in young, old and glaucomatous retina

#### 6.1. Introduction

Retinal ganglion cell morphology in control and glaucomatous retinas was quantified and compared to glaucomatous retinas injected with chABC, BDNF, chABC+BDNF and negative control retinas injected with chABC (Chapter 5). The intravitreal injection of chABC resulted in digestion of CSPGs and generation of chondroitin sulphate stub epitopes as confirmed by immunohistochemistry (Chapter 5). Further digestion with chABC resulted in a strong immunostaining throughout the retina that was strongest in the photoreceptor layer, indicating that not all epitopes had been exposed by the intravitreal injection (Chapter 5). That led us to a question whether the tissue localisation of CS-GAGs might be different in glaucomatous and young retinas. In addition, the localisation of aggrecan core protein in the whole rat retina was examined.

In addition, in Chapter 5, the possibility that RGC dendrite remodelling and shrinkage could be reversed and act as a neural substrate for the recovery of vision in glaucoma was investigated. Since the perineuronal net (PNN) represents a substantial barrier for recovery, digestion of the PNN to enhance the ability of RGCs to regenerate following the removal of the effect of elevated IOP was attempted. The data from Chapter 5 suggested that chABC might be useful in the recovery of neuronal damage in glaucoma. However, this raises the concern of whether chABC digestion may have a harmful effect on the retina.

PNNs are a highly condensed matrix surrounding the somas and proximal dendrites of some types of neurons. They develop postnatally and finally emerge as net-like features on the cell surface as a consequence of extracellular matrix (ECM) materials deposited around synaptic endings, as well as in the space between neurons and astrocytic processes (Rhodes and Fawcett, 2004). There are several possibilities for the function of PNNs: synaptic stabilisation and limitation of synaptic plasticity (Hockfield et al., 1990), neuroprotection (Morawski et al., 2004) or support of ion homeostasis in the region of very active neurons (Härtig et al., 1999). Extracellular matrix is composed of (1) glycosaminoglycans (GAGs), either bound to proteins, as proteoglycans, or unbound in the form of hyaluronan; (2) fibrous proteins (e.g., collagens and elastin); (3) adhesive glycoproteins (e.g., fibronectin, laminin and

tenascin) and various secreted growth factors and other molecules, many of which bind with different affinities to GAGs and other ECM components (Galtrey et al., 2007). In the CNS, unlike in other tissues, ECM contains a small quantity of fibrous proteins and a high quantity of GAGs (Novak and Kaye, 2000) and is organised around certain neurons to produce specialised condensed ECM, i.e. PNNs (Yamaguchi, 2000). The main components of the ECM in the CNS are hyaluronan, chondroitin sulphate proteoglycans (CSPGs), link protein and tenascin (Galtrey et al., 2007).

A number of *in vitro* studies demonstrated inhibitory properties of CSPGs on neurite outgrowth, either via their CS chains or their core proteins (Dou and Levine, 1997; Dou and Levine, 1994; Friedlander et al., 1994). Moreover, large aggregating proteoglycans, such as aggrecan and versican, can indirectly inhibit neurite outgrowth by high-affinity binding to the cell adhesion molecules, N-CAM and Ng-CAM/L1 (Friedlander et al., 1994; Grumet et al., 1993). Most CSPGs are secreted from cells and contribute to the formation of extracellular matrix (ECM) (Galtrey and Fawcett, 2007). Extracellular matrix changes, predominantly the formation of CSPG-containing perineuronal nets, restrict plasticity after the end of critical periods. Enzymatic removal of chondroitin sulphate (CS) chains with chondroitinase ABC has been shown to promote axonal regeneration and plasticity (Pizzorusso et al., 2002).

#### Experimental design

The aim of the present study was to investigate and compare the presence of chondroitin sulphate glycosaminoglycans (CS-GAGs) and aggrecan core protein epitopes in young, old and glaucomatous retinas. This was to enhance the understanding of the changes that occur in the extracellular matrix in glaucoma and aging. Therefore, the molecular weight distribution and immunohistochemical tissue localisation of GAGs in young, old and glaucomatous retinas were investigated (sections 2.4 & 6.2). Monoclonal antibodies [(Mab): 2B6, 3B3 and 1B5 specific to chondroitinase-generated chondroitin-4-sulphate (C4S), chondroitin-6-sulphate (C6S), chondroitin-0-sulphate (C0S) disaccharide epitopes (Caterson et al., 1983; Caterson et al., 1985; Caterson et al., 2000; Caterson et al., 1990; Ilic et al., 1992)] were employed. The C0S, C4S and C6S epitopes are located proximal to the tetrasaccharide bridge (glucuronic acid-galactose-galactose-xylose) that connects the

chondroitin GAG chain to the consensus serine residues of proteoglycan core proteins. Chondroitinase ABC removes all repeating chondroitin sulphate disaccharide units, leaving the hexasaccharide attached to serine (Hollyfield et al., 1999).

Other monoclonal antibodies used in the study were specific to aggrecan core protein IgD domain (394EPEEPFTFAPEI405) (6B4) (Ilic et al., 1992; Little et al., 2002; Maeda et al., 1992), an epitope shared by both the globular 1 (G1) and the chondroitin sulphate (CS) attachment domains on aggrecan (7D1) (Calabro et al., 1992), the new C-terminus (FVDIPEN) on aggrecan degradation products produced by the proteolytic action of matrix metalloproteinases (BC-4) (Hughes et al., 1995), and the C-terminal neoepitope sequence (NITEGE) generated after 'aggrecanase' catabolism at the same site within the aggrecan IGD (BC-13) (Caterson et al., 2000).

The core protein of the large human cartilage proteoglycan aggrecan consists of six distinct domains: globular 1 (G1), interglobular, globular 2 (G2), keratan sulphate attachment, chondroitin sulphate (CS) attachment, and globular 3 (G3) (Hughes et al., 1995) (Figure 6.1).

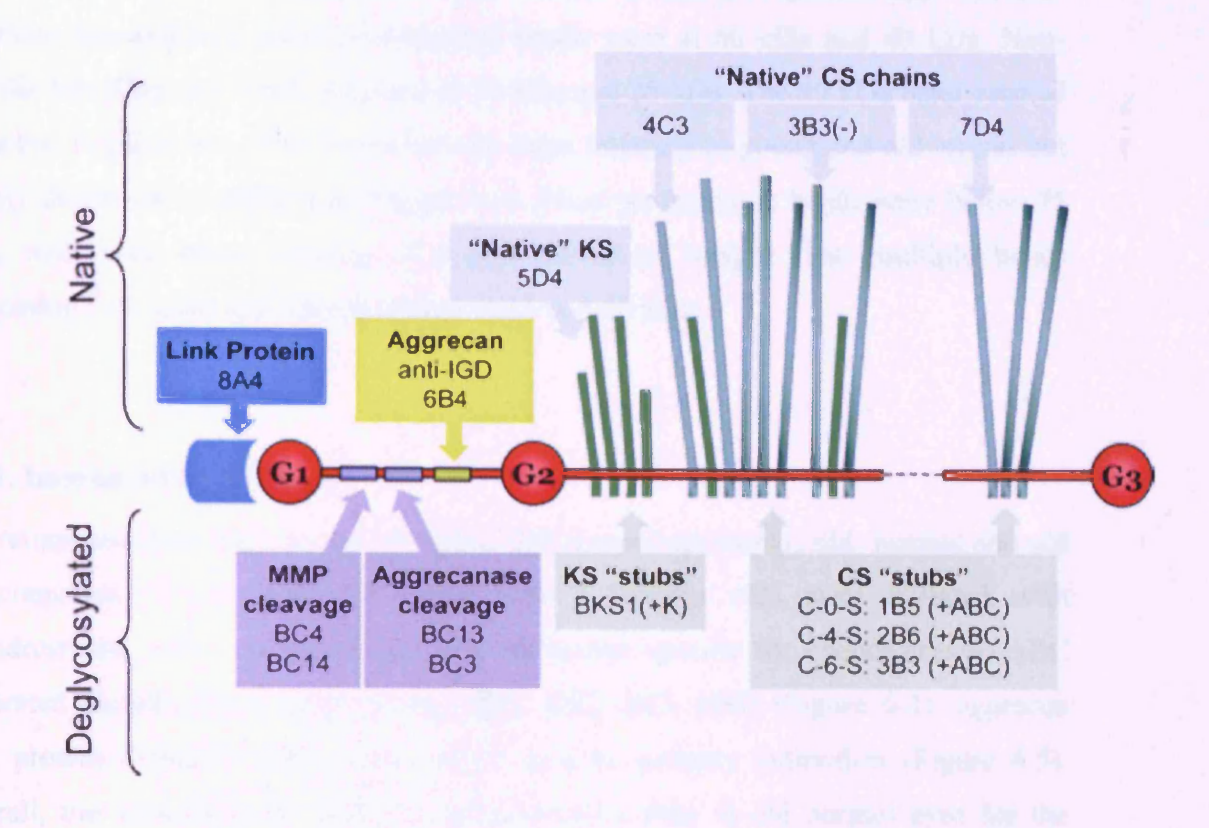


**Figure 6.1.** Diagrammatic representation of the structural epitopes and catabolic neoepitopes on aggrecan (native and deglycosylated) and link protein (copied from Haye et al., 2008).

Retinas used for biochemical analysis were obtained from young normal (3 weeks old), old normal and old glaucomatous rat eyes (old eyes were over 6 months old) (section 2.4.1.1). Immunohistochemical analysis was conducted on retinal sections obtained from young (8 weeks old), old normal and old glaucomatous rat eyes (old eyes were over 6 months old) (see section 2.4.2.1).

### 6.2. Results

## 6.2.1. Western blotting

Positive immunoreactivity with 6B4 and 2B6 mAbs for GAGs was present in rat retina (Figures 6.2 & 6.3). All 6B4 bands appeared to increase in intensity during aging, however the staining was reduced in bands from glaucomatous retinas (Figure

6.2). The multiple bands indicated the presence of highly degraded aggrecan (i.e. aggrecan metabolites); most predominant bands were at 60 kDa and 40 kDa. Non-specific labelling (IgG) was detected at 50 kDa and 25 kDa. The 60 kDa band seemed to be lost in glaucoma. 2B6 bands had the same intensity in young and old retinas but slighty decreased in glaucoma (Figure 6.3). Most predominant bands were below 75 kDa, with very weak staining of higher molecular weight. The multiple bands containing C4S were most predominant at 55 and 40 kDa.

## 6.2.2. Immunohistochemistry

Rat retinal sections from young (8 weeks old) normal rat retinas, old normal and old glaucomatous retinas (old eyes were over 6 months old) were digested with chondroitinase ABC and incubated with antibodies specific for chondroitinase ABC generated chondroitin-sulphate stubs (1B5, 2B6, 3B3, 6B4) (Figure 6.4), aggrecan core protein domains (7D1, BC4, BC13) and no primary antibodies (Figure 6.5). Overall, the staining was weaker in glaucomatous than in old normal eyes for the antibodies specific for chondroitin sulphate epitopes and slightly weaker for antibodies specific to aggrecan core protein domain or neoepitopes. 1B5 staining was weak throughout the retinas in young, slightly increased in old and reduced in glaucomatous retinas. 2B6 labelling was seen in the photoreceptor layer and weakly throughout the retina in young retinas; it was restricted to the photoreceptor layer in normal retinas and was not present in glaucomatous retinas. Very intense 6B4 staining was seen throughout the young retina with slightly weaker staining in the photoreceptor layer. In contrast, 6B4 immunoreactivity in glaucomatous and normal retinas was again detected throughout the retina, however stronger in RGC and photoreceptor layer. 3B3 immunolabeling was restricted to the photoreceptor layer in young, glaucomatous and normal retinas but stronger in the inner segments in young retinas. 7D1 immunoreactivity was detected throughout the retina, with stronger staining in photoreceptor layer in young and old retinas. In glaucomatous retinas, stronger 7D1 staining was present in the retinal ganglion cell and photoreceptor layers. BC-4 immunostaining was present throughout the retina with stronger staining in the photoreceptor layer in old and glaucomatous retinas. No staining was present in

retinas incubated with BC-13. Immunolabelling was completely absent in sections that were not incubated with primary antibodies.

# 6B4 secondary Ab

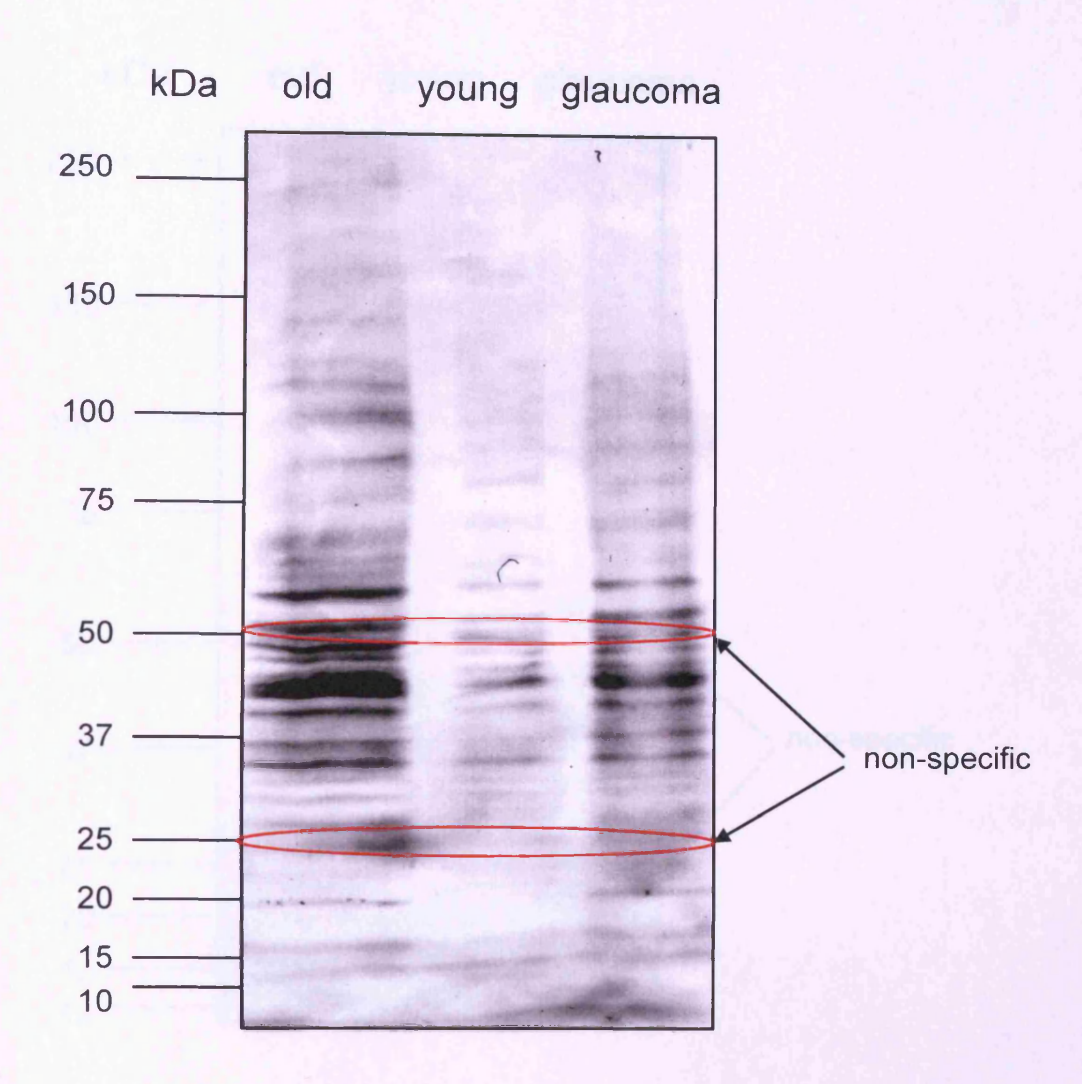


**Figure 6.2.** Western blot analysis of GAGs from old, young (3 weeks old), old normal and old glaucomatous rat retinas. 6B4 recognises aggrecan and aggrecan metabolites. Bands from old normal retinas were stained more intensely than those from old glaucomatous eyes. The weakest staining intensity was present in a track with bands from young retinas. Molecular weight standards are shown on the left hand side of the gel. Non-specific bands, 50 and 25 kDa, are marked by red oval lines.

# 2B6 secondary Ab

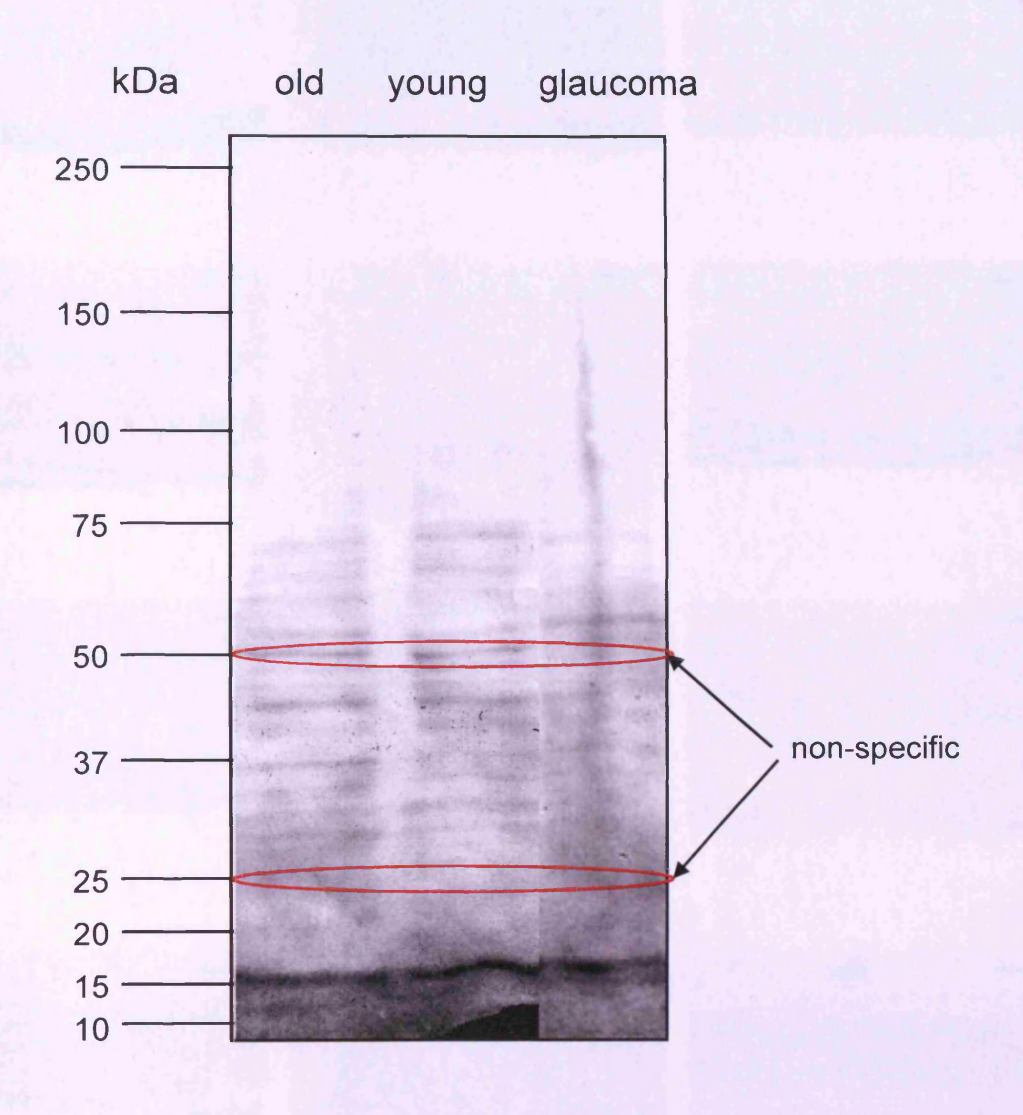


**Figure 6.3.** Western blot analysis of GAGs from old, young (3 weeks old), old normal and old glaucomatous rat retinas. 2B6 recognises chondroitinase-generated chondroitin-4-sulphate (C4S). Molecular weight standards are shown on the left hand side of the gel. Non-specific bands, 50 and 25 kDa, are marked by red oval lines.

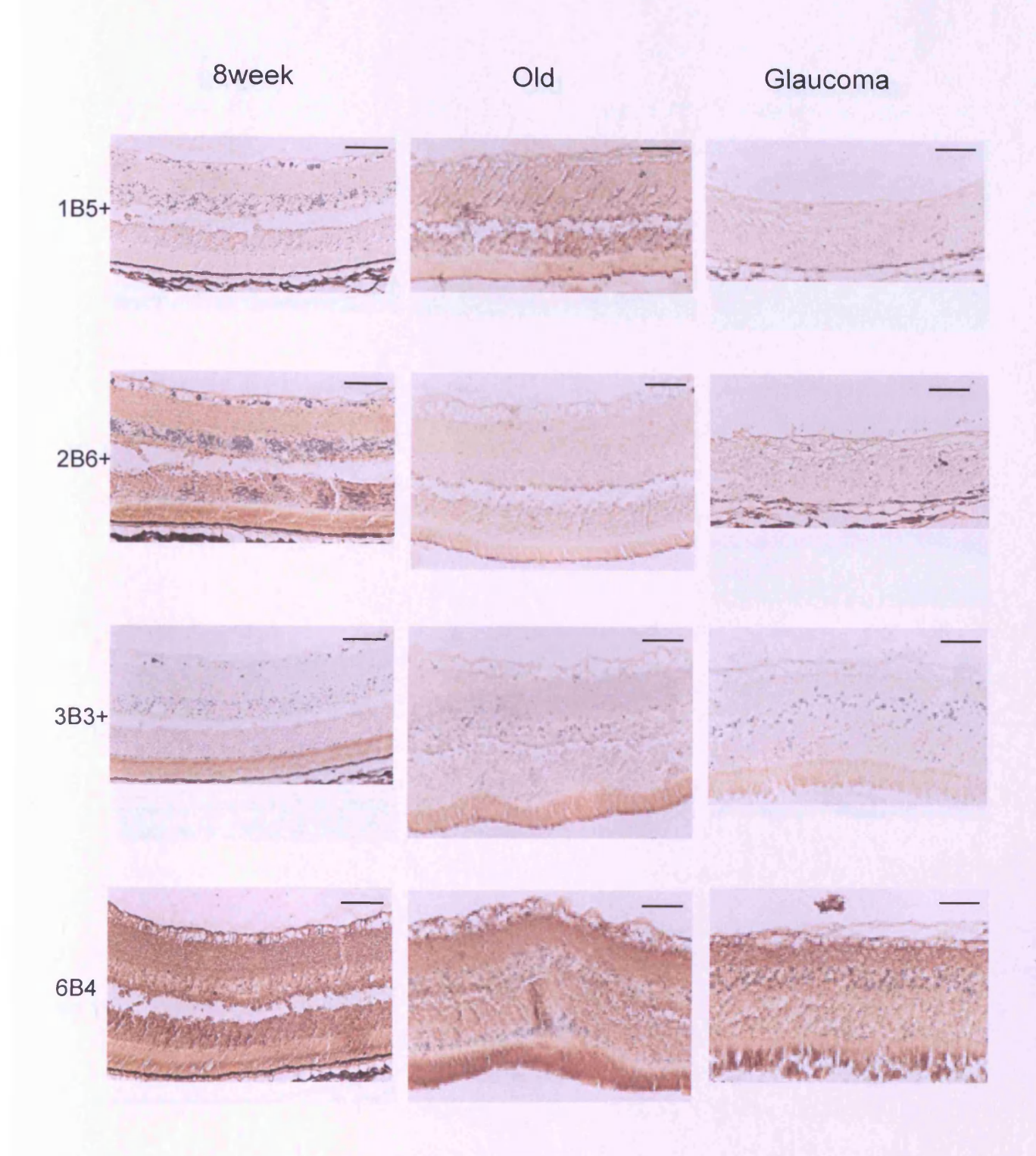


**Figure 6.4.** Rat retinal sections from 8 weeks old, old normal and old glaucomatous eyes (both over 6 months old) were incubated with antibodies specific for chondroitin-0-sulphate (1B5), chondroitin-4-sulphate (2B6), chondroitin-6-sulphate (3B3) and aggrecan core protein IgD domain (6B4). The (+) notation indicates that the sections were predigested with chondroitinase ABC to expose the stub epitopes prior to incubation with 1B5, 2B6 and 3B3 antibodies.

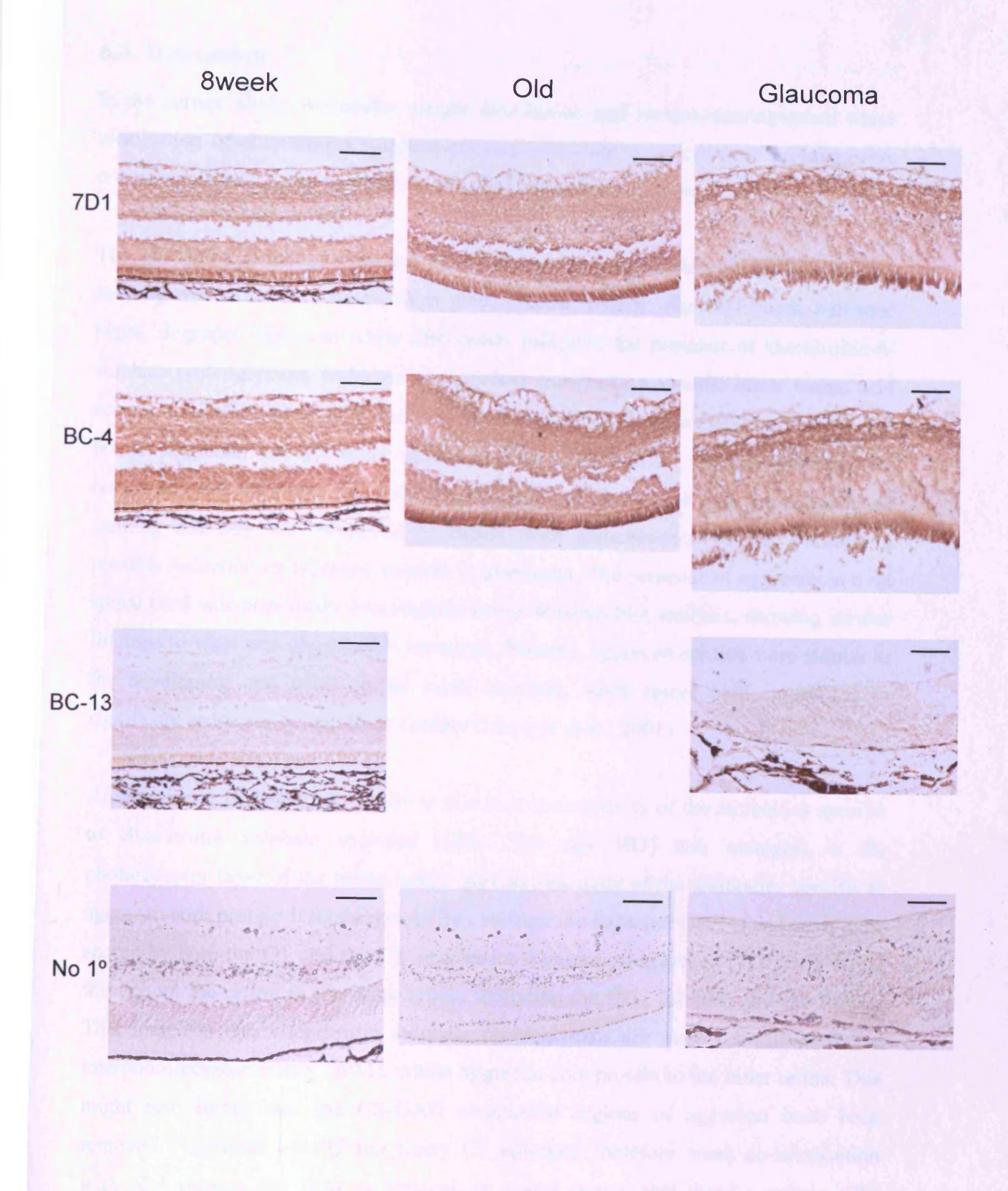


**Figure 6.5.** Rat retinal sections from 8 weeks old, old normal and old glaucomatous eyes (both over 6 months old) were incubated were incubated with antibodies specific for (7D1), (BC-4), (BC-13) and no primary antibodies (No 1°).

#### 6.3. Discussion

In the current study, molecular weight distribution and immunohistochemical tissue localisation of chondroitin sulphate proteoglycans and aggrecan core proteins were compared in young, old normal and old glaucomatous rat retinas.

The 6B4 and 2B6 bands appeared to increase in intensity during aging, however the staining was reduced in bands from glaucomatous retinas. The 6B4 bands indicated highly degraded aggrecan while 2B6 bands indicated the presence of chondroitin-4-sulphate proteoglycans. MAb anti-IGD (6B4) recognises a specific linear amino acid sequence EPEEPFTFAPEI present in the interglobular domain (IGD) of human and bovine aggrecan but not other animal species (Hayes et al., 2008). However, our results showed the presence of 6B4 epitopes in rat retina. The fact that the reduced staining intensity was observed in bands from glaucomatous retinas indicates a possible reduction in aggrecan content in glaucoma. The presence of aggrecan in a rat spinal cord was previously investigated using Western blot analysis, showing similar findings to what was observed in rat retina. Namely, aggrecan species were similar in the developing and adult spinal cord; however, adult spinal cord injury led to significant reduction in aggrecan content (Lemons et al., 2001).

An interesting finding of the study is that immunoreactivity of the antibodies specific to chondroitin sulphate epitopes (1B5, 2B6 and 3B3) was strongest in the photoreceptor layer of the retina, while immunoreactivity of the antibodies specific to aggrecan core protein IGD domain (6B4), neoepitope sequence (BC-4) and an epitope shared by both the G1 and the CS attachment domains on aggrecan (7D1) was found throughout the retina in the inner retina, including the INL, the IPL, and the RGCL. This indicates that chondroitin sulphate proteoglycans are mainly localised to the interphotoreceptor matrix (IPM), whilst aggrecan core protein to the inner retina. This might also imply that the CS-GAG attachment regions of aggrecan have been removed. Aggrecan usually has many CS epitopes, therefore weak co-localisation with 6B4 outside the IPM is unusual. It would appear that these aggrecan 6B4 fragments do not contain detectable CS epitopes. Also, Western blotting analysis indicates that aggrecan was highly digested, but the reason is unknown. It could be that the aggrecan breakdown is needed for a normal retinal function. In addition,

Western blotting analysis of 2B6 implies some aggrecan fragments have C4S but the staining was weak.

Since BC-4 antibody is specific to aggrecan degradation products generated by metalloproteinases while BC-13 to aggrecan degradation products generated by aggrecanases, the fact that only BC-4 staining was observed might imply that retinal aggrecan is digested predominantly by metalloproteinases. These findings raise the possibility that neuronal plasticity in the RGCL could be enhanced by digestion with enzymes other than chondroitinase ABC. Since the CS-PGS are involved in retinal attachment, digestion with ABC could cause retinal detachments. There is a possibility that an upregulation of metalloproteinases in the inner retina might prevent outer retinal damage.

Hollyfield et al. (1999) investigated the distribution of chondroitin-type proteoglycans in interphotoreceptor matrix (IPM) of Brown Norway rat retinas and aimed to identify the chondroitin-type proteoglycan core proteins present in IPM samples. According to Hageman et al. (1991), "The interphotoreceptor matrix (IPM) occupies the extracellular space between the photoreceptors of the retina and the apical surface of the retinal pigmented epithelium". A great proportion of the IPM consists of aqueousinsoluble glycoconjugates, including chondroitin sulphate-containing proteoglycans (Hageman et al., 1991). Immunohistochemical analysis showed intense staining against chondroitin-6-sulphate (3B3) in IPM in both digested and undigested retinas with chondroitinase ABC. This is consistent with our results as no labelling was observed in the IPM stained with the chondroitin-0-sulphate (unsulphated) (1B5) or the chondroitin-4-sulphate (2B6) antibodies before or after chondrotinase ABC digestion. In contrast, we detected 1B5 and 2B6 immunoreactivity in the photoreceptor layer and weakly throughout the normal retina and 2B6 immunoreactivity in young retinas. However, 1B5 immunoreactivity was absent in young and glaucomatous retinas, and 2B6 immunoreactivity was absent in glaucomatous retinas. Hollyfield et al. (1999) observed some scleral labelling in chondrotinase ABC treated samples with all three antibodies that was eliminated after double digestion with chondrotinase ABC and chondrotinase AC II. In Western blots using 2B6 antibody, two prominent immunoreactive bands were observed, one at approximately 230 kDa and the other at approximately 150 kDa in chondroitinase

ABC treated IPM samples. These results were different from our findings, showing multiple 2B6 bands most predominant at 100, 75, 70 kDa.

Degradation of cartilage is characteristic to arthropathies and involves proteolytic cleavage of its main structural elements, i.e. aggrecan and type II collagen. As an early event in cartilage degeneration, proteolysis and subsequent loss of the GAG rich region of aggrecan from cartilage occur (Cawston et al., 1998). Although there was a degradation of aggrecan within the retina, no consequent damage to the retina was observed. Thus, the function of aggrecan in retina remains unknown.

## 6.4. Chapter summary

The present study confirmed the existence of a perineuronal net in the rat retina and demonstrated the distribution of CS-GAGs and aggrecan core proteins in young, old and glaucomatous retinas. Our preliminary results indicate that molecular weight distribution and immunohistochemical tissue localisation of glycosaminoglycans might vary in younger, older and glaucomatous rat retinas. Chondroitin sulphate proteoglycans were mainly localised to the photoreceptor layer, while aggrecan core protein to the inner retina. Aggrecan was highly degraded in young, old and glaucomatous retinas. Future study could involve further investigation on molecular immunohistochemical tissue localisation of weight distribution and glycosaminoglycans in younger, older and glaucomatous rat retinas.

171

**Chapter 7: General discussion** 

## 7.1. Summary

Glaucoma is the second leading cause of vision loss in the world (Thylefors et al., 1995; Quigley, 1996). In the commonest form of the disease, chronic open angle glaucoma, increased intraocular pressure (IOP) is associated with accelerated death of retinal ganglion cells (RGCs) and consequent loss of visual field. Although lowering IOP can stop or slow the progression of glaucoma, currently there is no treatment to recover lost vision. Neuroplasticity is the ability for a neural system to remodel and repair following injury. If surviving damaged tissue could be regenerated on the basis of its intrinsic plasticity in glaucomatous eye, visual impairment associated with glaucoma might be potentially reversed. The principal aim of the project was to determine if RGC remodelling in glaucoma could be driven by the combined therapeutic intervention of IOP reduction and manipulation of retinal perineuronal nets.

There are conflicting opinions about the events that occur prior to RGC cell death in glaucoma. While some early studies suggested that larger RGCs were more susceptible to the effects of increased intraocular pressure (Quigley et al., 1989; Quigley et al., 1987), more recent studies showed that RGCs actually shrink (Morgan et al., 2000; Morgan 2002; Shou et al., 2003; Weber and Harman, 2005; Weber and Harman, 2008; Weber et al., 1998) prior to cell death. These later observations suggested that morphological changes can occur in RGCs that would affect cell function some time before cell death (Weber and Harman, 2005). Therefore, there is a possibility that there is a window opportunity for the administration of neuroprotective agents in order to prevent RGC death. It also raises a question about how the reduction in the number of RGCs would affect the dendrodendritic interactions that delimit the size of the dendritic tree. The loss of RGC caused by the elevated IOP is known to result in an expansion of adjacent dendritic trees to fill regions vacated by the dendritic trees of dead cells (Ahmed et al., 2001a), similar to what was previously observed in the developing retina (Perry and Linden, 1982). This neuroplastic response, when combined with the administration of neurotrophic agents, could potentially lead to the restoration of cellular morphology (Weber and Harman, 2008). Such a neuroplastic response in adult tissue could be exploited by the coadministration of agents (such as chondroitinase ABC) that disrupt the

glycosaminoglycan perineuronal net that limits the extent to which adult neurons can recover from injury. The manipulation of the perineuronal ECM can promote plasticity with beneficial effects on neuronal structure and function (Crespo et al., 2007; Fawcett, 2009; Pizzorusso et al., 2002). To evaluate the extent to which retinal neuroplasticity and retinal neuronal survival can be enhanced to permit visual recovery in experimental glaucoma, both *in vivo* (Chapters 4, 5 & 6) and *ex vivo* (Chapter 3) models of glaucoma were employed.

The purpose of the initial part of the study was to establish an in vitro model of glaucoma to analyse morphological changes of RGCs over a period of time (Chapter 3). Retinal explant cultures serve as a highly suitable model of glaucoma since the explanation of the retina requires the severing of all axons within the optic nerve and the consequential degeneration of RGCs; axonal damage is the chief suspect in the development of glaucoma. This system is particularly useful for experiments that cannot be performed in vivo due to limitations involving tissue access, confounding systemic factors, or control over microenvironment (Johnson and Tomarev, 2010). To establish retinal explant culture, culture conditions and biolistic transfection parameters were optimised. During the course of experiments, it was established that the helium pressure for the gene gun, the pore size of the filter used to protect from the shock wave and the age of animals were critical to the survival and the successful transfection. Once the conditions were optimised, further experiments were conducted using a broad-spectrum caspase inhibitor and BDNF to study their effects on neuronal survival and the formation of axonal growth cones. Broad-spectrum caspase inhibitor enhanced RGC survival and the number of axons in the proximity of the optic disc whereas exogenous BDNF enhanced the number of growth cones on the axons of RGCs. The present observations showing that caspase inhibitor had an effect on the survival of RGCs in culture are consistent with previous studies (Manabe et al., 2002; Oshitari and Adachi-Usami et al., 2003). The findings from this in vitro study implied that the regrowth of RGC axons could potentially be stimulated in the adult retina, encouraging further investigation with the use of in vivo rat models of glaucoma.

The main part of the project was conducted using two rat glaucoma models, induced by either injection of hypertonic saline into the episcleral veins to sclerose the trabecular meshwork (Morrison et al., 1997) or injection of paramagnetic microbeads

174

into the anterior chamber (Chapter 4). Since the induction of glaucoma with hypertonic saline resulted in a low rate of rats with a sustained increase in IOP (33%), we developed a novel technique for the induction of ocular hypertension using paramagnetic microbeads (Chapter 4). Glaucoma models based on obstruction of the trabecular meshwork with microscopic beads have been used both in rats (Urcola et al., 2006) and in primates (Weber and Zelenak, 2001). The injection of paramagnetic microbeads into the anterior chamber was technically undemanding and provided a measure of control over the distribution of beads within the anterior segment. Using a handheld magnet, the beads could be drawn away from the visual axis and distributed around the iridocorneal angle to optimise occlusion of the trabecular meshwork and facilitate visualisation of the retina and optic disc. A sustained IOP increase was obtained in 64% of rats and a fluctuating increase in 36% of rats. The degree of cell loss in our model (36.4%) was similar to that reported for other models (Ahmed et al., 2001a; Ahmed et al., 2001b; Naskar et al., 2002; Neufeld et al., 1999). The use of Optical Coherence Tomography validated the bead and hypertonic saline glaucoma models, by revealing a thinning of the retinal fibre layer over time in vivo as well as optic nerve head cupping in vivo and ex vivo (Chapter 4).

Following the successful development of a magnetic bead model (Chapter 4), it was time to determine whether dendritic tree morphology of RGCs in glaucoma could be influenced by the administration of agents that have previously been shown to promote plasticity in the CNS. Since chondroitinase ABC (chABC) influences plasticity by enzymatic digestion of the PNN (Kwok et al., 2008), the enzyme was injected intravitreally to promote retinal ganglion cells regeneration in glaucoma (Chapter 5). In addition, the effect of brain-derived neurotrophic factor on the preservation of the dendritic field complexity (Weber and Herman, 2008) was also investigated. The combined treatment of BDNF and chABC had effects on axon growth and synapse formation by the sprouting axons, implying the potential of this approach in therapies for the repair of the damaged adult CNS (Tropea et al., 2003).

Our results indicated that chABC promoted recovery of RGCs dendritic tree, when used alone or in combination with BDNF. Only treatment with chABC demonstrated a significant increase with respect to all the morphological parameters measured compared to the RGCs of glaucomatous eyes (Chapter 5). This represents an

important potential therapy for glaucoma and other neurogenerative diseases. However, the results from the injection of chABC alone suggest that it should be used with caution (Chapter 5). Since chondroitin sulphate proteoglycans (CS-PGs) are found mainly in the interphotoreceptor matrix (Hollyfield et al., 1999; Inatani and Tanihara, 2002) (Chapter 6), it is possible that the use of chABC may increase the risk of retinal damage, e.g. retinal detachment.

CS-PGs have been demonstrated to have inhibitory properties on neurite outgrowth, either via their CS chains or their core proteins (Dou and Levine, 1997; Dou and Levine, 1994; Friedlander et al., 1994). Moreover, large aggregating proteoglycans, such as aggrecan and versican, can indirectly inhibit neurite outgrowth by highaffinity binding to the cell adhesion molecules, N-CAM and Ng-CAM/L1 (Friedlander et al., 1994; Grumet et al., 1993). The intravitreal injection of chABC resulted in digestion of CSPGs and generation of chondroitin sulphate stub epitopes as confirmed by immunohistochemistry (Chapter 5). Further digestion with chABC resulted in a strong immunostaining throughout the retina that was strongest in the photoreceptor layer, indicating that not all epitopes had been exposed by the intravitreal injection (Chapter 5). That led us to question whether the tissue localisation of CS-GAGs might be different in glaucomatous, old and young retinas. In addition, the localisation of aggrecan core protein in the whole rat retina was examined. Our study confirmed the existence of a perineuronal net in the rat retina and indicated that the molecular weight distribution and immunohistochemical tissue localisation of glycosaminoglycans varied in young, old and glaucomatous rat retinas (Chapter 6). Chondroitin sulphate proteoglycans were mainly localised to the photoreceptor layer, while aggrecan core protein was limited to the inner retina (Chapter 6). An interesting finding was that the positive staining with BC-4 but not BC-13 antibody suggested that aggrecan is digested predominantly by metalloproteinases, raising the possibility that neuronal plasticity in the RGCL could be enhanced by digestion with enzymes other than chondroitinase ABC (Chapter 6). This alternative approach might reduce likelihood of retinal detachment that could be caused by chondroitinase ABC digestion of CS-PGs, since CS-PGs are specifically involved in retinal attachment. Aggrecan was highly degraded in young, old and glaucomatous retinas, without any consequent damage to the tissue, leaving an unanswered question about its role in retina.

#### 7.2. Future work

In Chapter 3, we have magnified the potential for increased RGC survival and the number of axons in the proximity to the optic disc in explants treated with caspase inhibitor. In addition, the number of growth cones was increased in explants treated with BDNF. It will be interesting to see if we can observe axonal and dendritic changes in RGCs in retinal explants over a period of time following the use of chondroitinase ABC and BDNF.

In Chapter 4, we introduced and evaluated a novel model of induction of experimental glaucoma using paramagnetic microspheres. The model could be further improved by testing different sizes of magnetic beads and different hand-held magnets to prolong the period of an elevated IOP following a single injection. Also, further investigation using Optical Coherence Tomography should be conducted to evaluate changes in the retinal fibre layer over a period of time *in vivo*.

.

Of all the types of intravitreal injections studied in Chapter 5, treatment with chABC demonstrated the most significant results. RGCs of chABC-treated retinas displayed a highly significant increase in all of the morphological parameters measured as compared to the RGCs of glaucomatous eyes. With respect to all types of tested agents and their combinations, a more detailed, more statistically robust analysis is needed, including testing the effects of different doses and times of injections.

We have characterised the tissue localisation and protein expression of CS-GAGs and aggrecan core proteins in young, aged and glaucomatous retinas immunohistochemical and western-blotting analyses (Chapter 6). Further experiments should be conducted to confirm these results and to further characterise protein expression in these groups of retinas. Also, the role of aggrecan in retina should be further examined.

#### 7.3. Conclusion

In conclusion, the study led to the development of a novel rat glaucoma model and, more importantly, demonstrated potential for dendritic regeneration of RGCs in glaucoma.

177

### **REFERENCES**

Agarwal, N., Agarwal, R., Kumar, D. M., Ondricek, A., Clark, A. F., Wordinger, R. J., and Pang, I. H. (2007). Comparison of expression profile of neurotrophins and their receptors in primary and transformed rat retinal ganglion cells. Mol Vis 13, 1311-1318.

AGIS-Investigators (2000). The advanced glaucoma intervention study (AGIS): 7. the relationship between control of intraocular pressure and visual field deterioration. Am J Ophthalmol 130, 429-440.

Ahmed, F. A. K. M., Chaudhary, P., and Sharma, S. C. (2001a). Effects of increased intraocular pressure on rat retinal ganglion cells. Int J Dev Neurosci 19, 209-218.

Ahmed, F. A. K. M., Hegazy, K., Chaudhary, P., and Sharma, S. C. (2001b). Neuroprotective effect of [alpha]2 agonist (brimonidine) on adult rat retinal ganglion cells after increased intraocular pressure. Brain Res 913, 133-139.

Aihara, M., Lindsey, J. D., and Weinreb, R. N. (2002). Reduction of Intraocular Pressure in mouse eyes treated with latanoprost. Invest Ophthalmol Vis Sci 43, 146-150.

Aihara, M., Lindsey, J. D., and Weinreb, R. N. (2003). Experimental mouse ocular hypertension: establishment of the Model. Invest Ophthalmol Vis Sci 44, 4314-4320.

Albrecht May, C. (2008). Comparative anatomy of the optic nerve head and inner retina in non-primate animal models used for glaucoma research. Open Ophthalmol J 2, 94-101.

Ames, A. d., Li, Y. Y., Heher, E. C., and Kimble, C. R. (1992). Energy metabolism of rabbit retina as related to function: high cost of Na+ transport. J Neurosci 12, 840-853.

Anderson, D. R. (1969). Ultrastructure of human and monkey lamina cribrosa and optic nerve head. Arch Ophthal 82, 800-814.

Anderson, D. R. (1970). Ultrastructure of the optic nerve head. Arch Ophthal 83, 63-73

Anderson, M., Nair, K. S., Amonoo, L., Mehalow, A., Trantow, C., Masli, S., and John, S. (2008). GpnmbR150X allele must be present in bone marrow derived cells to mediate DBA/2J glaucoma. BMC Genet 9, 30.

Anderson, M. G., Libby, R. T., Gould, D. B., Smith, R. S., and John, S. W. M. (2005). High-dose radiation with bone marrow transfer prevents neurodegeneration in an inherited glaucoma. PNAS 102, 4566-4571.

Anderson, M. G., Smith, R. S., Savinova, O. V., Hawes, N. L., Chang, B., Zabaleta, A., Wilpan, R., Heckenlively, J. R., Davisson, M., and John, S. W. (2001). Genetic modification of glaucoma associated phenotypes between AKXD-28/Ty and DBA/2J mice. BMC Genet 2, 1.

Andrade, M. A., Muro, E. M., and Moran, F. (2001). Simulation of plasticity in the adult visual cortex. Biol Cybern 84, 445-451.

Ansari, E. A., Morgan, J. E., and Snowden, R. J. (2002). Psychophysical characterisation of early functional loss in glaucoma and ocular hypertension. Br J Ophthalmol 86, 1131-1135.

Armaleo, D., Ye, G. N., Klein, T. M., Shark, K. B., Sanford, J. C., and Johnston, S. A. (1990). Biolistic nuclear transformation of Saccharomyces cerevisiae and other fungi. Curr Genet 17, 97-103.

Avila, M. Y., Carre, D. A., Stone, R. A., and Civan, M. M. (2001). Reliable Measurement of Mouse Intraocular Pressure by a Servo-Null Micropipette System. Invest Ophthalmol Vis Sci 42, 1841-1846.

Avwenagha, O., Campbell, G., and Bird, M. M. (2003). The outgrowth response of the axons of developing and regenerating rat retinal ganglion cells in vitro to neurotrophin treatment. J Neurocytol 32, 1055-1075.

Bahr, M. (2000). Live or let die - retinal ganglion cell death and survival during development and in the lesioned adult CNS. Trends in Neurosciences 23, 483-490.

Bahr, M., Wizenmann, A., and Thanos, S. (1992). Effect of bilateral tectum lesions on retinal ganglion cell morphology in rats. J Comp Neurol *320*, 370-380.

Barritt, A. W., Davies, M., Marchand, F., Hartley, R., Grist, J., Yip, P., McMahon, S. B., and Bradbury, E. J. (2006). Chondroitinase ABC Promotes Sprouting of Intact and Injured Spinal Systems after Spinal Cord Injury. J Neurosci 26, 10856-10867.

Beazley, L. D., Perry, V. H., Baker, B., and Darby, J. E. (1987). An investigation into the role of ganglion cells in the regulation of division and death of other retinal cells. Brain Res *430*, 169-184.

Becker, M., and Funk, J. (2001). [Diode laser cyclophotocoagulation as the primary surgical intervention in glaucoma]. Ophthalmologe 98, 1145-1148.

Bessero, A. C., and Clarke, P. G. Neuroprotection for optic nerve disorders. Curr Opin Neurol 23, 10-15.

Bradbury, E. J., Moon, L. D. F., Popat, R. J., King, V. R., Bennett, G. S., Patel, P. N., Fawcett, J. W., and McMahon, S. B. (2002). Chondroitinase ABC promotes functional recovery after spinal cord injury. Nature 416, 636-640.

Bray, D., Thomas, C., and Shaw, G. (1978). Growth cone formation in cultures of sensory neurons. Proc Natl Acad Sci U S A 75, 5226-5229.

Brewer, G. J. (1997). Isolation and culture of adult rat hippocampal neurons. J Neurosci Methods 71, 143-155.

- Brewer, G. J., Torricelli, J. R., Evege, E. K., and Price, P. J. (1993). Optimized survival of hippocampal neurons in B27-supplemented Neurobasal, a new serum-free medium combination. J Neurosci Res 35, 567-576.
- Bruckner, G., Seeger, G., Brauer, K., Hartig, W., Kacza, J., and Bigl, V. (1994). Cortical areas are revealed by distribution patterns of proteoglycan components and parvalbumin in the Mongolian gerbil and rat. Brain Res 658, 67-86.
- Buell, S. J., and Coleman, P. D. (1979). Dendritic growth in the aged human brain and failure of growth in senile dementia. Science 206, 854-856.
- Buell, S. J., and Coleman, P. D. (1981). Quantitative evidence for selective dendritic growth in normal human aging but not in senile dementia. Brain Research 214, 23-41.
- Bull, N. D., Irvine, K.-A., Franklin, R. J. M., and Martin, K. R. (2009). Transplanted Oligodendrocyte Precursor Cells Reduce Neurodegeneration in a Model of Glaucoma. Invest Ophthalmol Vis Sci 50, 4244-4253.
- Bull, N. D., Limb, G. A., and Martin, K. R. (2008). Human Muller stem cell (MIO-M1) transplantation in a rat model of glaucoma: survival, differentiation, and integration. Invest Ophthalmol Vis Sci 49, 3449-3456.
- Burgoyne, C. F., Mercante, D. E., and Thompson, H. W. (2002). Change detection in regional and volumetric disc parameters using longitudinal confocal scanning laser tomography. Ophthalmology 109, 455-466.
- Burr, J., Azuara-Blanco, A., and Avenell, A. (2005). Medical versus surgical interventions for open angle glaucoma. Cochrane Database Syst Rev, CD004399.
- Caggiano, A. O., Zimber, M. P., Ganguly, A., Blight, A. R., and Gruskin, E. A. (2005). Chondroitinase ABCI improves locomotion and bladder function following contusion injury of the rat spinal cord. J Neurotrauma 22, 226-239.
- Calabro, A., Hascall, V. C., and Caterson, B. (1992). Monoclonal antibodies directed against epitopes within the core protein structure of the large aggregating proteoglycan (aggrecan) from the swarm rat chondrosarcoma. Arch Biochem Biophys 298, 349-360.
- Caprioli, J., Kitano, S., and Morgan, J. E. (1996). Hyperthermia and hypoxia increase tolerance of retinal ganglion cells to anoxia and excitotoxicity. Invest Ophthalmol Vis Sci 37, 2376-2381.
- Carpenter, P., Sefton, A. J., Dreher, B., and Lim, W. L. (1986). Role of target tissue in regulating the development of retinal ganglion cells in the albino rat: effects of kainate lesions in the superior colliculus. J Comp Neurol 251, 240-259.
- Caserta, F., Eldred, W. D., Fernandez, E., Hausman, R. E., Stanford, L. R., Bulderev, S. V., Schwarzer, S., and Stanley, H. E. (1995). Determination of fractal dimension of physiologically characterized neurons in two and three dimensions. J Neurosci Methods 56, 133-144.

- Caspi, O., Lesman, A., Basevitch, Y., Gepstein, A., Arbel, G., Habib, I. H. M., Gepstein, L., and Levenberg, S. (2007). Tissue Engineering of Vascularized Cardiac Muscle From Human Embryonic Stem Cells. Circ Res *100*, 263-272.
- Caterson, B., Christner, J. E., and Baker, J. R. (1983). Identification of a monoclonal antibody that specifically recognizes corneal and skeletal keratan sulfate. Monoclonal antibodies to cartilage proteoglycan. J Biol Chem 258, 8848-8854.
- Caterson, B., Christner, J. E., Baker, J. R., and Couchman, J. R. (1985). Production and characterization of monoclonal antibodies directed against connective tissue proteoglycans. Fed Proc 44, 386-393.
- Caterson, B., Flannery, C. R., Hughes, C. E., and Little, C. B. (2000). Mechanisms involved in cartilage proteoglycan catabolism. Matrix Biol 19, 333-344.
- Caterson, B., Mahmoodian, F., Sorrell, J. M., Hardingham, T. E., Bayliss, M. T., Carney, S. L., Ratcliffe, A., and Muir, H. (1990). Modulation of native chondroitin sulphate structure in tissue development and in disease. J Cell Sci 97, 411-417.
- Cawston, T. E., Curry, V. A., Summers, C. A., Clark, I. M., Riley, G. P., Life, P. F., Spaull, J. R., Goldring, M. B., Koshy, P. J., Rowan, A. D., and Shingleton, W. D. (1998). The role of oncostatin M in animal and human connective tissue collagen turnover and its localization within the rheumatoid joint. Arthritis Rheum 41, 1760-1771.
- Celio, M. R., and Blumcke, I. (1994). Perineuronal nets--a specialized form of extracellular matrix in the adult nervous system. Brain Res Brain Res Rev 19, 128-145.
- Cellerino, A., Pinzon-Duarte, G., Carroll, P., and Kohler, K. (1998). Brain-Derived Neurotrophic Factor Modulates the Development of the Dopaminergic Network in the Rodent Retina. J Neurosci 18, 3351-3362.
- Cense, B., Chen, T. C., Park, B. H., Pierce, M. C., and de Boer, J. F. (2004). Thickness and Birefringence of Healthy Retinal Nerve Fiber Layer Tissue Measured with Polarization-Sensitive Optical Coherence Tomography. Invest Ophthalmol Vis Sci 45, 2606-2612.
- Cepurna, W. O., Kayton, R. J., Johnson, E. C., and Morrison, J. C. (2005). Age related optic nerve axonal loss in adult Brown Norway rats. Exp Eye Res 80, 877-884.
- Charalambous, P., Hurst, L. A., and Thanos, S. (2008). Engrafted chicken neural tube-derived stem cells support the innate propensity for axonal regeneration within the rat optic nerve. Invest Ophthalmol Vis Sci 49, 3513-3524.
- Chaturvedi, N., Hedley-Whyte, E. T., and Dreyer, E. B. (1993). Lateral geniculate nucleus in glaucoma. Am J Ophthalmol 116, 182-188.

Chaudhary, P., Ahmed, F., Quebada, P., and Sharma, S. C. (1999). Caspase inhibitors block the retinal ganglion cell death following optic nerve transection. Brain Res Mol Brain Res 67, 36-45.

Chauhan, B. C., LeVatte, T. L., Garnier, K. L., Tremblay, F., Pang, I.-H., Clark, A. F., and Archibald, M. L. (2006). Semiquantitative Optic Nerve Grading Scheme for Determining Axonal Loss in Experimental Optic Neuropathy. Invest Ophthalmol Vis Sci 47, 634-640.

Chauhan, B. C., Pan, J., Archibald, M. L., LeVatte, T. L., Kelly, M. E., and Tremblay, F. (2002). Effect of intraocular pressure on optic disc topography, electroretinography, and axonal loss in a chronic pressure-induced rat model of optic nerve damage. Invest Ophthalmol Vis Sci 43, 2969-2976.

Chen, H., and Weber, A. J. (2001). BDNF Enhances Retinal Ganglion Cell Survival in Cats with Optic Nerve Damage. Invest Ophthalmol Vis Sci 42, 966-974.

Chierzi, G. R., T. Pizzorusso and L. Maffei (2005). Effects of chondroitin sulphate proteoglycan digestion on dendritic spine motility in the visual cortex of adult mice. 979.914.

Chiu, K., Chang, R., and So, K. F. (2007). Laser-induced chronic ocular hypertension model on SD rats. J Vis Exp, 549.

Choma, M., Sarunic, M., Yang, C., and Izatt, J. (2003). Sensitivity advantage of swept source and Fourier domain optical coherence tomography. Opt Express 11, 2183-2189.

Cohan, B. E., and Bohr, D. F. (2001). Goldmann applanation tonometry in the conscious rat. Invest Ophthalmol Vis Sci 42, 340-342.

Collaborative Normal-Tension Glaucoma Study, G. (1998). The effectiveness of intraocular pressure reduction in the treatment of normal-tension glaucoma. American Journal of Ophthalmology 126, 498-505.

Corvetti, L., and Rossi, F. (2005). Degradation of Chondroitin Sulfate Proteoglycans Induces Sprouting of Intact Purkinje Axons in the Cerebellum of the Adult Rat. J Neurosci 25, 7150-7158.

Crespo, D., Asher, R. A., Lin, R., Rhodes, K. E., and Fawcett, J. W. (2007). How does chondroitinase promote functional recovery in the damaged CNS? Exp Neurol 206, 159-171.

Cui, Q., and Harvey, A. R. (2000). CNTF promotes the regrowth of retinal ganglion cell axons into murine peripheral nerve grafts. Neuroreport 11, 3999-4002.

Cynader, M., Berman, N., and Hein, A. (1976). Recovery of function in cat visual cortex following prolonged deprivation. Exp Brain Res 25, 139-156.

- Dacey, D. M. (1993). The mosaic of midget ganglion cells in the human retina. J Neurosci 13, 5334-5355.
- Dacey, D. M. (1994). Physiology, morphology and spatial densities of identified ganglion cell types in primate retina. Ciba Found Symp 184, 12-28; discussion 28-34, 63-70.
- Dacey, D. M., and Petersen, M. R. (1992). Dendritic Field Size and Morphology of Midget and Parasol Ganglion Cells of the Human Retina. Proc Natl Acad Sci U S A 89, 9666-9670.
- Dacey, D. M., Peterson, B. B., Robinson, F. R., and Gamlin, P. D. (2003). Fireworks in the Primate Retina: In Vitro Photodynamics Reveals Diverse LGN-Projecting Ganglion Cell Types. Neuron 37, 15-27.
- Dahlmann-Noor, A. H., Vijay, S., Limb, G. A., and Khaw, P. T. (2010). Strategies for optic nerve rescue and regeneration in glaucoma and other optic neuropathies. Drug Discov Today 15, 287-299.
- Danias, J., Kontiola, A. I., Filippopoulos, T., and Mittag, T. (2003). Method for the Noninvasive Measurement of Intraocular Pressure in Mice. Invest Ophthalmol Vis Sci 44, 1138-1141.
- Davies, A. M., Lee, K.-F., and Jaenisch, R. (1993). p75-Deficient trigeminal sensory neurons have an altered response to NGF but not to other neurotrophins. Neuron 11, 565-574.
- Daw, N. W., and Wyatt, H. J. (1976). Kittens reared in a unidirectional environment: evidence for a critical period. J Physiol 257, 155-170.
- Dawson, V. L., and Dawson, T. M. (1996). Nitric oxide actions in neurochemistry. Neurochem Int 29, 97-ccc110ddd.
- de Boer, J. F., Cense, B., Park, B. H., Pierce, M. C., Tearney, G. J., and Bouma, B. E. (2003). Improved signal-to-noise ratio in spectral-domain compared with time-domain optical coherence tomography. Opt Lett 28, 2067-2069.
- Decherchi, P., Cochard, P., and Gauthier, P. (1997). Dual staining assessment of Schwann cell viability within whole peripheral nerves using calcein-AM and ethidium homodimer. Journal of Neuroscience Methods 71, 205-213.
- Di Polo, A., Aigner, L. J., Dunn, R. J., Bray, G. M., and Aguayo, A. J. (1998). Prolonged delivery of brain-derived neurotrophic factor by adenovirus-infected Muller cells temporarily rescues injured retinal ganglion cells. PNAS 95, 3978-3983.
- Dietlein, T. S., Hermann, M. M., and Jordan, J. F. (2009). The medical and surgical treatment of glaucoma. Dtsch Arztebl Int 106, 597-605; quiz 606.

Dou, C.-L., and Levine, J. M. (1997). Identification of a Neuronal Cell Surface Receptor for a Growth Inhibitory Chondroitin Sulfate Proteoglycan (NG2). Journal of Neurochemistry 68, 1021-1030.

Dou, C. L., and Levine, J. M. (1994). Inhibition of neurite growth by the NG2 chondroitin sulfate proteoglycan. J Neurosci 14, 7616-7628.

Drexler, W. (2004). [Methodological advancements. Ultrahigh-resolution OCT]. Ophthalmologe 101, 804-812.

Dreyer, E. B. (1998). A proposed role for excitotoxicity in glaucoma. J Glaucoma 7, 62-67.

Duan, H., Wearne, S. L., Rocher, A. B., Macedo, A., Morrison, J. H., and Hof, P. R. (2003). Age-related Dendritic and Spine Changes in Corticocortically Projecting Neurons in Macaque Monkeys. Cereb Cortex 13, 950-961.

Duenker, N., Valenciano, A. I., Franke, A., Hernandez-Sanchez, C., Dressel, R., Behrendt, M., De Pablo, F., Krieglstein, K., and de la Rosa, E. J. (2005). Balance of pro-apoptotic transforming growth factor-beta and anti-apoptotic insulin effects in the control of cell death in the postnatal mouse retina. Eur J Neurosci 22, 28-38.

Elliot (1917). Glaucoma: A Handbook for the General Practitioner.

Elizabeth, W., Mercy, W., and Guadalupe, R. (2004). Muller cell response to laser-induced increase in intraocular pressure in rats. Glia 47, 109-119.

Erickson-Lamy, K. A., Kaufman, P. L., McDermott, M. L., and France, N. K. (1984). Comparative anesthetic effects on aqueous humor dynamics in the cynomolgus monkey. Arch Ophthal 102, 1815-1820.

Ervin, J. C., Lemij, H. G., Mills, R. P., Quigley, H. A., Thompson, H. W., and Burgoyne, C. F. (2002). Clinician change detection viewing longitudinal stereophotographs compared to confocal scanning laser tomography in the LSU Experimental Glaucoma (LEG) Study. Ophthalmology 109, 467-481.

Eysel, U. T., Peichl, L., and Wassle, H. (1985). Dendritic plasticity in the early postnatal feline retina: quantitative characteristics and sensitive period. J Comp Neurol 242, 134-145.

Eysel, U. T., and Wolfhard, U. (1984). The effects of partial retinal lesions on activity and size of cells in the dorsal lateral geniculate nucleus. The Journal Of Comparative Neurology 229, 301-309.

Fawcett, J., Joost Verhaagen, Elly M. Hol Inge Huitenga Jan Wijnholds Arthur B. Bergen Gerald J. Boer and Dick F. Swaab (2009). Molecular control of brain plasticity and repair. Prog Brain Res, 501-509.

Fechtner, R. D., and Weinreb, R. N. (1994). Mechanisms of optic nerve damage in primary open angle glaucoma. Surv Ophthalmol 39, 23-42.

- Feigenspan, A., Bormann, J., and Wassle, H. (1993). Organotypic slice culture of the mammalian retina. Vis Neurosci 10, 203-217.
- Fercher, A. F., Hitzenberger, C. K., Kamp, G., and El-Zaiat, S. Y. (1995). Measurement of intraocular distances by backscattering spectral interferometry. Opt Commun 117, 43-48.
- Flammer, J., Orgul, S., Costa, V. P., Orzalesi, N., Krieglstein, G. K., Serra, L. M., Renard, J.-P., and Stefansson, E. (2002). The impact of ocular blood flow in glaucoma. Prog Retin Eye Res 21, 359-393.
- Floel, A., Hummel, F., Breitenstein, C., Knecht, S., and Cohen, L. G. (2005). Dopaminergic effects on encoding of a motor memory in chronic stroke. Neurology 65, 472-474.
- Frassetto, L. J., Schlieve, C. R., Lieven, C. J., Utter, A. A., Jones, M. V., Agarwal, N., and Levin, L. A. (2006). Kinase-Dependent Differentiation of a Retinal Ganglion Cell Precursor. Invest Ophthalmol Vis Sci 47, 427-438.
- Friedlander, D. R., Milev, P., Karthikeyan, L., Margolis, R. K., Margolis, R. U., and Grumet, M. (1994). The neuronal chondroitin sulfate proteoglycan neurocan binds to the neural cell adhesion molecules Ng-CAM/L1/NILE and N-CAM, and inhibits neuronal adhesion and neurite outgrowth. J Cell Biol 125, 669-680.
- Frost, D. O., Ma, Y. T., Hsieh, T., Forbes, M. E., and Johnson, J. E. (2001). Developmental changes in BDNF protein levels in the hamster retina and superior colliculus. J Neurobiol 49, 173-187.
- Fu, Q. L., Li, X., Yip, H. K., Shao, Z., Wu, W., Mi, S., and So, K. F. (2009). Combined effect of brain-derived neurotrophic factor and LINGO-1 fusion protein on long-term survival of retinal ganglion cells in chronic glaucoma. Neuroscience 162, 375-382.
- Fujikawa, D. G. (1995). Neuroprotective effect of ketamine administered after status epilepticus onset. Epilepsia 36, 186-195.
- Gaasterland, D., Tanishima, T., and Kuwabara, T. (1978). Axoplasmic flow during chronic experimental glaucoma. 1. Light and electron microscopic studies of the monkey optic nervehead during development of glaucomatous cupping. Invest Ophthalmol Vis Sci 17, 838-846.
- Gahwiler, B. H. (1981). Organotypic monolayer cultures of nervous tissue. J Neurosci Methods 4, 329-342.
- Galtrey, C. M., Asher, R. A., Nothias, F., and Fawcett, J. W. (2007). Promoting plasticity in the spinal cord with chondroitinase improves functional recovery after peripheral nerve repair. Brain 130, 926-939.

- Galtrey, C. M., and Fawcett, J. W. (2007). The role of chondroitin sulfate proteoglycans in regeneration and plasticity in the central nervous system. Brain Res Rev 54, 1-18.
- Gan, W.-B., Grutzendler, J., Wong, W. T., Wong, R. O. L., and Lichtman, J. W. (2000). Multicolor "DiOlistic" Labeling of the Nervous System Using Lipophilic Dye Combinations. Neuron 27, 219-225.
- Garrett, W. T., McBride, R. L., Williams Jr, J. K., and Feringa, E. R. (1991). Fluoro-Gold's toxicity makes it inferior to True Blue for long-term studies of dorsal root ganglion neurons and motoneurons. Neurosci Lett 128, 137-139.
- Gastinger, M. J., Kunselman, A. R., Conboy, E. E., Bronson, S. K., and Barber, A. J. (2008). Dendrite Remodeling and Other Abnormalities in the Retinal Ganglion Cells of Ins2Akita Diabetic Mice. Invest Ophthalmol Vis Sci 49, 2635-2642.
- Gerd, H., and Michael Walter, L. (1998). "Coherence Radar" and "Spectral Radar"--- New Tools for Dermatological Diagnosis. J Biomed Opt 3, 21-31.
- Giese, K. P., Peters, M., and Vernon, J. (2001). Modulation of excitability as a learning and memory mechanism: A molecular genetic perspective. Physiol Behav 73, 803-810.
- Glovinsky, Y., Quigley, H. A., and Dunkelberger, G. R. (1991). Retinal ganglion cell loss is size dependent in experimental glaucoma. Invest Ophthalmol Vis Sci 32, 484-491.
- Glovinsky, Y., Quigley, H. A., and Pease, M. E. (1993). Foveal ganglion cell loss is size dependent in experimental glaucoma. Invest Ophthalmol Vis Sci 34, 395-400.
- Goldberg, J. L., Espinosa, J. S., Xu, Y., Davidson, N., Kovacs, G. T. A., and Barres, B. A. (2002). Retinal Ganglion Cells Do Not Extend Axons by Default: Promotion by Neurotrophic Signaling and Electrical Activity. Neuron *33*, 689-702.
- Goldblum, D., and Mittag, T. (2002). Prospects for relevant glaucoma models with retinal ganglion cell damage in the rodent eye. Vision Res 42, 471 478.
- González-García, A. O., Vizzeri, G., Bowd, C., Medeiros, F. A., Zangwill, L. M., and Weinreb, R. N. (2009). Reproducibility of RTVue Retinal Nerve Fiber Layer Thickness and Optic Disc Measurements and Agreement with Stratus Optical Coherence Tomography Measurements. Am J Ophthalmol 147, 1067-1074.e1061.
- Gordon, M. O., Beiser, J. A., Brandt, J. D., Heuer, D. K., Higginbotham, E. J., Johnson, C. A., Keltner, J. L., Miller, J. P., Parrish, R. K., 2nd, Wilson, M. R., and Kass, M. A. (2002). The Ocular Hypertension Treatment Study: baseline factors that predict the onset of primary open-angle glaucoma. Arch Ophthalmol 120, 714-720; discussion 829-730.
- Graham, S. L., Drance, S. M., Chauhan, B. C., Swindale, N. V., Hnik, P., Mikelberg, F. S., and Douglas, G. R. (1996). Comparison of psychophysical and

electrophysiological testing in early glaucoma. Invest Ophthalmol Vis Sci 37, 2651-2662.

Gross, R. L., Ji, J., Chang, P., Pennesi, M. E., Yang, Z., Zhang, J., and Wu, S. M. (2003). A mouse model of elevated intraocular pressure: retina and optic nerve findings. Trans Am Ophthalmol Soc 101, 163-169; discussion 169-171.

Grozdanic, S. D., Betts, D. M., Sakaguchi, D. S., Allbaugh, R. A., Kwon, Y. H., and Kardon, R. H. (2003). Laser-Induced Mouse Model of Chronic Ocular Hypertension. Invest Ophthalmol Vis Sci 44, 4337-4346.

Grumet, M., Flaccus, A., and Margolis, R. U. (1993). Functional characterization of chondroitin sulfate proteoglycans of brain: interactions with neurons and neural cell adhesion molecules. J Cell Biol 120, 815-824.

Grumet, M., Milev, P., Sakurai, T., Karthikeyan, L., Bourdon, M., Margolis, R. K., and Margolis, R. U. (1994). Interactions with tenascin and differential effects on cell adhesion of neurocan and phosphacan, two major chondroitin sulfate proteoglycans of nervous tissue. J Biol Chem 269, 12142-12146.

Grutzendler, J., Kasthuri, N., and Gan, W.-B. (2002). Long-term dendritic spine stability in the adult cortex. Nature 420, 812-816.

Guerin, M. B., McKernan, D. P., O'Brien C, J., and Cotter, T. G. (2006). Retinal ganglion cells: dying to survive. Int J Dev Biol 50, 665-674.

Gugleta, K., Orgul, S., Stumpfig, D., Dubler, B., and Flammer, J. (1999). Fludrocortisone in the treatment of systemic hypotension in primary open-angle glaucoma patients. Int Ophthalmol 23, 25-30.

Guimaraes, A., Zaremba, S., and Hockfield, S. (1990). Molecular and morphological changes in the cat lateral geniculate nucleus and visual cortex induced by visual deprivation are revealed by monoclonal antibodies Cat-304 and Cat-301. J Neurosci 10, 3014-3024.

Guterman, Y. (2007). A neural plasticity perspective on the schizophrenic condition. Conscious Cogn 16, 400-420.

Gutierrez, H., and Davies, A. M. (2007). A fast and accurate procedure for deriving the Sholl profile in quantitative studies of neuronal morphology. J Neurosci Methods 163, 24-30.

Gutierrez, H., Dolcet, X., Tolcos, M., and Davies, A. (2004). HGF regulates the development of cortical pyramidal dendrites. Development 131, 3717-3726.

Gutierrez, H., Hale, V. A., Dolcet, X., and Davies, A. (2005). NF-κB signalling regulates the growth of neural processes in the developing PNS and CNS. Development 132, 1713-1726.

- Haas, K., Li, J., and Cline, H. T. (2006). AMPA receptors regulate experience-dependent dendritic arbor growth in vivo. Proc Natl Acad Sci USA 103, 12127-12131.
- Hageman, G. S., Kirchoff-Rempe, M. A., Lewis, G. P., Fisher, S. K., and Anderson, D. H. (1991). Sequestration of basic fibroblast growth factor in the primate retinal interphotoreceptor matrix. Proc Natl Acad Sci USA 88, 6706-6710.
- Hanninen, V. A., Pantcheva, M. B., Freeman, E. E., Poulin, N. R., and Grosskreutz, C. L. (2002). Activation of caspase 9 in a rat model of experimental glaucoma. Curr Eye Res 25, 389-395.
- Harbin, T. S., Jr., Podos, S. M., Kolker, A. E., and Becker, B. (1976). Visual field progression in open-angle glaucoma patients presenting with monocular field loss. Transactions Section On Ophthalmology American Academy Of Ophthalmology And Otolaryngology 81, 253-257.
- Hartig, W., Brauer, K., and Bruckner, G. (1992). Wisteria floribunda agglutinin-labelled nets surround parvalbumin-containing neurons. Neuroreport 3, 869-872.
- Härtig, W., Derouiche, A., Welt, K., Brauer, K., Grosche, J., Mäder, M., Reichenbach, A., and Brückner, G. (1999). Cortical neurons immunoreactive for the potassium channel Kv3.1b subunit are predominantly surrounded by perineuronal nets presumed as a buffering system for cations. Brain Res 842, 15-29.
- Hausen, D., Bruckner, G., Drlicek, M., Hartig, W., Brauer, K., and Bigl, V. (1996). Pyramidal cells ensheathed by perineuronal nets in human motor and somatosensory cortex. Neuroreport *7*, 1725-1729.
- Hayes, A. J., Hughes, C. E., and Caterson, B. (2008). Antibodies and immunohistochemistry in extracellular matrix research. Methods 45, 10-21.
- Hebb, D. O. (1949). The organization of behaviour (New York Wiley).
- Hedman, K., Watson, P. G., and Alm, A. (2002). The effect of latanoprost on intraocular pressure during 2 years of treatment. Surv Ophthalmol 47 Suppl 1, S65-76.
- Herzog, K. H., and von Bartheld, C. S. (1998). Contributions of the optic tectum and the retina as sources of brain-derived neurotrophic factor for retinal ganglion cells in the chick embryo. J Neurosci 18, 2891-2906.
- Hockfield, S., Kalb, R. G., Zaremba, S., and Fryer, H. (1990). Expression of neural proteoglycans correlates with the acquisition of mature neuronal properties in the mammalian brain. Cold Spring Harb Symp Quant Biol 55, 505-514.
- Hollyfield, J. G., Rayborn, M. E., Midura, R. J., Shadrach, K. G., and Acharya, S. (1999). Chondroitin Sulfate Proteoglycan Core Proteins in the Interphotoreceptor Matrix: A Comparative Study using Biochemical and Immunohistochemical Analysis. Exp Eye Res 69, 311-322.

- Homma, K., Koriyama, Y., Mawatari, K., Higuchi, Y., Kosaka, J., and Kato, S. (2007). Early downregulation of IGF-I decides the fate of rat retinal ganglion cells after optic nerve injury. Neurochem Int 50, 741-748.
- Honkanen, R. A., Baruah, S., Zimmerman, M. B., Khanna, C. L., Weaver, Y. K., Narkiewicz, J., Waziri, R., Gehrs, K. M., Weingeist, T. A., Boldt, H. C., et al. (2003). Vitreous Amino Acid Concentrations in Patients With Glaucoma Undergoing Vitrectomy. Arch Ophthalmol 121, 183-188.
- Huang, D., Swanson, E. A., Lin, C. P., Schuman, J. S., Stinson, W. G., Chang, W., Hee, M. R., Flotte, T., Gregory, K., Puliafito, C. A., and et al. (1991). Optical coherence tomography. Science 254, 1178-1181.
- Huang, J., Liu, X., Wu, Z., and Sadda, S. (2010). Comparison of full-thickness traumatic macular holes and idiopathic macular holes by optical coherence tomography. Graefes Arch Clin Exp Ophthalmol.
- Hughes, C. E., Caterson, B., Fosang, A. J., Roughley, P. J., and Mort, J. S. (1995). Monoclonal antibodies that specifically recognize neoepitope sequences generated by 'aggrecanase' and matrix metalloproteinase cleavage of aggrecan: application to catabolism in situ and in vitro. Biochem J 305 ( Pt 3), 799-804.
- Huxlin, K. R., and Goodchild, A. K. (1997). Retinal ganglion cells in the albino rat: revised morphological classification. J Comp Neurol 385, 309-323.
- Ilic, M. Z., Handley, C. J., Robinson, H. C., and Mok, M. T. (1992). Mechanism of catabolism of aggrecan by articular cartilage. Arch Biochem Biophys 294, 115-122.
- Inatani, M., and Tanihara, H. (2002). Proteoglycans in retina. Prog Retin Eye Res 21, 429-447.
- Ip, E. Y.-Y., Giza, C. C., Griesbach, G. S., and Hovda, D. A. (2002). Effects of Enriched Environment and Fluid Percussion Injury on Dendritic Arborization within the Cerebral Cortex of the Developing Rat. J Neurotrauma 19, 573-585.
- Isaacs, K. R., Hanbauer, I., and Jacobowitz, D. M. (1998). A Method for the Rapid Analysis of Neuronal Proportions and Neurite Morphology in Primary Cultures. Exp Neurol 149, 464-467.
- Isenmann, S., Kretz, A., and Cellerino, A. (2003). Molecular determinants of retinal ganglion cell development, survival, and regeneration. Progress in Retinal and Eye Research 22, 483-543.
- Ishikawa, H., Takano, M., Matsumoto, N., Sawada, H., Ide, C., Mimura, O., and Dezawa, M. (2005). Effect of GDNF gene transfer into axotomized retinal ganglion cells using in vivo electroporation with a contact lens-type electrode. Gene Ther 12, 289-298.
- Jaffe, G. J., and Caprioli, J. (2004). Optical coherence tomography to detect and manage retinal disease and glaucoma. Am J Ophthalmol 137, 156-169.

- Jakobs, T. C., Libby, R. T., Ben, Y., John, S. W. M., and Masland, R. H. (2005). Retinal ganglion cell degeneration is topological but not cell type specific in DBA/2J mice. J Cell Biol 171, 313 325.
- Ji, J.-Z., Elyaman, W., Yip, H. K., Lee, V. W. H., Yick, L.-W., Hugon, J., and So, K.-F. (2004). CNTF promotes survival of retinal ganglion cells after induction of ocular hypertension in rats: the possible involvement of STAT3 pathway. Eur J Neurosci 19, 265-272.
- Jia, L., Cepurna, W. O., Johnson, E. C., and Morrison, J. C. (2000). Effect of General Anesthetics on IOP in Rats with Experimental Aqueous Outflow Obstruction. Invest Ophthalmol Vis Sci 41, 3415-3419.
- John, S. W. (2005). Mechanistic insights into glaucoma provided by experimental genetics the cogan lecture. Invest Ophthalmol and Vis Sci 46, 2649-2661.
- John, S. W., Anderson, M. G., and Smith, R. S. (1999). Mouse genetics: a tool to help unlock the mechanisms of glaucoma. J Glaucoma 8, 400-412.
- John, S. W., Hagaman, J. R., MacTaggart, T. E., Peng, L., and Smithes, O. (1997). Intraocular pressure in inbred mouse strains. Invest Ophthalmol Vis Sci 38, 249 253.
- John, S. W. M., Smith, R. S., Savinova, O. V., Hawes, N. L., Chang, B., Turnbull, D., Davisson, M., Roderick, T. H., and Heckenlively, J. R. (1998). Essential iris atrophy, pigment dispersion, and glaucoma in DBA/2J mice. Invest Ophthalmol Vis Sci 39, 951 962.
- Johnson, E. C., Deppmeier, L. M. H., Wentzien, S. K. F., Hsu, I., and Morrison, J. C. (2000). Chronology of Optic Nerve Head and Retinal Responses to Elevated Intraocular Pressure. Invest Ophthalmol Vis Sci 41, 431-442.
- Johnson, E. C., Jia, L., Cepurna, W. O., Doser, T. A., and Morrison, J. C. (2007). Global Changes in Optic Nerve Head Gene Expression after Exposure to Elevated Intraocular Pressure in a Rat Glaucoma Model. Invest Ophthalmol Vis Sci 48, 3161-3177.
- Johnson, E. C., Morrison, J. C., Farrell, S., Deppmeier, L., Moore, C. G., and McGinty, M. R. (1996). The Effect of Chronically Elevated Intraocular Pressure on the Rat Optic Nerve Head Extracellular Matrix. Exp Eye Res 62, 663-674.
- Johnson, T. V., Bull, N. D., Hunt, D. P., Marina, N., Tomarev, S. I., and Martin, K. R. (2010). Neuroprotective Effects of Intravitreal Mesenchymal Stem Cell Transplantation in Experimental Glaucoma. Invest Ophthalmol Vis Sci 51, 2051-2059.
- Johnson, T. V., and Martin, K. R. (2008). Development and Characterization of an Adult Retinal Explant Organotypic Tissue Culture System as an In Vitro Intraocular Stem Cell Transplantation Model. Invest Ophthalmol Vis Sci 49, 3503-3512.

- Johnson, T. V., and Tomarev, S. I. (2010). Rodent models of glaucoma. Brain Res Bull 81, 349-358.
- Johnston, S. A., Anziano, P. Q., Shark, K., Sanford, J. C., and Butow, R. A. (1988). Mitochondrial transformation in yeast by bombardment with microprojectiles. Science 240, 1538-1541.
- Jonas, J. B., Budde, W. M., and Panda-Jonas, S. (1999). Ophthalmoscopic Evaluation of the Optic Nerve Head. Surv Ophthalmol 43, 293-320.
- Kalb, R. G., and Hockfield, S. (1990). Induction of a neuronal proteoglycan by the NMDA receptor in the developing spinal cord. Science 250, 294-296.
- Kandel, E. R. (1970). Nerve cells and behavior. Sc Am 223, 57-67 passim.
- Kandel, E. R., and Schwartz, J. H. (1982). Molecular biology of learning: modulation of transmitter release. Science 218, 433-443.
- Karim, M. Z., Sawada, A., Mizuno, K., Kawakami, H., Ishida, K., and Yamamoto, T. (2009). Neuroprotective effect of nipradilol [3,4-dihydro-8-(2-hydroxy-3-isopropylamino)-propoxy-3-nitroxy-2H-1-benzopyran] in a rat model of optic nerve degeneration. J Glaucoma 18, 26-31.
- Karimi-Abdolrezaee, S., Eftekharpour, E., Wang, J., Schut, D., and Fehlings, M. G. (2010). Synergistic Effects of Transplanted Adult Neural Stem/Progenitor Cells, Chondroitinase, and Growth Factors Promote Functional Repair and Plasticity of the Chronically Injured Spinal Cord. J Neurosci 30, 1657-1676.
- Karten, Y. J. G., Olariu, A., and Cameron, H. A. (2005). Stress in early life inhibits neurogenesis in adulthood. Trends in Neurosciences 28, 171-172.
- Kass, M. A., Heuer, D. K., Higginbotham, E. J., Johnson, C. A., Keltner, J. L., Miller, J. P., Parrish Ii, R. K., Wilson, M. R., and Gordon, M. O. (2002). The Ocular Hypertension Treatment Study: A randomized trial determines that topical ocular hypotensive medication delays or prevents the onset of primary open-angle glaucoma. Arch Ophthalmol 120, 701-713.
- Kaufman, P. L., and Davis, G. E. (1980). "Minified" Goldmann applanating prism for tonometry in monkeys and humans. Arch Ophthalmol 98, 542-546.
- Kawaguchi, I., Higashide, T., Ohkubo, S., Takeda, H., and Sugiyama, K. (2006). In Vivo Imaging and Quantitative Evaluation of the Rat Retinal Nerve Fiber Layer Using Scanning Laser Ophthalmoscopy. Invest Ophthalmol Vis Sci 47, 2911-2916.
- Kermer, P., Ankerhold, R., Klöcker, N., Krajewski, S., Reed, J. C., and Bähr, M. (2000). Caspase-9: Involvement in secondary death of axotomized rat retinal ganglion cells in vivo. Molecular Brain Research 85, 144-150.

- phenomenon with wide-ranging implications in tissue kinetics. Br J Cancer 26, 239-257.
- Kerrigan, L. A., Zack, D. J., Quigley, H. A., Smith, S. D., and Pease, M. E. (1997). TUNEL-positive ganglion cells in human primary open-angle glaucoma. Arch Ophthalmol 115, 1031-1035.
- Khaw, P. T., Shah, P., and Elkington, A. R. (2004). Glaucoma--1: Diagnosis. BMJ 328, 97-99.
- Khaw, P. T., Shah, P., and Elkington, A. R. (2004). Glaucoma--2: Treatment. BMJ 328, 156-158.
- Kheirandish, L., Gozal, D., Pequignot, J. M., Pequignot, J., and Row, B. W. (2005). Intermittent hypoxia during development induces long-term alterations in spatial working memory, monoamines, and dendritic branching in rat frontal cortex. Pediatr Res 58, 594-599.
- Kipnis, J., Avidan, H., Markovich, Y., Mizrahi, T., Hauben, E., Prigozhina, T. B., and Slavin, S. (2004). Low-dose gamma-irradiation promotes survival of injured neurons in the central nervous system via homeostasis-driven proliferation of T cells. Eur J Neurosci 19, 1191-1198.
- Kipnis, J., Yoles, E., Porat, Z., Cohen, A., Mor, F., Sela, M., Cohen, I. R., and Schwartz, M. (2000). T cell immunity to copolymer 1 confers neuroprotection on the damaged optic nerve: possible therapy for optic neuropathies. Proc Natl Acad Sci U S A 97, 7446-7451.
- Kirby, M. A., and Chalupa, L. M. (1986). Retinal crowding alters the morphology of alpha ganglion cells. J Comp Neurol 251, 532-541.
- Klein, R. M., Wolf, E. D., Wu, R., and Sanford, J. C. (1992). High-velocity microprojectiles for delivering nucleic acids into living cells. 1987. Biotechnology 24, 384-386.
- Ko, M.-L., Hu, D.-N., Ritch, R., Sharma, S. C., and Chen, C.-F. (2001). Patterns of retinal ganglion cell survival after brain-derived neurotrophic factor administration in hypertensive eyes of rats. Neurosci Lett 305, 139-142.
- Koizumi, A., Zeck, G., Ben, Y., Masland, R. H., and Jakobs, T. C. (2007). Organotypic culture of physiologically functional adult mammalian retinas. PLoS One 2, e221.
- Kolb, B., Gibb, R., and Robinson, T. E. (2003). Brain plasticity and behavior. Current Directions in Psychological Science 12, 1-5.
- Kolb, H., Linberg, K. A., and Fisher, S. K. (1992). Neurons of the human retina: a Golgi study. J Comp Neurol 318, 147-187.

- Konorski, J. C. r. a. n. o., Cambridge University Press, Cambridge, UK. (1948). Conditioned reflexes and neuron organization.
- Krekoski, C. A., Neubauer, D., Zuo, J., and Muir, D. (2001). Axonal Regeneration into Acellular Nerve Grafts Is Enhanced by Degradation of Chondroitin Sulfate Proteoglycan. J Neurosci *21*, 6206-6213
- Kretz, A., Hermening, S. H., and Isenmann, S. (2004). A novel primary culture technique for adult retina allows for evaluation of CNS axon regeneration in rodents. J Neurosci Methods *136*, 207-219.
- Krishnamoorthy, R. R., Agarwal, P., Prasanna, G., Vopat, K., Lambert, W., Sheedlo, H. J., Pang, I. H., Shade, D., Wordinger, R. J., Yorio, T., et al. (2001). Characterization of a transformed rat retinal ganglion cell line. Brain Res Mol Brain Res 86, 1-12.
- Krott, R., Diestelhost, M., Zollweg, M., and Krieglstein, G. K. (1997). [Dose-response relationship of trans-scleral contact cyclophotocoagulation]. Ophthalmologe 94, 273-276.
- Krusius, T., Gehlsen, K. R., and Ruoslahti, E. (1987). A fibroblast chondroitin sulfate proteoglycan core protein contains lectin-like and growth factor-like sequences. J Biol Chem 262, 13120-13125.
- Kuehn, Fingert, and Kwon (2005). Retinal Ganglion Cell Death in Glaucoma: Mechanisms and Neuroprotective Strategies. Ophthalmol Clin North Am 18, 383-395.
- Kwok, J. C., Afshari, F., Garcia-Alias, G., and Fawcett, J. W. (2008). Proteoglycans in the central nervous system: plasticity, regeneration and their stimulation with chondroitinase ABC. Restor Neurol Neurosci 26, 131-145.
- Laquis, S., Chaudhary, P., and Sharma, S. C. (1998). The patterns of retinal ganglion cell death in hypertensive eyes. Brain Res 784, 100-104.
- Lawrence, J. M., Singhal, S., Bhatia, B., Keegan, D. J., Reh, T. A., Luthert, P. J., Khaw, P. T., and Limb, G. A. (2007). MIO-M1 cells and similar muller glial cell lines derived from adult human retina exhibit neural stem cell characteristics. Stem Cells 25, 2033-2043.
- Leaver, S. G., Cui, Q., Plant, G. W., Arulpragasam, A., Hisheh, S., Verhaagen, J., and Harvey, A. R. (2006). AAV-mediated expression of CNTF promotes long-term survival and regeneration of adult rat retinal ganglion cells. Gene Ther 13, 1328-1341.
- Leitgeb, R., Drexler, W., Unterhuber, A., Hermann, B., Bajraszewski, T., Le, T., Stingl, A., and Fercher, A. (2004). Ultrahigh resolution Fourier domain optical coherence tomography. Opt Express 12, 2156-2165.
- Leitgeb, R., Hitzenberger, C., and Fercher, A. (2003). Performance of fourier domain vs. time domain optical coherence tomography. Opt Express 11, 889-894.

- Lemons, M. L., Sandy, J. D., Anderson, D. K., and Howland, D. R. (2001). Intact aggrecan and fragments generated by both aggrecanse and metalloproteinase-like activities are present in the developing and adult rat spinal cord and their relative abundance is altered by injury. J Neurosci 21, 4772-4781.
- Leske, M. C., Heijl, A., Hussein, M., Bengtsson, B., Hyman, L., Komaroff, E., and Early Manifest Glaucoma Trial, G. (2003). Factors for glaucoma progression and the effect of treatment: the early manifest glaucoma trial. Arch Ophthal 121, 48-56.
- Levin, L. A. (1999). Direct and indirect approaches to neuroprotective therapy of glaucomatous optic neuropathy. Surv Ophthalmol 43 Suppl 1, S98-101.
- Levine, J. M., and Card, J. P. (1987). Light and electron microscopic localization of a cell surface antigen (NG2) in the rat cerebellum: association with smooth protoplasmic astrocytes. J Neurosci 7, 2711-2720.
- Levkovitch-Verbin, H., Harizman, N., Dardik, R., Nisgav, Y., Vander, S., and Melamed, S. (2007). Regulation of cell death and survival pathways in experimental glaucoma. Exp Eye Res 85, 250-258.
- Levkovitch-Verbin, H., Martin, K. R., Quigley, H. A., Baumrind, L. A., Pease, M. E., and Valenta, D. (2002). Measurement of amino acid levels in the vitreous humor of rats after chronic intraocular pressure elevation or optic nerve transection. J Glaucoma 11, 396-405.
- Lewis, G. P., Linberg, K. A., and Fisher, S. K. (1998). Neurite outgrowth from bipolar and horizontal cells after experimental retinal detachment. Investigative Ophthalmology & Visual Science 39, 424-434.
- Li, Q., Timmers, A. M., Hunter, K., Gonzalez-Pola, C., Lewin, A. S., Reitze, D. H., and Hauswirth, W. W. (2001). Noninvasive Imaging by Optical Coherence Tomography to Monitor Retinal Degeneration in the Mouse. Invest Ophthalmol Vis Sci 42, 2981-2989.
- Li, S., Wang, X., Li, S., Wu, G., and Wang, N. (2010). Evaluation of optic nerve head and retinal nerve fiber layer in early and advance glaucoma using frequency-domain optical coherence tomography. Graefes Arch Clin Exp Ophthalmol 248, 429-434.
- Li, W., Rusiniak, M. E., Chintala, S., Gautam, R., Novak, E. K., and Swank, R. T. (2004). Hermansky-Pudlak syndrome genes: regulators of lysosome-related organelles. Bioessays 26, 616 628.
- Libby, R. T., Anderson, M. G., Pang, I. H., Robinson, Z. H., Savinova, O. V., Cosma, I. M., Snow, A., Wilson, L. A., Smith, R. S., Clark, A. F., and John, S. W. (2005). Inherited glaucoma in DBA/2J mice: pertinent disease features for studying the neurodegeneration. Vis Neurosci 22, 637-648.
- Libersat, F., and Duch, C. (2002). Morphometric analysis of dendritic remodeling in an identified motoneuron during postembryonic development. J Comp Neurol 450, 153-166.

194

- Limb, G. A., Salt, T. E., Munro, P. M. G., Moss, S. E., and Khaw, P. T. (2002). In Vitro Characterization of a Spontaneously Immortalized Human Muller Cell Line (MIO-M1). Invest Ophthalmol Vis Sci 43, 864-869.
- Lindsey, J. D., and Weinreb, R. N. (2005). Elevated intraocular pressure and transgenic applications in the mouse. J Glaucoma 14, 318-320.
- Little, C. B., Hughes, C. E., Curtis, C. L., Janusz, M. J., Bohne, R., Wang-Weigand, S., Taiwo, Y. O., Mitchell, P. G., Otterness, I. G., Flannery, C. R., and Caterson, B. (2002). Matrix metalloproteinases are involved in C-terminal and interglobular domain processing of cartilage aggrecan in late stage cartilage degradation. Matrix Biol 21, 271-288.
- Lo, D. C. (2001). Neuronal transfection using particle-mediated gene transfer. Curr Protoc Neurosci *Chapter 3*, Unit 3 15.
- Lom, B., and Cohen-Cory, S. (1999). Brain-Derived Neurotrophic Factor Differentially Regulates Retinal Ganglion Cell Dendritic and Axonal Arborization In Vivo. J Neurosci 19, 9928-9938.
- Lowndes, M., Stanford, D., and Stewart, M. G. (1990). A system for the reconstruction and analysis of dendritic fields. J Neurosci Methods 31, 235-245.
- Mabuchi, F., Aihara, M., Mackey, M. R., Lindsey, J. D., and Weinreb, R. N. (2003). Optic Nerve Damage in Experimental Mouse Ocular Hypertension. Invest Ophthalmol Vis Sci 44, 4321-4330.
- Maeda, K., Sawada, A., Matsubara, M., Nakai, Y., Hara, A., and Yamamoto, T. (2004). A novel neuroprotectant against retinal ganglion cell damage in a glaucoma model and an optic nerve crush model in the rat. Invest Ophthalmol Vis Sci 45, 851-856.
- Maeda, N., Matsui, F., and Oohira, A. (1992). A chondroitin sulfate proteoglycan that is developmentally regulated in the cerebellar mossy fiber system. Dev Biol 151, 564-574.
- Manabe, S.-i., Kashii, S., Honda, Y., Yamamoto, R., Katsuki, H., and Akaike, A. (2002). Quantification of axotomized ganglion cell death by explant culture of the rat retina. Neuroscience Letters 334, 33-36.
- Mansour-Robaey, S., Clarke, D. B., Wang, Y., Bray, G. M., and Aguayo, A. J. (1994). Effects of Ocular Injury and Administration of Brain-Derived Neurotrophic Factor on Survival and Regrowth of Axotomized Retinal Ganglion Cells. PNAS *91*, 1632-1636.
- Margolis, R. K., and Margolis, R. U. (1993). Nervous tissue proteoglycans. Experientia 49, 429-446.
- Martin, K. R., Quigley, H. A., Zack, D. J., Levkovitch-Verbin, H., Kielczewski, J., Valenta, D., Baumrind, L., Pease, M. E., Klein, R. L., and Hauswirth, W. W. (2003).

Gene therapy with brain-derived neurotrophic factor as a protection: retinal ganglion cells in a rat glaucoma model. Invest Ophthalmol Vis Sci 44, 4357-4365.

Martin, K. R. G., Levkovitch-Verbin, H., Valenta, D., Baumrind, L., Pease, M. E., and Quigley, H. A. (2002). Retinal glutamate transporter changes in experimental glaucoma and after optic nerve transection in the rat. Invest Ophthalmol Vis Sci 43, 2236-2243.

Massey, J. M., Hubscher, C. H., Wagoner, M. R., Decker, J. A., Amps, J., Silver, J., and Onifer, S. M. (2006). Chondroitinase ABC Digestion of the Perineuronal Net Promotes Functional Collateral Sprouting in the Cuneate Nucleus after Cervical Spinal Cord Injury. J Neurosci 26, 4406-4414.

May, C. A., and Lutjen-Drecoll, E. (2002). Morphology of the Murine Optic Nerve. Invest Ophthalmol Vis Sci 43, 2206-2212.

McKinnon, S. J., Lehman, D. M., Kerrigan-Baumrind, L. A., Merges, C. A., Pease, M. E., Kerrigan, D. F., Ransom, N. L., Tahzib, N. G., Reitsamer, H. A., Levkovitch-Verbin, H., et al. (2002). Caspase Activation and Amyloid Precursor Protein Cleavage in Rat Ocular Hypertension. Invest Ophthalmol Vis Sci 43, 1077-1087.

Michael Maleski, S. H. (1997). Glial cells assemble hyaluronan-based pericellular matrices in vitro. Glia 20, 193-202.

Mittag, T. W., Danias, J., Pohorenec, G., Yuan, H.-M., Burakgazi, E., Chalmers-Redman, R., Podos, S. M., and Tatton, W. G. (2000). Retinal Damage after 3 to 4 Months of Elevated Intraocular Pressure in a Rat Glaucoma Model. Invest Ophthalmol Vis Sci 41, 3451-3459.

Mizrahi, A., and Libersat, F. (2002). Afferent input regulates the formation of distal dendritic branches. The Journal of Comparative Neurology 452, 1-10.

Mo, X., Yokoyama, A., Oshitari, T., Negishi, H., Dezawa, M., Mizota, A., and Adachi-Usami, E. (2002). Rescue of axotomized retinal ganglion cells by BDNF gene electroporation in adult rats. Invest Ophthalmol Vis Sci 43, 2401-2405.

Mohammadi, K., Bowd, C., Weinreb, R. N., Medeiros, F. A., Sample, P. A., and Zangwill, L. M. (2004). Retinal nerve fiber layer thickness measurements with scanning laser polarimetry predict glaucomatous visual field loss. Am J Ophthalmol 138, 592-601.

Moon, L. D., Asher, R. A., Rhodes, K. E., and Fawcett, J. W. (2001). Regeneration of CNS axons back to their target following treatment of adult rat brain with chondroitinase ABC. Nat Neurosci 4, 465-466.

Moore, C. G., Johnson, E. C., and Morrison, J. C. (1996). Circadian rhythm of intraocular pressure in the rat. Curr Eye Res 15, 185-191.

Morawski, M., Brückner, M. K., Riederer, P., Brückner, G., and Arendt, T. (2004). Perineuronal nets potentially protect against oxidative stress. Exp Neurol 188, 309-315.

Morgan, J., Caprioli, J., and Koseki, Y. (1999). Nitric oxide mediates excitotoxic and anoxic damage in rat retinal ganglion cells cocultured with astroglia. Arch Ophthalmol 117, 1524-1529.

Morgan, J. E., Datta, A. V., Erichsen, J. T., Albon, J., and Boulton, M. E. (2006). Retinal ganglion cell remodelling in experimental glaucoma. Adv Exp Med Biol 572, 397-402.

Morgan, J. E., Uchida, H., and Caprioli, J. (2000). Retinal ganglion cell death in experimental glaucoma. Br J Ophthalmol 84, 303-310.

Morgan, J. E. D. F. (2002). Retinal Ganglion Cell Shrinkage in Glaucoma. J Glaucoma 11, 365-370.

Morrison, J., Farrell, S., Johnson, E., Deppmeier, L., Moore, C. G., and Grossmann, E. (1995). Structure and composition of the rodent lamina cribrosa. Exp Eye Res 60, 127-135.

Morrison, J. C., Johnson E. C., Cepurna W. (1998). Animal models in glaucoma research. Ophthalmic Practice 16, 12–20.

Morrison, J. C. (2005). Elevated intraocular pressure and optic nerve injury models in the rat. J Glaucoma 14, 315-317.

Morrison, J. C., Johnson, E., Cepurna, W. O., and Carlo Nucci, L. C. N. N. O. a. G. B. (2008). Rat models for glaucoma research. Prog Brain Res (Elsevier), pp. 285-301.

Morrison, J. C., Johnson, E. C., Cepurna, W., and Jia, L. (2005). Understanding mechanisms of pressure-induced optic nerve damage. Prog Retin Eye Res 24, 217-240.

Morrison, J. C., Moore, C. G., Deppmeier, L. M. H., Gold, B. G., Meshul, C. K., and Johnson, E. C. (1997). A Rat Model of Chronic Pressure-induced Optic Nerve Damage. Exp Eye Res 64, 85-96.

Murakami, T., Ohtsuka, A., Taguchi, T., and Piao, D. X. (1995). Perineuronal sulfated proteoglycans and dark neurons in the brain and spinal cord: a histochemical and electron microscopic study of newborn and adult mice. Arch Histol Cytol 58, 557-565.

Nagata, A., Higashide, T., Ohkubo, S., Takeda, H., and Sugiyama, K. (2009). In Vivo Quantitative Evaluation of the Rat Retinal Nerve Fiber Layer with Optical Coherence Tomography. Invest Ophthalmol Vis Sci 50, 2809-2815.

- Naskar, R., Wissing, M., and Thanos, S. (2002). Detection of Early Neuron Degeneration and Accompanying Microglial Responses in the Retina of a Rat Model of Glaucoma. Invest Ophthalmol Vis Sci 43, 2962-2968.
- Nassif, N., Cense, B., Park, B., Pierce, M., Yun, S., Bouma, B., Tearney, G., Chen, T., and de Boer, J. (2004). In vivo high-resolution video-rate spectral-domain optical coherence tomography of the human retina and optic nerve. Opt Express 12, 367-376.
- Neale, E. A., Bowers, L. M., and Smith, T. G., Jr. (1993). Early dendrite development in spinal cord cell cultures: a quantitative study. J Neurosci Res 34, 54-66.
- Neufeld, A. H., Hernandez, M. R., and Gonzalez, M. (1997). Nitric oxide synthase in the human glaucomatous optic nerve head. Arch Ophthalmol 115, 497-ccc503ddd.
- Neufeld, A. H., Sawada, A., and Becker, B. (1999). Inhibition of nitric-oxide synthase 2 by aminoguanidine provides neuroprotection of retinal ganglion cells in a rat model of chronic glaucoma. Proc Natl Acad Sci U S A 96, 9944-9948.
- Nickells, R. W., Jampel, H. D., and Zack, D. J. (2002). Glaucoma. Emery & Rimoins Principles and Practices of Medical Genetics 3, 3491 3512.
- Nissirios, N., Chanis, R., Johnson, E., Morrison, J., Cepurna, W. O., Jia, L., Mittag, T., and Danias, J. (2008). Comparison of Anterior Segment Structures in Two Rat Glaucoma Models: An Ultrasound Biomicroscopic Study. Invest Ophthalmol Vis Sci 49, 2478-2482.
- Nouri-Mahdavi, K., Hoffman, D., Coleman, A. L., Liu, G., Li, G., Gaasterland, D., and Caprioli, J. (2004). Predictive factors for glaucomatous visual field progression in the Advanced Glaucoma Intervention Study. Ophthalmology 111, 1627-1635.
- Novak, U., and Kaye, A. H. (2000). Extracellular matrix and the brain: components and function. J Clin Neurosci 7, 280-290.
- Oakley, R. A., and Tosney, K. W. (1991). Peanut agglutinin and chondroitin-6-sulfate are molecular markers for tissues that act as barriers to axon advance in the avian embryo. Developmental Biology *147*, 187-206.
- Ogilvie, J. M., Speck, J. D., Lett, J. M., and Fleming, T. T. (1999). A reliable method for organ culture of neonatal mouse retina with long-term survival. J Neurosci Methods 87, 57-65.
- Oohira, A., Shuo, T., Tokita, Y., Nakanishi, K., and Aono, S. (2004). Neuroglycan C, a brain-specific part-time proteoglycan, with a particular multidomain structure. Glycoconj J 21, 53-57.
- Oshitari, T., and Adachi-Usami, E. (2003). The effect of caspase inhibitors and neurotrophic factors on damaged retinal ganglion cells. Neuroreport 14, 289-292.
- Otori, Y. (2008). Use of Purified Retinal Ganglion Cells for an In Vitro Model to Study Glaucoma, in: J.Tombran-Tink, C.J. Barnstable, M.B. Shields (Eds.),

Opthalmology Research: Mechanisms of the Glaucomas (Totowa, NJ, Humana Press), 601-607.

Ozden, S., and Isenmann, S. (2004). Neuroprotective properties of different anesthetics on axotomized rat retinal ganglion cells in vivo. J Neurotrauma 21, 73-82.

Pang, I.-H., Johnson, E. C., Jia, L., Cepurna, W. O., Shepard, A. R., Hellberg, M. R., Clark, A. F., and Morrison, J. C. (2005). Evaluation of Inducible Nitric Oxide Synthase in Glaucomatous Optic Neuropathy and Pressure-Induced Optic Nerve Damage. Invest Ophthalmol Vis Sci 46, 1313-1321.

Pante, G., Thompson, J., Lamballe, F., Iwata, T., Ferby, I., Barr, F. A., Davies, A. M., Maina, F., and Klein, R. (2005). Mitogen-inducible gene 6 is an endogenous inhibitor of HGF/Met-induced cell migration and neurite growth. J Cell Biol 171, 337-348.

Parrilla-Reverter, G., Agudo, M., Sobrado-Calvo, P., Salinas-Navarro, M., Villegas-Perez, M. P., and Vidal-Sanz, M. (2009). Effects of different neurotrophic factors on the survival of retinal ganglion cells after a complete intraorbital nerve crush injury: a quantitative in vivo study. Exp Eye Res 89, 32-41.

Paulsson, M., Morgelin, M., Wiedemann, H., Beardmore-Gray, M., Dunham, D., Hardingham, T., Heinegard, D., Timpl, R., and Engel, J. (1987). Extended and globular protein domains in cartilage proteoglycans. Biochem J 245, 763-772.

Pease, M. E., McKinnon, S. J., Quigley, H. A., Kerrigan-Baumrind, L. A., and Zack, D. J. (2000). Obstructed Axonal Transport of BDNF and Its Receptor TrkB in Experimental Glaucoma. Invest Ophthalmol Vis Sci 41, 764-774.

Pease, M. E., Zack, D. J., Berlinicke, C., Bloom, K., Cone, F., Wang, Y., Klein, R. L., Hauswirth, W. W., and Quigley, H. A. (2009). Effect of CNTF on retinal ganglion cell survival in experimental glaucoma. Invest Ophthalmol Vis Sci 50, 2194-2200.

Pease, M. E., Zack, D. J., Berlinicke, C. A., Bloom, K. M., Cone, F. E., Wang, Y., Klein, R. L., Hauswirth, W. W., and Quigley, H. A. (2008). CNTF over-expression leads to increased retinal ganglion cell survival in experimental glaucoma. Invest Ophthalmol Vis Sci, iovs.08-3013.

Peichl, L., and Bolz, J. (1984). Kainic acid induces sprouting of retinal neurons. Science 223, 503-504.

Pena, J. D., Agapova, O., Gabelt, B. T., Levin, L. A., Lucarelli, M. J., Kaufman, P. L., and Hernandez, M. R. (2001). Increased elastin expression in astrocytes of the lamina cribrosa in response to elevated intraocular pressure. Invest Ophthalmol Vis Sci 42, 2303-2314.

Perry, V. H., and Cowey, A. (1981). The morphological correlates of X- and Y-like retinal ganglion cells in the retina of monkeys. Exp Brain Res 43, 226-228.

Perry, V. H., and Linden, R. (1982). Evidence for dendritic competition in the developing retina. Nature 297, 683-685.

- Peterson, B. B., and Dacey, D. M. (2000). Morphology of wide-field bistratified and diffuse human retinal ganglion cells. Vis Neurosci 17, 567-578.
- Peterson, J. A., Kiland, J. A., Croft, M. A., and Kaufman, P. L. (1996). Intraocular pressure measurement in cynomolgus monkeys. Tono-Pen versus manometry. Invest Ophthalmol Vis Sci 37, 1197-1199.
- Pizzorusso, T., Medini, P., Berardi, N., Chierzi, S., Fawcett, J. W., and Maffei, L. (2002). Reactivation of Ocular Dominance Plasticity in the Adult Visual Cortex. Science 298, 1248-1251.
- Pizzorusso, T., Medini, P., Landi, S., Baldini, S., Berardi, N., and Maffei, L. (2006). Structural and functional recovery from early monocular deprivation in adult rats. Proc Natl Acad Sci U S A 103, 8517-8522.
- Pollock, G. S., Robichon, R., Boyd, K. A., Kerkel, K. A., Kramer, M., Lyles, J., Ambalavanar, R., Khan, A., Kaplan, D. R., Williams, R. W., and Frost, D. O. (2003). TrkB Receptor Signaling Regulates Developmental Death Dynamics, But Not Final Number, of Retinal Ganglion Cells. J Neurosci *23*, 10137-10145.
- Poole, A. R., Pidoux, I., Reiner, A., Cöster, L., and Hassell, J. R. (1982). Mammalian eyes and associated tissues contain molecules that are immunologically related to cartilage proteoglycan and link protein. J Cell Biol 93, 910-920.
- Povazay, B., Hermann, B., Unterhuber, A., Hofer, B., Sattmann, H., Zeiler, F., Morgan, J. E., Falkner-Radler, C., Glittenberg, C., Blinder, S., and Drexler, W. (2007a). Three-dimensional optical coherence tomography at 1050 nm versus 800 nm in retinal pathologies: enhanced performance and choroidal penetration in cataract patients. J Biomed Opt 12, 041211.
- Povazay, B., Hofer, B., Hermann, B., Unterhuber, A., Morgan, J. E., Glittenberg, C., Binder, S., and Drexler, W. (2007b). Minimum distance mapping using three-dimensional optical coherence tomography for glaucoma diagnosis. J Biomed Opt 12, 041204.
- Prashar, A., Guggenheim, J. A., Erichsen, J. T., Hocking, P. M., and Morgan, J. E. (2007). Measurement of intraocular pressure (IOP) in chickens using a rebound tonometer: Quantitative evaluation of variance due to position inaccuracies. Exp Eye Res 85, 563-571.
- Qin, Y., Xu, G., and Wang, W. (2006). Dendritic abnormalities in retinal ganglion cells of three-month diabetic rats. Curr Eye Res 31, 967-974.
- Quigley, H. A. (1986). Examination of the retinal nerve fiber layer in the recognition of early glaucoma damage. Trans Am Ophthalmol Soc 84, 920-966.
- Quigley, H. A. (1996). Number of people with glaucoma worldwide. Br J Ophthalmol 80, 389-393.
- Quigley, H. A. (1999). Neuronal death in glaucoma. Prog Retin Eye Res 18, 39-57.

•

- Quigley, H. A., and Addicks, E. M. (1980). Chronic experimental glaucoma in primates. I. Production of elevated intraocular pressure by anterior chamber injection of autologous ghost red blood cells. Invest Ophthalmol Vis Sci 19, 126-136.
- Quigley, H. A., Dunkelberger, G. R., and Green, W. R. (1988). Chronic human glaucoma causing selectively greater loss of large optic nerve fibers. Ophthalmology 95, 357-363.
- Quigley, H. A., Dunkelberger, G. R., and Green, W. R. (1989). Retinal ganglion cell atrophy correlated with automated perimetry in human eyes with glaucoma. Am J Ophthalmol 107, 453-464.
- Quigley, H. A., Hohman, R. M., Addicks, E. M., and Green, W. R. (1984). Blood vessels of the glaucomatous optic disc in experimental primate and human eyes. Invest Ophthalmol Vis Sci 25, 918-931.
- Quigley, H. A., McKinnon, S. J., Zack, D. J., Pease, M. E., Kerrigan-Baumrind, L. A., Kerrigan, D. F., and Mitchell, R. S. (2000). Retrograde Axonal Transport of BDNF in Retinal Ganglion Cells Is Blocked by Acute IOP Elevation in Rats. Invest Ophthalmol Vis Sci 41, 3460-3466.
- Quigley, H. A., Nickells, R. W., Kerrigan, L. A., Pease, M. E., Thibault, D. J., and Zack, D. J. (1995). Retinal ganglion cell death in experimental glaucoma and after axotomy occurs by apoptosis. Invest Ophthalmol Vis Sci 36, 774-786.
- Quigley, H. A., Sanchez, R. M., Dunkelberger, G. R., L'Hernault, N. L., and Baginski, T. A. (1987). Chronic glaucoma selectively damages large optic nerve fibers. Invest Ophthalmol Vis Sci 28, 913-920.
- Rapaport, D. H., and Stone, J. (1983). Time course of morphological differentiation of cat retinal ganglion cells: influences on soma size. J Comp Neurol 221, 42-52.
- Reichardt, L. F. (2006). Neurotrophin-regulated signalling pathways. Philos Trans R Soc Lond B Biol Sci 361, 1545-1564.
- Reitsamer, H. A., Kiel, J. W., Harrison, J. M., Ransom, N. L., and McKinnon, S. J. (2004). Tonopen measurement of intraocular pressure in mice. Exp Eye Res 78, 799-804.
- Resnikoff, S., Pascolini, D., Etya'ale, D., Kocur, I., Pararajasegaram, R., Pokharel, G. P., and Mariotti, S. P. (2004). Global data on visual impairment in the year 2002. Bull World Health Organ 82, 844-851.
- Rhodes, K. E., and Fawcett, J. W. (2004). Chondroitin sulphate proteoglycans: preventing plasticity or protecting the CNS? J Anat 204, 33-48.
- Ristanovic, D., Milosevic, N. T., and Stulic, V. (2006). Application of modified Sholl analysis to neuronal dendritic arborization of the cat spinal cord. J Neurosci Methods 158, 212-218.

- Ritch, R., Shields, M., Krupin, T. (1989). The Glaucomas, 1st edn (St Louis, Mosby).
- Robinson, T. E., and Kolb, B. (1997). Persistent Structural Modifications in Nucleus Accumbens and Prefrontal Cortex Neurons Produced by Previous Experience with Amphetamine. J Neurosci 17, 8491-8497.
- Rodieck, R. W., Binmoeller, K. F., and Dineen, J. (1985). Parasol and midget ganglion cells of the human retina. J Comp Neurol 233, 115-132.
- Rohrer, B., LaVail, M. M., Jones, K. R., and Reichardt, L. F. (2001). Neurotrophin Receptor TrkB Activation Is Not Required for the Postnatal Survival of Retinal Ganglion Cells in Vivo. Experimental Neurology 172, 81-91.
- Rothblat, L. A., and Schwartz, M. L. (1979). The effect of monocular deprivation on dendritic spines in visual cortex of young and adult albino rats: evidence for a sensitive period. Brain Research *161*, 156-161.
- Rousseau, V., Engelmann, R., and Sabel, B. A. (1999). Restoration of vision III: soma swelling dynamics predicts neuronal death or survival after optic nerve crush in vivo. Neuroreport 10, 3387-3391.
- Ruiz-Ederra, J., and Verkman, A. S. (2006). Mouse model of sustained elevation in intraocular pressure produced by episcleral vein occlusion. Exp Eye Res 82, 879-884. Sanford, J. C., Klein, T. M., Wolf, E. D., and Allen, N. (1987). Delivery of substances into cells and tissues using a particle bombardement process. Part Sci Technol 5, 27–37.
- Sapieha, P. S., Peltier, M., Rendahl, K. G., Manning, W. C., and Di Polo, A. (2003). Fibroblast growth factor-2 gene delivery stimulates axon growth by adult retinal ganglion cells after acute optic nerve injury. Mol Cell Neurosci 24, 656-672.
- Sappington, R. M., Carlson, B. J., Crish, S. D., and Calkins, D. J. (2010). The microbead occlusion model: a paradigm for induced ocular hypertension in rats and mice. Invest Ophthalmol Vis Sci 51, 207-216.
- Sawada, A., and Neufeld, A. H. (1999). Confirmation of the Rat Model of Chronic, Moderately Elevated Intraocular Pressure. Exp Eye Res 69, 525-531.
- Schlamp, C. L., Johnson, E. C., Li, Y., Morrison, J. C., and Nickells, R. W. (2001). Changes in Thy1 gene expression associated with damaged retinal ganglion cells. Mol Vis 7, 192-201.
- Schori, H., Kipnis, J., Yoles, E., WoldeMussie, E., Ruiz, G., Wheeler, L. A., and Schwartz, M. (2001). Vaccination for protection of retinal ganglion cells against death from glutamate cytotoxicity and ocular hypertension: implications for glaucoma. Proc Natl Acad Sci U S A 98, 3398-3403.
- Schori, H., Yoles, E., Wheeler, L. A., Raveh, T., Kimchi, A., and Schwartz, M. (2002). Immune-related mechanisms participating in resistance and susceptibility to glutamate toxicity. Eur J Neurosci 16, 557-564.

- Schwartz, K., and Budenz, D. (2004). Current management of glaucoma. Curr Opin Ophthalmol 15, 119 126.
- Schwartz, M. (2004). Vaccination for glaucoma: dream or reality? Brain Res Bull 62, 481-484.
- Seigel, G. M. (1999). The golden age of retinal cell culture. Mol Vis 5, 4.
- Sena, D. F., Ramchand, K., and Lindsley, K. (2010). Neuroprotection for treatment of glaucoma in adults. Cochrane Database Syst Rev 2, CD006539.
- Shareef, S., Sawada, A., and Neufeld, A. H. (1999). Isoforms of nitric oxide synthase in the optic nerves of rat eyes with chronic moderately elevated intraocular pressure. Invest Ophthalmol Vis Sci 40, 2884-2891.
- Shareef, S. R., Garcia-Valenzuela, E., Salierno, A., Walsh, J., and Sharma, S. C. (1995). Chronic ocular hypertension following episcleral venous occlusion in rats. Exp Eye Res 61, 379-382.
- Shatz, C. J. (1996). Emergence of order in visual system development. Proc Natl Acad Sci U S A 93, 602-608.
- Sheldon, W. G., Warbritton, A. R., Bucci, T. J., and Turturro, A. (1995). Glaucoma in food-restricted and ad libitum-fed DBA/2NNia mice. Lab Anim Sci 45, 508-518.
- Shi, S. H., Cox, D. N., Wang, D., Jan, L. Y., and Jan, Y. N. (2004). Control of dendrite arborization by an Ig family member, dendrite arborization and synapse maturation 1 (Dasm1). Proc Natl Acad Sci U S A 101, 13341-13345.
- Sholl, D. A. (1953). Dendritic organization in the neurons of the visual and motor cortices of the cat. J Anat 87, 387-406.
- Shors, T. J., Miesegaes, G., Beylin, A., Zhao, M., Rydel, T., and Gould, E. (2001). Neurogenesis in the adult is involved in the formation of trace memories. Nature 410, 372-376.
- Shou, T., Liu, J., Wang, W., Zhou, Y., and Zhao, K. (2003). Differential Dendritic Shrinkage of {alpha} and {beta} Retinal Ganglion Cells in Cats with Chronic Glaucoma. Invest Ophthalmol Vis Sci 44, 3005-3010.
- Singhal, S., Lawrence, J. M., Bhatia, B., Ellis, J. S., Kwan, A. S., Macneil, A., Luthert, P. J., Fawcett, J. W., Perez, M. T., Khaw, P. T., and Limb, G. A. (2008). Chondroitin sulfate proteoglycans and microglia prevent migration and integration of grafted Muller stem cells into degenerating retina. Stem Cells 26, 1074-1082.
- Siu, A. W., Leung, M. C. P., Ho To, C., Siu, F. K. W., Ji, J. Z., and Fai So, K. (2002). Total Retinal Nitric Oxide Production is Increased in Intraocular Pressure-elevated Rats. Exp Eye Res 75, 401-406.

- Smith, F. D., Harpending, P. R., and Sanford, J. C. (1992). Biolistic transformation of prokaryotes: factors that affect biolistic transformation of very small cells. J Gen Microbiol 138, 239-248.
- Smith, K. J., Self, R. L., Butler, T. R., Mullins, M. M., Ghayoumi, L., Holley, R. C., Littleton, J. M., and Prendergast, M. A. (2007). Methamphetamine exposure antagonizes N-methyl-d-aspartate receptor-mediated neurotoxicity in organotypic hippocampal slice cultures. Brain Research 1157, 74-80.
- Smith, R. S., Zabaleta, A., Savinova, O. V., and John, S. W. (2001). The mouse anterior chamber angle and trabecular meshwork develop without cell death. BMC ev Biol 1, 3.
- Snow, D. M., Lemmon, V., Carrino, D. A., Caplan, A. I., and Silver, J. (1990). Sulfated proteoglycans in astroglial barriers inhibit neurite outgrowth in vitro. Experimental Neurology *109*, 111-130.
- Spalding, K. L., Dharmarajan, A. M., and Harvey, A. R. (2005). Caspase-independent retinal ganglion cell death after target ablation in the neonatal rat. Eur J Neurosci 21, 33-45.
- Spires, T. L., Grote, H. E., Garry, S., Cordery, P. M., Van Dellen, A., Blakemore, C., and Hannan, A. J. (2004). Dendritic spine pathology and deficits in experience-dependent dendritic plasticity in R6/1 Huntington's disease transgenic mice. Eur J Neurosci 19, 2799-2807.
- Srinivasan, V. J., Ko, T. H., Wojtkowski, M., Carvalho, M., Clermont, A., Bursell, S.-E., Song, Q. H., Lem, J., Duker, J. S., Schuman, J. S., and Fujimoto, J. G. (2006). Noninvasive Volumetric Imaging and Morphometry of the Rodent Retina with High-Speed, Ultrahigh-Resolution Optical Coherence Tomography. Invest Ophthalmol Vis Sci 47, 5522-5528.
- Stallcup, W. B., and Beasley, L. (1987). Bipotential glial precursor cells of the optic nerve express the NG2 proteoglycan. J Neurosci 7, 2737-2744.
- Steward, O., and Vinsant, S. L. (1978). Identification of the cells of origin of a central pathway which sprouts following lesions in mature rats. Brain Research 147, 223-243.
- Stiles, J. (2000). Neural plasticity and cognitive development. Developmental Neuropsychology 18, 237-272.
- Sugiura, S., Kitagawa, K., Tanaka, S., Todo, K., Omura-Matsuoka, E., Sasaki, T., Mabuchi, T., Matsushita, K., Yagita, Y., and Hori, M. (2005). Adenovirus-Mediated Gene Transfer of Heparin-Binding Epidermal Growth Factor-Like Growth Factor Enhances Neurogenesis and Angiogenesis After Focal Cerebral Ischemia in Rats. Stroke 36, 859-864.
- Sun, W., Li, N., and He, S. (2002). Large-scale morophological survey of rat retinal ganglion cells. Vis Neurosci 19, 483-493.

Sur, M., Frost, D. O., and Hockfield, S. (1988). Expression of a surface-associated antigen on Y-cells in the cat lateral geniculate nucleus is regulated by visual experience. J Neurosci 8, 874-882.

Sycha, T., Vass, C., Findl, O., Bauer, P., Groke, I., Schmetterer, L., and Eichler, H. (2003). Interventions for normal tension glaucoma. Cochrane Database Syst Rev, CD002222.

Takano, M., Horie, H., Iijima, Y., Dezawa, M., Sawada, H., and Ishikawa, Y. (2002). Brain-derived Neurotrophic Factor Enhances Neurite Regeneration from Retinal Ganglion Cells in Aged Human Retina in vitro. Experimental Eye Research 74, 319-323.

Tawara, A., Varner, H. H., and Hollyfield, J. G. (1989). Proteoglycans in the mouse interphotoreceptor matrix II. Origin and development of proteoglycans. Exp Eye Res 48, 815-839.

Teitelbaum, D., Meshorer, A., Hirshfeld, T., Arnon, R., and Sela, M. (1971). Suppression of experimental allergic encephalomyelitis by a synthetic polypeptide. Eur J Immunol 1, 242-248.

Tezel, G., Edward, D. P., and Wax, M. B. (1999). Serum autoantibodies to optic nerve head glycosaminoglycans in patients with glaucoma. Arch Ophthalmol 117, 917-924.

Tezel, G., Li, L. Y., Patil, R. V., and Wax, M. B. (2001). TNF-alpha and TNF-alpha receptor-1 in the retina of normal and glaucomatous eyes. Invest Ophthalmol Vis Sci 42, 1787-1794.

Tezel, G., and Wax, M. B. (2000). Increased production of tumor necrosis factoralpha by glial cells exposed to simulated ischemia or elevated hydrostatic pressure induces apoptosis in cocultured retinal ganglion cells. J Neurosci 20, 8693-8700.

Thylefors, B., Negrel, A. D., Pararajasegaram, R., and Dadzie, K. Y. (1995). Global data on blindness. Bull World Health Organ 73, 115-121.

Tomita, G., Niwa, Y., Shinohara, H., Hayashi, N., Yamamoto, T., and Kitazawa, Y. (1999). Changes in optic nerve head blood flow and retrobular hemodynamics following calcium-channel blocker treatment of normal-tension glaucoma. Int Ophthalmol 23, 3-10.

Toris, C. B., Zhan, G. L., Wang, Y. L., Zhao, J., McLaughlin, M. A., Camras, C. B., and Yablonski, M. E. (2000). Aqueous humor dynamics in monkeys with laser-induced glaucoma. J Ocul Pharmacol Ther 16, 19-27.

Toris, C. B., Zhan, G.-L., and McLaughlin, M. A. (2003). Effects of brinzolamide on aqueous humor dynamics in monkeys and rabbits. J Ocul Pharmacol Ther 19, 397-404.

•

- Tropea, D., Caleo, M., and Maffei, L. (2003). Synergistic Effects of Brain-Derived Neurotrophic Factor and Chondroitinase ABC on Retinal Fiber Sprouting after Denervation of the Superior Colliculus in Adult Rats. J Neurosci 23, 7034-7044.
- Uchida, M., Li, X. W., Mertens, P., and Alpar, H. O. (2009). Transfection by particle bombardment: Delivery of plasmid DNA into mammalian cells using gene gun. Biochim Biophys Acta (BBA) General Subjects 1790, 754-764.
- Ullian, E. M., Barkis, W. B., Chen, S., Diamond, J. S., and Barres, B. A. (2004). Invulnerability of retinal ganglion cells to NMDA excitotoxicity. Mol Cell Neurosci 26, 544-557.
- Urcola, J. H., Hernández, M., and Vecino, E. (2006). Three experimental glaucoma models in rats: Comparison of the effects of intraocular pressure elevation on retinal ganglion cell size and death. Exp Eye Res 83, 429-437.
- Valverde, F. (1967). Apical dendritic spines of the visual cortex and light deprivation in the mouse. Exp Brain Res 3, 337-352.
- van Adel, B. A., Kostic, C., Deglon, N., Ball, A. K., and Arsenijevic, Y. (2003). Delivery of ciliary neurotrophic factor via lentiviral-mediated transfer protects axotomized retinal ganglion cells for an extended period of time. Hum Gene Ther 14, 103-115.
- van der Valk, R., Webers, C. A., Schouten, J. S., Zeegers, M. P., Hendrikse, F., and Prins, M. H. (2005). Intraocular pressure-lowering effects of all commonly used glaucoma drugs: a meta-analysis of randomized clinical trials. Ophthalmology 112, 1177-1185.
- Varner, H. H., Rayborn, M. E., Osterfeld, A. M., and Hollyfield, J. G. (1987). Localization of proteoglycan within the extracellular matrix sheath of cone photoreceptors. Exp Eye Res 44, 633-642.
- Vickers, J. C., Schumer, R. A., Podos, S. M., Wang, R. F., Riederer, B. M., and Morrison, J. H. (1995). Differential vulnerability of neurochemically identified subpopulations of retinal neurons in a monkey model of glaucoma. Brain Res 680, 23-35.
- Vizzeri, G., Weinreb, R. N., Gonzalez-Garcia, A. O., Bowd, C., Medeiros, F. A., Sample, P. A., and Zangwill, L. M. (2009). Agreement between spectral-domain and time-domain OCT for measuring RNFL thickness. Br J Ophthalmol 93, 775-781.
- von Bartheld, C. S., Byers, M. R., Williams, R., and Bothwell, M. (1996). Anterograde transport of neurotrophins and axodendritic transfer in the developing visual system. Nature 379, 830-833.
- Wamsley, S., Gabelt, B. T., Dahl, D. B., Case, G. L., Sherwood, R. W., May, C. A., Hernandez, M. R., and Kaufman, P. L. (2005). Vitreous glutamate concentration and axon loss in monkeys with experimental glaucoma. Arch Ophthalmol 123, 64-70.

206

- Wang, S. W., Mu, X., Bowers, W. J., and Klein, W. H. (2002). Retinal ganglion cell differentiation in cultured mouse retinal explants. Methods 28, 448-456.
- Wang, W.-H., Millar, J. C., Pang, I.-H., Wax, M. B., and Clark, A. F. (2005). Noninvasive Measurement of Rodent Intraocular Pressure with a Rebound Tonometer. Invest Ophthalmol Vis Sci 46, 4617-4621.
- Wang, X., Tay, S. S., and Ng, Y. K. (2000). An immunohistochemical study of neuronal and glial cell reactions in retinae of rats with experimental glaucoma. Exp Brain Res 132, 476-484.
- Wang, L., Zhang, Z., Wang, Y., Zhang, R., and Chopp, M. (2004). Treatment of Stroke With Erythropoietin Enhances Neurogenesis and Angiogenesis and Improves Neurological Function in Rats. Stroke 35, 1732-1737.
- Watanabe, M., and Rodieck, R. W. (1989). Parasol and midget ganglion cells of the primate retina. J Comp Neurol 289, 434-454.
- Wax, M. B. (2000). Is there a role for the immune system in glaucomatous optic neuropathy? Curr Opin Ophthalmol 11, 145-150.
- Weber, A. J., and Harman, C. D. (2005). Structure-Function Relations of Parasol Cells in the Normal and Glaucomatous Primate Retina. Invest Ophthalmol Vis Sci 46, 3197-3207.
- Weber, A. J., and Harman, C. D. (2008). BDNF Preserves the Dendritic Morphology of {alpha} and {beta} Ganglion Cells in the Cat Retina after Optic Nerve Injury. Invest Ophthalmol Vis Sci 49, 2456-2463.
- Weber, A. J., Kaufman, P. L., and Hubbard, W. C. (1998). Morphology of single ganglion cells in the glaucomatous primate retina. Invest Ophthalmol Vis Sci 39, 2304-2320.
- Weber, A. J., and Zelenak, D. (2001). Experimental glaucoma in the primate induced by latex microspheres. J Neurosci Methods 111, 39-48.
- Wieloch, T., and Nikolich, K. (2006). Mechanisms of neural plasticity following brain injury. Current Opinion in Neurobiology 16, 258-264.
- Will, B., Galani, R., Kelche, C., and Rosenzweig, M. R. (2004). Recovery from brain injury in animals: relative efficacy of environmental enrichment, physical exercise or formal training (1990-2002). Progress in Neurobiology 72, 167-182.
- Wojtkowski, M., Srinivasan, V., Ko, T., Fujimoto, J., Kowalczyk, A., and Duker, J. (2004). Ultrahigh-resolution, high-speed, Fourier domain optical coherence tomography and methods for dispersion compensation. Opt Express 12, 2404-2422.
- Woldemussie, E., Ruiz, G., Wijono, M., and Wheeler, L. A. (2001). Neuroprotection of Retinal Ganglion Cells by Brimonidine in Rats with Laser-Induced Chronic Ocular Hypertension. Invest Ophthalmol Vis Sci 42, 2849-2855.

- Woldemussie, E., Wijono, M., and Ruiz, G. (2004). Muller cell response to laser-induced increase in intraocular pressure in rats. Glia 47, 109-119.
- Wolpaw, J. R., and Carp, J. S. (2006). Plasticity from muscle to brain. Progress in Neurobiology 78, 233-263.
- Wood, G. E., Young, L. T., Reagan, L. P., Chen, B., and McEwen, B. S. (2004). Stress-induced structural remodeling in hippocampus: Prevention by lithium treatment. Proc Natl Acad Sci U S A 101, 3973-3978.
- Wyllie, A. H., Morris, R. G., Smith, A. L., and Dunlop, D. (1984). Chromatin cleavage in apoptosis: association with condensed chromatin morphology and dependence on macromolecular synthesis. J Pathol 142, 67-77.
- Xin, H., Yannazzo, J. A., Duncan, R. S., Gregg, E. V., Singh, M., and Koulen, P. (2007). A novel organotypic culture model of the postnatal mouse retina allows the study of glutamate-mediated excitotoxicity. J<sup>4</sup>Neurosci Methods 159, 35-42.
- Yamada, E. S., Bordt, A. S., and Marshak, D. W. (2005). Wide-field ganglion cells in macaque retinas. Vis Neurosci 22, 383-393.
- Yamada, H., Watanabe, K., Shimonaka, M., and Yamaguchi, Y. (1994). Molecular cloning of brevican, a novel brain proteoglycan of the aggrecan/versican family. J Biol Chem 269, 10119-10126.
- Yamaguchi, Y. (2000). Lecticans: organizers of the brain extracellular matrix. Cell Mol Life Sci 57, 276-289.
- Yan, D. B., Coloma, F. M., Metheetrairut, A., Trope, G. E., Heathcote, J. G., and Ethier, C. R. (1994). Deformation of the lamina cribrosa by elevated intraocular pressure. Br J Ophthalmol 78, 643-648.
- Yick, L.-W., Cheung, P.-T., So, K.-F., and Wu, W. (2003). Axonal regeneration of Clarke's neurons beyond the spinal cord injury scar after treatment with chondroitinase ABC. Experimental Neurology 182, 160-168.
- Zagrebelsky, M., Holz, A., Dechant, G., Barde, Y.-A., Bonhoeffer, T., and Korte, M. (2005). The p75 Neurotrophin Receptor Negatively Modulates Dendrite Complexity and Spine Density in Hippocampal Neurons. J Neurosci 25, 9989-9999.
- Zaia, J. (2009). On-line separations combined with MS for analysis of glycosaminoglycans. Mass Spectrom Rev 28, 254-272.
- Zangwill, L. M., Weinreb, R. N., Beiser, J. A., Berry, C. C., Cioffi, G. A., Coleman, A. L., Trick, G., Liebmann, J. M., Brandt, J. D., Piltz-Seymour, J. R., et al. (2005). Baseline topographic optic disc measurements are associated with the development of primary open-angle glaucoma: the Confocal Scanning Laser Ophthalmoscopy Ancillary Study to the Ocular Hypertension Treatment Study. Arch Ophthalmol 123, 1188-1197.

Zaremba, S., Guimaraes, A., Kalb, R. G., and Hockfield, S. (1989). Characterization of an activity-dependent, neuronal surface proteoglycan identified with monoclonal antibody Cat-301. Neuron *2*, 1207-1219.

Zelenin, A. V., Titomirov, A. V., and Kolesnikov, V. A. (1989). Genetic transformation of mouse cultured cells with the help of high-velocity mechanical DNA injection. FEBS Lett 244, 65-67.

Zuo, J., Neubauer, D., Graham, J., Krekoski, C. A., Ferguson, T. A., and Muir, D. (2002). Regeneration of Axons after Nerve Transection Repair Is Enhanced by Degradation of Chondroitin Sulfate Proteoglycan. Experimental Neurology *176*, 221-228.

209